

# **Declaration**

I, Abdelaziz Ismail Abualshawareb, hereby affirm that the material contained within this thesis has not been previously submitted for any other academic award and is in compliance with the University's guidelines and regulations for research. Additionally, I certify that all the work presented in this thesis is my own original work and that any assistance received in conducting the research and composing the thesis has been appropriately acknowledged and cited.

Signature:

Date: May 2025

# Acknowledgments

I would like to express my deepest gratitude to Dr. Ioana Pisica. From our very first meeting, she believed in me and in this work, and stood by my side through every phase of this PhD. Her support, guidance, and encouragement were unwavering, especially during the most difficult moments. I genuinely wouldn't have made it without her.

I am also thankful to Dr. Carola Koenig, whose support and thoughtful input were valuable during the final months of the VPP4Islands project and its successful conclusion. I appreciate Dr. Ximena Schmidt, who stepped in at a critical time and helped keep the project on track with clear direction. My thanks go as well to Dr. Zahir Dehouche, who supervised me during the first two years and whose early mentorship laid the foundation for this work. Though he had to step back due to health reasons, his guidance left a lasting impact.

Special thanks to the VPP4Islands partners, Seifeddine Benghali, Sergi, Victor, and Habib and to Bornholm Island, especially Torben and Jorgen, for generously sharing their time and expertise.

To my family, especially my sister and my wife, thank you for your love, patience, and constant support. You've been the heart of this journey. To all my friends, your friendship, humour, and shared struggles made this experience not only bearable but unforgettable. Finally, I would like to express my deepest gratitude to everyone who supported me throughout this PhD journey.

## **Abstract**

The transition to high-renewable energy systems at the community level demands optimisation frameworks that balance economic efficiency, operational flexibility, and sustainability. While many existing studies focus on either static sizing or simplified dispatch heuristics, they often fail to co-optimise key system parameters such as inverter capacity, grid constraints, and hybrid storage integration under dynamic conditions. This thesis addresses that gap by developing a deeply integrated optimisation architecture that unites long-horizon sizing with short-horizon control, tailored for islanded and weak-grid energy communities.

The central objective is to design a techno-economically robust and energy sustainable hybrid PV-battery-hydrogen system that minimises lifecycle cost and enhances renewable self-consumption while accounting for real-world constraints. To this end, a nested optimisation approach is proposed, integrating a Genetic Algorithm (GA) for capacity sizing with a Mixed Integer Linear Programming (MILP) framework that embeds a Model Predictive Control (MPC) dispatch strategy. The GA generates candidate system layouts, each of which is validated via the MILP model that co-optimises hourly dispatch under fixed tariff structures and inverter-grid limits with AC/DC nodal representation. To capture operational uncertainty and improve flexibility, a rolling-horizon MPC layer executes every 12 hours using a 24-hour forecast window, incorporating flexible loads up to 8% of daily average demand, a level selected to reflect realistic load-shifting potential based on typical non-critical applications such as water pumps.

Results show that the framework achieves Net Present Cost (NPC) and Levelised Cost of Energy (LCOE) reductions of 10% and 10.2%, respectively, compared to static or rule-based baselines. Grid-related operational charges fall by 46% under MPC with load flexibility, and self-consumption rises to 44.56%. A novel, extended Energy Return on Investment (EROI) metric is introduced to capture full energy pathways, revealing battery storage as the dominant contributor to lifecycle efficiency. To explore trade-offs between system size, energy return, and cost, generalisation heatmaps of EROI and NPC are developed around the optimised Formentera case study design from Chapter 4, which serves as the baseline (i.e. the configuration with the lowest NPC). These heatmaps identify design "sweet spots" around 1.0−1.1× the baseline capacity, where high EROI (>5.0) and low NPC (≤€610,000) are simultaneously achieved. Beyond which oversizing leads to diminishing energy and cost returns due to increased curtailment and underutilisation of grid infrastructure.

The proposed GA–MILP–MPC framework thus provides a replicable, scalable, and practical tool for optimising community-scale energy systems. By tightly linking planning, operation, and sustainability metrics, it enables planners to make data-driven decisions that are financially

sound, operationally feasible, and environmentally justified. As distributed energy infrastructures continue to evolve, such integrative methods will be crucial for shaping resilient and sustainable energy futures.

## Nomenclature and Abbreviations

## Acronyms:

Acronym **Definition** AC **Alternating Current** AEM Anion Exchange Membrane BIR Battery-to-Inverter Ratio CapEx Capital Expenditure DC **Direct Current DEAP** Distributed Evolutionary Algorithms in Python **EROI Energy Return on Investment ESOI Energy Stored on Invested ESS Energy Storage System** GΑ Genetic Algorithm  $H_2$ Hydrogen **HRES** Hybrid Renewable Energy System IC **Inverter-Capacity Optimisation LCOE** Levelised Cost of Electricity Level of Hydrogen LoH **MILP** Mixed Integer Linear Programming **MPC** Model Predictive Control NC **Nominal Capacity NPC Net Present Cost NOCT** Nominal Operating Cell Temperature O&M Operation and Maintenance PEM Proton Exchange Membrane PS **Peak Shaving** PV **Photovoltaic** RH Rolling Horizon SA Simulated Annealing SH Static Hourly Dispatch

Acronym	Definition
SOC	State of Charge
SPT	Smart Planning Tool
ToU	Time-of-Use
TPR	Tank-to-Inverter Ratio
VPP	Virtual Power Plant

# Variables:

Symbol Description		Unit
$\mathcal{C}_r$ Vector of decision variables for system component capacities		-
$P_{PV}$	Photovoltaic array capacity	kW
$N_{WT}$	Number of wind turbines	units
$N_{bt}$	Number of battery modules (4.8 kWh each)	units
$P_{inv}$	Inverter rated capacity	kW
$\overline{P_{gr}}$	Grid exchange power limit (buy/sell)	kW
$P_{fc}$	Fuel cell electrical output power	kW
$P_{el}$	Electrolyser electrical input power	kW
$P_{HT}$	Hydrogen tank capacity	kg
$C_{NPC}$	Net Present Cost over the system lifetime	€
CapEX <sub>k,t</sub>	Capital expenditure for component $\boldsymbol{k}$ at time $t$	€
$OpEX_t$	Operational expenditure at time t	€
$RepEX_{k,t}$	Replacement expenditure for component $\boldsymbol{k}$ at time $\boldsymbol{t}$	€
$RecVal_{k,t}$	Recovery value of component $k$ at time $t$	€
$D_t$	Discount factor at time t	-
i	Real discount rate	- or %
i'	Nominal discount rate	- or %
f	Inflation rate	- or %
CRF	Capital Recovery Factor	-
$R_v$	Recovery value of component at project end	€
$C_{Rep}$	Replacement cost of a component	€

$T_{rem}$	Remaining life of a component at project end	years
$T_{com}$	Expected lifetime of the component	years
$E_{load}$	Total energy demand/load served	kWh
$P_{PV-\text{ output }}[t]$	PV array output power at time $t$	kW
$f_{PV}$	PV derating factor	-
$G_{module}\left[t ight]$	Irradiance on tilted PV module at time $t$	$\frac{kW}{m^2}$
$G_{T,STC}$	Standard test condition irradiance	$\frac{kW}{m^2}$
$K_p$	Temperature coefficient of power	%°C
$T_c[t]$	PV cell temperature at time t	°C
$T_S$	Standard cell temperature ( 25°C )	°C
δ	Solar declination angle	degrees
d	Day of the year (1-365)	-
T <sub>ambient</sub> [t]	Ambient temperature at time t	°C
$T_{c,NOCT}$	Nominal Operating Cell Temperature	°C
$T_{a,NOCT}$	Ambient temp. under NOCT conditions	°C
$G_{ m NOCT}$	Irradiance under NOCT conditions	$\frac{kW}{m^2}$
$\eta_{\sf mp,STC}$	PV efficiency at standard test conditions	-
$\alpha_P$	Temperature coefficient of power	%— °C
τα	Optical factor (transmissivity × absorptivity)	-
Т	Set of time steps in the optimisation	-
$\pi_{buy}\left[t ight]$	Grid electricity buying price at time t	€/kWh
$\pi_{sell}\left[t ight]$	Grid electricity selling price at time t	€/kWh
P <sub>grid,buy</sub> [t]	Power bought from grid at time t	kWh
$P_{grid,sell[t]}$	Power sold to grid at time t	kWh
penalty <sub>ummet</sub>	Penalty cost per unit unmet energy	€/kWh
penalty <sub>excess</sub>	Penalty cost per unit excess energy	€/kWh
$E_{wmmet}[t]$	Unmet energy demand at time t	kWh
$E_{excess}[t]$	Excess energy at time t	kWh
P <sub>battery,charge</sub> [t]	Battery charging power at time t	kW

$P_{battery}$ , discharge $[t]$	Battery discharging power at time $t$	kW
$\eta_{b-}$	Battery charging efficiency	-
$\eta_b$ +	Battery discharging efficiency	-
$B_m$	Battery module capacity	kWh
SoC[t]	Battery state of charge at time <i>t</i>	%
SoC <sub>min</sub>	Minimum state of charge	%
SoC <sub>max</sub>	Maximum state of charge	%
LoH[t]	Hydrogen level in tank at time $t$	% or kg
LoH <sub>min</sub>	Minimum allowed hydrogen tank level	%
LoH <sub>max</sub>	Maximum allowed hydrogen tank level	%
$\eta_{el ext{-}}$	Electrolyser efficiency	- or %
$\overline{\eta_{fc+}}$	Fuel cell efficiency	- or %
$H_{LHV}$	Lower Heating Value of hydrogen	kWh/kg
$x_{\text{grid}}[t]$	Binary gid direction (1 = buy, 0 = sell)	Binary
x <sub>battery</sub> [t]	Binary battery direction (0 = charge, 1 = discharge)	Binary
x <sub>hydrogen</sub> [t]	Binary control for H <sub>2</sub> system operation	Binary
$x_{\text{ren-gen}}[t]$	Binary indicating the remaining DC renewable generation	Binary
x <sub>hydrogen</sub> [t]	Binary control for H <sub>2</sub> system operation	Binary
x <sub>ren-gen</sub> [t]	Binary indicating the remaining DC renewable generation	Binary
M	Large number used in linearisation (Big-M method)	-
$\epsilon$	Small positive value used in constraints	-
$F_{CP}$	Fixed contracted power charge	€
$R_{t,p}$	Contracted rate for power at time $t$ , period $p$	€/kW/day
$D_{month}$	Number of days in billing month	days
$E_{cc}$	Electricity consumption charge	€
$F_{EP}$	Peak power penalty charge	€
$P_d^j$	Demand peak in billing interval <i>j</i>	kW
$S_{BC}$	Selling back charge (revenue from selling electricity)	€

Penalty <sub>excess</sub> Penalty for total excess energy (if > 100 kWh) €		€
Penalty <sub>unmet</sub>	Penalty for total unmet energy (if > 100 kWh)	€
P <sub>excess</sub>	Large penalty value for excess energy	€
P <sub>ummet</sub>	Large penalty value for unmet energy	€
Fitness Value( $p,g$ )	Final fitness function (NPC + penalties)	€
W	Index of the current rolling window	-
h	Starting hour of the current window in the global 8,760-hour timeline	hours
Т	Local hourly set in a window (typically { $0,1,,23$ )	hours
P <sub>flexible</sub> [t]	Flexible (shiftable) load power at time t	kW
$P_{flexible,rated}$	Rated power of the flexible load	kW
$x_{\overline{\text{flexible,on}}}[t]$	Binary variable: 1 if flexible load is ON at time $t$	Binary (0 or 1)
$H_{flexible,daily}$	Required total operation time of flexible load per day	hours/day
$T_d$	Set of global hours that belong to day $\emph{d}$	hours
$\phi_d^{(w-1)}$	Number of flexible-load hours already used for day $\boldsymbol{d}$ in previous window	hours
$SoC_b[t]$	Battery state of charge in MPC formulation at time $\boldsymbol{t}$	%
$SoC_{init}^{(w)}$	Initial battery SoC passed into window w	%
LoH[t]	Hydrogen level in tank in MPC formulation at time $\boldsymbol{t}$	% or kg
LoH <sub>init</sub> <sup>(w)</sup>	Initial hydrogen level passed into window w	% or kg
ESOI <sub>e</sub>	Energy Stored on Invested for electricity-only storage	- (dimensionless)
E <sub>out</sub> , st	Total lifetime energy dispatched from storage	MJ
$E_{emb}$ , st	Embodied energy used in manufacturing the storage system	MJ
EROI <sub>gen</sub>	Energy Return on Investment of the generation subsystem	-
$E_{emb,gen}$	Embodied energy required for constructing the generation subsystem	MJ
$arphi_{ extsf{pv\_load}}$	Fraction of generation directly consumed by the local load	-

$arphi_{bat}$	Fraction of generation routed through the battery system	-
$arphi_{ m H_2}$	Fraction of generation routed through the hydrogen system	-
$arphi_{ extsf{pv\_grid}}$	Fraction of generation exported to the grid	-
$arphi_{ ext{curt}}$	Fraction of generation curtailed (unused or dumped)	-
$E_{ m disp,total}$	Total energy dispatched to end uses (load + grid) accounting for efficiency losses	MJ
ESOI <sub>i</sub>	ESOI value for storage technology $i$ (e.g., battery, hydrogen)	-
$\eta_i$	Round-trip efficiency of storage technology i	-
$E_{emb,i}$	Embodied energy associated with storage technology $\emph{i}$	MJ
$E_{emb,total}$	Total embodied energy (generation + all storages)	MJ
EROI community	Novel extended EROI metric for hybrid energy community system	-
$arepsilon_{ ext{gen}}$	Energy intensity of generation (MJ embodied per MJ generated), equals $\frac{1}{EROI_{gen}}$	MJ/MJ
$arepsilon_{ ext{st}}$	Energy intensity of storage (MJ embodied per MJ delivered), equals $\frac{1}{\mathrm{ESOI}_e}$	MJ/MJ
φ	Fraction of generation $E_{\rm gen}$ routed through the storage system	-
EROI <sub>grid</sub>	Energy Return on Investment of the combined generation-plus-storage grid system	-
$E_{\sf disp,gen}$	Dispatched energy directly from generation (bypassing storage)	MJ
$E_{\sf disp,st}$	Dispatched energy from storage (after round-trip losses)	MJ
$\eta_{st}$	Round-trip efficiency of the storage system	-

# **Table of Contents**

Declaration	2
Acknowledgments	3
Abstract	4
Nomenclature and Abbreviations	6
Table of Contents	12
List of Figures	15
List of Tables	20
1 Introduction	22
1.1 Motivation	22
1.2 The Role of Regenerative Hydrogen Storage in Decarbonisation	
1.3 Research Aim and Objectives	29
1.4 Principal Research Contributions	30
1.5 Thesis Structure	30
1.6 List of Publications	33
2 Literature Review	34
2.1 Introduction	34
2.1.1 Review Scope and Research Relevance	34
2.1.2 Structure of the Chapter	35
2.2 Hybrid Renewable Energy Storage Systems: Concept	ts and Challenges36
2.2.1 Hybrid Systems and Grid Integration	36
2.2.2 Specific Challenges for Island Energy Communities	38
2.3 Optimisation Methods for Hybrid System Sizing and D	Dispatch41
2.3.1 Genetic Algorithms (GA) for System Sizing	42
2.3.2 Mixed Integer Linear Programming for Sizing and F	dourly Dispatch45
2.3.3 Nested Optimisation Approaches	53
2.4 Theoretical Background: Penalty-Guided Nested Obje	ective61

	2.5	Life-Cycle Energy Assessment in Hybrid Renewable Systems	64
	2.6	Literature Gap	70
3	Syst	em Sizing of Renewable Fuel Cell Battery Storage Systems with Hourly D	ispatch
O	ptimisa	tion	73
	3.1	Introduction	73
	3.2	System Description and Governance	74
	3.2.1	Physical Configuration of the REC	74
	3.2.2	Governance, Contracted-Power Limits, and Tariff Context	75
	3.3	Comparative Methods for Dispatch and Sizing	76
	3.3.1	Overview of Comparative Framework	76
	3.3.2	2 GA-Yearly Horizon Method	77
	3.3.3	GA-Based Load Following and HOMER Pro Comparison	89
	3.4	Model Inputs and System Parameters	92
	3.4.1	Geographical Location and Targeted Island	92
	3.4.2	2 Grid Tariff Structure	95
	3.4.3	Cost Assumptions and Sensitivity Analysis for Economic Inputs	96
	3.5	Results	98
	3.5.1	System Sizing	99
	3.5.2	P. Energy Flow and Dynamics	103
	3.5.3	B Economic Analysis	106
	3.6	Summary	112
4	Impr	oving Renewable System Sizing Accuracy through Model Predictive Control C	oncept
a	nd Flexi	ble Load Operation	114
	4.1	Introduction	114
	4.2	Methodology	114
	4.2.1	MPC-Flexible Load Formulation	116
	4.2.2	2 Water Pump as a Flexible Load	119
	4.2.3	B Summary	121
	4.3	Results	121
	431	System Sizing	121

		4.3.2		Energy Flow and Dynamics	125
		4.3.3	3	Economic Analysis	130
		4.3.4		GA and MILP Solvers parameter tunning	138
	4.	.4	Sι	ımmary	142
5		Life-0	Сус	cle Energy Cost Analysis through a New Index for Hybrid Renewable-Fuel	Cell
В	att	ery S	tor	age Systems in Energy Communities	144
	5.	.1	Int	troduction	144
	5.	.2	No	ovel Index for Energy Systems in Communities	146
	5.	.3	Αp	oplying the EROI Community Metric: Sensitivity and Scaling Analysis	150
	5.	.4	Re	esults	155
		5.4.1		Parametric Sensitivity Analysis with Fixed Capacities	155
		5.4.2		Capacity Scaling and Generalisation Framework	161
	5.	.5	Sι	ımmary	174
6		Integ	ırat	ed Analysis of Sizing, Operation, and Life-Cycle Performance	176
	6.	.1	Ma	ain Findings from Integrated System Design	176
	6.	.2	Ro	obustness Under Economic and Environmental Variability	183
	6.	.3	De	esign Decision Support Using EROI–NPC Trade-offs	185
	6.	.4	Co	omparative Benchmarking with Literature	186
		6.4.1		Sizing Ratios and Operational Load Matching	190
		6.4.2	) -	Grid Dependency and Storage Utilisation Trends	193
		6.4.3	}	Seasonal Energy Balancing and Storage Role Separation	195
	6.	.5	Sı	ımmary	196
7		Conc	clus	sion	196
8		Futur	re \	Work and Research Directions Work	199
9		Appe	end	lices	200
	9.	.1	Lit	erature Table Nomenclature	200
	9.	.2	Αl	gorithmic Setup and Implementation (Python)	203
		9.2.1		Genetic Algorithm (GA) Implementation (DEAP)	203
		922	,	MILP Implementation (PLILP)	208

9.2.3 MILP Decision Variables	210
9.3 Rule-Based Load Following	211
9.4 The Foundational Theoretical Framework	217
10 Reference	219
List of Figures	
Figure 1-1: Most recent carbon emissions world total (2024) with the 2	-
scenarios [2], [3], [4]	22
Figure 1-2: The historical energy consumption by source in EJ and GT	CO2 emissions [6]. 23
Figure 1-3: IEA Global hydrogen demand by production technology in	the Net Zero Scenario,
2020-2030 [27]	25
Figure 1-4: Hydrogen Production, consumption and transport pathway	s26
Figure 1-5: Comparison of ESS in terms of storage capacity, discharge	duration, and services
provided [34].	27
Figure 1-6: Flow of information and chapter dependencies throughout	the thesis 31
Figure 2-1: Diagram of a typical HRES adapted from [57]	36
Figure 3-1: Energy flow for the integrated hybrid energy system and its	s energy vector 74
Figure 3-2: Nested optimisation approach with progressive parameter	adjustment76
Figure 3-3: Proposed Benchmarking GA-Yealy Horizon Methodologi	cal for two layers Grid
Time of Use driven Optimisation approach. The detailed algorithm imp	lementation is provided
in Appendix 9.2.	78
Figure 3-4: Flow Diagram for Load-Following Energy Management Str	ategy90
Figure 3-5: Geographical Context of Formentera Island location	93
Figure 3-6: The geographical location of energy community buildings	west of Sant Francesc
Xavier capital of Formentera Island. Building 1: Culture Building ele	ctrical demand 44,995
kWh/year. Building 2: primary school with electrical demand 47,189	kWh/year. Building 3:
Radio and Youth Centre with electrical demand 19,616 kWh/year. But	ilding 4: Preschool with
electrical demand 26,596 kWh/year. Building 5: Vehicle inspection	station with electrical
demand 11,486 kWh/year. Building 6: Fire station with electrical deman	d 23,584 kWh. Building
7: 29,437 kWh/year	93
Figure 3-7: Data Input for Formentera case study	94
Figure 3-8: Endesa Grid Tariff structure adopted from [120]	95
Figure 3-9: Winter Operational Dynamics for Load Following (a), HO	MER - Load Following
(b), and GA-Yealy Horizon (c). The positive values for hydrogen repres	sent the fuel cell output

in kW, and the negative values indicate electrolyser consumption. For the battery, positive
values indicate discharge, and negative values indicate charging. Grid interactions show
positive values for electricity purchases and negative values for sales104
Figure 3-10: Summer Operational Dynamics for Load Following (a), HOMER - Load Following
(b), and GA-Yealy Horizon (c). The positive values for hydrogen represent the fuel cell output
in kW, and the negative values indicate electrolyser consumption. For the battery, positive
values indicate discharge, and negative values indicate charging. Grid interactions show
positive values for electricity purchases and negative values for sales105
Figure 3-11: Breakdown of Net Present Costs and Annualized Expenditures. a) Total system
costs by category, (b) GA-Load Following cost distribution, (c) HOMER-Load Following cost
distribution, (d) Annualized costs by component across all strategies
Figure 3-12: Benchmarking Methods Monthly Escalated Grid-Related Financial Performance.
a) Monthly energy revenue from grid sales, (b) Monthly grid-related costs, including power
purchases and fixed charges across GA-Yearly Horizon, GA-Load Following, and HOMER-
Load Following
Figure 3-13: Cumulative Discounted Cash Flow Over a 25-Year Horizon for Different Energy
Management111
Figure 4-1: Proposed Novel GA-MILP-MPC Flexible Load Methodological for two layers Grid
Time of Use driven Optimisation approach
Figure 4-2: Winter Operational Dynamics for MPC rolling horizon with 0% flexibility (a), 4%
flexibility (b), 6% flexibility (c), and 8% flexibility (d). The positive values for hydrogen represent
the fuel cell output in kW, and the negative values indicate electrolyser consumption. For the
battery, positive values indicate discharge, and negative values indicate charging. Grid
interactions show positive values for electricity purchases and negative values for sales. 125
Figure 4-3: Summar Operational Dynamics for MPC rolling horizon with 0% flexibility (a), 4%
flexibility (b), 6% flexibility (c), and 8% flexibility (d). The positive values for hydrogen represent
the fuel cell output in kW, and the negative values indicate electrolyser consumption. For the
battery, positive values indicate discharge, and negative values indicate charging. Grid
interactions show positive values for electricity purchases and negative values for sales. 127
Figure 4-4: Hourly load profiles and pricing dynamics for MPC 8% flexible operation across
four representative days: (a) 5 <sup>th</sup> January 2022 and (b) 12 <sup>th</sup> January 2022, representing winter
days with low PV availability, whereas (c) 20 <sup>th</sup> July 2022 and (d) 21 <sup>st</sup> July 2022, reflecting
summer days with abundant solar energy. Shaded regions indicate load shifts (green:
increase, blue: decrease), highlighting MPC's adaptive strategy to minimize energy costs by
aligning demand with low-tariff hours and PV generation windows. Dual-axis plots show both
power demand (left y-axis) and electricity prices (right y-axis)

Figure 4-5: Breakdown of Net Present Costs for the total system costs by category for MPC rolling horizon with 0% flexibility (a), 4% flexibility (b), 6% flexibility (c), and 8% flexibility (d)
Figure 4-6: Monthly breakdown of grid escalated charges and revenues for MPC rolling horizon with 0% flexibility (a), 4% flexibility (b), 6% flexibility (c), and 8% flexibility (d) 135 Figure 4-7: Discounted Cashflow for the GA-MPC approach with different flexibility scenarios
Figure 4-8: The influence of solver parameter tunning in Gurobi MIPFocus parameter 139
Figure 4-9: The Influence of MILPGap on accuracy and convergence speed
Figure 4-10: Convergence plots for different mutation and crossover mutation 140
Figure 4-11: Interaction plot of final fitness versus crossover probability for different mutation rates (μ)
Figure 5-1: Normalised measured hourly data for whole year days and their average values for energy generation, prices and consumption
Figure 5-2: Energy flow comparison between (A) a simple grid-connected system with single
storage and (B) a hybrid energy community with multiple storage paths and direct load consumption, highlighting the need for an extended EROI metric
Figure 5-3: Two-stage methodological framework for applying the derived EROI-community
metric. Step A (left) conducts parametric sensitivity analysis using fixed, optimised system
capacities while varying key technical parameters, efficiency, durability, and embodied energy
Step B (right) applies uniform scaling to system capacities to assess the impact of system size
on performance. Both steps use rolling-horizon MILP dispatch to extract operational metrics
which are then used to compute and analyse the life cycle EROI and associated sustainability indicators
Figure 5-4: Sensitivity of system EROI and storage ESOI to variations in round-trip efficiency
The four subplots show that battery efficiency ( $R^2 = 0.99$ for EROI and 1.00 for ESOI) has a
stronger impact than hydrogen efficiency (R² = 0.33 for EROI and 0.85 for ESOI), with each point coloured by NPC.
Figure 5-5: Sensitivity of system-level EROI and component-specific ESOI to variations in
component durability (battery, fuel cell, electrolyser). Data points are coloured according to ne
present cost (NPC), illustrating economic impacts associated with differing durability levels
Figure 5-6: Sensitivity of system-level EROI and storage-specific ESOI to variations in
embodied energy intensity for PV, battery, and hydrogen storage components. Points are
coloured by the corresponding system-level EROI, illustrating how manufacturing energy
inputs influence overall energy life-cycle metrics

Figure 5-7: Surrogate model accuracy shown via predicted vs. actual plots for NPC, EROI,
Unmet, and Excess energy (10-fold cross-validation)
Figure 5-8: System EROI and NPC across PV and battery scales, overlaid with unmet and
excess energy contours (MWh/year), highlighting trade-offs between cost, sustainability, and
energy utilisation
Figure 5-9: System EROI and NPC across PV and hydrogen tank capacity scales, overlaid
with unmet and excess energy contours (MWh/year), illustrating the diffuse trade-offs between
cost, sustainability, and renewable energy utilisation in hydrogen-based storage
configurations
Figure 5-10: Capacity scaling analysis of PV and fuel cell systems showing trade-offs between
system EROI and NPC
Figure 5-11: Capacity scaling analysis of PV-electrolyser systems, illustrating trade-offs
between economic cost and energy sustainability
Figure 5-12: Battery and hydrogen tank capacity scaling analysis showing four performance
regions that capture the trade-offs between system-level EROI and NPC 168
Figure 5-13: Battery-Fuel Cell capacity scaling delineates four distinct regions of trade-off
between lifecycle energy efficiency (EROI) and economic cost (NPC), underscoring the
importance of balanced storage sizing for sustainable hybrid systems
Figure 5-14: Battery-Electrolyser capacity scaling analysis showing how moderate storage
configurations yield optimal trade-offs between system-level EROI and NPC 170
Figure 5-15: Tank and fuel cell scaling reveals optimal cost-sustainability trade-offs near
baseline configurations, with under sizing or oversizing degrading performance 171
Figure 5-16: System EROI and NPC response to hydrogen tank and electrolyser capacity
scaling, highlighting cost-optimal and energy-efficient regions
Figure 5-17: Balanced fuel cell and electrolyser scaling yields optimal cost-efficiency trade-
offs; extreme sizing degrades performance
Figure 6-1: Comparison of solar-to-inverter (SIR), battery-to-inverter (BIR), and
tank-to-inverter (TIR) sizing ratios for the Load-Following baseline and MPC strategies with 0
%, 4 %, 6 %, and 8 % load-shifting
Figure 6-2: Annual hourly PV generation (yellow), theoretical AC (blue), and actual AC (red)
outputs, together with average battery (dashed blue) and hydrogen tank (dashed green) SoC,
for (a) Load-Following with a 120 kW inverter (Battery $\approx$ 46 %, H <sub>2</sub> $\approx$ 23 %), (b) MPC 0 % with
a 77 kW inverter (Battery $\approx$ 33 %, $H_{2}$ $\approx$ 55 %), and (c) MPC 8 % with a 72 kW inverter and 8 %
load shifting (Battery $\approx$ 34 %, H <sub>2</sub> $\approx$ 51 %)

Figure 6-3: Contracted-power ratios (SPR, BPR, TPR) for Load-Following vs. MF	'C (0–8 %);
MPC greatly boosts storage versus grid capacity, enabling higher PV capture an	d seasonal
balancing.	180
Figure 6-4: PV vs. grid import/export for Load-Following ( $\pm78$ kW) and MPC 8 $\%$	(±37 kW):
MPC achieves import-free operation 86 $\%$ of hours and uses storage discharge	at zero PV,
flattening grid exchanges.	181
Figure 6-5: Annual dynamics of Battery SoC and Hydrogen LoH for (a) Load Follow	ing and (b)
MPC 8%. Each subplot shows hourly values (faded), daily means, and 30-	day rolling
averages. MPC 8% maintains the battery at a lower SoC set point with red	luced daily
fluctuation while using hydrogen for long-term seasonal storage, in contrast to Loa	d Following
which underutilises hydrogen and experiences frequent battery saturation	182
Figure 6-6: Interactive Cost-EROI dashboard. Baseline optimal mix with ability	to compare
different equipment sizes	185
Figure 6-7: Interactive Cost–EROI dashboard, PV-heavy what-if scenario	186
Figure 9-1: Chromosome layout for capacity sizing showing the decision val	riables: PV
capacity, number of battery units, inverter rating, contracted grid limit, fuel	cell power,
electrolyser power, and hydrogen tank capacity. The bounds of each variable ar	e indicated
below the corresponding gene.	204
Figure 9-2: DEAP initialisation of decision variables	204
Figure 9-3: Population size setup in DEAP framework	205
Figure 9-4: DEAP setup for the NPC fitness function	205
Figure 9-5: Tournament setup for the DEAP library	206
Figure 9-6: Crossover method selection and setup range of offsprings	207
Figure 9-7: Mutation method selection and setup on DEAP	207
Figure 9-8: Pulp initialisation of the problem	208
Figure 9-9: Objective problem method of implementation	209
Figure 9-10: Grid Constraint method of application	210
Figure 9-11: Focused snippet Between Process 1-3	211
Figure 9-12: Focused snippet Process 4 and its two main decisions 4.1 and 4.2 $\dots$	212
Figure 9-13: Focused on Decision Branches from 4.1 to 4.1.4	212
Figure 9-14: Focused on Decision Branch es from 4.1.8 to 4.1.12	214
Figure 9-15: Focused on Decision Branch es from 4.1.4 to 4.1.8	214
Figure 9-16: Focused on Decision Branches from 4.2 to 4.2.4	215
Figure 9-17: Focused on Decision Branches from 4.2.4 to 4.2.8	216
Figure 9-18: Focused on Decision Branch es from 4.2.8 to 4.2.12	216
Figure 9-19: Focused on Decision Branch es from 5. to 5.2.1 and 5. To 5.1	217

# **List of Tables**

Table 2-1: Optimisation Methods for HRES Sizing with Objective Functions adapted from [84],
[85]42
Table 2-2: Summary of recent studies on grid-connected PV-battery-hydrogen systems,
highlighting key components (BT: Battery, HR: Hydrogen, GR: Grid, WT: Wind, PV:
Photovoltaic, INV: Inverter), methodologies, and limitations
Table 2-3: Detailed MILP comparative summary of these studies, including their energy
balance formulations, bus structures, decision variables, and key findings (refer to appendix
9.1 for energy balance nomenclature)
Table 2-4: Overview of recent nested optimisation studies combining heuristic sizing (e.g., GA,
GWO) with short-horizon MILP dispatch for hybrid renewable energy systems (HRES).
System architectures are denoted using the following component codes: PV - photovoltaic
panels, WT - wind turbines, BT - battery storage, FC - fuel cells, EL - electrolysers, TK -
$hydrogen\ storage\ tanks,\ IN-inverters\ or\ power\ electronics,\ GR-grid\ interface,\ OR-other and other and othe$
components such as heat pumps or thermal storage. Each study is assessed for control
structure, optimisation layers, component integration, and major limitations 54
Table 2-5: Summary of key studies assessing life-cycle energy performance in hybrid
renewable systems, highlighting EROI, ESOI, and curtailment-related outcomes across
scales. Abbreviations: Li-ion = Lithium-ion Battery, PHS = Pumped Hydro Storage, CAES =
Compressed Air Energy Storage, RHFC = Regenerative Hydrogen Fuel Cell, PtG = Power-to-
Gas, EROI = Energy Return on Investment, ESOI = Energy Stored on Energy Invested, VRE
= Variable Renewable Energy 65
Table 3-1: Key Operational Assumptions and Regulatory References for REC Model 75
Table 3-2: Key design and standard parameters employed in the PV output and cell
temperature modelling
Table 3-3: Sensitivity sweep for penalty selection across 21 edge-case designs 84
Table 3-4: Technical and Economic Data Inputs for the Modelling
Table 3-5: Financial Parameters Used in Economic Assessment
Table 3-6: Comparison of the sizing outcomes for the three Benchmarking methods99
Table 3-7: Performance metrics for benchmarking methods
Table 3-8: Key Financial Metrics of Benchmarking Approaches
Table 4-1:Flexible Load: Water Pump Specifications for the Formentera Energy Community
Table 4-2 : Scenarios defined for the flexibility investigation
Table 4-3: GA-MPC novel approach capacity sizing results
Table 4-4 Performance metrics comparison for MPC approach with different flexibility % 124

Table 4-5 Year-1 grid-trading cash-flow by scenario, separating export revenue from import
costs and reporting net grid cash-flow and avoided import cost (Grid-Only - scenario) 131
Table 5-1: Comparison of life-cycle energy-return metrics and their suitability for community
hybrid systems
Table 5-2: Sample Parameter Ranges for Efficiency, Durability, and Embodied Energy
Sensitivity Studies
Table 5-3: Illustrative Capacity Variations Relative to the MPC-4% Baseline
Table 6-1: Sensitivity Analysis of System Components under External Variations (MPC-4%
selected)
Table 6-2: Comparison of optimisation studies, showing grid/island context, cost reductions ( $\Delta$
NPC, $\Delta$ LCOE) against each paper's benchmark, and which advanced features are
implemented; shortcuts: GS = meta-heuristic sizing, DO = Dispatch Optimisation, RH = rolling-
horizon/MPC, SH = static-hourly assumption, LS = load-shifting, CG = contracted-grid
optimisation, IC = inverter-capacity optimisation, AD = detailed AC/DC buses, TO = time-of-
use tariffs, PS = peak-shaving
Table 9-1: Type of variables and with pulp syntax example

# 1 Introduction

#### 1.1 Motivation

Global energy demand is projected to rise in the coming years, driven by factors such as urbanisation, increased access to electricity, and population growth. The 2023 COP28 summit marked a pivotal moment in climate policy, with commitments to triple renewable energy capacity by 2030 and accelerate the transition away from fossil fuels. Although the summit marked the "beginning of the end of the fossil fuel era," it also confirmed that the earth is not on track to keep global warming to 1.5 °C [1]. The IPCC projects two scenarios where appropriate climate action will reduce emissions by 2050. Figure 1-1 displays the historical carbon dioxide emissions and the projected two scenarios' ranges [2], [3], [4]. Researchers quantified energy system changes between the different IPCC scenarios and explored different metrics to identify whether global efforts were on track [5]. They concluded that the world must likely deepen the decarbonisation of energy systems to limit temperature change below 2°C.

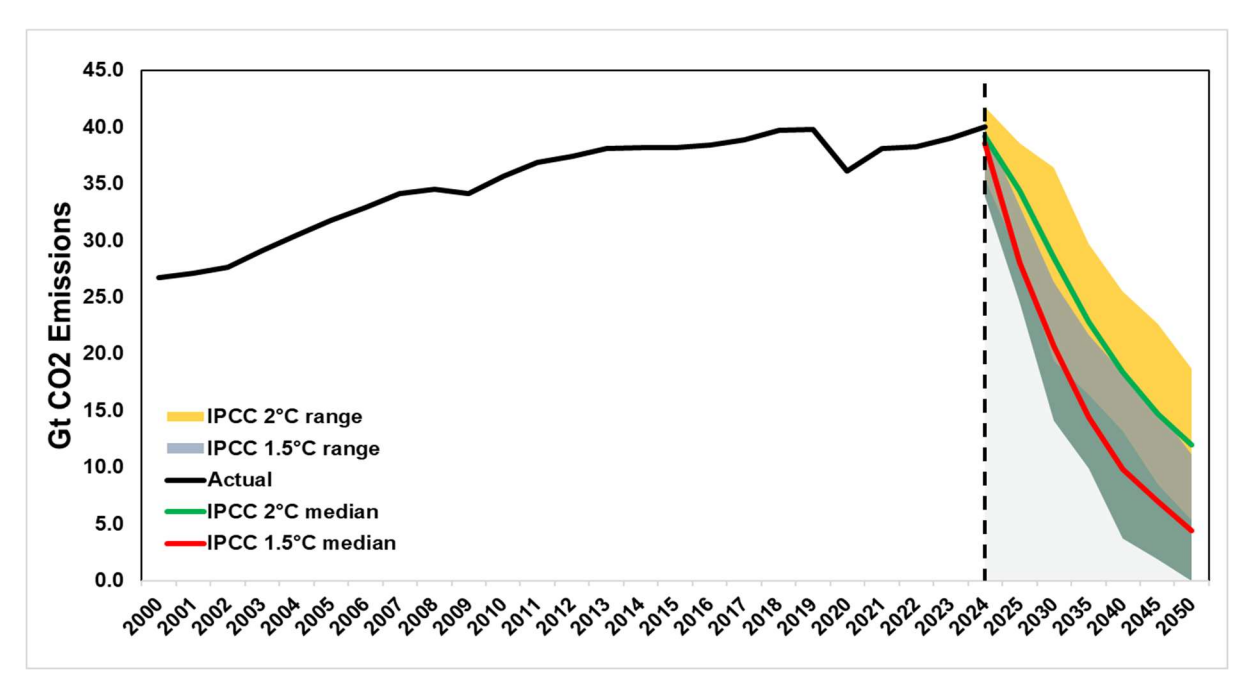


Figure 1-1: Most recent carbon emissions world total (2024) with the 2 and 1.5 degrees IPCC scenarios [2], [3], [4]

The scientific community has emphasised the urgent need for accelerated mitigation efforts to prevent severe climate impacts, driven by rising atmospheric concentrations of key greenhouse gases such as carbon dioxide (CO<sub>2</sub>), methane (CH<sub>4</sub>), and nitrous oxide (N<sub>2</sub>O), which are the principal contributors to global warming. Figure 1-2 presents the past global energy consumption by type of fuel in EJ, as well as the carbon dioxide emissions in MTCO<sub>2</sub> [6]. Over the past thirty years, global energy demand has increased by 76%, accompanied by a 64% rise in greenhouse gas emissions. In 2020, the COVID-19 pandemic led to a temporary decline, with energy consumption falling by 3.5% and emissions decreasing by 5.1%, the most significant drop since 1965. However, by 2021 and 2022, emissions had rebounded sharply, reaching their highest recorded levels, thereby underscoring the urgency for accelerated climate action.

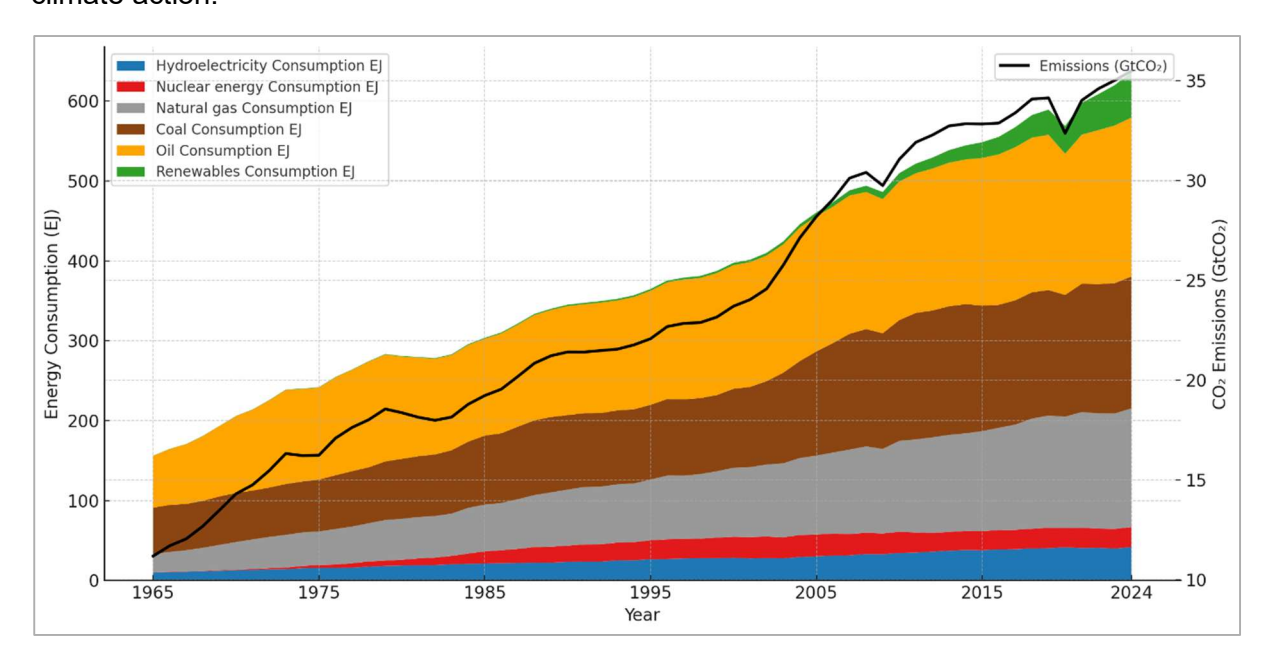


Figure 1-2: The historical energy consumption by source in EJ and GTCO2 emissions [6].

Driven by population increase and economic development, worldwide energy consumption is rising; hence, the construction industry ranks as one of the primary causes of greenhouse emissions. About 26% of world emissions and 30% of world energy consumption come from building sector activities [7]. In the EU, buildings are responsible for approximately 40% of energy consumption and 36% of total greenhouse gas emissions, making the sector a key focus of the EU's strategy to achieve carbon neutrality by 2050, as outlined in the European Green Deal and the 2024 Energy Performance of Buildings Directive [8], [9].

The electricity consumption in the EU remains high, notably in the building sector, despite the growing commitment to renewable energy. With renewable energy accounting for 38.2% of the EU's 2,824 TWh gross electricity generation in 2022, nuclear power and gas-fired plants were second followed by [10]. The consumption of this electricity is distributed among

households, services, and industry, with households alone accounting for approximately 25% of the total consumption [11]. In residential buildings, electricity demand is primarily driven by lighting and electrical appliances, which account for approximately 15% and 85% of total residential electricity use, respectively [12]. However, in colder regions such as the UK, space and water heating, often powered by gas or electricity, represent a substantial portion of overall residential energy use [13]. This underscores the importance of adopting energy-efficient appliances, improved heating systems such as heat pumps, and advanced control technologies to manage and optimise residential energy consumption.

Many EU nations still struggle to reduce their dependency on fossil fuels for power generation, despite attempts to decarbonise the energy supply [14]. The high energy consumption patterns in the EU building sector highlight the urgent need for the integration of smart energy systems into residential and commercial infrastructure. This need becomes even more critical in geographically isolated regions, such as island communities, where limited energy infrastructure and reliance on imported fossil fuels heighten their energy insecurity and make them especially vulnerable to the impacts of global warming [15], [16]. Rising sea levels, catastrophic weather events, and increasing energy prices resulting from their isolation make islands front lines of climate change [17]. Their particular weaknesses draw attention to the need for transformative energy solutions and resilience-building initiatives.

About 4% of the total EU population resides on these islands, which house nearly 16 million people living on almost 2,200 inhabited islands spread over Europe alone [18]. Due in great part to the logistical challenges of fuel delivery and maintenance of the energy infrastructure, energy production on these islands can be up to ten times pricier than on the mainland [18]. This dependence on imported fuels also makes island people more sensitive to price fluctuations and supply disruptions [19].

Seasonal population fluctuations, mostly related to tourism, cause considerable variations in energy demand patterns on many islands depending on non-islanders' consumption practices [20]. These variations, especially in cooling, lighting, and other basic services, place additional pressure on already fragile infrastructure during high travel seasons. Infrastructure stress on islands is driven not only by tourism-related demand surges but also by persistent structural challenges, such as the integration of intermittent renewable sources, the maintenance of stable grid operations, and the logistical difficulties inherent to remote locations [21], [22]. Although islands play a strategic role in the global transition to clean energy, they often receive inadequate investment in essential energy infrastructure. Efforts to scale up smart technologies and energy storage systems are frequently constrained by outdated grid networks, a shortage of technical expertise, and limited access to financial resources [23].

Tackling these challenges requires comprehensive energy planning that integrates advanced system management, flexible demand-side responses, and robust storage capacity to ensure long-term efficiency, reliability, and sustainability [24].

# 1.2 The Role of Regenerative Hydrogen Storage in Community Energy System Decarbonisation

Hydrogen is a versatile energy carrier that may be converted into electricity, utilised as a transportation fuel, heated and cooled, and employed in various other industrial uses. Hydrogen is expected to play a key role in the future design of energy systems as part of efforts to achieve green energy independence and enhance energy security [25]. Hydrogen energy is increasingly being explored as a potential storable fuel and energy carrier, particularly for long-duration or seasonal energy storage applications. Batteries offer high efficiency and fast response and are well-suited for short-term grid stabilisation. However, hydrogen storage may be more viable for extended durations and applications requiring very low self-discharge or versatility across sectors [26]. Unlike batteries, which are limited by shorter discharge durations, hydrogen can be scaled to meet multi-day energy demands, making it especially valuable for deep decarbonisation of power systems with high renewable penetration [27]. Hydrogen production is expected to double in the next eight years to fulfil the IEA's Net-Zero scenario [28]. Figure 1-3 depicts the predicted global demand for hydrogen by production technology between 2020 and 2030. Electrolysis from renewable sources is expected to provide the most hydrogen (80 Mt).

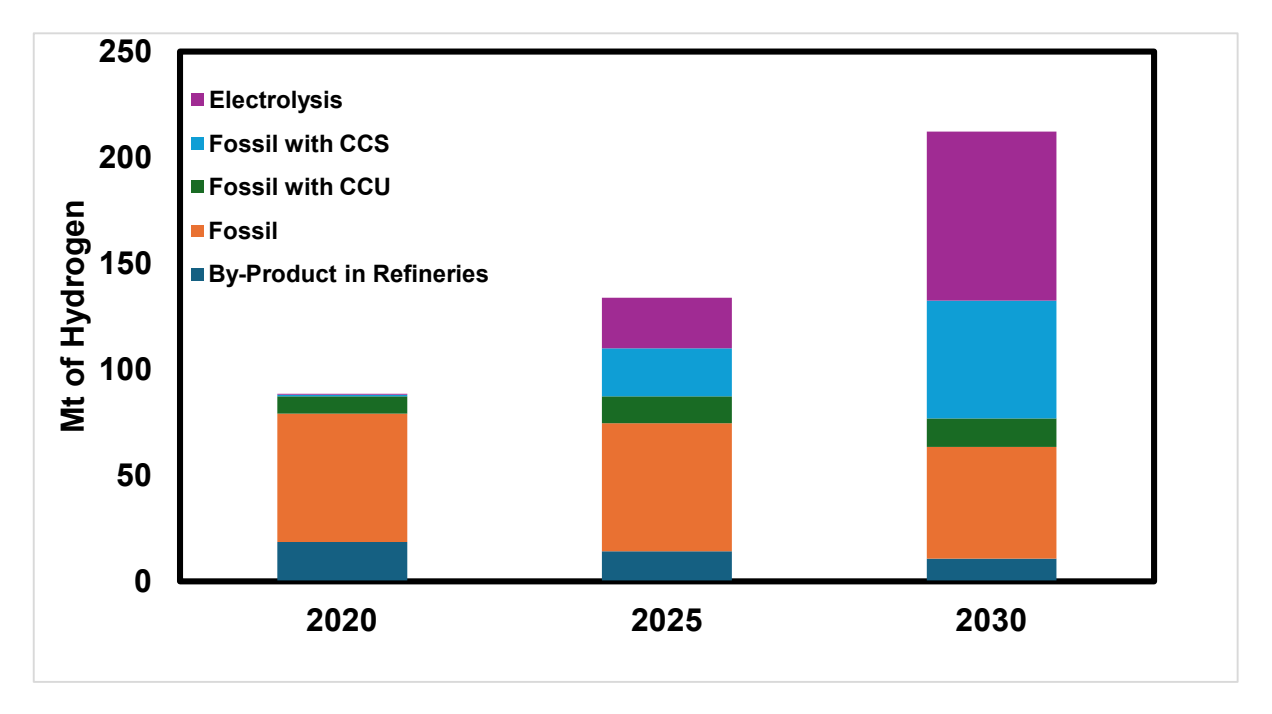


Figure 1-3: IEA Global hydrogen demand by production technology in the Net Zero Scenario, 2020-2030 [27].

Colours are used to refer to different ways of producing hydrogen to couple the production technology with the carbon footprint of hydrogen production [29]. Figure 1-4 depicts hydrogen production, use and storage pathways. Black and brown-coloured hydrogen is produced with high carbon emissions from coal and lignite through partial oxidation technologies such as gasification. Grey and blue-tagged hydrogen are produced through steam methane reforming at pressure up to 25 bar and a high temperature ranging from 700-1000 °C [30]. The difference between Grey and Blue is that the latest is produced from fossil fuels with less CO<sub>2</sub> emission using carbon capture utilisation and storage. The carbon emissions of steam-reforming methane sourced from natural gas are less than coal and lignite. The least impact hydrogen is produced from renewable electricity. Electrolysis uses electricity and water to produce hydrogen. It is important to mention that the environmental impact of these hydrogen production ways can vary depending on the energy source, country, and type of carbon capture technology deployed. The largest consumption segment of hydrogen is expected to be mobility, industrial uses for heating and feedstock, accounting for around 90 % of the demand by 2050 [31]. Increasing the share of renewable energy generation is expected to play a central role in future decarbonisation efforts. However, the intermittent nature of sources like solar and wind power necessitates both short- and long-duration energy balancing solutions within the system. Hydrogen plays a vital role in decarbonising the electrical demand since it can offer long-duration and seasonal storage and peak shaving, which will be essential for grid stabilisation.

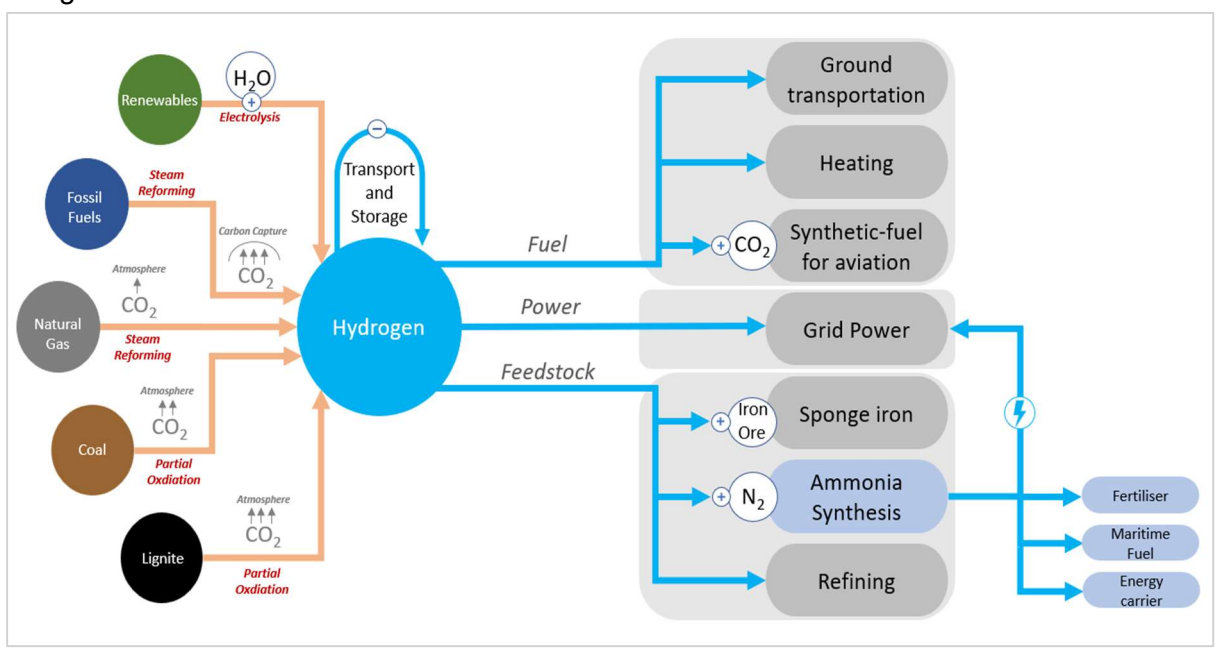


Figure 1-4: Hydrogen Production, consumption and transport pathways

Energy storage systems can provide different services to local stabilisation and management of grid use depending on the application timescale. For instance, frequency and voltage control require rapid response within milliseconds and up to seconds. By contrast, applications such as peak shaving and seasonal storage operate on much longer timescales, ranging from several hours to multiple months [32]. Hydrogen and battery storage systems are particularly suited for grid stabilisation and short- to long-term storage applications [33], [34]. It has been shown that if combined, they will provide higher reliability and lower cost than both technologies standing alone for specific applications [35]. Batteries are preferred for short-term storage, while hydrogen storage systems are better for seasonal ones, as shown in Figure 1-5 [36].

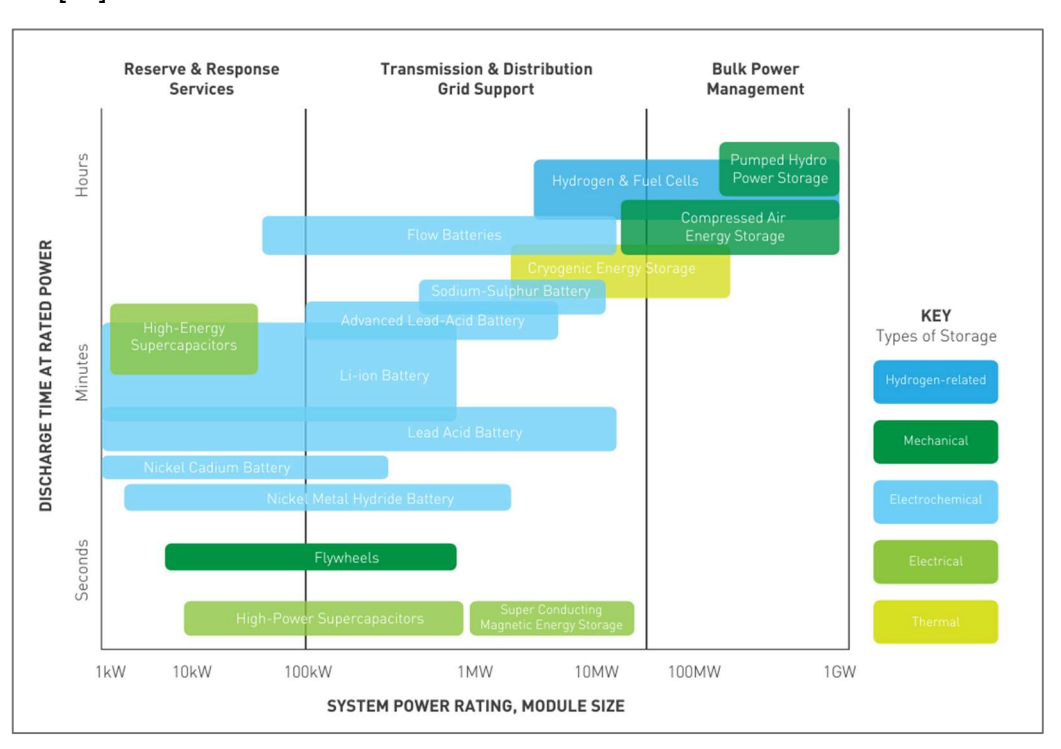


Figure 1-5: Comparison of ESS in terms of storage capacity, discharge duration, and services provided [34].

Hydrogen as energy carrier in regenerative hydrogen fuel cell systems, can be an answer to smart grids' long-term storage dilemma since it can complement batteries. A typical regenerative hydrogen integrated for grid support consists of an electrolyser, hydrogen storage and a fuel cell. Electrolysis transforms surplus electricity to hydrogen, which is then stored and used in fuel cells to produce power, therefore balancing supply and demand and helping system stability [37]. Including hydrogen and battery storage into energy systems, however, adds considerable complexity, especially in terms of system configuration and operational control. Ensuring that these hybrid systems function reliably, efficiently, and cost-effectively depends on their optimised sizing and operational strategies. A wide range of methods, from traditional computational approaches to advanced metaheuristic algorithms, have been explored to address these optimisation challenges. Chapter 2 of this thesis reviews

these methods in detail, summarises their limitations, and highlights the need for a more integrated, hybrid optimisation approach, justifying the novel framework introduced in this chapter. Before advancing to the optimisation methodology, it is important to first delineate the target community energy system configuration, the role of aggregators, and the functional scope of energy actors involved.

In this study, a community energy system refers to a decentralised, geographically defined energy network where local actors collectively generate, consume, and manage energy, often using distributed renewable sources, with shared economic and social benefits [38]. These systems may be governed by community members, local authorities, or cooperative entities, and are designed to support decarbonisation, enhance local resilience, and advance energy justice [39], [40]. The focused area in this research targets a community-sized deployment (e.g. a small island or town) comprising distributed PV, hydrogen, and battery storage under aggregated energy management, aligning with academic definitions and recent European implementations [41]. A virtual trading layer is assumed to allocate shared energy among members, prioritising smaller loads, a flexible model adaptable to RED(III) REC policies. While this logic is not location-specific, it provides a flexible baseline that can be adapted to different REC governance policies [42].

Establishing these structural and governance parameters is fundamental to ensuring that the subsequent modelling and optimisation strategies reflect both operational feasibility and policy-aligned implementation. Numerous studies have investigated the optimisation of hybrid renewable energy systems that combine hydrogen and battery storage, particularly through classical methods such as MILP for component sizing and cost evaluation in off-grid or partially connected environments [43], [44]. Metaheuristic and hybrid optimisation approaches, such as PSO, GA, and their variants, have also been widely applied to tackle design complexity under uncertainty [45], [46], [47]. While these methods represent notable advancements, much of the existing research remains grounded in idealised planning scenarios, frequently neglecting the practical challenges of system integration and day-to-day operations and operational behaviour. This highlights the ongoing need for more unified frameworks, ones that can bridge between architecture and operation, especially under the nuanced constraints typical of distributed, community-scale energy systems.

Optimising the design and operation of hybrid energy storage systems that incorporate both hydrogen and battery technologies requires innovative optimisation strategies, ones that thoughtfully combine the strengths of classical and metaheuristic approaches. Enhancing these methods can significantly support the effective integration of hybrid storage into smart grids, contributing to improved system reliability, cost-effectiveness, and long-term

sustainability. Nevertheless, many existing approaches struggle to reconcile the complexity of real-world operations with economic and environmental constraints. With a particular focus on energy communities and grid-connected applications, this study introduces a new optimisation framework aimed at advancing the integration of PV-battery-hydrogen systems under practical, scalable conditions.

## 1.3 Research Aim and Objectives.

Integrating hybrid energy storage systems, such as photovoltaic (PV), battery, and hydrogen fuel cell configurations, into grid-connected energy systems is becoming more and more important as the global effort for decarbonisation accelerates. Recent developments are making these hybrid systems more appealing for energy communities trying to combine renewable energy integration with grid stability, even if cost and technical constraints prevent their broad deployment now. Optimising their design and operation is crucial to guarantee that these systems are both sustainable and reasonably affordable.

The aim of this research is to develop a novel optimisation approach for energy community to find the optimal design parameters for the hybrid PV- regenerative fuel cell-battery storage based on grid driven unit commitment energy management.

#### **Objectives:**

#### O1. To Develop Novel Energy Optimisation Technique:

The first objective is to develop a layered optimisation approach combining yearly-horizon mixed-integer linear programming (MILP) with genetic algorithms (GA) for capacity sizing. Focusing on PV-battery-hydrogen storage, this hybrid system will combine grid-driven unit commitment. This method co-optimises inverter rating, contracted grid power and time-of-use tariffs while meeting hourly energy balance constraints. Validation versus HOMER Pro confirms techno-economic gains.

#### O2. To incorporate MPC and Flexible Load Optimisation:

Building on the first optimisation, the second objective is to introduce novel flexible loads capabilities by including a model predictive control (MPC) layer. This layer will employ MILP to improve operational optimisation for time-of- usage energy management. By integrating a short-horizon MPC layer with flexible load shifting and peak shaving, this objective aims to improve short-term reliability and minimise curtailment.

#### O3. Develop a New Environmental Performance Metric

Building on objective 1 and 2, this objective focuses on developing novel dynamic, operationally coupled Energy Return on Investment and Energy Stored on Invested (EROI/ESOI) index that evaluates energy pay-back under the GA-MILP-MPC schedule, capturing AC/DC losses, curtailment and multi-path storage flows. This novel index will combine environmental and financial performance indicators to provide holistic measure for evaluating hybrid PV-battery-hydrogen systems. It will provide a balanced view reflecting environmental sustainability as well as financial viability as interactive visualisation for energy communities.

## 1.4 Principal Research Contributions

- 1. A GA–MILP sizing framework that jointly optimises PV, battery, electrolyser, fuel-cell capacities in conjunction with inverter rating and contracted grid power against realistic time-of-use tariffs.
- 2. A two-stage unit-commitment and MPC dispatch architecture that incorporates flexible-load shifting and AC/DC hybrid balancing, delivering peak-demand shaving and seasonal-storage synergy.
- 3. A dynamic life-cycle energy metric (EROI/ESOI) explicitly linked to the rolling dispatch, enabling planners to weigh energy sustainability against cost in community-scale hybrid renewable energy systems (HRES).
- 4. Demonstration on the Formentera Island energy community, evidencing cost, and energy-return improvements relative to conventional rule-based or single-layer methods.

#### 1.5 Thesis Structure

This thesis is organised into seven main chapters, each building upon the previous to develop and evaluate a comprehensive optimisation framework for hybrid PV-battery-hydrogen systems in community-based applications. The structure is designed to guide the reader from conceptual foundations through methodological development, system implementation, and comparative performance analysis as shown in Figure 1-6:

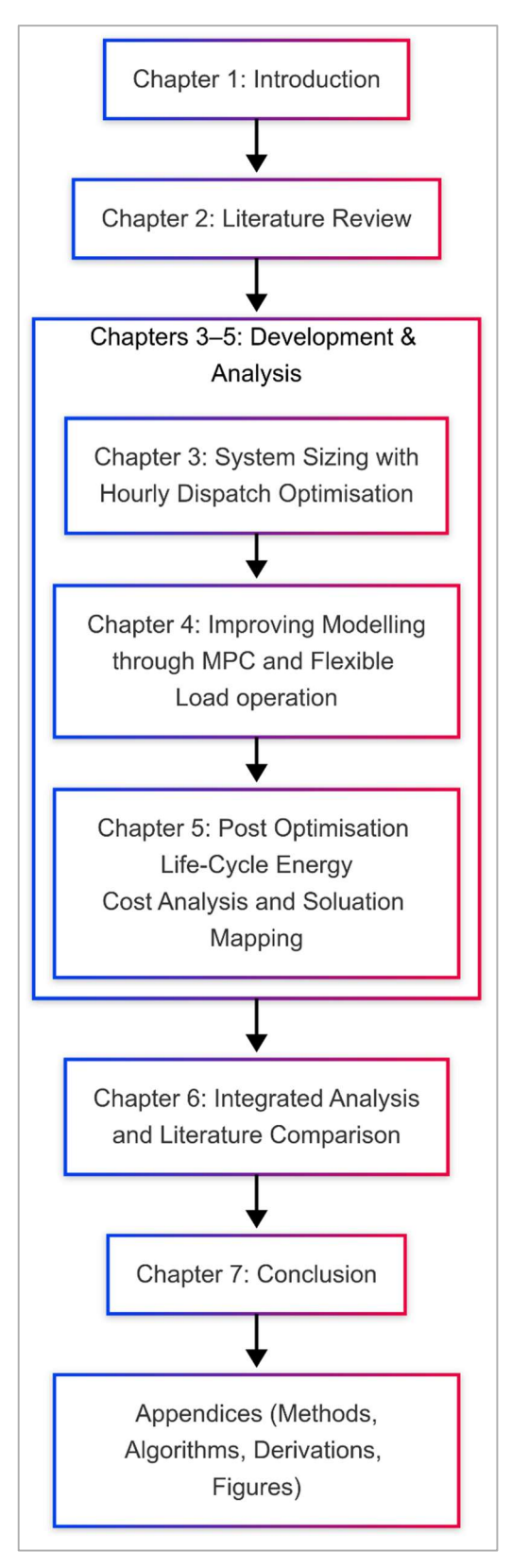


Figure 1-6: Flow of information and chapter dependencies throughout the thesis

- Chapter 1: Introduction outlines the motivation for the research, defines the central aim and objectives, and introduces the core contributions of the study within the broader context of renewable energy and decarbonisation strategies.
- Chapter 2: Literature Review critically evaluates existing work across hybrid energy systems, optimisation techniques, and life-cycle energy assessment. It identifies specific methodological limitations in current approaches, especially those related to inverter treatment, hybrid dispatch, and sustainability metrics.
- Chapter 3: System Sizing with Hourly Dispatch Optimisation presents the initial GA-MILP framework used to co-optimise component capacities and dispatch logic under grid tariff constraints. Comparative simulations and baseline results are discussed.
- Chapter 4: Improving Accuracy through MPC and Flexible Load Operation
  introduces the rolling-horizon Model Predictive Control (MPC) layer, incorporating
  flexible loads to refine operational realism. The chapter contrasts sizing outcomes and
  dispatch performance with static control methods.
- Chapter 5: Life-Cycle Energy Cost Analysis develops a novel EROI-based metric
  for hybrid systems, capturing multi-path energy flow and embodied energy
  contributions. The new index is applied to conduct parametric sensitivity and capacity
  scaling analyses, enabling deeper understanding of design and performance tradeoffs.
- Chapter 6: Integrated Analysis and Literature Comparison synthesises the results from Chapters 3–5, analysing how system sizing, control, and energy return interact. The proposed method is benchmarked against key peer-reviewed studies and tested under scenario uncertainty to assess its robustness and planning relevance.
- Chapter 7: Conclusion summarises the research findings, highlights the original contributions, and outlines limitations and potential directions for future work.

The thesis is supported by detailed appendices, including implementation notes, algorithm descriptions, extended derivations, and additional figures that complement the main discussion.

## 1.6 List of Publications

- Abualshawareb, A., Dehouche, Z. (2024). Economic and Environmental Analysis of a Hybrid Energy Storage System for an Energy Community on the Renewable Energy. ICEER 2023. Environmental Science and Engineering. Springer, Cham. https://doi.org/10.1007/978-3-031-54394-4 32
- 2. Abualshawareb, A. & Pisica, I. (2024). Modelling of hydrogen-enabled port energy systems. Presented at the 22nd Intelligent Systems Applications to Power Systems (ISAP) Conference, Budapest, Hungary.
- 4. Abualshawareb, A. & Pisica, I. Optimising Hybrid Renewable Energy Systems: A Review of Grid-Constrained Sizing, Dispatch, and Life-Cycle Energy Metrics for Island Communities Microgrids (Under Review).
- Abualshawareb, A. & Pisica, I. (2024). System Sizing of Hybrid Renewable Systems
   Under Inverter and Contracted Grid Power Constraints with Flexible Load Integration.
   60th International Universities Power Engineering Conference (UPEC) Conference,
   London, UK (Under Review).

## 2 Literature Review

#### 2.1 Introduction

#### 2.1.1 Review Scope and Research Relevance

The deployment of HRES, typically integrating renewable sources such as PV panels with battery and hydrogen-based energy storage system, has been introduced to address the challenges faces by climate change and the increased reliance on fossil fuels [48]. The hybridisation between two storage technologies is often used to balance between cost and environmental burden when compared individually [49]. These systems offer significant potential for enhancing grid reliability, reducing intermittent renewable generation, particularly for isolated communities and island-based microgrids that face unique operational and technical constraints [50], [51].

Despite the various advantages of HRES, their effective implementation remains technically challenging, particularly in the context of accurately sizing system components and ensuring optimal operational management and realistic integration [52]. Conventional sizing methodologies often overlook critical infrastructure limitations in accurately modelling the contracted grid-power constraints or the power type (AC/DC) interactions and constraints in the planning and operational methods [53]. Similarly, attempts at reducing strain on the grid by introducing demand side management such as load shifting are not explored enough in a planning context since the existing operational control strategies frequently rely on rule-based, static dispatching strategies that limit the adoptability of flexible loads, thereby reducing their practical relevance [47], [54].

Parallel to these operational and sizing challenges, the assessment of HRES is often conducted using traditional targeted metrics such as life cycle cost, environmental indicators, or technical performance measures. Energy life cycle indices are metrics used to evaluate the efficiency and sustainability of energy systems. The Energy Return on Investment (EROI) and Energy Stored on Invested (ESOI) are established metrics on large grid scale but remain limited when applied to HRES with community-based applications that involve multiple interacting storage pathways with diverse operational scenarios [55]. They typically do not fully capture the complexity and interactive nature between the hybrid storage systems, necessitating the development of new methodologies that better evolve with the current hybrid storage community-based taxonomy.

Therefore, the main motivation of this literature review chapter is to critically analyse and study the current body of knowledge on the sizing and operational management of HRES, together with evaluation techniques that measure their life-cycle energy performance. Thus, the scope of the literature review specifically covers two interconnected areas: the sizing and optimisation approaches for HRES with enhanced operational dispatch strategies focused on multi-nested methods, and the study of EROI and ESOI derivation and their applications in integrated hybrid configurations that combine multiple storage pathways and dispatch mechanisms.

#### 2.1.2 Structure of the Chapter

The literature review begins with the fundamental concepts of HRES and continues with optimisation methods, operational planning, and energy lifecycle cost metrics. Section 2.2 outlines the major features of hybrid systems, the challenges of including them into the grid, and the specific issues experienced by isolated or island communities, including intermittency, seasonal variation, and cost concerns. Section 2.3 advances the understanding of the optimisation methods by discussing established techniques such as Genetic Algorithms and Linear Programming, and more sophisticated nested approaches. Recent developments in adaptable load management are also reviewed, underscoring the benefits how flexible operations can improve system reliability and reduce cost.

Section 2.4 focuses on energy life cycle metrics that are used to assess renewable system, with closer look at EROI and ESOI and integrated methods. It also considers the limitations of these metrics when applied to hybrid, community-based applications, and reviews emerging approaches designed to address the complexity of multi-path energy flows.

Finally, Section 2.5 synthesises key gaps in the literature, specifically in system sizing, operational control, and sustainability assessment. This structured review thus provides a clear foundation for the technical methodologies developed in chapters 3, 4, and 5. By means of this methodical process, the literature review offers a strong basis on which the new techniques and studies of this dissertation are constructed.

# 2.2 Hybrid Renewable Energy Storage Systems: Concepts and Challenges

#### 2.2.1 Hybrid Systems and Grid Integration

HRES are systems that combine various storage technologies, like batteries and hydrogen systems, with renewable energy sources, like wind and photovoltaics to reduce the effects of intermittency and variability inherent in renewable generation. Various microgrid topologies are used to structure hybrid energy systems depending on the number and type of power buses involved, as outlined in [56], [57]. Some configurations assign a dedicated AC/DC converter to each major component. While this modular approach increases flexibility and control granularity, it also adds to system cost and coordination complexity. Figure 2-1 illustrates three representative architectures: Figure 2-1A shows a DC microgrid, where all components, including PV panels, battery storage, fuel cells, and loads, interact via a common DC bus with appropriate DC-DC or DC-AC converters. In contrast, Figure 2-1B illustrates an AC microgrid, where a single AC bus connects all components, and converters are used to manage the interface between DC sources and AC loads. Finally, Figure 2-1C shows a hybrid setup that includes both AC and DC buses. This hybrid bus configuration helps reduce

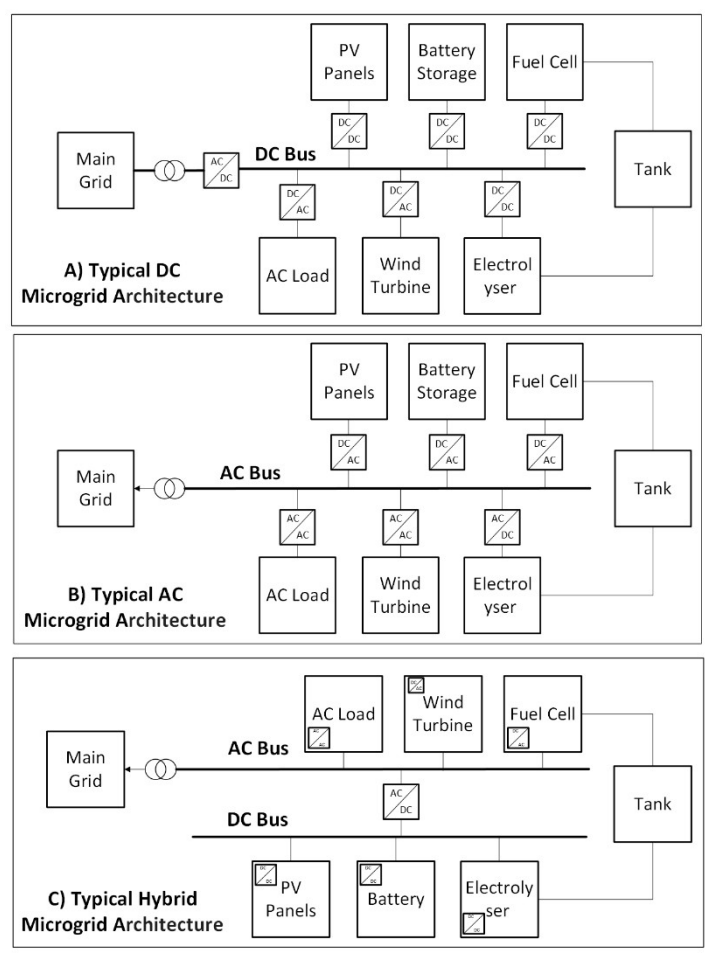


Figure 2-1: Diagram of a typical HRES adapted from [57].

conversion losses and boosts reliability, as emphasised in [58]. While it is suitable for both residential and industrial uses, it also demands careful coordination and precise inverter control, as discussed in [54].

Hydrogen storage can act as a complementary long-duration energy buffer in hybrid renewable energy systems, helping to mitigate multi-day to seasonal mismatches between renewable generation and demand. In the so-called "power-to-gas-to-power" loop, surplus PV or wind electricity is channelled through a DC-coupled electrolyser, producing hydrogen that is compressed and stored in tanks for later use [59]. During extended low-irradiance or low-wind periods, a fuel cell stack reconverts the hydrogen into electricity, injecting it into the AC side through the same bidirectional inverter used by the battery bank [60]. Integrating hydrogen storage becomes especially effective in systems with high seasonal variability and where renewables supply over 80% of total electricity demand, complementing batteries by addressing longer-duration storage needs [61]. A study modelled an islanded Canadian microgrid combining PV, wind, batteries, and a 700 kg hydrogen storage tank. The hydrogen tank maintained levels above 200 kg for over 5,000 hours each year [62]. These results suggests that hydrogen can effectively support extended energy storage needs, working well alongside traditional batteries, especially in hybrid renewable setups operating in isolated or weak-grid environments.

Reviewing the wider body of research, the main obstacles to deploying HRES include intermittency, high capital expenditure, and complex integration [63]. The critical role of sophisticated modelling tools and adaptive operational strategies in sustaining energy reliability and maintaining grid balance, given the unpredictability of renewable resources, has been highlighted in the literature [60]. Reliability remains a major technical issue for HRES, as it requires sophisticated forecasting methods, improved storage solutions, and enhanced grid-management strategies, as noted in [64], [65].

A pivotal aspect in the deployment of hybrid renewable energy systems is the techno-economic optimisation of inverter stages. Acting as the interface between the DC produced by photovoltaic arrays and battery banks and the AC requirements of utility networks and building loads, inverters have a decisive influence on overall efficiency and power-quality compliance [66], [67]. For instance, A study of an off-grid PV/Wind/Tidal/Fuel Cell hybrid system tailored to the Urmia region found that a 425 kWp PV array paired with a 54.98 kW inverter yielded the lowest net present cost under reliability constraints [68]. However, the inverter was treated as an independent decision variable, unconstrained by PV size and optimised only to meet peak load, resulting in an extreme DC/AC ratio (7.7:1). This raises concerns about implicit curtailment, as excess PV beyond the electrolyser's capacity was not

penalised or quantified in the model. Inverter sizing in HRES configurations must be precise. Oversizing adds unnecessary capital cost, while under sizing restricts renewable utilisation and reduces overall project revenues through clipping and curtailment. Apart from internal component sizing, HRES's interaction with the utility grid introduces another important degree of complexity.

Most studies on grid-connected microgrids have treated the power grid as an infinite power supply or power sink, guaranteeing the energy balance inside the microgrid when energy storage systems are either full or empty. A grid-linked PV/fuel-cell/hydrogen storage system sized using HOMER Pro for a university lab demonstrated that a 54.7 kW PV array, 7 kW fuel cell, 3 kW electrolyser, and 8 kg H<sub>2</sub> tank could supply 96.7% of the laboratory's annual electrical demand with renewable energy at a cost of just 0.0418 \$/kWh [69]. In the simulation, the utility grid was treated as an infinite sink for excess generation and an unlimited import source, as the sell-back price was set to zero. However, distribution-network constraints such as maximum contracted power or feeder thermal limits frequently prevent that idealised flexibility. When renewable output exceeds these limits, utilities may curtail generation or impose demand penalties to maintain balance. Hence a realistic techno-economic optimisation must include the full tariff structure, particularly the fixed charge for contracted power and the variable penalties for demand peak overruns, so that the selected operating strategy respects those network constraints throughout the project life cycle [67]. In the Spanish industrial sector, even a 10-20% reduction in contracted power can significantly increase penalties under coincident tariff systems. In one study [70], reducing the contracted capacity from 260 kW to 220 kW in a meat-processing plant led to a €564 increase in annual variable charges, from €1,263 to €1,827, due to more frequent peak overruns. This largely offset the expected savings and revealed a U-shaped cost relationship between contracted power and total demand charges.

#### 2.2.2 Specific Challenges for Island Energy Communities

There are approximately 11,000 permanently inhabited islands globally with 730 million people across various oceans, lakes and seas as of 2020 [71]. Europe has 2200 inhabited islands with a total of approximately 16 million residents, which corresponds to nearly 4% of the total EU population [18]. The energy generation on these islands has difficulties and has high costs, reaching up to ten times the expenses incurred on the mainland [72]. Furthermore, relying on non-renewable energy sources produces enormous greenhouse gas emissions and other pollutants, which have a detrimental impact on the ecology and human health.

Island communities have recently demonstrated growing interest in solar and wind energy as part of a transition toward more sustainable power sources. However, high-renewable penetration systems often experience pronounced seasonal mismatches between energy supply and demand, necessitating long-duration energy storage solutions. Hybrid systems that combine hydrogen fuel cells with battery storage are especially appealing as they provide short term and seasonal storage [73]. The prompt adoption of these renewable solutions requires a focus on the optimisation for the community renewable generation and management at the planning phase to ensure technical performance, cost-effectiveness, and environmental sustainability.

Many island power systems operate on diesel, which produces very high LCOE by generating high share of their power. For example, Galápagos' diesel plants produced 91.5% of its power in 2021 at up to 500 \$/MWh, about an order of magnitude higher than mainland Ecuador's average wholesale cost. Despite subsidised retail prices, Fernando de Noronha imports more than 6.6 million litres of diesel annually, which raises wholesale generation costs to 310 \$/MWh [74]. Due to severe supply fragility, Príncipe Island experiences scheduled blackouts of up to 12 hours per day when diesel supplies run low [74]. A 25-year techno-economic assessment of a proposed zero-emission community microgrid in Arandun, Nigeria shows how radically costs and emissions can fall when diesel is displaced [75]. The renewable configuration (photovoltaic, concentrated solar power, micro-hydro and battery energy storage) lowered the net present cost from \$408 million (diesel) to \$55.7 million and cut the LCOE from 1.01 \$/kWh to 0.26 \$/kWh. Importantly, it eliminated all operational CO<sub>2</sub> emissions, replacing an annual output of approximately 7.45 kilotons.

In response to these high costs and reliability challenges, islands have also emerged as strategic platforms for testing next-generation hybrid renewable systems. Islands can serve as proving grounds for cutting-edge operational models by integrating deep reinforcement learning for hybrid hydrogen-battery energy management, thereby validating new control methods under real-world microgrid conditions [76]. Furthermore, European projects such as REACT<sup>1</sup>, IANOS<sup>2</sup>, and LOCALRES<sup>3</sup> illustrate the innovative role of islands in piloting community-integrated renewables and storage, yet emphasize the continued need for custom-tailored energy planning that considers local load profiles and tariff structures [23]. While academic and policy interest in island energy systems is growing, recent literature reviews suggest that only a limited number of island-specific energy models have been developed.

-

<sup>&</sup>lt;sup>1</sup> https://react2020.eu/

<sup>&</sup>lt;sup>2</sup> https://ianos.eu/

<sup>&</sup>lt;sup>3</sup> https://localres.eu/

Many existing studies tend to focus on technical aspects and may not fully capture real-world challenges such as political instability, constrained financing, and the complexities of pursuing energy autonomy [77]. These findings highlight islands not only as urgent cases of energy transition but also as replicable test beds for the global shift toward decentralised, hybrid renewable systems.

Orkney, a Scottish archipelago with approximately 20,000 residents, exemplifies both the promise and complexity of advanced renewable integration in island communities. Since 2013, Orkney has consistently met more than 100% of its annual electricity demand through local renewable generation [78]. It hosts the highest density of community micro-wind turbines in the UK, prompting the launch of Britain's first distribution-level Active Network Management (ANM) system in 2009 [79]. By 2012, the island's 33 kV distribution feeders were saturated, and ANM now curtails nearly 30% of the output from North Isles turbines [79]. To recapture lost revenue, Shapinsay's Development Trust joined the €10.9 million EU-funded BIG-HIT project, deploying a 1 MW proton exchange membrane (PEM) electrolyser that converts otherwise curtailed wind energy into hydrogen for school heating, local council vehicles, and ferry auxiliary loads [80], [81]. However, life cycle costing analyses show that hydrogen remains expensive due to high input electricity costs, meaning grid congestion and curtailment risks persist even after integrating storage technologies.

The Isle of Wight, home to around 140,000 people and connected to the UK mainland via cable, presents a contrasting case where grid stability constraints still limit renewable deployment despite interconnection [82]. Using the REACT-DECARB planning platform, researchers assessed two main development scenarios. The first, a fully autonomous design, requires 663 MWp of solar PV and 1,731 MWh of batteries, resulting in a LCOE between €0.45 and €0.58/kWh, roughly ten times current wholesale prices [82]. A more moderate, grid-connected configuration with 405 MWp of PV, 187 MW of wind, and 400 MWh of battery storage offers better economic performance but still struggles to undercut prevailing market rates [82]. Nevertheless, multi-criteria decision analysis consistently ranks the autonomy pathway highest when metrics such as per-capita energy yield and CO₂ reduction are prioritised over cost [83]. This underscores the continuing challenge: storage expansion alone cannot make high-renewable systems viable without coordinated demand response and smart controls.

In summary, the development of hybrid renewable storage systems, especially for isolated grids, calls for solutions that are efficient, robust, and cost effective. The present study seeks to contribute by examining advanced control concepts, refined grid integration methods, and financing models tailored to small, resource-constrained communities. Overcoming these

hurdles would position hybrid renewables as a cornerstone of sustainable energy supply in communities that need it most. Having discussed the foundational components and unique challenges of HRES, particularly in island settings, the next section explores the suite of optimisation methods used to size and manage these systems effectively.

# 2.3 Optimisation Methods for Hybrid System Sizing and Dispatch

A variety of methods has been advanced for determining the optimal size of HRES, each tuned to design goals and levels of model complexity. Table 2-1, compiled from recent surveys, sets these approaches side by side [84], [85]. Metaheuristic, especially GA and Particle Swarm Optimisation (PSO) are popular for strongly nonlinear problems because their global searches are less likely to stall in local optima. Deterministic formulations such as MILP can deliver mathematically exact solutions when discrete choices dominate, but they often perform poorly in the presence of complex nonlinearities. New hybrid strategies (for instance, GA-PSO combinations or mathematical with Metaheuristic) blend the strengths of their originating algorithms and often reach high-quality solutions more rapidly, though at the cost of greater computational effort. Commercial packages like HOMER Pro remain valuable for early-stage feasibility checks, though their built-in solvers allow only limited algorithmic customisation. Collectively, these trends point toward the need for integrated optimisation frameworks capable of tackling both design-phase sizing and operational management in a unified fashion.

Table 2-1: Optimisation Methods for HRES Sizing with Objective Functions adapted from [84], [85].

Optimisation Method	Category	Use Case	Strengths	Limitations
Genetic Algorithm (GA)	Metaheuristic	Component sizing and reliability cost trade-offs	Handles nonlin- earities, wide adoption	Parameter sensitive, may converge prema- turely
Particle Swarm Optimisation (PSO)	Metaheuristic	Sizing + dispatch un- der varying load	Fast conver- gence, simple coding	Prone to local optima, weak in multi-objective scenarios
Simulated Anneal- ing (SA)	Heuristic	Optimal cost under limited design space	Global search potential	Slower, high tuning effort
Grey Wolf Opti- mizer (GWO)	Metaheuristic	Cost-efficient storage integration	Balanced search-exploit trade-off	Limited experimental validation
Multi-objective Evolutionary Algo- rithms (NSGA-II)	Multi-objective	Pareto-front design (cost vs. emissions)	Efficient Pareto ranking, elite selection	Complex implementation
Mixed Integer Linear Programming (MILP)	Deterministic/ Classical	Dispatch optimisation, inverter sizing	Accurate, con- straint-friendly	Struggles with nonlinear-ities
Stochastic Programming	Probabilistic	Uncertainty in load/solar generation	Real-world mod- elling	Requires data, hard to solve large instances
Artificial Intelli- gence (AI) / Ma- chine Learning (ML)	Soft Computing	Forecasts and decision-making via trained models	Learns complex patterns from data	Data-intensive; prone to overfitting
Hybrid Techniques (GA-PSO, PSO- GWO)	Combined	Optimized design with better convergence	Synergistic strengths	High computational cost
Software Tools (HOMER, iHOGA)	Simulation + Optimisation	Rapid system sizing with predefined libraries	User-friendly, scenario analy- sis	Limited customization, black-box nature

#### 2.3.1 Genetic Algorithms (GA) for System Sizing

HRES that combine both batteries and hydrogen storage is increasingly dimensioned with metaheuristic algorithms, especially when the installation remains grid connected. Algorithms such as the GA and PSO are well suited to the non-linear, high-dimensional search space that arises when multiple storage facilities share power flows. This review examines recent single-objective studies, each centred on either cost or performance, to highlight the current state of the art and the limitations still present in grid-connected battery-hydrogen configurations as summarised in Table 2-2.

Table 2-2: Summary of recent studies on grid-connected PV-battery-hydrogen systems, highlighting key components (BT: Battery, HR: Hydrogen, GR: Grid, WT: Wind, PV: Photovoltaic, INV: Inverter), methodologies, and limitations.

	<u>.</u>	- · · ·			Sys	tem				
Ref.	Study	Strengths	ВТ	HR	GR	WT	PV	INV	Results	Limitations
[86]	Zhang et al. (2017)	Early comparative analysis of hydrogen vs. battery in a grid-connected PV system; employs rulebased operation logic with cost sensitivity	✓	✓	✓	×	<b>√</b>	×	Useful baseline for demonstrating economic role of hydrogen, but outdated methodologically for today's dynamic load management needs	Uses fixed, rule-based operation; lacks stochastic or forecast-driven control; simple load profile
[87]	Singh et al. (2020)	Applies hybrid ABC–PSO to grid- connected PV–hydrogen–battery system; includes grid exchange lim- its as decision variables	<b>√</b>	<b>√</b>	<b>√</b>	×	<b>√</b>	×	Highlights grid-limit integration in hybrid optimisation; demonstrates feasibility under static tariff assumptions	Assumes flat tariff; omits inverter dynamics and demand flexibility
[88]	Le et al. (2023)	Strong focus on seasonal dynamics, storage degradation, and LCOE minimization; multi-year load scenarios included	<b>√</b>	<b>√</b>	<b>√</b>	×	<b>√</b>	×	Excellent techno-economic frame- work for long-term planning, but lacks algorithmic novelty; could benefit from hybrid GA–MILP style nesting	Metaheuristic method not detailed; more of a parametric approach than algorithmic innovation
[89]	Hassanza- dehFard et al. (2021)	Introduces novel waste-reuse aspect in cost modelling; uses improved PSO variant; grid participation is included	✓	✓	✓	✓	<b>√</b>	×	Pushes boundaries on cost mod- elling scope (waste reuse), but still omits key operational constraints for hybrid hydrogen-battery sys- tems	Simplified energy flow and control strategy; no consideration of AC/DC interactions or inverter constraints
[90]	Modu et al. (2023)	Applies Levy Flight Algorithm (LFA) in real seasonal RES scenarios; includes stochastic resource profiles and grid logic	✓	✓	<b>√</b>	×	✓	×	Rule-based operation is only slightly optimized via LFA; lacks demand-side flexibility or price-responsive dispatch	Most recent work in the set — marks a step toward adaptive seasonal strategies, but still falls short of full dispatch realism (e.g., MPC integration)

A recent study examined a grid-connected PV-hydrogen-battery system for a Gothenburg apartment complex, using the NSGA-II algorithm to optimize cost versus self-sufficiency ratio across four rule-based dispatch scenarios. In their study energy flows were simulated on an hourly basis using linear programming, accounting for a 100 kW PV export limit and Nord Pool electricity prices (0.83 SEK/kWh retail). The setup achieved uninterrupted power supply (LPSP = 0) and also quantified financial gains from peak shaving at a rate of 1500 SEK/kW-year. Inverter and grid exchange capacities were treated as fixed inputs during capacity planning [86]. Expanding the optimisation criteria, A study examined capacity sizing for a campus-scale PV-hydrogen-battery microgrid in India using a hybrid Artificial Bee Colony-Particle Swarm Optimisation approach. Their optimal design yielded a levelized cost of electricity of 0.104 \$/kWh. A distinctive aspect of the study is that the upper bounds on grid imports (30 kW) and exports (25 kW) were themselves treated as decision variables. Even with an export tariff (0.80 \$/kWh) exceeding the import tariff (0.70 \$/kWh), the model still favoured purchasing power from the grid (37,660 kWh/year) over selling (12,352 kWh/year), underscoring the influence of temporal mismatches between demand and on-site generation. Nonetheless, the reliance on a flat tariff and the omission of inverter reduce the direct applicability of the results to operational settings, though the methodological contribution remains noteworthy [87].

Over a 25-year horizon, a hybrid PV-battery-hydrogen system in tropical Vietnam was optimised using a Multi-Objective Modified Firefly Algorithm [88]. The optimal setup included a 2360 kWp PV array, a 1890 kWh battery bank, a 362 kW electrolyser, and a 90 kg hydrogen tank, achieving a levelised cost of electricity (LCOE) nearly 50% lower than comparable systems in the literature, along with a 98.7% self-sufficiency ratio and a net present value (NPV) of \$0.27 million [88]. In comparison, a battery-only configuration reached 75% self-sufficiency (NPV \$3.00 million), while the hydrogen-only system achieved 95% but resulted in a negative NPV, highlighting the hybrid system's superior balance between energy autonomy and economic performance. However, inverter and grid limits are not planning variables; grid access is assumed unlimited, and feed-in tariffs are excluded, overlooking export revenue. Their rule-based seasonal dispatch limits adaptability, despite realistic ageing and storage modelling [88].

A grid-connected hybrid microgrid including PV, wind, battery, and hydrogen was optimised using PSO over 20 years [89]. The system achieved a 27% fuel saving and 19% cost-of-energy reduction via municipal waste reuse. However, dispatch logic is schematic and static; inverter and grid limits (e.g., max import/export) are imposed as constants but not decision variables, limiting operational flexibility. Forecasting, dynamic tariffs, or adaptive scheduling are not considered [89]. The Levy Flight Algorithm was applied to size and manage a standalone PV-wind-hydrogen-battery microgrid under seasonal scenarios [90]. The

annualised system cost reaches \$1.86 million, approximately 10% lower than the HOMER benchmark, while the LCOE reaches 0.93 \$/kWh, undercutting the diesel baseline by 8% and HOMER by 13%, all while meeting a 5% loss-of-power-supply threshold. Dispatch is governed by static, rule-based logic rather than an optimised, forecast-driven energy management system. Inverter rating and grid-connection capacity are treated as fixed inputs rather than decision variables, and the model ignores contractual grid interactions and time-varying tariffs, which reduces the practical realism of an otherwise season-aware optimisation [90].

Despite their strength in global exploration, current metaheuristic-based sizing studies fall short in integrating dispatch-aware operational constraints. Grid limits, inverter capacities, and tariff dynamics are often predefined rather than co-optimised, while dispatch strategies tend to rely on static or rule-based heuristic strategies. As summarised in Table 2-2, even the most recent and season-aware studies neglect co-optimisation of grid-integration variables, storage flexibility, and contractual constraints. This disconnects between design-phase optimisation and operational feasibility restricts the real-world applicability of these methods, particularly in community or islanded systems. These observations motivate the transition to more rigorous formulations like Mixed-Integer Linear Programming (MILP), which can explicitly model hourly dispatch, enforce power balance, and embed infrastructure limits. The following section explores MILP's role in bridging this critical optimisation gap.

### 2.3.2 Mixed Integer Linear Programming for Sizing and Hourly Dispatch

GA techniques coupled with rule-based energy-management heuristics dominated the early hybrid-microgrid literature because they explored extensive design spaces with only modest mathematical effort [91], [92]. Their primary limitation, however, is that every candidate system is judged under a fixed schedule of dispatch rules that cannot adjust to the subtle, hour-by-hour interplay among batteries, hydrogen loops, and time-varying grid tariffs. MILP has become the prevailing analytical framework for sizing and dispatching hybrid renewable-energy systems: its linear structure accommodates on/off logic, physical constraints, and layered cost terms while retaining global optimality [93], [94], [95]. A close reading of the literature shows both the trajectory of that transition and the outstanding gaps it leaves behind. A detailed comparative summary of these studies, including their energy balance formulations, bus structures, decision variables, and key findings, is provided in Table 2-3.

Table 2-3: Detailed MILP comparative summary of these studies, including their energy balance formulations, bus structures, decision variables, and key findings (refer to appendix 9.1 for energy balance nomenclature)

No.	Reference	Horizon	Energy Balance	Energy Balance commentary	Inverter Limits	Grid Con- nected	Bus Struc- ture	Decision Variables	Key Findings	Limitations
[43]	Marocco et al. (2021)	Full 8760 hours (1 year)	$\begin{aligned} & P_{RES}(t) + P_{BT,dc}(t) \\ & + P_{FC}(t) + P_{NS}(t) \\ & = P_{LD}(t) + P_{BT,ch}(t) \\ & + P_{EL}(t) + P_{CT}(t) \end{aligned}$	DC-side strict bal- ance + binary ex- clusivity	Implicit through inverter effi- ciency, not de- tailed limits	Off-grid	DC bus	PV, bat- tery, elec- trolyser, H <sub>2</sub> tank, fuel cell sizes	Load flexibility (30%) reduces bat- tery sizing by 35%, LCOE by ~12%	Perfect fore- sight, no de- tailed inverter or network limits, AC/DC not clearly sepa- rated
[96]	Zhang et al. (2020)	24-hour synthetic typical day	$\begin{aligned} & P_{PV}(t) + P_{WT}(t) \\ & + P_{o,bat}(t) + P_{o,H}(t) \\ & = P_{i,bat}(t) + P_{i,H}(t) \\ & + P_{inv}(t) + E_{dis}(t) \end{aligned}$	Aggregated DC side balance with- out device-specific allocation	Single inverter limit modelled, but shared among all de- vices	Off-grid	DC bus with AC side load matching	PV, wind, battery, hy- drogen system	Battery cheaper now; hydrogen only becomes competitive with 53% CAPEX cut	No device dis- patch disaggre- gation, AC/DC not clearly sep- arated
[97]	Gabrielli et al. (2020)	Full year clustered into 24 "design days"	$\sum_{i \in \mathcal{M}} (U_{j,i,t} + P_{j,i,t} - V_{j,i,t} - F_{j,i,t}) - L_{j,t} = 0$	Generalised multi- energy carrier bal- ance	Not detailed for individual components	Grid-con- nected neighbour- hood	Multi- carrier AC/DC	PV, bat- tery, H <sub>2</sub> PtG sys- tems, heat pumps	Hydrogen essential for full decarbonization; heat and electricity coupling save 80% CO <sub>2</sub>	Clustering intro- duces small (1%) sizing er- rors, oversimpli- fied real dynam- ics (full year horizon), AC/DC not clearly sep- arated
[98]	Kassab et al. (2024)	Full 8760 hours	$\begin{aligned} p_{\text{bus}}(t_{i}) &= p_{L}^{D}(t_{i}) - \gamma_{PV}^{co} \\ &= p_{L}^{D}(t_{i}) - \gamma_{PV}^{co} \\ &\cdot p_{PV}^{MPPT}(t_{i}) + \frac{\mu_{c}}{\gamma_{b}^{co}} \\ &+ p_{b}^{d}(t_{i}) \cdot \gamma_{b}^{co} \cdot \mu_{d} \\ &+ p_{g}^{s}(t_{i}) \cdot \gamma_{g}^{co} + \frac{p_{g}^{in}(t_{i})}{\gamma_{g}^{co}} \\ &\leq 0 \end{aligned}$	Detailed DC-side balance	Explicit inverter efficiencies modelled, but fixed values	Both grid- connected and off-grid options compared	DC mi- crogrid	PV, battery size, grid contract peak (sen- sitivity)	Grid connection cuts LCOE from €0.98/kWh to €0.22/kWh	Perfect full year prediction and no inverter and grid constraint, AC/DC not clearly separated
[99]	Giovanniello & Wu (2023)	Full 8760 hours (no clus- tering)	$\max \left( \sum_{t=1}^{8760} \sum_{i} E_i(t) \right), i$ $\in \{LIB, HS\}$	LIB and H <sub>2</sub> storage energy balances independently tracked	Inverter limit applied but simplified	Off-grid	DC bus, fully is- landed	Wind tur- bines, bat- teries, hy- drogen tanks	Hybrid storage reduces cost by ~40%, overbuilding ratio 2.6x	Simplified con- trol without dy- namic re- sponse, no grid backup, AC/DC

										not clearly sep- arated
[100]	Zelaschi et al. (2025)	10 representative days	$P_{GT}(t) + P_{PV}(t)$ $+ P_{B,dis}(t)$ $= P_{load}(t) + P_{B,ch}(t)$ $+ P_{curt}(t)$	Single AC-bus balance couples PV, gas turbines, battery charge/discharge, curtailment; re- serve & start-up constraints guar- antee supply if one generator fails	Fixed efficiency factor; inverter rating not a deci- sion variable	Off-grid	AC bus	Sizes of gas tur- bines (incl. spare), PV ca- pacity, battery energy	Annual cost modestly (≈ 3–10 %); optimal design shifts toward larger battery and slightly smaller PV to meet reserve without oversizing turbines	24h window misses sea- sonal effects, simplified bat- tery dynamics, AC/DC not clearly sepa- rated
[101]	Talent and Du (2018)	Full year (17,520 periods); 10-yr NPV	$\begin{aligned} y_i A_i \text{GHI}_h \\ &= P_{i,p}^{PG} + P_{i,p}^{PL} + \sum_{j=1}^{J} P_{ij,p}^{PB} \\ , P_p &= P_p^{GL} + \\ \sum_{i=1}^{J} \underbrace{h_{\text{PV inv}}}_{\text{inverter}} P_{i,p}^{PL} + \\ &= \text{efficiency} \\ \sum_{j=1}^{J} P_{j,p}^{BL} \end{aligned}$	Power flows are aggregated; inverter efficiency at 97% applies to DC→AC conversion, no disaggregated device-level flow	Fixed efficiency, capacity not a decision variable	Yes, both TOU and demand tar- iff scenarios	Single AC/DC abstrac- tion (no nodal model- ling)	Binary PV & battery selection from dis- crete cata- logues	Tariff type alters dispatch patterns but not sizing; large PV, minimal battery chosen un- der both tariffs	No co-optimised inverter/grid siz- ing; no AC/DC separation; static perfect foresight; no flexible demand
[102]	Kassab et al. (2023)	Full 8760 hours	$ \begin{aligned} & p_{\text{bus}}\left(t_{i}\right) \\ &= p_{L}^{D}(t_{i}) - \gamma_{PV}^{co} \\ &\cdot p_{PV}^{MPPT}(t_{i}) + \frac{\mu_{c}}{\gamma_{b}^{co}} \\ &+ p_{b}^{d}(t_{i}) \cdot \gamma_{b}^{co} \cdot \mu_{d} \\ &+ p_{g}^{s}(t_{i}) \cdot \gamma_{g}^{co} + \frac{p_{g}^{in}(t_{i})}{\gamma_{g}^{co}} \\ &\leq 0 \end{aligned} $	DC-side balance	Inverter efficiencies considered; inverter rated capacity respected	Both is- landed and grid-con- nected	DC mi- crogrid	PV, battery sizing	Curtailment im- proves economics, grid link reduces LCOE by 67%	Static compo- nent efficien- cies, no network congestion modelled, AC/DC not clearly sepa- rated
[103]	Marocco et al. (2024)	Full 8760 hours	$\begin{split} P_{PV}(t) + P_{BS,dc}(t) &= \\ P_{BS,ch}(t) + P_{PV,BS}(t) , \\ P_{PV,BS}(t) + P_{GR,buy}(t) &= \\ P_{EL,in}(t) + P_{GR,sell}(t), \\ P_{EL, \text{out}}(t) + P_{HS,dc}(t) \\ &= P_{HS, \text{ch}}(t) + P_{LD,H_2}(t) \end{split}$	Separate AC and DC balances, electrolyser mod- elled in partial load	Partial load electrolyser efficiency modelled in PWA form	Grid-con- nected (in- dustrial H <sub>2</sub> production)	Hybrid AC/DC coupling	PV, bat- tery, elec- trolyser sizing	PV oversizing be- comes optimal >€120/MWh elec- tricity price	Full year perfect prediction, dis- tinguished but inverter sizing is simplified, AC/DC not clearly sepa- rated

A comprehensive MILP framework tailored for off-grid PV-battery-hydrogen systems was developed to jointly optimise the sizing of photovoltaic arrays, battery banks, electrolysers, hydrogen tanks, and fuel cells, while performing a full dispatch over all 8,760 hours of the year [43]. A notable strength of this work is the detailed treatment of component performance through piecewise-affine (PWA) representations of stack efficiencies and capital costs, embedded directly into the MILP. In addition, operating costs are linked to component degradation, and a simple demand-response program (DRP) is included to allow 30% of the load to shift based on time-of-use electricity rates with the off-grid configuration [43]. The system's energy balance enforces strict supply-demand matching on a singular DC bus topology, reflecting limited accounting for power type conversions and providing minimal details regarding inverter functionality. In this Mediterranean island case study (Stromboli Island, Italy), a LCOE reduction from €0.455/kWh to €0.402/kWh when flexible load shifting is enabled, mainly through a 35% downsizing of battery capacity. The results highlight that introducing even basic load flexibility at the design stage can substantially improve economic outcomes for isolated renewable hydrogen systems.

Building upon their earlier work, [103] explored the optimal design of PV-based grid-connected hydrogen production systems using a detailed MILP framework. This study significantly advanced the methodology by shifting from a single DC bus topology to a more nuanced multinode approach distinguishing between DC power, AC power, and hydrogen balances [103]. The model separately tracks DC-side balances for PV-battery subsystems and AC-side balances for grid-electrolyser interactions. Crucially, electrolyser partial-load behaviour is modelled using PWA approximations to capture efficiency variations over the operating range. Sensitivity analysis across grid electricity prices shows that at prices above €120/MWh, it becomes economically optimal to oversize PV arrays and electrolyser capacities to minimise grid reliance. The study finds that grid availability substantially reduces the need for large hydrogen storage capacities, with hydrogen levelized costs ranging between €3.5 and €7 per kilogram depending on market conditions [103].

Despite these enhancements, the mathematical model presented in [103] still exhibits limited detail concerning power conversion components such as inverters, along with relatively sparse treatment of grid constraints and inverter operational parameters. This progression clearly shows growing recognition of the importance of explicitly distinguishing AC/DC power balances in system optimisation models, though future work may benefit from a more thorough consideration of inverter operations and grid interaction constraints to further enhance technoeconomic results.

Building upon a related framework, the authors in [96] proposed a MILP model that cooptimises PV, wind, battery and hydrogen storage over a single 24-hour window derived from averaged annual weather data. The formulation minimises total annualised cost (capital, replacement and O&M) while meeting both electrical and thermal loads. It enforces binary exclusivity between battery charging/discharging and electrolyser/fuel cell operation, ensuring operational realism. Under current technology costs, the optimiser selects a battery-only system at approximately 6,989 \$/year, outperforming a hydrogen-only configuration at \$7,764 \$/year. However, if hydrogen CAPEX falls to around 47% of present levels, the two configurations achieve cost parity [96]. Incorporating fuel-cell cogeneration reduces annual costs by a further 3–5% when thermal demand is substantial, highlighting hydrogen's longer-term promise. A notable simplification is that the DC-side energy balance aggregates all generation and storage outputs into a single inverter stream, which is forced to match total AC demand and is capped by the inverter limit. Because this flow is not disaggregated by source, the model cannot resolve the hourly contribution of each technology to the AC load, leaving the detailed energy mix unidentified [96].

Reference [97] extended the multi-carrier optimisation paradigm by formulating a MILP that captures the interactions among electricity, heat, gas, and hydrogen flows within a neighbourhood-scale system. The energy-balance formulation generalises supply-demand matching across all carriers, incorporating imports, on-site generation, feed-in exports, and device fuel requirements. To maintain computational tractability over the full 8,760-hour horizon, daily profiles are clustered into a limited number of "design days" using k-means techniques, preserving critical peak demand values. Coupling rules are introduced to pass each storage device's state from one design day to the next, allowing the optimiser to plan multi-day and seasonal charging cycles [97]. In a case study for a Zurich neighbourhood, around 24 design days were sufficient to recover storage sizing within 1% accuracy compared to a full-year model. Results indicate that CO<sub>2</sub> emissions can be reduced by up to 80% using only heat pumps and thermal storage, while deeper decarbonisation requires integrating battery and hydrogen-based power-to-gas (PtG) systems. Hydrogen becomes indispensable for achieving long-term seasonal shifting and near-zero carbon operations.

In [100], a reliability-oriented MILP framework is presented to co-optimize the sizing of gas turbines, PV arrays, battery storage, and a standby backup unit, while performing hourly dispatch. To maintain computational feasibility, the 8,760-hour year is condensed into six "typical" days (average conditions) and four "extreme" days (periods of peak demand or very low renewable output) using a clustering algorithm. The formulation imposes explicit reserve and starts-up constraints so the islanded microgrid can still cover demand if any one major generator unexpectedly goes offline. Meeting this explained reliability requirement raises total

annual cost by 2.8 % for a remote gas plant and 10.4 % for an isolated airport yet guarantees uninterrupted service during such an outage. The optimised design shifts investment toward a larger battery and a slightly smaller PV array, allowing the battery to supply spinning reserve without oversizing conventional generators. Inverter losses are modelled by a fixed efficiency factor, and no contracted-peak charges are included due to the fully off-grid nature of the system [100].

A notable contribution is presented in [99], where a single-layer MILP simultaneously optimizes the sizing and dispatch for a fully islanded, 100% wind-powered microgrid combining lithium-ion batteries and hydrogen storage. The model captures all 8,760 hours without clustering, offering a credible representation of both daily and seasonal balancing requirements [99]. Hybridising lithium-ion batteries with hydrogen storage reduces the annualized system cost from \$75 million per year (battery-only) or \$59 million (hydrogen-only) down to \$43 million per year for the combined system, achieving a 40% cost reduction. Under projected 2050 technology costs, this drops further to \$19 million per year. In the optimised hybrid configuration, lithium-ion batteries operate for 90% of the time, while hydrogen systems support around 27%, bridging long-duration winter deficits. The results also reveal that 84 MW of installed wind capacity supports a peak demand of 33 MW, resulting in a generation-to-demand overbuild ratio of approximately 2.6 times, essential to maintain supply reliability without grid backup The results also reveal that 84 MW of installed wind capacity supports a peak demand of 33 MW, resulting in a generation-to-demand overbuild ratio of approximately 2.6 times, essential to maintain supply reliability without grid backup [99].

A detailed MILP method is introduced in [101] for planning and scheduling the use of PV-battery systems under two pricing structures: time-of-use (TOU) and demand-based pricing. The model first maximises the net present value (NPV) of capacity selection over a 10-year horizon, followed by hourly dispatch to minimise first-year electricity bills using half-hourly load data. To maintain tractability across 17,520 time periods per year, PV and battery sizes were discretised into a small, actionable decision set [101]. In both residential and commercial scenarios, the optimiser favoured the largest PV capacity with minimal or no battery storage, highlighting limited value for batteries under current tariff regimes. A fixed inverter efficiency of 97% is assumed whenever power crosses the DC/AC boundary, but no upper limit or associated cost is imposed, allowing the inverter to act as an unrestricted conduit. Grid-contracted power is also fixed, eliminating clipping risk and enabling oversized PV outputs to remain uncurtailed. This helps explain the model's bias toward large PV and minimal storage. Overall, the study provides strong evidence that tariff structure, rather than storage economics, plays a dominant role in capacity decisions, an insight with major implications for both policy-makers and investors [101].

A MILP-based optimisation framework is developed in [102] for sizing and dispatch strategies in a DC microgrid, primarily examining the trade-offs between isolated and grid-connected scenarios over a full-year horizon. The results show that grid support significantly reduces PV and battery sizing requirements, yielding a cost of €0.28/kWh compared to €0.85/kWh for the isolated case. Sensitivity analysis reveals that lower battery costs favour greater battery capacity, whereas higher battery prices incentivise PV oversizing and curtailment to minimise storage reliance [102]. Across all scenarios, battery replacement costs, due to their 5-year operational life, emerge as the largest contributor to total system expenditure. The study also confirms that incorporating PV curtailment into the optimisation process helps avoid unnecessary battery oversizing, thereby enhancing the economic feasibility of microgrids without compromising reliability [102].

Building significantly on [102] initial contribution, [98] further advanced their MILP framework by incorporating more realistic grid constraints and market conditions, explicitly introducing TOU electricity tariffs, grid subscription charges based on contracted power peaks, and detailed modelling of inverter sizing constraints. The model uses single DC bus bar topology with inverter/converter ratings as explicit decision variables, limiting instantaneous power flows according to rated inverter/converter capacities, though without associating inverter/converter sizing with explicit capital or replacement costs [98]. Simulating a PV-battery microgrid under French electricity market conditions, they find that grid-connected designs achieve an LCOE of approximately €0.22/kWh, compared to €0.98/kWh for fully isolated systems. Furthermore, tightening contracted peak limits from 36 kVA to 18 kVA (36, 30, 24 and 18 kVA as sensitivity limits) reduces dependence on grid electricity but increases both costs and emissions due to the need for larger local generation and storage [98]. The study highlights that carefully choosing the contracted grid subscription level is crucial to balancing cost and environmental targets and confirms that inverter sizing constraints and TOU tariff structures strongly influence system design.

Overall, the progression from [102] to [98] reflects a clear transition from simplified economic optimisation towards comprehensive techno-economic and environmental modelling, explicitly incorporating grid limit constraints, dynamic tariffs, inverter sizing decisions, and environmental metrics. Nevertheless, remaining simplifications, such as the assumption of perfect foresight and the omission of inverter capital and lifetime costs, highlight important methodological gaps, aligning closely with the research advancements proposed in this thesis.

Across the reviewed literature, a recurring structural limitation emerges co-optimising system sizing and hourly dispatch in a single MILP formulation becomes increasingly complex when

both long-term coverage and detailed operational modelling are pursued together. To manage this, most studies adopt one of two modelling strategies.

The first strategy retains the full 8,760-hour horizon but simplifies the operational layer. Several [43], [98], [99], [102], [103] follow this approach. These models preserve hourly resolution across the year but adopt structural simplifications, for instance, by fixing inverter capacity outside the model, aggregating all power flows on a DC bus, or avoiding binary charge/discharge exclusivity. While most of these studies do not explicitly discuss how dimensionality is controlled, their formulations are typically binary light, relying on continuous sizing variables and restricting integer variables to a handful of logical switches such as PV/load imbalance or electrolyser on/off states. Importantly, this approach also assumes perfect foresight of demand, generation, and market conditions across the full year, an assumption that may lead to overly optimistic dispatch and sizing decisions compared to what could be achieved under limited or real-time information

The second strategy preserves more operational realism but reduces the temporal scope. Some studies [96], [97], [100] compress the year into synthetic or representative days. For instance, [96] uses a single 24-hour synthetic day; [97] clusters the time series into 24 "design days" and introduces continuity constraints to maintain storage behaviour; and [100] approximates the year with ten representative days—six typical and four extremes—preserving key peaks while keeping the model compact. These models accommodate features such as partial-load efficiency, battery cycling penalties, and inverter performance, but the time compression inherently limits their ability to capture long-term storage dynamics and rare high-demand periods.

Across both groups, the underlying constraint is structural: maintaining fine operational detail over an extended horizon leads to an increase in variables and constraints that most MILP frameworks avoid by design. This helps explain why inverter sizing and grid contract parameters are frequently treated as exogenous inputs, and why component sizes are often selected from continuous ranges or predefined list.

To address these trade-offs, the next section introduces frameworks that hybridise metaheuristic sizing loops with mathematical-programming dispatch submodule. In this configuration, outer loop explores capacity configurations, while an inner loop evaluates each size proposal using short-horizon dispatch with detailed operational constraints. This decoupled structure provides a way to reintroduce operational complexity without significantly expanding the overall model scale. The next subsection therefore critically reviews state-of-the-art nested models, evaluating their claims and highlighting persistent gaps: fixed or neglected inverter sizing alongside effectively unlimited contracted grid power; reliance on full-

year, perfect-foresight horizons; oversimplified tariff structures; and the absence of explicit AC/DC nodal representation.

### 2.3.3 Nested Optimisation Approaches

Nested optimisation techniques, which couple long-term sizing heuristics with short-horizon dispatch models, have emerged as a powerful strategy for hybrid renewable energy systems (HRES) that must navigate complexity across timescales, resource variability, and technical constraints. In particular, the integration of GA, Evolutionary Programming, or Grey Wolf Optimisation (GWO) at the outer loop with MILP at the inner loop has become a common structure in recent studies. These approaches bridge the common disconnect between static design-phase models and dynamic operational constraints, especially relevant in systems with multi-path energy flows and grid-tied operation. Table 2-4 and discussion critically examine recent studies that exemplify this nested framework, highlighting their methodological strengths, techno-economic outcomes, and persistent modelling limitations.

One of the earliest fully implemented examples of a coupled nested framework combines a GA-based sizing layer with a 24-hour rolling-horizon MILP-MPC dispatch strategy across an off-grid DC-coupled microgrid [104]. Across a simulated full-year horizon (365 × 24 h subproblems), the integrated strategy reduced the annualised system cost by 7% (from \$18,095 to \$16,819 per year) and levelized cost of electricity (LCOE) by 8.7% (from \$0.599 to \$0.547/kWh) compared to a rule-based dispatch baseline. Component downsizing followed: PV capacity was reduced from 23 to 20 kW, and battery capacity from 80 to 76 kWh [104]. Simultaneously, reliability improved, with the loss-of-load probability reduced by 75% (from 0.0032 to 0.00079). However, the modelling assumes a perfectly ideal DC bus, omitting both inverter losses and any explicit AC layer, limiting the applicability of the results in real-world systems that require AC supply or bidirectional grid exchange [104].

Table 2-4: Overview of recent nested optimisation studies combining heuristic sizing (e.g., GA, GWO) with short-horizon MILP dispatch for hybrid renewable energy systems (HRES). System architectures are denoted using the following component codes: PV – photovoltaic panels, WT – wind turbines, BT – battery storage, FC – fuel cells, EL – electrolysers, TK – hydrogen storage tanks, IN – inverters or power electronics, GR – grid interface, OR – other components such as heat pumps or thermal storage. Each study is assessed for control structure, optimisation layers, component integration, and major limitations.

				Energy				Syste	m Stru	ıcture				Energy					
Ref.	Study	Sizing Method	Dispatch Method	Manageme nt Energy Balance	P V	W T	B T	F C	E L	T K	I N	G R	O R	Balance Commentary	Inverter Limits	Bus Structure	Grid Connected	Key Findings	Limitations
[104	Rullo et al. (2019)	GA minimises annualised system cost	Rolling- horizon MILP- MPC for 24 horizons	DC-bus energy balance (PV + WT - curtailment - served- load = Batt + Electrolyser - Fuel-cell)	✓	✓	✓	✓	✓	✓	×	×	×	Single DC bus, no explicit AC bus; renewable and storage flows balanced directly on DC side	No inverter limit considered (implicit inverter assumed ideal)	Single DC bus structure	No (Off-grid, standalone microgrid)	MPC dispatch saves ~15% COE compared to rule-based; predictive flexibility improves component sizing	Single bus with aggregated DC/and AC nodes. Inverter and grid limits and not considered
[105	Tamashiro et al. (2023)	Multi- objective optimisation using e- constraint (min. cost + CO <sub>2</sub> )	Model Predictive Control (MPC) with rolling horizon (3- day prediction, 1-day control)	Power balance: Pgrid(t) + PBESS(t) +  ΣPFC(t) = Pload(t) - PPV(t) With PBESS = Pdis - Pcha, Pgrid = Ppur - Psell	V	V	√	√	×	×	×	√	1	Electrical balance includes PV, BESS, FC, load, and grid. No explicit AC/DC conversion. No modelling of inverters. No curtailment or flexible loads included.	No inverter component or limits considered in equations or model assumption s. Inverter assumed ideal.	Single power flow bus (implicitly DC). No separation of AC/DC mathematicall y.	Yes, electricity can be purchased/so Id from grid. Grid import/export modelled, still no limit	MPC dispatch (Case C) reduces costs by 44.4% and CO <sub>2</sub> emissions by 54.7% vs. no DER case; shows predictive scheduling significantly outperforms day-by-day planning.	No inverter modelling: grid limits modelled only as max fluctuation, not capacity limit.

[106	Li et al. (2017)a	GA minimises total system cost (capex + opex + maintenanc e)	MILP-based Unit over one-week average input data, 1-year rolling horizon validation)	$PPV(t)$ $-P_{\text{curt}}(t)$ $-(P_{\text{load}}(t)$ $-P_{LS}(t))$ $=Z_{\text{ele}}(t)$ $-Z_{fc}(t)$ $+Z_{ch}(t)$ $-Z_{\text{dis}}(t)$	1	×	1	√	√	√	×	×	×	Multi-vector electrical and heat balance modelled; AC/DC distinction not considered; inverters assumed ideal.	No inverter component or limits modelled (ideal assumed)	Single energy bus, no AC/DC separation modelled	No	Degradation -aware co- optimisation improves long-term sizing; ±10% forecast errors increase hydrogen and thermal storage significantly.	Inverter limits are not modelled; sizing evaluated over one-week average input data; no wind integration; off- grid only. open-loop UC (no MPC)
[107	Li et al. (2017)b	$GA$ searches over sizing set U to minimise F $= C_{a_pex} + C_{o_pex} + C_{main} \text{ via}$ MILP-based dispatch.	12-day evaluation horizon, 1- year rolling horizon validation	Electrical:  PV -  curtailed -  load +  shedding =  FC + battery  +  electrolyser  +  auxiliaries,  Thermal:  Solar heater  - curtailed -  heating load  + shedding  = FC heat +  boiler + heat  storage,	1	×	1	1	1	✓	x	x	J	Four parallel buses (Power, Heat, Cooling, H <sub>2</sub> ); scheduling MILP enforces each balance; no inverter losses or ratings are modelled.	No inverter constraints	Single electrical aggregated bus	No	Demonstrat es linearized EL/FC models, simple battery SOC, and bi-level UC- sizing coupling achieves feasible off- grid operation	Using just 12 representative days can hinder finding the global optimum, No inverter/grid limits; no WT, no multi- energy; follower only UC, no receding horizon; single bus idealization

[108]	Pu et al. (2021)	Two-level RT-GWO & MILP: RT- GWO for capacities (PV, WT, FC, EL, EB, CO, Batt, HES, H <sub>2</sub> seasonal & short) minimises life-cycle cost	MILP scheduling on clustered "typical days"	$\begin{aligned} P_{\text{EB}}(t) \\ + P_{\text{CO}}(t) \\ + P_{\text{EL}}(t) \\ + P_{\text{I}}(t) \\ = P_{\text{PV}}(t) \\ + P_{\text{WT}}(t) \\ + P_{\text{FC}}(t) \\ + P_{\text{BAT}}(t) \end{aligned}$	1	1	1	1	1	1	×	x	x	Power balance enforced by MILP; accounts for PV, load, BSS, HSS, curtailment, and shedding; no grid support assumed.	Ideal inverters	Single bus	No	Integrates degradation (PEMFC, EL, Batt), seasonal H <sub>2</sub> storage; RT- GWO outperforms PSO/GWO; typical-day clustering; finds seasonal H <sub>2</sub> 5× battery cost- effective; ~9.47 M ¥ lifecycle cost	No inverter sizing/losses; no receding horizon (UC only); thermal/hydrog en network idealized; single location; clustering may omit extremes
[109	Al-Quran & Al- Mhairat (2024)	MOGA: multi- objective GA minimises annualized cost & maximizes REF	EMPC- MILP, 3 h receding horizon (economic MPC)	$\begin{aligned} P_{\text{PV}} + P_{\text{WT}} \\ + P_{\text{FC}} \\ + P_{\text{bat, dis}} \\ + P_{\text{grid}} \\ = P_{\text{load}} \\ + P_{\text{BL}} \\ + P_{\text{bat, ch}} \\ + P_{\text{loss}} \end{aligned}$	✓	✓	✓	1	1	√	×	✓	×	DC-bus: PV+WT – Batt charge + Batt discharge + EZ – FC – grid import + grid export balanced hourly; includes degradation and grid trades	Constant efficiencies, no sizing limits	Single DC bus + single- phase inverter	Yes	Bi-level GA + 3 h EMPC co-optimizes cost vs. REF; EMPC delivers true MPC; grid export/impor t at \$0.135 /kWh; seasonal case study shows 60% REF, net export in summer	No inverter/inverter sizing; only four weeks of data; no full-year stochastic analysis
[110	Eltamaly & Almutairi (2025)	Nested LEA (Lotus Effect Optimisatio n Algorithm)	Hourly inner-loop optimisation via LEA (or ANN	-	✓	<b>√</b>	✓	✓	✓	<b>√</b>	×	×	×	DC-side energy balance, including PV, WT, battery charge/discharg	No power- rating or dynamic inverter constraints	Single DC bus (no separate AC bus)	No	Nested LEA cuts sizing convergenc e by 43%; ANN	Linearized DR & storage models; no inverter/inverter sizing; hourly

		with multi- objective weighting of LCOE + LOLP	surrogate); static economic dispatch (not MPC)											e, electrolyser & fuel-cell flows; no AC/DC conversion or inverter losses				surrogate speeds it to 1.08% of that time; DEMAND RESPONSE cuts cost ~28%; co- optimisation balances cost vs. REF Embedding	resolution; single-site case; no stochastic uncertainty beyond stepwise REPF
[111	Mohseni & Bre nt (2022)	Particle Swarm Optimisatio n minimises LCOE	72 h rolling-horiz on LP dispatch	$\begin{aligned} P_{im} + P_{pv} \\ + P_{wt} \\ + P_{bat, dis} \\ = + P_{load} \\ = P_{ex} \\ + P_{bat, ch} \end{aligned}$	✓	✓	✓	×	×	×	×	×	✓	Aggregated DC-coupled energy balance including PV, wind, battery, grid import/export and curtailment; no AC/DC split modelled.	Fixed converter efficiency; no explicit power-ratin g or clipping constraints.	DC-coupled microgrid + AC grid via multi-mode inverter	Yes	72 h look-ahead dispatch in PSO sizing cuts whole-life cost by up to 8 % and boosts battery arbitrage value.	Assumes perfect forecasts (no uncertainty); inverter losses modelled via fixed η; no feeder or contracted-pea k limits; deterministic LP.

Earlier foundational work introduced a bi-level system sizing framework in which a GA acts as the upper-level leader, proposing candidate plant configurations [106]. These are subsequently evaluated by a lower-level, hourly mixed integer linear programming unit commitment (UC-MILP) model with the objective of minimising total annual cost. To reduce computational effort, the GA is applied to weekly-averaged profiles of demand and solar irradiance. Once an optimal configuration is identified, it is subjected to a more granular 1hour rolling-horizon simulation, executed daily over an entire year. If the simulation reveals energy shortages, the fuel cell and electrolyser capacities are iteratively adjusted. When a 10% forecast error is introduced, the robust analysis produces a cost range from €174k (bestcase) to €279k (worst-case), highlighting a 38% range attributable to uncertainty rather than to changes in the optimisation strategy [106]. Comparing the MILP dispatcher with classic rulebased control method nearly triples the battery size, from 189 kWh to 407 kWh, and raises the capital cost from €128k to €175k. This result underscores the inefficiency of fixed heuristic approaches in hybrid microgrid applications. Although the model accounts for battery ageing and enforces strict constraints on state-of-charge (SOC), level-of-hydrogen (LOH), and power limits, it assumes ideal, lossless static converters, thereby neglecting AC/DC conversion losses and their associated operational impacts [106].

The work in [107] builds directly on earlier foundations by extending the same GA + UC-MILP co-optimisation approach to a stand-alone multi-vector micro-grid with parallel AC, hydrogen, and thermal buses. A GA-driven sizing layer is coupled to an hourly UC-MILP solved on 12 representative days and validated in a year-long rolling-horizon run. The preferred design contains 121 kWp of PV, a 396-kW electrolyser and a 1065 N·m³ hydrogen store, giving 25 hours of fuel-cell autonomy and keeping capital costs below €0.4 million. Eliminating the last instances of PV curtailment requires scaling the hydrogen tank to approximately 1.4 × 10⁵ N·m³, pushing the CAPEX to €2.26 million [107]. However, the simplification of using just 12 representative days may hinder global optimality. Additionally, no aggregate limit or dynamics are applied to the AC interface. Effectively, the inverter linking devices to the electric bus is treated as loss-less and unconstrained, potentially overlooking performance bottlenecks present in practical deployments [107].

To address the scale and runtime challenges of full-year optimisation, the authors in [108] introduced a two-level hybrid model using Real-Time Grey Wolf Optimisation (RT-GWO) for sizing and a clustered MILP schedule based on 30 "typical days," representing an entire year. Applied to an island microgrid with seasonal hydrogen storage, their model revealed that substituting the seasonal H<sub>2</sub> tank with batteries would increase the capital investment from ¥5.6 million to ¥29.7 million, a more than fivefold jump [108]. Inclusion of degradation models raised overall lifecycle costs by 13.1%, underscoring the financial implications of ageing. While

the model captures thermal, battery, and hydrogen interactions effectively, it simplifies the power electronics by assuming ideal inverters. The absence of rolling horizon or demand forecasting limits the adaptability of the dispatch algorithm to extreme or atypical days [108].

Further enhancing temporal resolution, the authors in [111] propose a recent nested framework that couples a PSO outer loop with a linear programming (LP) inner loop executing rolling 72-hour dispatch, a departure from the 24-hour look-ahead used in most prior cooptimisation models. Applied to a grid-tied, DC-coupled community microgrid, the PSO determines optimal sizes for PV, wind turbines, and lithium-ion batteries, while the LP leverages three-day forecasts to co-optimise arbitrage revenue and battery degradation costs. Compared to their own baseline PSO + 24 h model, their 72-hour dispatch strategy reduces life-cycle cost by up to 8% and lowers the risk of PV overbuild by preserving battery headroom across multi-day price cycles [111]. The model achieves computational efficiency by solving 72 sub-problems per year, instead of tackling the entire year in a single large-scale optimisation, though it retains common simplifications, notably fixed inverter efficiencies and the absence of explicit AC-bus constraints. Consequently, phenomena like inverter clipping or peak penalties remain outside the optimisation scope.

Pursuing computational efficiency, the authors in [110] introduced an innovative nested Lotus Effect Algorithm (LEA) with Artificial Neural Network (ANN) surrogates, cutting the computational runtime from 21.3 hours to just 0.23 hours, about 1.08% of the full loop, while maintaining an LCOE near \$0.057/kWh. Their system, set within a smart-grid context, uses real-time pricing and demand response [110]. The study stands out for balancing computational efficiency with techno-economic rigour, showing that integrating ANN models can dramatically reduce optimisation time without major loss in fidelity. However, their inverter models remain idealised and the ANN lacks interpretability, making sensitivity analysis difficult [110].

In a similarly performance-conscious approach, the authors in [109] merged a Multi-Objective GA (MOGA) with a 3-hour economic MPC (EMPC) layer to model grid-connected residential HRES under seasonal variability. In this study, the summer week emerged as the optimal configuration, yielding an annualised cost of \$99,484 (10% less versus the next-cheapest spring week) and the highest renewable energy fraction while maintaining the lowest aggregated degradation index of  $\Sigma$  = 50 (a reduction of 72% versus winter) [109]. Their inverter efficiencies were fixed (between 90–95%), and clipping was ignored, an omission that may underestimate the true LCOE and misrepresent periods of surplus generation. The model horizon spans only four weeks, limiting the ability to extrapolate to long-term operation and seasonal variability [109].

Culminating recent advances, the authors in [105] advanced the state-of-the-art by embedding a multi-objective e-constraint GA within a rolling-horizon 3-day MPC-MILP scheme tailored for grid-connected residential systems. Their setup evaluates 3-day forecasts with daily reoptimisation, emulating real operational settings under dynamic pricing. The case study demonstrated a 44.4% reduction in operating cost and a 54.7% cut in CO<sub>2</sub> emissions compared to static dispatch, confirming the potential of predictive control when co-optimised with system sizing [105]. Yet, grid interaction is simplified by infinite import/export capacities, and inverter dynamics are omitted. The assumption of unconstrained grid exchange significantly affects the model's flexibility, risking unrealistic cost reductions in high-penetration scenarios [105].

In comparing these nested models, several patterns emerge. First, coupling heuristic sizing methods like GA or GWO with short-horizon, constraint-rich dispatch models (MILP, MPC) consistently outperforms static or sequential approaches in both cost and reliability. However, most models assume infinite size for the inverters, neglect power rating limits, and oversimplify AC/DC interactions. This can obscure operational limits such as curtailment due to undersized inverters or overloading of DC links. Only a few studies, such as [105], model demand-side flexibility forward-looking scheduling mechanisms, and even fewer incorporate contracted grid constraints or dynamic tariffs, despite their potential influence on system design and investment outcomes. Second, system performance and cost sensitivity are tightly linked to the granularity and realism of temporal modelling. Studies relying on representative or typical days risk under-capturing rare but critical stress periods, especially in island systems where energy autonomy must span full seasonal cycles. While clustering reduces computational burden, it must be paired with robust cross-day storage coupling or validation to retain credibility. Third, hydrogen storage consistently proves its value for long-duration, lowfrequency balancing, reducing battery size, curtailment, and life-cycle cost, particularly when paired with electrochemical storage for short-term flexibility. The results in [108] and [99] reinforce this synergy quantitatively. Still, hydrogen systems introduce a second layer of conversion losses and require precise inverter planning to ensure peak demands are met. Inverter oversizing to accommodate fuel cell peaks can inflate CAPEX unless modelled jointly with power-sharing strategies and peak-shaving algorithms.

Despite the advances in computational strategy, incomplete modelling of inverter and grid interfaces remains the most persistent and consequential omission in nested HRES optimisation. Even when rolling horizons or stochasticity are present, assuming infinite grid exchange or ideal conversion masks significant techno-economic trade-offs. As energy systems become increasingly integrated and prosumer-oriented, these assumptions erode the external validity of simulation results.

In conclusion, while nested optimisation frameworks offer a powerful pathway to co-optimise HRES sizing and operation, their full potential is unlocked only when grid constraints, inverter dynamics, and demand-side flexibility are explicitly incorporated. This thesis addresses several of these gaps by incorporating MILP-based formulations that embed contracted power limits, partial-load inverter constraints, flexible load scheduling, and high-fidelity AC/DC hybrid modelling into the sizing and dispatch process. Additionally, the approach integrates realistic tariff structures to better reflect techno-economic constraints in grid-connected scenarios. Moreover, incorporating elements inspired by adaptive control models such as MPC framework allows this approach to simulate anticipatory, constraint-aware dispatch strategies within the design phase, enhancing the alignment between techno-economic planning and operational feasibility.

The preceding review has surveyed decomposition strategies and practical implementations of nested sizing-and-dispatch frameworks in the literature. To make explicit the theoretical mechanism that underpins many of those implementations, the next subsection formalises a penalty-guided formulation that links hourly dispatch outcomes to long-term design objectives. The aim is to show, at a conceptual level, how aggregated reliability indicators produced by the dispatch layer can be used to shape the design search in a manner that is both tractable and consistent with common practice in the field.

# 2.4 Theoretical Background: Penalty-Guided Nested Objective

In nested metaheuristic–MILP frameworks, the upper-level design problem can be expressed as a penalised objective that couples economic cost with annual reliability indicators computed by the dispatch layer. This provides a clean theoretical mechanism by which the design search (e.g. GA) is guided by the total annual unmet and excess energy arising from hourly operation.

Let  $x \in \mathcal{X}$  be the capacity vector and let y(x) be the optimal hourly dispatch over a representative year returned by the MILP. Define the annual indicators from the lower layer as:

$$U(x) = \sum_{t \in T} u_t(x) \Delta t, E(x) = \sum_{t \in T} e_t(x) \Delta t$$
 (2-1)

where  $u_t$  and  $e_t$  are, respectively, unmet-load and excess-energy slacks at hour t. A general penalised upper-level problem can then be written as:

$$\min_{x \in \mathcal{X}} \underbrace{\text{NPC}(x; y(x))}_{\text{economic term}} + \underbrace{\lambda_U \widehat{U}(x) + \lambda_E \widehat{E}(x)}_{\text{annual penalty guiding the search}}$$
 (2-2)

with  $\widehat{U}$ ,  $\widehat{E}$  taken as either the raw annual totals U, E or normalised versions, for example as fractions of annual demand, and with weights  $\lambda_U$ ,  $\lambda_E \geq 0$  that set the selection pressure. The lower-level dispatch is a MILP of the form:

$$y(x) \in \arg\min_{y \in \mathcal{Y}(x)} \sum_{t \in T} \left( p_t^{\text{buy}} g_t^{\text{buy}} - p_t^{\text{sell}} g_t^{\text{sell}} \right) + c_U u_t + c_E e_t$$
 (2-3)

where the coefficients  $c_U$ ,  $c_E$  enforce operational feasibility for a fixed x. The upper-level weights  $\lambda_U$ ,  $\lambda_E$  then steer design choices by penalising the annual totals returned by the dispatch solution y(x).

This structure guides a GA in a transparent way. If  $\lambda_U$  is large relative to marginal changes in capital and operating costs, any design with non-zero annual unmet  $\widehat{U}(x)$  becomes dominated, so the population drifts toward capacity mixes that allow the lower layer to meet demand over the year. A moderate  $\lambda_E$  discourages chronic curtailment and nudges the search to right-size generation, inverter and storage so that production is absorbed efficiently. Because  $\widehat{U}(x)$  and  $\widehat{E}(x)$  are annual aggregates rather than hourly quantities, the GA receives a stable fitness signal that reflects the whole year rather than hour-to-hour noise.

There are equivalent theoretical variants of the same idea. An  $\varepsilon$ -constraint form minimises NPC(x; y(x)) subject to  $\widehat{U}(x) \leq \varepsilon_U$ ,  $\widehat{E}(x) \leq \varepsilon_E$ . A guard-rail or hinge-penalty form replaces hard penalties by  $[\cdot]_+ = \max(\cdot,0)$ , for example NPC +  $\lambda_U[\widehat{U}(x) - \varepsilon_U]_+ + \lambda_E[\widehat{E}(x) - \varepsilon_E]_+$ , which is often numerically gentler than very large fixed penalties. A multi-objective view treats (NPC,  $\widehat{U},\widehat{E}$ ) directly and then uses a scalarisation such as a weighted sum or an  $\varepsilon$ -constraint to obtain a single fitness value. The penalised form in (equations 2-2 and 2-3) is precisely such a scalarisation.

Weight selection should be unit consistent, and theory aligned. Normalising first, for example  $\widehat{U}=U/D$  and  $\widehat{E}=E/D$  with D the annual demand, yields dimensionless percentages and makes  $\lambda_U$  and  $\lambda_E$  comparable across different cases. An ordering with  $\lambda_U\gg\lambda_E$  encodes the fact that unmet demand is more critical than curtailment. If raw kWh units are kept, the weights can be set in Euros/kWh as present-value costs, with  $\lambda_U$  approximating a value of lost load and  $\lambda_E$  approximating the opportunity cost of curtailed energy. Robustness should be confirmed by simple sensitivity checks, for example scaling  $\lambda$  by factors of 1/10 , 1 and 10; designs that remain stable across this range indicate adequate selection pressure rather than artefacts of arbitrary scaling.

It is helpful to be clear about the role split between layers. The lower layer uses  $c_U$ ,  $c_E$  to resolve operational feasibility for a given x and if feasibility exists the MILP will typically drive  $u_t$  to zero at most hours. The upper layer then uses  $\lambda_U$ ,  $\lambda_E$  on the annual aggregates to steer the

design toward regions where the dispatch can keep those slacks acceptably small throughout the year. Writing the upper-level objective as:

$$\min_{x \in \mathcal{X}} NPC(x; y(x)) + \lambda_U \widehat{U}(x) + \lambda_E \widehat{E}(x)$$
 (2-4)

The formulation above therefore provides a compact, literature-grounded mechanism by which annual aggregates of unmet and excess energy influence design search through penalty-weighted objectives, while preserving a clear separation between high-fidelity operational evaluation and global design exploration.

While penalty-guided objectives reconcile operational fidelity with tractable design search, economic metrics alone do not capture the full sustainability implications of competing storage strategies. This observation underscores the need to move beyond purely financial indicators like LCOE or net present cost. Metrics such as Energy Return on Investment (EROI) and Energy Stored on Invested (ESOI) provide a complementary and essential dimension to performance evaluation, shifting focus from "cost-effectiveness" to "energy effectiveness." These life-cycle metrics quantify how much usable energy a system returns relative to what it consumes or embodies across its entire lifespan, including manufacturing, maintenance, and eventual decommissioning. In doing so, they introduce a distinct 'energy life cycle' perspective that is particularly well suited to multi-vector systems with layered energy storage and seasonal variability.

For community energy planners, especially in remote or island settings, EROI and ESOI are not just abstract metrics, they are practical tools for identifying design pathways that maximise energy autonomy, system resilience, and environmental return. They help quantify how wisely energy is invested across competing storage strategies (batteries vs. hydrogen), and how operational patterns like curtailment or inverter clipping affect not just cost, but overall system sustainability. Moreover, they provide a language to anticipate performance bottlenecks, test design robustness, and guide transition strategies under real-world constraints.

Building on the operational and optimisation models explored in this section, the next section introduces these energy-centric metrics, reviews their application in the HRES context, and evaluates their role in supporting long-term sustainability, especially for decentralised and community-based systems.

# 2.5 Life-Cycle Energy Assessment in Hybrid Renewable Systems

A growing body of literature has applied life-cycle energy metrics, particularly Energy Return on Investment (EROI) and Energy Stored on Energy Invested (ESOI), to evaluate the long-term sustainability of renewable generation and storage technologies. These indicators quantify the net energy performance of a system over its lifetime by relating usable energy output to the energy required for its manufacturing and deployment. However, in most applications, these metrics are computed under simplified conditions that overlook the dynamic interactions present in hybrid energy systems, especially at the community scale, where generation, demand, curtailment, and storage operate under fluctuating, sub-hourly profiles. This section reviews a broad body of contributions spanning various system scales and modelling approaches, with the aim of identifying common assumptions, methodological gaps, and their implications for community-scale hybrid energy systems. The studies reviewed are summarised in Table 2-5.

The Energy Stored on Investment (ESOI) metric was first introduced at the device level in [112], which benchmarked seven storage technologies, including pumped hydro storage (PHS) and lithium-ion batteries, by comparing cycle life, efficiency, and depth of discharge. The methodology translated lifecycle energy data into clear ESOI ratios. For instance, the results showed that compressed air energy storage (CAES) and PHS had ESOI values of approximately 240 and 210, respectively, far exceeding battery-based technologies. However, the analysis was static, excluding balance-of-system elements and operational constraints pertinent to case study- or community-scale implementations [112].

While the ESOI was originally established as a device-level benchmark in [112], a subsequent study in [107] analytically coupled ESOI with generation-side Energy Returned on Investment (EROI), shifting the focus toward system-level energy logic [113]. This study developed a mathematical framework for integrating EROI and ESOI to identify conditions under which energy storage is preferable to curtailment. Based on literature averages, the authors derived an inequality that predicts whether storage increases or reduces net energy return. In a representative case, photovoltaic (PV) systems with an EROI of 8 could benefit from battery storage, while wind systems with an EROI of 86 would require storage technologies with an ESOI exceeding 700, effectively restricting viable options to pumped hydro [113]. While this formulation provides a theoretical boundary for storage viability, it omits practical considerations such as inverter efficiency, grid constraints, and real-world load dynamics, limiting its relevance for community-scale microgrids.

Table 2-5: Summary of key studies assessing life-cycle energy performance in hybrid renewable systems, highlighting EROI, ESOI, and curtailment-related outcomes across scales. Abbreviations: Li-ion = Lithium-ion Battery, PHS = Pumped Hydro Storage, CAES = Compressed Air Energy Storage, RHFC = Regenerative Hydrogen Fuel Cell, PtG = Power-to-Gas, EROI = Energy Return on Investment, ESOI = Energy Stored on Energy Invested, VRE = Variable Renewable Energy.

Ref	Study	Storage Type	Application Scale	Metric Evaluated	Base EROI	EROI with Storage	ESOI Mentioned	Curtailment Scenario Considered	Key Takeaways
[114]	Davidsson Kurland & Benson (2019)	Lithium-ion Battery	Residential	EROI	14–27 (PV- only)	Decreased by >20%	Implicit (Battery Production Energy)	Yes	Storage increases self-con- sumption but reduces overall EROI; in curtailment scenarios, EROI can fall as low as 7
[113]	Barnhart et al. (2013)	Batteries (Li-ion, PbA, NaS), Pumped Hydro (PHS), Compressed Air (CAES)	Grid-scale	EROI + ESOI	PV: ~8; Wind: ~86	PV improves; Wind decreases unless using high-ESOI storage like PHS	Yes – detailed for each technology (Li- ion: 32, NaS: 20, PHS/CAES: ~700– 800)	Yes	Developed inequality showing when storage is preferable; PV supports even low-ESOI stor- age, wind requires high-ESOI like PHS
[55]	Pellow et al. (2015)	Regenerative Hydrogen Fuel Cell (RHFC)	Grid-scale (Wind/PV overgeneration mitigation)	ESOI, Round- trip Efficiency, EROI_grid	PV: 8, Wind: ~86	PV: maintained/improved, Wind: reduced unless high ESOI <sub>e</sub> storage used	RHFC: 59, Li-ion: 35, PHS: 830, CAES: 1100	Yes, directly compared using derived inequality	RHFCs outperform batteries in ESOI <sub>e</sub> but lag in round-trip effi- ciency; suitable for PV curtail- ment recovery, less so for wind.
[115]	Ghiassi- Farrokhfal et al. (2014)	Li-ion, PbA, CAES	Grid-scale (RE farms)	EROI	PV: 9, Wind: 18	Varies by tech: PbA < baseline, Li-ion/CAES > baseline	Implicit via storage parameters	Yes (access line capacity constraint)	PbA often lowers EROI; Li-ion and CAES improve it; solar re- quires more grid capacity to stay above the net-energy cliff
[116]	Limpens & Jeanmart (2018)	Battery, PHES, PtG	National grid (Belgium)	Gross and Net EROI	~11 (wind), ~7 (PV)	Down to 5.37	22–36 (batt), ~700 (PHES)	Yes, opti- mized ~3.5%	Storage-heavy 100% RE drops EROI; PtG needed beyond 40% RE
[117]	Palmer (2017)	Li-ion, PHS	Grid-scale (ERCOT)	EROI	~20–30	Li-ion: 0.8 at 60% VRE; PHS: ~7.2 at 60% VRE	Implicit via embodied energy	Yes (captured via storage, VRE surplus)	PHS is energetically viable at high VRE levels; Li-ion loses viability quickly as VRE share grows.
[118]	Dumas et al. (2022)	Multiple (battery, power-to-gas, etc., implicitly via system modelling)	National (Belgium, 2035 energy system)	EROI	8.9	3.9 (when GHG targets are most stringent)	No	Yes (curtail- ment affects storage and import deci- sions)	Demonstrates how deep decar- bonization reduces system-wide EROI; imported renewable gas significantly affects EROI varia- bility; highlights trade-offs in net energy vs. emissions goals.
[119]	Kittner et al. (2016)	Mini hydro and PV hybrid systems in Thailand	Community-scale mini-grid (village- level)	EROI	Hydro: 41–78 (up to 145–284 with extended life), PV: 6–30	Hybrid mini-grid: 21–62	No	Indirectly, via integration of PV with hydro	Demonstrates that hybrid mini- grids can rival or exceed fossil grid EROI; rich in empirical data but limited treatment of load vari- ability and network dynamics.
[112]	Barnhart & Benson (2013)	Li-ion, NaS, PbA, CAES, PHS	Grid-scale	ESOI	Not used directly	N/A	Yes (2-100+)	No load model; yes curtailment	ESOI highlights energy-intensity gaps between battery and geo- logical storage; long cycle life critical for viability
[120]	Clerjon & Perdu (2018)	Li-ion, PHS, CAES, P2P	National (France) grid	ESOI by time scale	Not single- valued	Time-scale dependent	Yes (per device)	Indirect via re- sidual de- mand smooth- ing	ESOI > 1 for Li-ion (hours– days), PHS (days–weeks), P2P (seasonal) if H <sub>2</sub> storage is free

To address temporal variability and storage applications across different timescales, a step forward was taken in [120], where a frequency-domain decomposition of residual demand was introduced. The authors applied Haar wavelet decomposition to four years of residual demand data (load minus variable renewables), breaking it into seven-time bands ranging from 45 minutes to one year. For each band, they extract three sizing metrics, peak power, energy capacity and cycle count, and use these to size storage options and compute ESOI ratio. Their dynamic ESOI profiles show that lithium-ion batteries peak at sub-daily scales (up to ESOI 8.0 in the hybrid mix), pumped hydro excels at weekly scales (up to ESOI 7.2 in the wind mix), and power-to-gas-to-power becomes competitive at multi-day to seasonal scales (up to ESOI 4.5 in the hybrid mix). Despite these valuable insights across hourly to seasonal scales, their analysis does not include detailed dispatch modelling or local network constraints, both of which are critical for community-scale applications.

While wavelet analysis mapped storage technologies to temporal bands, more granular operational realism was introduced in [115], where physical constraints such as power limits, degradation, and export caps were embedded into ESOI-aware dispatch modelling. The authors evaluated the impact of energy storage on the life-cycle energy return of a 3 MW windsolar farm by imposing a fixed export limit on the feeder; any generation above this cap was diverted into storage [115]. Using a recursive state-of-charge model that captures limits, round-trip efficiency, charge/discharge power self-discharge losses, depth-of-discharge constraints, they calculate system EROI as the long-term ratio of total delivered energy (direct generation to be exported plus discharged from the battery) to the embodied energy invested in both the PV farm and storage [115]. For a 10 MWh storage system, they demonstrate that lithium-ion batteries elevate the farm's EROI above the critical threshold of 8 when the export limit is approximately 0.5 MW for wind and 0.9 MW for solar; compressed-air storage yields comparable gains, whereas lead-acid batteries never exceed an EROI of 8 under realistic export constraints. Although this work accurately captures storage physics (power limits, efficiencies, and cycle life) and applies export-or-curtailment logic at the grid scale, it does not model how stored energy could be dispatched into community loads [115].

Yet, the framework in [115] abstracted away from long-duration storage. In contrast, [55] shifted focus to seasonal balancing, comparing hydrogen, batteries, and pumped hydro across daily and multi-month surpluses. A net-energy framework was adopted to evaluate regenerative hydrogen fuel cell (RHFC) systems against lithium-ion batteries and pumped hydro storage for both daily and seasonal applications. In a reference case with a wind farm generating 5 MW of surplus power for eight hours per day, the authors sized an RHFC system comprising a 5 MW electrolyser, a 2.6 MW fuel cell, and 84 MWh of hydrogen storage, yielding

an ESOI of 59, compared to 35 for lithium-ion batteries and approximately 830 for pumped hydro storage. When scaled to handle four months of surplus electricity, the RHFC's ESOI dropped into single digits with steel tanks, though improved to about 78 when using underground salt caverns [55]. These results effectively capture the energy trade-offs and round-trip efficiency penalties of hydrogen-based seasonal storage. However, the model in [55] assumes a constant daily overgeneration profile and idealised storage durations, omitting real-world load variability, dispatch constraints, and temporal resolution, thus offering useful conceptual insight but lacking the operational depth required for practical community-scale hybrid energy systems.

Building on these system-scale insights, a study re-centred the analysis on household-scale PV-battery systems, highlighting how storage oversizing erodes EROI even under modest self-consumption improvements [114]. They evaluate the energy impact of integrating a 12-kWh lithium-ion battery with a 6 kWp residential PV system using hourly SAM simulations across five U.S. climates. In a "grid-available" case all excess PV is exported to an assumed infinite sink, whereas in a "curtailment" case surplus must charge the battery or be lost. In their work, system EROI is defined as the lifetime ratio of delivered electricity (direct load/export + battery-discharged) to embodied energy inputs for PV and battery components [114]. Results highlight that adding the 12 kWh battery boosts self-consumption from 40–66% to 72–93% but lowers EROI by 21% (27 to 21 in Arizona) and by 50% (14 to 7 in Alaska) under curtailment; doubling to 24 kWh further cuts EROI by 34% due to poor utilisation of oversized storage. While the study offers valuable insights into the autonomy–EROI trade-off across climates, its simplified demand representation and absence of grid-export constraints limit its applicability to more complex, community-scale systems [114].

Moving beyond residential systems, [119] evaluated real-world micro-hydro and PV projects in Thailand, comparing empirical life cycle EROI values and showing how hybridisation affects overall system energetics. They apply a comprehensive life cycle EROI framework to five runof-river mini hydro plants (1.15–5.1 MW each) in northern Thailand and to a 3 MWp grid-connected solar PV system modelled in PVSYST, compiling embodied energy inputs for manufacturing, operation, and other phases over each technology's lifespan [119]. They calculate EROI as the ratio of total lifetime electricity output to the sum of all energy investments, finding that mini hydro plants deliver EROI values between 41 and 78 under base assumptions, rising to 145–284 if plant life is extended to 100 years and transport energy halved, while PV systems range from 6–12 for crystalline modules to 11–30 for amorphous silicon [119]. When these resources are combined in hybrid mini-grid scenarios with PV contributing 20–50% of annual generation, the overall mini-grid EROI falls into the 21–62 range, rivalling or exceeding that of conventional coal-based grids (EROI ≈ 46). While the

study offers detailed life cycle accounting at the village scale, its treatment of local demand and network dynamics is simplified, limiting its ability to fully capture operational realities in community-based systems.

While authors in [119] used real-world infrastructure data, [117] returned to a modelled approach, introducing a reliability-constrained system EROI framework that captures diminishing returns from increased storage capacity. They build a system level framework tying net energy accounting to reliability by defining inclusive EROI as gross lifetime energy from renewables plus storage divided by their embodied energy, aligned with a loss of load expectation (LOLE) of 0.1 days per decade [117]. Using three years of hourly loads (2010-2012) and wind/solar profiles, they runs a capacity expansion and dispatch model that minimises using linear programming embodied energy under hourly balance, state of charge dynamics and reliability constraints, drawing inputs from assumed EROI ratios (30 wind, 25 PV) and energy intensities (400 MJ/kWh PHS, 960 MJ/kWh Li ion) [117]. The EROI curves show steeply diminishing returns: early storage yields high marginal gains but beyond modest renewable shares storage's embodied energy drags system EROI below practical thresholds, for instance 7.2 with PHS and 0.8 with Li ion over fifty years. Despite its rigor, the model abstracts from local grid dynamics and assumes uniform reliability constraints, making it less suited for capturing the operational diversity and control needs typical of community-scale systems.

However, the model in [117] was still limited in spatial detail. Researchers in [116] introduced a geographically resolved, hourly-optimised national model, illustrating how high renewable shares drive down net EROI without diverse storage. They build an hourly-resolution, cell-based linear optimisation model of the Belgian electricity system, split into mainland and offshore cells, to size and dispatch a mix of PV, wind, batteries, PHS and power-to-gas (PtG) to maximise net EROI [116]. The model's decision variables include hourly power flows (generation, storage charge/discharge, imports/exports) and installed capacities (PV, wind, batteries, PHS, PtG), while constraints enforce hourly energy balance, transmission and pipeline capacities, storage state-of-charge dynamics (round-trip efficiency, power limits, depth-of-discharge, self-discharge, cycle life), minimum PtG capacity factor, and periodicity of storage (start-end SoC match) [116]. They distinguish gross EROI, total renewable generation including curtailed energy over embodied energy of renewables, from net EROI, which subtracts the energy costs and losses of storage and curtailment and cast EROI maximization as a linear program. Applied across scenarios from 10 % to 100 % renewable share (with imports fixed at 10 %), the optimised net EROI falls by up to 50 % as storage and curtailment grow, batteries driving the steepest decline, while a diverse storage portfolio becomes indispensable beyond = 40 % renewables [116]. While this top-down approach offers valuable

insights into system-level energy return dynamics, its spatial and operational abstractions limit its resolution for analysing the finer-grained, context-specific behaviours of community-scale hybrid systems. Notably, as in [111], [116] evaluate storage options in isolation, examining batteries, PHS and PtG individually, rather than exploring potential synergies from their simultaneous deployment.

Finally, the work in [118] built upon this with a full-sectoral model that directly embeds EROI into a national-scale optimisation, marking the methodological frontier, though at the cost of sub-hourly resolution and community-level relevance[118]. Their study represents a comprehensive endpoint in this review. They embed EROI directly into a comprehensive, multi-sector, hourly-resolved optimisation of Belgium's entire energy system, thereby combining the temporal granularity seen in earlier power farm and microgrid studies with national-scale scope. By framing their model as a linear program that maximises final-stage EROI under real-world constraints, hourly balances, storage dynamics, emissions caps, and technology limits, they show how deep decarbonisation decisions (e.g. importing renewable gas) can halve system EROI even while satisfying service demands [118]. A global sensitivity analysis reveals that imported renewable gas accounts for over two-thirds of the uncertainty in system EROI, and that cutting emissions by 80% reduces it from 8.9 to 3.9, suggesting potential socio-economic implications of deep decarbonisation. However, like other top-down models, it abstracts away sub-hourly operational dynamics and local grid constraints that are vital for distributed energy systems [118]. As such, it illustrates the potential of integrating net energy metrics into whole-system planning, while also indicating the relevance of complementary bottom-up models to resolve the local dynamics essential for community-scale systems.

The reviewed studies collectively trace the methodological evolution of life-cycle energy metrics from static, device-level ratios to increasingly integrated, system-wide evaluations. Early work introduced ESOI as a benchmark for comparing storage technologies [112], while subsequent research extended this concept by linking it analytically to generator EROI [113]. However, both relied on static assumptions and excluded dynamic operational features such as curtailment, inverter losses, or dispatch flexibility.

The field advanced by decomposing residual demand into temporal bands, aligning ESOI to the time scales best served by specific storage types [120]. Further developments incorporated sub-hourly dispatch constraints, and round-trip efficiency, illustrating how export-limited systems dynamically alter EROI [115]. Seasonal hydrogen-based storage was introduced, showing that ESOI collapses under long-duration assumptions unless supported by low-energy-intensity storage such as hydrogen underground salt cavern [55]. Then authors

in [114] demonstrated how oversizing storage in residential PV-battery systems reduces EROI, especially under curtailment. Further scaling the scope, [119] calculated empirical life cycle EROIs for real-world hybrid mini-grids in Thailand, while [111] introduced system-level EROI linked to reliability constraints, revealing diminishing returns as storage capacity expands. [116] embedded net EROI into a national linear optimisation model, and [118] extended this by integrating final-stage EROI into a multi-sector MILP for Belgium under emissions constraints.

Collectively, the reviewed studies demonstrate a gradual shift in the application of life-cycle energy metrics, from static, technology-specific indicators to more integrated, system-level evaluations. Nonetheless, most applications treat EROI and ESOI as static outcome metrics, typically calculated after fixed system designs are established, rather than as tools for exploring trade-offs or informing iterative design adjustments within broader techno-economic planning frameworks. Operational factors such as inverter sizing, contracted grid exchange limits, and temporal resolution are often treated simplistically or omitted entirely. Moreover, existing work tends to examine storage technologies independently, evaluating batteries or hydrogen systems separately, rather than analysing their combined use within hybrid configurations. Few studies assess how different energy storage pathways interact with curtailment, grid exports, or demand patterns to shape overall energy life cycle costing performance. The next section discusses the knowledge gaps that must be addressed to fully align energy metrics with the operational and planning needs of community-scale hybrid renewable systems.

# 2.6 Literature Gap

The literature on HRES, particularly those integrating battery and hydrogen storage, has advanced significantly in terms of optimisation algorithms, operational strategies, and energy sustainability metrics. However, several methodological limitations persist and continue to affect the practical relevance and applicability of most frameworks, especially in community-based and islanded contexts with complex operational constraints.

A notable shortcoming is the static treatment of inverter sizing and contracted grid power. In several studies, including [86], [87], [88], inverter capacities are fixed during design-phase optimisation, without being dynamically linked to system costs or grid interaction dynamics. Even in detailed MILP-based models such as those in [43] and [98], inverter constraints are simplified to infinite throughput or constant efficiency penalties without accounting for clipping losses or cost-driven trade-offs. Contracted grid power is similarly simplified; for instance, [69] assumes an unconstrained grid exchange, neglecting real-world cost penalties and capacity limits. Even when grid contracts are considered, such as in[70], they are only evaluated after

the optimisation, rather than being embedded within the optimisation framework. This disconnection can lead to PV oversizing or underestimation of curtailment, reducing the practical value of the derived system configurations.

Operational dispatch modelling also remains predominantly static. Several studies, including [90], [89], and [88], apply heuristic dispatch logic, which cannot adapt to load variability and renewable generation availability. Although more advanced control strategies are evident in the works of [104] and [105], these remain uncommon. Even when predictive frameworks like MPC are employed in system sizing, integration with load shifting or demand response remains limited, as demonstrated by [43], where it was applied only in an off-grid system. Consequently, most models limit the ability to capture the potential of flexible loads to reduce peak demand or storage requirements, especially under tariff-driven operating constraints.

Hybrid storage dynamics are often oversimplified. While many studies simulate battery-hydrogen combinations, their interactions are usually modelled on a common DC bus or through idealised converters. The works by [99] and [86] use simplified energy balances where AC and DC flows are aggregated, omit AC/DC prioritisation and dynamic switching, or inverter constraints. Even in multi-bus frameworks like those of [103], nodal interactions are treated abstractly, and inverter capacities are not co-optimised across storage pathways. This abstraction may reduce the fidelity of dispatch simulations, particularly for systems that rely on dynamic switching between battery and hydrogen storage to cover short- and long-duration deficits.

Further, life-cycle energy performance metrics such as EROI and ESOI are typically derived from fixed system designs, with minimal operational coupling. Similar studies like [55], [112], [117] present valuable methodologies but apply them under idealised load and generation profiles. Researchers in [115] made important progress by incorporating grid export constraints and battery degradation, but even this work isolates storage dynamic dispatch decisions. Similarly, while [114] demonstrate how storage oversizing can reduce EROI, but do not link these outcomes to dispatch or grid constraints. As a result, energy return metrics are often used as post-optimisation diagnostics rather than being integrated into design decisions, limiting their utility for real-world HRES planning.

Across these themes, there is a clear convergence of gaps: inverter sizing is often omitted or simplified; grid contracts are rarely embedded within the optimisation loop; operational control remains predominantly heuristic; and energy performance metrics are decoupled from system dynamics with hybrid storage streams. These limitations are particularly consequential for small-scale, islanded, or tariff-sensitive communities, where marginal changes in design or dispatch can yield outsized impacts on reliability and cost. This thesis addresses these

limitations by proposing a unified optimisation framework that embeds inverter sizing, grid constraints, and adaptive dispatch into both techno-economic and energy return evaluations, tailored specifically to the operational and planning realities of community-scale hybrid renewable systems.

In summary, the key knowledge gaps identified in the literature include:

- The absence of explicit inverter sizing co-optimisation within integrated sizing and dispatch frameworks.
- Inadequate integration of contracted grid exchange constraints and dynamic tariff structures into optimisation routines.
- The limited integration of rolling-horizon dispatch strategies, including flexible load management within system sizing frameworks.
- Insufficient modelling of AC/DC nodal behaviour and hybrid battery-hydrogen storage interactions at operational time scales.
- The use of static EROI and ESOI metrics that are not dynamically integrated into energy dispatch and planning models with hybrid storage streams.

These gaps collectively underscore the necessity for a comprehensive, integrated methodological framework. The subsequent chapters in this thesis propose and validate novel strategies explicitly designed to simultaneously resolve these gaps, enabling the practical deployment of effective, sustainable, and economically viable hybrid renewable energy solutions in island-based communities.

# 3 System Sizing of Renewable Fuel Cell Battery Storage Systems with Hourly Dispatch Optimisation

# 3.1 Introduction

This chapter presents a novel approach for sizing and operating renewable-based hybrid energy systems, using a nested Genetic Algorithm (GA)–Mixed Integer Linear Programming (MILP) framework. Building on the foundations of optimisation techniques introduced in Chapter 2, here the GA conducts a global search over potential capacities, photovoltaic (PV), battery banks, and fuel cells, while the MILP subproblem enforces realistic hour-by-hour dispatch constraints across a full year. Combining a high-level search with thorough operational cycles helps the layered approach to find reasonably priced system designs that is applied on real-world case study of resource and load patterns.

The chapter compares this annual GA-MILP approach versus two often used, shorter-horizon approaches. First is a straightforward rule-based load-following scheme, which makes reactive decisions using local hourly steps only. Second is the well-known HOMER Pro tool, widely used in microgrid planning. These comparisons offer perspective on how long-horizon foresight compares to simpler, hour-to-hour logic. Recognising that an annual, single-horizon view can be optimistic in practical terms, because real systems often operate with rolling forecasts or limited foresight, this framework is further improved in Chapter 4.

# 3.2 System Description and Governance

## 3.2.1 Physical Configuration of the REC

The integrated energy system presented in Figure 3-1 is designed to combine renewable energy production assets focused on PV, and hybrid energy storage units at the community level with a connection to the grid at a nodal or transformer level. Three main power flow types of DC power, AC power, and Hydrogen Energy flows are distinguished through different colours in the figure. On the DC side, the PV system, battery, and PEM fuel cell are connected to a common DC bus whose power is balanced on the DC bus at each time step with the ability to invert from DC to AC when required (one direction). On the AC side, the grid interacts bidirectionally with the AC bus, enabling energy exchange based on the load demand, generation, and storage conditions, while also responding to a typical six-period tariff structure. Different physical constraints, such as maximum contracted power and the three phases being equally balanced since power levels are high, are represented in this study as aggregated power. On the hydrogen side, the electrolysers are powered with AC electricity converting power to hydrogen to store in a hydrogen tank that has a regenerative hydrogen design, feeding this stored hydrogen to the fuel cell when needed. The complex energy system requires accurate modelling of the physical system behaviour, constraints, and technical and economic performance of an optimisation problem, to ensure precise planning for energy communities and accurately gauge investment scales.

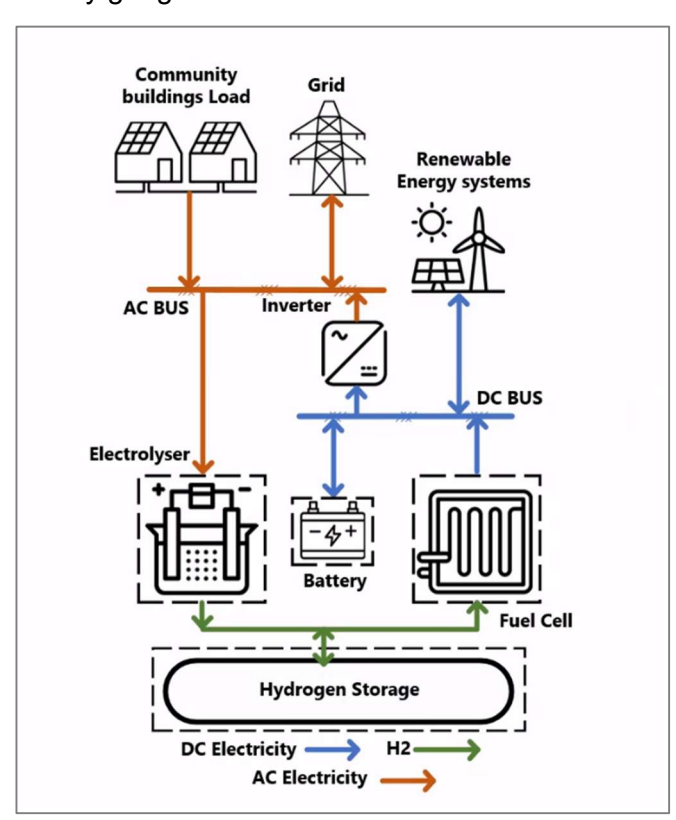


Figure 3-1: Energy flow for the integrated hybrid energy system and its energy vector.

### 3.2.2 Governance, Contracted-Power Limits, and Tariff Context

All distributed energy resources (DER), building-mounted PV arrays, the communal lithiumion battery, electrolyser, and fuel-cell are dispatched by a single centralised community-level Energy Management System (EMS). The EMS executes the MILP schedules generated by the optimisation engine, refreshes forecast each hour, and issues set points to inverter and BESS controllers. In regulatory terms, the EMS functions as the aggregator under Spain's Royal Decree 244/2019 (Art. 11), which enables collective self-consumption and surplus compensation for organized communities [121], [122], [123]. Physically, the Renewable Energy Community (REC) is grid-connected at a single point-of-common-coupling (PCC) on the low-voltage side of transformer. All community participant buildings share this PCC, which is constrained by a contracted power limit  $P_{gr}^{\max} \in [50,100]$  kW that the MILP selects to minimise the overall NPC, subject to the step-wise access-charge schedule in 3.3.2.2.

Because the optimiser restricts  $P_{gr}^{\max}$  to values below 100 kW, the REC remains in the simplified collective self-consumption export bracket [121]. Any surplus is credited by the supplier/retailer at the applicable price (0.051  $\in$ /kWh reference value here), capped each billing period (monthly) by the energy imported in that same period. There is no carry-over of credits between periods. The DSO provides metering and allocation to participants; settlement is performed by the supplier, as shown in Table 3-1. The MILP enforces that cap for both import and export and prices energy using the six-period 3.0 TD tariff that is explained in section 3.4.2. Although the present study is a planning and sizing exercise, it incorporates detailed operational constraints to ensure that the chosen capacities are technically feasible under real dispatch conditions. Internal trading layer is treated as a virtual ledger applied as described in the energy community definition in section 1.2; because it does not influence technical dispatch and sizing at community scale, it is kept outside the MILP to avoid combinatorial growth, a structure consistent with Spanish LEC pilot projects [124], [125], [126]. With the physical architecture and regulatory boundaries established, the next section compares alternative sizing-and-dispatch strategies that operate within these constraints.

Table 3-1: Key Operational Assumptions and Regulatory References for REC Model

Element	Specification in Model	Purpose / relevance	Regulatory [Ref]	
Controller type	Centralised community EMS	Single decision-maker	_	
A maramatar rala	EMS as REC representative; supplier settles	Manages grid contracts and	DD 244/2040 A# 44 [424]	
Aggregator role	compensation, DSO handles metering/allocation	surplus credits	RD 244/2019 Art. 11 [121]	
Grid interface	One PCC, bidirectional smart meter on LV side	Defines where imports/exports are	UNE EN 50549 1 / general PCC	
Grid interface	One PCC, bidirectional smart meter on EV side	constrained	definition [127]	
Contracted limit	Optimised variable, range 50–100 kW	Keeps REC ≤ 100 kW for simplified	RD 244/2019 Art. 4 [121]	
Contracted little	Optimised variable, range 50–100 kW	compensation	RD 244/2019 AIT. 4 [121]	
Tariff class	Six-period 3.0 TD tariff for imports	Mandatory threshold > 15 kW	CNMC Circular 3/2020 [128]	
Surplus	Simplified compensation at 0.051 €/ kWh (2022	Provides realistic export pricing	PD 244/2010 Art 7 [121]	
remuneration	average), capped at annual imports	Frovides realistic export pricing	RD 244/2019 Art. 7 [121]	

# 3.3 Comparative Methods for Dispatch and Sizing

### 3.3.1 Overview of Comparative Framework

In this section, a detailed structure of the energy system including PV systems, batteries, and fuel cells is presented. These components are modelled to facilitate realistic, grid-connected operational strategies for commercial microgrids. Figure 3-2 shows the optimisation approach

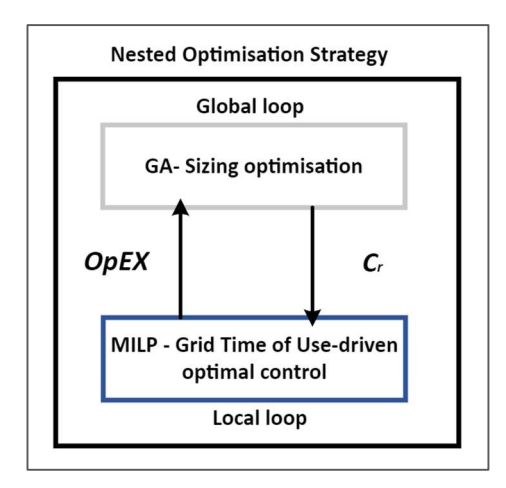


Figure 3-2: Nested optimisation approach with progressive parameter adjustment

where the global search for the minimum Net Present Cost (NPC) interacts with the local loop by passing different component sizes  $C_r$  to find the minimum grid operation OpEX.

For a thorough evaluation in this section, two different energy management (local loop) methods are compared:

- 1. **GA-Yearly Horizon:** Single-year, hourly energy management unit commitment.
- 2. **GA-Load Following (Rule-based)**: Utilises GA with traditional load-following, rule-based energy management validated with HOMER Pro.

The Load Following method adopts a rule-based, heuristic approach to energy management. It relies on predefined operational logic to make decisions based on the current state of generation, demand, and storage at each time step. The method prioritises local energy consumption, followed by battery usage, hydrogen conversion, and grid exchange, depending on resource availability. In contrast to the GA-Yearly Horizon method, this approach does not incorporate long-term optimisation but operates reactively in hourly increments. While it offers a simpler and more intuitive control structure, it may not capture potential cost-efficiency improvements that could arise from long-horizon coordination. To facilitate validation and benchmarking, this method is implemented in Python and cross-compared using HOMER Pro, a widely recognised microgrid simulation tool.

# 3.3.2 GA-Yearly Horizon Method

A layered bi-layer optimisation strategy was developed, combining a GA with MILP to optimise an energy system over a single year. Figure 3-3 illustrates the flowchart of the proposed layered optimisation framework. In the global loop, the GA generates a population of candidate solutions at each generation, where each individual encodes capacity values for system components, solar PV, battery storage, contracted power, and inverter systems, treated as decision variables. These capacity sets are passed to the MILP-based local loop, which performs hourly dispatch optimisation over a single representative year. The MILP determines optimal hourly scheduling decisions by minimising operating costs while satisfying system constraints under a six-period time-of-use tariff. It models energy flows among generation sources, storage units, and grid interaction to meet the hourly electrical demand. The MILP returns performance indicators, including energy shortages and curtailment, which are used to assess the feasibility and efficiency of each GA-generated configuration. Following MILP convergence, the GA evaluates each individual's fitness based on a full 25-year discounted cash flow analysis. Although the MILP simulates only a single representative year, its outputs, hourly energy balances, grid usage, and storage behaviour, are extrapolated over the project horizon. This allows the GA to estimate Net Present Cost (NPC) and Levelized Cost of Electricity (LCOE) while iteratively refining system capacities to converge toward a technically robust and economically optimal configuration. Although the MILP evaluates system performance over a single representative year, this annual operation is assumed to repeat consistently over the full 25-year project horizon. This assumes load and generation patterns are statistically representative and remain stable over time a simplification that balances fidelity and computational demands. This approach effectively decouples long-term investment planning from short-term operational optimisation, enabling a practical trade-off between dispatch resolution and computational tractability. In this study a population-based Genetic Algorithm is used as the global optimiser for capacity sizing. Population search samples multiple attraction basins in parallel, while selection, crossover and mutation progressively assemble high-performing gene combinations. Classical schema results explain why short, fit building blocks tend to proliferate under moderate variation, and evolutionary algorithms converge in probability to globally optimal solutions under mild conditions when computational effort is unbounded. In practice, near-optimality is achieved by maintaining diversity, preserving elites, and coupling the GA to a deterministic MILP evaluator that provides stable, near-optimal dispatch costs within a solver tolerance. This coupling reduces fitness noise and improves selection decisions, so the outer search intensifies around genuinely good designs rather than artefacts of noisy evaluation. The following section

presents the implementation details of the GA global loop, including its objective function, decision variables, and the financial modelling structure.

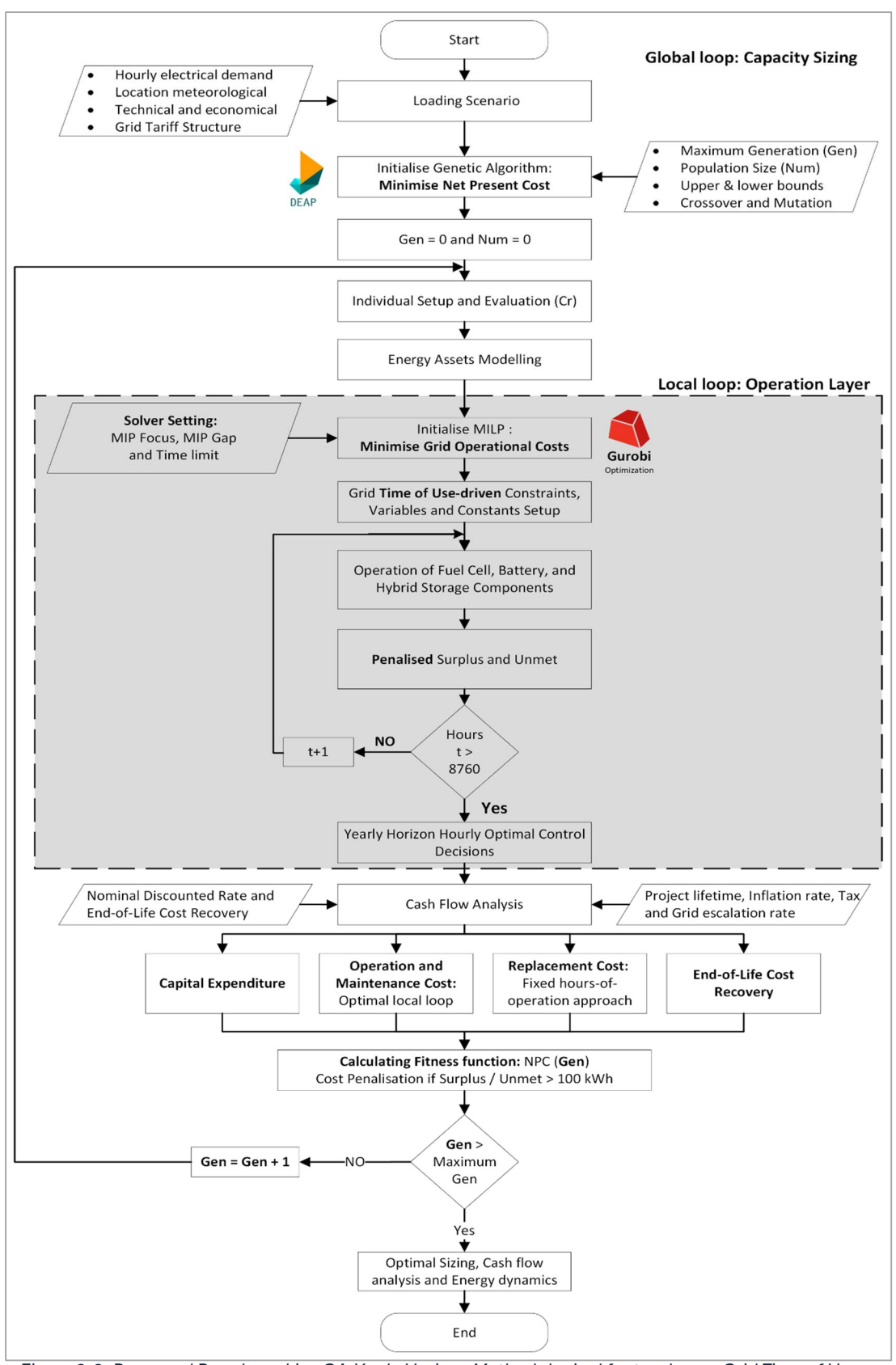


Figure 3-3: Proposed Benchmarking GA-Yealy Horizon Methodological for two layers Grid Time of Use driven Optimisation approach. The detailed algorithm implementation is provided in Appendix 9.2.

#### 3.3.2.1 Genetic Algorithm (GA): Upper Loop for Capacity Sizing

This study employs a comprehensive 25-year cash flow model that accounts for capital investment, grid operating expenses, maintenance, component replacement, and salvage value for the hybrid energy system. Grid prices are escalated annually over the 25-year planning horizon to reflect realistic operational cost trends. To evaluate the present value of future cash flows, all costs and revenues are discounted using a real discount rate derived from the nominal interest rate and expected inflation. The optimisation process uses NPC as the primary objective function, guiding the search for the most cost-effective system configuration. Following optimisation, the LCOE is calculated as a secondary financial metric to assess the economic performance of the resulting design. Together, this cash flow analysis provides a comprehensive basis for financial evaluation in community-scale energy systems.

Metaheuristic methods such as Particle Swarm Optimisation (PSO) and GAs are often used because their resilience in generating global solutions for complicated, nonlinear problems, such as those found in to the system modelling and cashflow analysis generated [129], [130]. In this study, a single-objective GA is implemented to minimise the NPC of the energy system. The algorithm is developed using DEAP (Distributed Evolutionary Algorithms in Python), an open-source Python framework for evolutionary computation. DEAP has been widely applied in energy system optimisation, including in [131], [132], [133]. The GA performs a global search across capacity sizing variables and evaluates each candidate's NPC to identify the most cost-effective configuration. Guided by principles of natural selection, the GA operates as the upper-level loop in the optimisation framework. Equation (3-1) defines the GA decision variables as follows:

$$C_r = [P_{PV}, N_{bt}, P_{inv}, P_{gr}, P_{fc}, P_{el}, P_{HT}]$$
(3-1)

Where  $P_{PV}$  is the photovoltaic capacity in (kW),  $N_{bt}$  is the number of battery modules, each with a commercially available capacity of 4.8 kWh,  $P_{inv}$  is the inverter capacity in kW,  $P_{gr}$  is the maximum power that can be bought or sold to the grid in kW,  $P_{fc}$  is the fuel cell electrical power output in kW,  $P_{el}$  is the electrolyser electrical power input in kW, and finally  $P_{HT}$  is hydrogen tank capacity in kg. The GA fitness function minimises the net present cost of the system during the project's lifecycle and its calculated using the equation (3-2):

$$Minimise\ C_{NPC} = \sum_{k \in Cr} \sum_{t=0}^{R_{proj}} \left( CapEX_{k,t} + OpEX_t + RepEX_{k,t} - RecVal_{k,t} \right) \cdot D_t$$
(3-2)

Where  $C_{NPC}$  is the total net present cost of the system, expressed in euros ( $\in$ ), accumulated over the entire project duration defined by  $R_{proj}$  years,  $CapEX_{k,t}$  represents the capital

expenditure for component at time t,  $OpEX_t$  is the operational expenditure at time t, including maintenance,  $RepEX_{k,t}$  is the replacement expenditure; and  $RecVal_{k,t}$  denotes the recovery (salvage) value of component k near the end of the project.  $D_t$  is the discounted factor at time t. The cash flow analysis is computed for each component k over each year t of the project. The discount factor  $D_t$  is calculated using the following equation:

$$D_t = \frac{1}{(1+i)^t} {(3-3)}$$

Where the discounted factor at time t is calculated for each year, i is the real discount rate considering inflation rate. The real discounted rate i is calculated using the following equation:

$$i = \frac{i' - f}{1 + f} \tag{3-4}$$

Where i' is the nominal discounted rate and f is the expected inflation rate. The capital recovery factor CRF is calculated using the following equation:

$$CRF = \frac{i \cdot (1+i)^{R_{proj}}}{(1+i)^{R_{proj}} - 1}$$
 (3-5)

Where the CRF is used to convert NPC to annualised payments. Near the end of the lifetime of the project, the recovery value of an equipment,  $R_v$  is considered and the following equation is used to calculate it:

$$R_v = C_{Rep} \frac{T_{rem}}{T_{com}} \tag{3-6}$$

Where  $C_{Rep}$  is the replacement cost of an equipment,  $T_{rem}$  is the component remaining life at the end of the lifecycle of the project, and  $T_{com}$  is the expected lifetime of the component. The levelized cost of electricity is calculated using the following equation:

$$LCOE = \frac{C_{NPC} \cdot CRF}{E_{load}}$$
 (3-7)

To enhance the financial analysis, two financial metrics are computed: Discounted Payback Period (DPP) and Internal Rate or Return (IRR). The DPP indicates the number of years required for the cumulative discounted cash flow difference between the base case and the optimised system to become positive. The IRR represents the discount rate at which the Net Present Value (NPV) equals zero, thereby reflecting the effective return on investment. A higher IRR suggests a more profitable project and serves as a key indicator of financial viability, particularly useful when comparing alternative investment options. The PV model is integrated into the GA upper loop and implemented in detail, with hourly solar generation

simulated for each candidate capacity configuration. This generation profile is passed to the MILP as available energy to be balanced against the load and storage components. In contrast, the operational behaviour of the electrolyser, fuel cell, battery, and hydrogen tank are modelled in the MILP operation layer using fixed component efficiencies. Each of these technologies is represented with a constant conversion efficiency (e.g., electrolyser, fuel cell, battery), where energy losses are applied deterministically at each hour based on defined rates. A full description of MILP operations and component modelling is provided in section 3.3.2.2.

The PV array output every time step t is calculated using Duffie–Beckman model with temperature correction as follows [134]:

$$P_{PV-\text{ output }}[t] = P_{PV} f_{PV} \left( \frac{G_{module}[t]}{G_{T,STC}} \right) \cdot \left[ 1 + \alpha_P (T_c[t] - T_S) \right]$$
(3-8)

In this equation,  $P_{\text{PV-output}}[t]$  represents the actual electrical power output of the PV system at time step t. The term  $P_{PV}$  denotes the rated power output of the PV module under standard test conditions (STC), while  $f_{PV}$  is a system-wide derating factor accounting for losses such as soiling, shading, wiring resistance, and inverter inefficiencies. The variable  $G_{\text{module}}[t]$  is the effective solar irradiance incident on the tilted module surface, and  $G_{\text{STC}}$  is the standard irradiance under test conditions. The final bracketed term corrects for the impact of temperature on power output, where  $\alpha_P$  is the temperature coefficient of power,  $T_c[t]$  is the cell temperature at time t, and t is the reference cell temperature under STC. The model captures both irradiance-dependent scaling and temperature-induced deviations in panel efficiency. To determine t is the reflects the irradiance on the tilted plane of the PV module, the following transformation is applied to the global horizontal irradiance [134]:

$$G_{module}[t] = G_T[t] \cdot \frac{\sin(\alpha + \beta)}{\sin(\alpha)}$$
 (3-9)

Where  $G_T[t]$  is the global horizontal irradiance measured in kW/m<sup>2</sup> at time step t,  $\alpha$  is the solar altitude angle and  $\beta$  is the tilt angle of the single PV module. The solar altitude angle  $\alpha$  is itself computed based on the geographic location and time of year using the expression [134]:

$$\alpha = 90^{\circ} - \emptyset - \delta \tag{3-10}$$

Where  $\emptyset$  is the site's geographic latitude, and  $\delta$  is the solar declination angle, which depends on the day of the year, and it's calculated as following:

$$\delta = 23.45 \cdot \sin\left(\frac{360}{365} \cdot (284 + d)\right) \tag{3-11}$$

Where d is the number of the day of the full year, ranging from 1 to 365 days. The PV cell temperature  $T_c[t]$  at each time step is estimated using the following semi-empirical formulation [134]:

$$T_{c}[t] = \frac{T_{ambient}[t] + \left(T_{c,NOCT} - T_{a,NOCT}\right) \left(\frac{G_{module}[t]}{G_{NOCT}}\right) \left[1 - \frac{\eta_{mp,STC}\left(1 - \alpha_{P}T_{c,STC}\right)}{\tau\alpha}\right]}{1 + \left(T_{c,NOCT} - T_{a,NOCT}\right) \left(\frac{G_{module}[t]}{G_{NOCT}}\right) \left[\frac{\alpha_{P}\eta_{mp,STC}}{\tau\alpha}\right]}$$
(3-12)

Where  $T_{\rm ambient}$  [t] In this expression,  $T_{\rm ambient}$  [t] is the ambient air temperature at time t. The terms  $T_{c, \rm NOCT}$  and  $T_{a, \rm NOCT}$  represent the nominal operating cell temperature and corresponding ambient temperature under NOCT (Nominal Operating Cell Temperature) conditions, respectively.  $G_{\rm NOCT}$  is the reference irradiance used in NOCT testing procedures. The quantity  $\eta_{mp,\rm STC}$  indicates the module's peak power efficiency under standard conditions, and  $\alpha_P$  is the temperature coefficient of power, reflecting the sensitivity of power output to temperature deviations.  $T_{c,\rm STC}$  is the reference cell temperature at STC, and  $\tau\alpha$  encapsulates the combined effect of the module's optical properties, specifically transmittance and absorptance. This thermal model accounts for the non-linear dependency of module temperature on irradiance and provides a realistic estimation of cell temperature, which significantly impacts power generation accuracy.

Table 3-2 summarises the PV model parameter assumptions used in this work. Selection rationale varies by parameter type: industry-standard assumptions are used where high consensus exists (e.g., optical loss factor, derating factor); empirical approximations are used where grounded in prior system deployments (e.g., tilt angle = latitude); and manufacturer datasheets inform performance-related parameters (e.g., module efficiency, temperature coefficient). This mixed-source approach ensures realistic modelling while maintaining model transparency and traceability.

Table 3-2: Key design and standard parameters employed in the PV output and cell temperature modelling.

Sym- bol	Parameter	Unit	Value	Source	Source Type
$f_{PV}$	Derating factor	-	0.8	[135]	Industry default assumption
β	Panel tilt angle	Degrees	38.7	[136]	Empirical value
$\eta_{mp,STC}$	Module efficiency at STC	%	20	[137]	Manufacturer datasheet median.
τα	Optical loss factor	-	0.9	[42]	Industry default assumption
$\alpha_P$	Temperature coefficient of power	%/°C	-0.45	[138]	Industry default assumption

### 3.3.2.2 MILP for Hourly Dispatch Optimisation

The unit commitment problem is formulated as a MILP model to minimise operational costs at the lower optimisation layer of the GA–Yearly Horizon framework. The MILP model operates on a fixed hourly time step ( $\Delta t = 1 \, h$ ), meaning all energy flow quantities are expressed in kilowatt-hours (kWh). For consistency with the MILP literature, power-based symbols are retained under the assumption of consistent units across all hourly intervals. The model is executed over an annual time horizon  $t \in \mathcal{T}$ , encompassing hourly time steps denoted by:

$$\mathcal{T} = \{0, 1, 2, \dots, 8759\}$$

The objective of the MILP is to determine optimal dispatch decisions that minimise total gridrelated expenditures over the year. This includes electricity purchases from the grid, revenue from energy exports, and penalties associated with unmet demand or curtailed excess energy. The objective function is presented in equation (3-14) as follows:

$$\min_{\text{all variables}} \sum_{t \in \mathcal{T}} \left( \pi_{\text{buy}} \left[ t \right] \cdot P_{\text{grid, buy}} \left[ t \right] - \pi_{\text{sell}} \left[ t \right] \cdot P_{\text{grid, sell}} [t] + \text{ penalty }_{\text{unmet}} \right.$$

$$\left. \cdot E_{\text{unmet}} \left[ t \right] + \text{ penalty }_{\text{excess}} \cdot E_{\text{excess}} \left[ t \right] \right)$$

$$(3-14)$$

Where  $\pi_{\text{buy}}$  [t] and  $\pi_{\text{sell}}$  [t] represent the electricity buying and selling prices in  $\in$ /kWh, and  $P_{\text{grid, buy}}$  [t] and  $P_{\text{grid, sell}}$ [t] represent the respective power exchanges in kWh. The terms  $E_{\text{unmet}}$  [t] and  $E_{\text{excess}}$  [t] denote unmet load and surplus generation, which are penalised to discourage infeasible dispatch.

Slack penalties are applied in the objective to guarantee feasibility while strongly discouraging unmet demand and excessive curtailment. A penalty of  $1000 \, \in \, \text{kWh}$  is applied to unmet energy (  $penalty_{unmet}$ ), and  $100 \, \in \, \text{kWh}$  to excess generation  $E_{\text{excess}}[t]$ . These magnitudes were selected through a grid-sweep sensitivity analysis over both penalty types, tested on 21 deliberately stressed "edge-case" system designs. Edge cases push the MILP to invoke unmet or excess slack variables by constraining capacities to extreme but feasible levels (e.g., very low battery, undersized inverter, large PV with small hydrogen storage), thus revealing the minimum penalty values that still eliminate unnecessary slack use. Results Table 3-3 show that guaranteeing the minimum attainable unmet energy across all edge cases requires 1000 €/kWh, while only  $10 \, \in \, \text{kWh}$  is needed to achieve minimum excess. a ratio of 10:1 is retained between unmet and excess penalties, consistent with common MILP practice in energy and industrial optimisation [139], [140], by setting excess to  $100 \, \in \, \text{kWh}$ .

Table 3-3: Sensitivity sweep for penalty selection across 21 edge-case designs

Penalty type	Tested penalty range (€/kWh)	Edge cases (n)	Minimum penalty meeting all cases (€/kWh)	Cases meet- ing target at ≤ 1	≤ 10	≤ 100	Selected value (€/kWh)
Unmet energy	{0, 0.1, 1, 10, 100, 1000}	21	1000	3	3	5	1000
Excess energy	{0, 0.1, 1, 10, 100, 1000}	21	10	21	21	21	100

These penalty parameters steer the GA-MILP framework toward feasible and balanced system configurations by penalising excessive unmet demand or curtailment. After solving the annual dispatch problem, the MILP provides the GA with operational outcomes, specifically the total unmet and excess energy associated with a given capacity design. These outcomes reflect how well a candidate system can meet demand and utilise generation under real-world constraints. The GA then uses this feedback to evaluate fitness and iteratively refine its capacity choices, avoiding over- or under-sized systems. The specific thresholds and penalty values used to guide this process are detailed in the subsequent section 3.3.2.3 on penalty functions.

The energy balance constraint is formulated to ensure that at each time step t, the total energy generated through renewable systems such as PV and exchanged within the system equals to the energy consumed responding to the load, accounting for any unmet and excess energy. It meant to distinguish between AC and DC components connected through an inverter, ensuring accurate tracking of energy flows. The energy balance equation is formulated and designed to distinguish between AC and DC components connected through the decision variable of the inverter capacity as follows in equation (3-15) and (3-16):

$$\begin{split} P_{ren, \ DC \ inverted} \left[ t \right] + P_{ren, \ DC \ remaining} \left[ t \right] + P_{battery, \ discharge} \left[ t \right] + P_{fuel-cell} [t] \\ &- P_{battery, \ charge} \left[ t \right] - P_{inverter} \left[ t \right] \cdot \left( 1 + 1 - \eta_{DC/AC \ inverter} \right) \\ &- E_{\text{excess}} \left[ t \right] = 0 \ , \qquad \forall t \in \mathcal{T} \end{split} \tag{3-15}$$

$$P_{inverter}[t] + P_{grid\_buy}[t] - P_{grid\_sell}[t] - P_{load}[t] - P_{electrolyser}[t] + E_{unmet}[t] = 0,$$

$$\forall t \in T$$
(3-16)

Where the  $P_{ren,\ DC\ inverted}$  [t] is PV renewable generation that is consumed by AC load, or used to start the electrolyser, or sold to the grid, giving priority to responding community electricity demand first. Any remaining renewable generation at the same time step is represented as  $P_{ren,\ DC\ remaining}$  [t] which is available at the DC bus side that can be used either to charge the battery or recorded as excess.  $P_{grid,\ buy}$  [t] and  $P_{grid,\ sell}$ [t] capture the system interaction from external grid.

The objective function and the energy balance constraint overlaps with the grid interaction variables, and unmet and excess energy are recorded each time steps. Every time step t decision is driven by the objective and in compliance with this energy balance constraint. Similarly,  $P_{battery,\ discharge}$  [t] and  $P_{battery,\ charge}$  [t] represent the energy discharged and charged to the storage battery in kWh at time t.  $P_{fuel-cell}$ [t] and  $P_{electrolyser}$  [t] manages the electrochemical conversion of energy between electrical and chemical form of hydrogen in kWh at time t.The total electrical load represented by  $P_{load}$  [t] must be satisfied at each time step.  $\eta_{DC/AC\ inverter}$  is the inverter efficiency, set to 95 %.

Any excess that can't be utilised locally or be sent back to the grid is recorded as  $E_{\rm excess}[t]$ , while any shortfall in meeting this load is represented by  $E_{\rm unmet}[t]$ . These penalty terms, embedded in the MILP formulation, reinforce the objective function by discouraging configurations with frequent curtailment or unmet demand. This supports more balanced dispatch outcomes and enhances self-consumption and cost-effective grid interaction. In order for this energy balance constraints provide mutually exclusive interaction that replicates the physical behaviour, the grid interaction is constrained, limiting direction and maximum values in equations (3-17) and (3-18):

$$P_{grid, buy}[t] \le P_{gr}^{\max} \cdot x_{grid}[t], \quad \forall t \in \mathcal{T}$$
 (3-17)

$$P_{grid, sell} \le P_{gr}^{\max} \cdot (1 - x_{grid}[t]), \quad \forall t \in \mathcal{T}$$
 (3-18)

The energy system at a given time step t either can buy or sell, but not both, and is limited to the max contracted power  $P_{gr}^{\max}$ . The binary decision  $x_{grid}$  [t] governs the grid interaction in the power system acting like a switch helping in deciding the direction of the power flow between the grid and energy system. Similarly, the battery interaction constraints can either charge or discharge, but not both, and are limited to the allowable battery power as shown in equation (3-19) and (3-20):

$$P_{battery,charge}[t] \le P_b^{-\max} \cdot (1 - x_{battery}[t]), \quad \forall t \in \mathcal{T}$$
 (3-19)

$$P_{battery,discharge}[t] \le P_b^{+\text{max}} \cdot x_{battery}[t], \quad \forall t \in \mathcal{T}$$
 (3-20)

Where  $P_{battery,max}$  and  $P_{battery,min}$  are the allowed power for charging and discharging in kW at time t. The charging and discharging state of charge SoC [t] are limited to the allowed state of charge limits as following in equation (3-21):

$$SoC_{min} \leq SoC[t] \leq SoC_{max}, \quad \forall t \in \mathcal{T}$$
 (3-21)

Where  $SoC_{min}$  is the lowest state of charge that the battery is bounded to 5%, and  $SoC_{max}$  is the highest state of charge of 100%. Each time step, the battery State of Charge SoC[t] is calculated using this equation (3-22):

$$SoC[t] = SoC[t-1] + \left(\frac{P_{battery,charge}[t] \times \eta_{b-} \times 100}{N_{bt} \times B_{m}}\right) - \left(\frac{P_{battery,discharge}[t] \times 100}{\eta_{b+} \times N_{bt} \times B_{m}}\right), \quad \forall t \in \mathcal{T}$$
(3-22)

Where SoC[t-1] is the state of charge for the previous time step,  $\eta_{b-}$  and  $\eta_{b+}$  are the charging and discharging efficiencies,  $N_{bt}$  is number of batteries, and  $B_m$  is the single battery energy capacity in kWh. Since the battery operation is mutually exclusive, at time step t, the battery state of charge can only increase its charge due to charging or decrease due discharge activity. Similarly, the level of hydrogen LoH[t] in the tank is tracked through this energy balance constraint as following in equation (3-23):

$$LoH[t] = LoH[t-1] + \left(\frac{P_{\text{electrolyser}}[t] \times \eta_{el-} \times 100}{P_{HT} \times H_{LHV}}\right) - \left(\frac{P_{\text{fuel-cell}}[t] \times 100}{\eta_{fc+} \times P_{HT} \times H_{LHV}}\right)$$
(3-23)

Where LoH[t-1] is the level of hydrogen at the previous time step,  $P_{\text{electrolyser}}$  [t] and  $P_{\text{fuel-cell}}[t]$  are electrical input power for electrolyser and electrical output of the fuel cell at time t,  $\eta_{el-}$  and  $\eta_{fc}$  are the efficiency of the electrolyser and fuel cell,  $P_{HT}$  is the hydrogen tank capacity in kg, and  $H_{LHV}$  is the Lower Heating Value of hydrogen in kWh/kg. The operation of the fuel cell and electrolyser is mutually exclusive, in a similar manner to the battery and grid bounded by the binary decision binary  $x_{\text{hydrogen}}[t]$  and by the rated power of the fuel cell  $P_{el}$  and the electrolyser  $P_{fc}$  as following in equations (3-24) and (3-25):

$$P_{electrolyser} [t] \le P_{el} \cdot (1 - x_{hydrogen}[t]), \quad \forall t \in \mathcal{T}$$
 (3-24)

$$P_{fuel-cell}[t] \le P_{fc} \cdot x_{hydrogen}[t], \quad \forall t \in \mathcal{T}$$
 (3-25)

LoH[t] in the tank is bounded by the tank lowest level of hydrogen  $LoH_{min}$  of 5% and the highest possible  $LoH_{max}$  is 100%, as showing in equation (3-26):

$$LoH_{min} \le LoH[t] \le LoH_{max}, \quad \forall t \in \mathcal{T}$$
 (3-26)

The sum of the possible DC power of the battery discharging  $P_{battery, discharge}[t]$ , fuel cell  $P_{fuel-cell}[t]$  and the portion of the renewable generation at the AC side  $P_{ren, DC inverted}[t]$  at time step t can be less or equal to the inverter power limit  $P_{inv}$  as following in equation (3-27):

$$P_{inverter}[t] \le P_{inv}^{max}, \quad \forall t \in \mathcal{T}$$
 (3-27)

After bounding AC and DC side to the inverter limit  $P_{inv}$ , it is important to establish that the total renewable generation  $P_{ren-output}$  [t] is fully accounted for in the model. This is achieved by ensuring that it equals the sum of the portion consumed on the AC bus  $P_{ren, AC}[t]$  and the remaining portion available on the DC bus  $P_{ren, DC \ remaining}[t]$ , as shown in equation:

$$P_{ren, DC inverted}[t] + P_{ren, DC remaining}[t] = P_{ren-output}[t], \quad \forall t \in \mathcal{T}$$
 (3-28)

After establishing this constraint, the remaining renewable generation at the DC side  $P_{ren, DC}[t]$  is either encouraged to be charged to the battery, if available, or recorded at this time step as excess  $E_{excess}[t]$ , accomplishing correct energy balance as following in equation (3-29):

$$P_{ren, DC remaining}[t] = P_{battery, charge}[t] + E_{excess}[t], \quad \forall t \in \mathcal{T}$$
 (3-29)

The battery is prevented from discharging when there is still remaining power at the DC bus which is limited by the inverter capacity conversion, prioritising charging and achieved by linearised big M-method for conditional situations as following in the equations (3-30), (3-31), and (3-32):

$$P_{ren, DC remaining}[t] \le (M \cdot x_{ren-gen}[t]) + \epsilon, \quad \forall t \in \mathcal{T}$$
 (3-30)

$$P_{ren, DC remaining}[t] \ge \epsilon \cdot x_{ren-gen}[t], \quad \forall t \in \mathcal{T}$$
 (3-31)

$$P_{battery, discharge}[t] \le (1 - x_{ren-gen}[t]) \cdot P_b^{+\text{max}}, \quad \forall t \in \mathcal{T}$$
 (3-32)

Where M and  $\epsilon$  are large and small numbers,  $X_{ren-g}$  [t] is a binary variable to capture the remaining renewable power at the DC side  $P_{ren, DC remaining}[t]$ .

#### 3.3.2.3 Penalty Function

Penalties are very important in the GA-MILP hybrid optimisation process in steering the algorithm toward practical and optimum answers. These penalties apply when system configurations violate important operational limits, including unmet energy demand or too high energy generation. These are meant to deter system designs that either fail to satisfy demand or produce too much unneeded energy, therefore guiding the optimisation toward dependable and reasonably priced solutions.

When the total excess energy accumulated over the year exceeds a predefined threshold, a penalty is imposed to discourage system configurations that lead to substantial energy curtailment. The penalty for excess energy is determined based on the total excess energy calculated as follows:

$$\hat{E} = \sum_{t=1}^{T} E_{\text{excess}}(t)$$
 (3-33)

Where T is the total number of time steps in the optimisation (8760 hours for a yearly horizon) and  $E_{\rm excess}(t)$  is the excess energy at time t. If the total excess energy exceeds a predefined design criteria 100 kWh, a penalty is added to the fitness function before passing this to value to GA evaluate function as following:

Penalty 
$$_{\text{excess}} = \begin{cases} P_{\text{excess}}, & \text{if the } \hat{E} > 100kWh \\ 0, & \text{otherwise} \end{cases}$$
 (3-34)

Where  $P_{\rm excess}$  is a large constant penalty, typically set to discourage and guide the GA away any significant violation (e.g.,  $\leq$  10,000,000). When the system fails to provide the needed load at any one moment, an unmet energy demand results. Similar to the penalty for excess energy, the penalty for unmet energy is determined based on the total unmet energy calculated as:

$$\widehat{U} = \sum_{t=1}^{T} E_{unmet}(t)$$
 (3-35)

 $E_{\text{unmet}}(t)$  is the unmet energy at time t. and similar to the excess of energy, the *Penalty*  $_{unmet}$  is calculated at the end of each iteration as follows:

Penalty 
$$_{unmet} = \begin{cases} P_{unmet}, & \text{if } \widehat{U} > 100kWh \\ 0, & \text{otherwise} \end{cases}$$
 (3-36)

 $P_{\text{unmet}}$  is another significant constant penalty number (e.g.,  $\leq$ 10,000,000) which guarantees the system avoids under-sizing system capacities. Then after that both penalties for excess  $Penalty_{\text{excess}}$  and unmet  $Penalty_{\text{unmet}}$  are added as following to the final a fitness function:

Fitness Value 
$$(p,g) = NPC + Penalty_{excess} + Penalty_{unmet}$$
 (3-37)

NPC represents the Net Present Cost of individual p at generation g. Ultimately, the hybrid GA-MILP (GA-Yearly horizon) optimisation framework integrates the strengths of Mixed-Integer Linear Programming for detailed operational dispatch and Genetic Algorithms for global capacity sizing. This combination enables both long-term financial assessment and enforcement of operational constraints in hybrid energy systems. By incorporating penalties for unmet demand and excess generation, the framework encourages designs that are both feasible and reliable. The resulting approach offers a structured and adaptable method to address the complexities of hybrid energy system optimisation.

Equation (3-37) defines a scalar fitness equal to NPC plus hard annual penalties that activate when total unmet or excess energy exceed design thresholds. Because NPC is in euros and the triggers are expressed in  $\[ \in \]$ /kWh, the scaling is unit-consistent; the chosen magnitudes make any violating design strictly dominated by feasible alternatives. In parallel, the MILP layer applies large per-hour slack costs ( $1000\]$ /kWh for unmet,  $100\]$ /kWh for excess), so for a fixed chromosome the dispatch solution already drives slacks toward zero whenever feasible. Together, these mechanisms yield strong selection pressure: tournament selection prefers individuals with  $(\bar{U}, \hat{E}) \to 0$ , and only then discriminates on NPC within the feasible set. This is exactly the pattern observed in the convergence/interaction plots, where parameter settings that sustain diversity also achieve lower NPC after 20–30 generations

# 3.3.3 GA-Based Load Following and HOMER Pro Comparison

# 3.3.3.1 GA-Rule-Based Load Following Method

The rule-based energy management has been used extensively in literature for energy planning and optimisation of energy systems. The technique allocates energy according to predefined rules, prioritising certain means to match or follow the energy production to the fluctuations in the load throughout the day. Rule-based load-following is a widely adopted control strategy in hybrid energy system planning and simulation. It operates through a predefined hierarchy of dispatch decisions to balance renewable energy production with hourly electrical demand. The logic prioritises local energy utilisation by sequentially dispatching available resources in the following order: (1) direct PV-to-load supply, (2) battery storage, (3) hydrogen production or consumption, and (4) grid interaction.

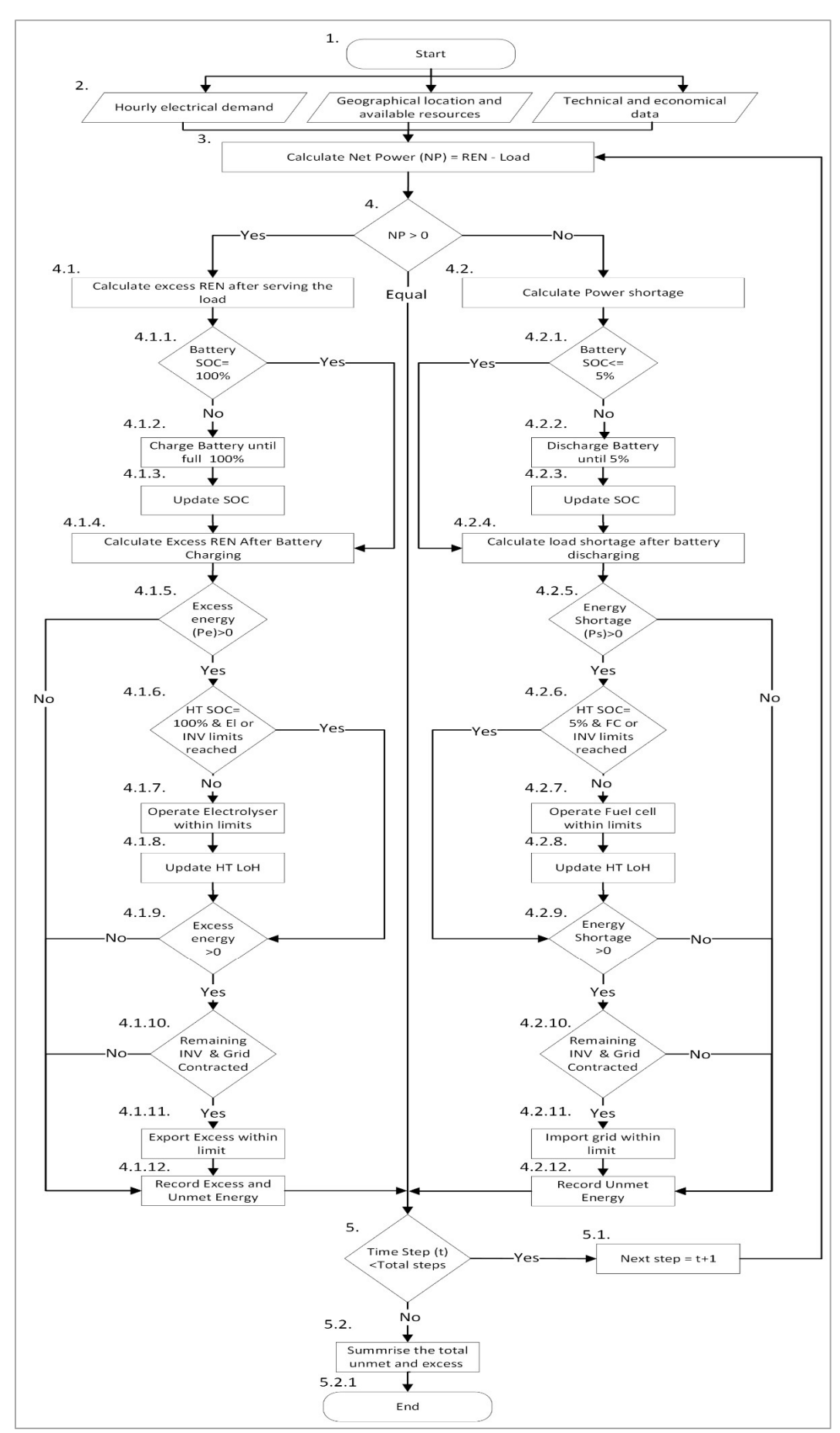


Figure 3-4: Flow Diagram for Load-Following Energy Management Strategy.

Figure 3-4 illustrates the flowchart of the implemented load-following control logic used in this study. At each time step, the algorithm calculates the net power (NP), defined as the difference between renewable generation (REN) and load demand. Depending on whether the system experiences surplus or shortage, the flow branches into two primary paths. If NP > 0, the system attempts to store or convert the excess energy, beginning with battery charging, followed by hydrogen generation through the electrolyser, and finally grid export. If NP < 0, the model sequentially discharges the battery, operates the fuel cell, and finally imports from the grid, if necessary. Any remaining mismatch is recorded as unmet or excess energy. This logic is deterministic and rule-based, making it computationally efficient and transparent, though limited in its ability to anticipate future states or perform multi-period optimisation. Importantly, this rule-based dispatch scheme is embedded within the same upper-layer GA framework described in Section 3.3.2. The GA conducts global capacity sizing by searching across PV, battery, fuel cell, electrolyser, hydrogen tank, and grid contract values. Its objective remains the minimisation of NPC over a 25-year horizon. However, instead of using MILP to simulate hourly dispatch, this configuration evaluates each candidate using the rule-based loadfollowing strategy. Operational results such as unmet and excess energy are computed for each annual simulation and passed to the GA for fitness evaluation. This substitution allows a direct comparison between MILP-based and heuristic dispatch strategies, while maintaining a consistent outer-loop optimisation structure. For full implementation details of this flowchart, including component prioritisation, SOC updates, and conditional constraints, refer to Appendix 9.3, which provides an expanded step-by-step description.

#### 3.3.3.2 Validation Using HOMER Pro

To assess the implementation of the rule-based load-following control logic used in this study, a comparative exercise was carried out using HOMER Pro, a widely used microgrid simulation platform known for its capability to model hybrid energy systems. The primary objective was to benchmark the Python-based GA-Load Following model against an established tool, examining the consistency of technical and economic outcomes across both modelling environments. The validation began by configuring HOMER Pro to approximate the same system specifications, operational constraints, and economic parameters as the Python model. Key components, including PV arrays, battery systems, fuel cells, electrolysers, and grid interaction terms, were aligned as closely as possible between both platforms to establish a comparable reference.

HOMER Pro was then used to simulate dispatch behaviour under its internal load-following logic, which prioritises renewable utilisation, storage management, and grid exchange. This served as a reference baseline for evaluating the Python model's output under similar rule-based conditions. Performance indicators such as NPC, unmet demand, excess energy,

battery SOC, and LoH were compared. Particular attention was given to assessing whether the Python implementation reproduced key aspects of HOMER Pro's operational logic, especially in the handling of storage and hydrogen subsystems.

In addition, GA-optimised capacity configurations generated in the Python model, including PV sizing, battery count, fuel cell and electrolyser ratings, and contracted grid limits, were manually replicated in HOMER Pro. Although HOMER Pro does not include evolutionary optimisation, this approach enabled a consistent evaluation of those configurations under the same dispatch logic for comparative analysis. Overall, the results revealed close agreement in key dynamic trends such as battery charging behaviour, PV energy use, and hydrogen LoH evolution. Some differences in indicators like unmet load or cycling frequency were investigated further as potential effects of variation in constraint modelling or degradation assumptions. These comparative outcomes support the applicability of the GA-Load Following model under the assumed conditions, offering a reference point for the broader optimisation results presented in the next chapter. Comparative performance results for the GA-Load Following, GA-Yearly Horizon, and HOMER Pro implementations are provided in Chapter 3 of the result section 3.5, where each method is evaluated across technical, economic, and operational metrics. Having benchmarked the alternative control schemes, the discussion now turns to the site-specific inputs and economic parameters that underpin the subsequent optimisation runs.

# 3.4 Model Inputs and System Parameters

In accordance with the European Directive on Renewable Energy, Sustainable Development Goal (SDG) 7: Affordable and Clean Energy, energy communities are encouraged to be renewable self-sufficient by generating, consuming, storing or selling electricity through community installation [141], [142]. The Balearic Island of Formentera, home to approximately 12,000 residents is part of this initiative under the VPP4islands project, employing innovative development of smart energy communities [143]. The following sections provide details of the case study, and the key information used, starting with the location and description of the energy community, grid tariff structure, and followed by the economical and performance model inputs.

# 3.4.1 Geographical Location and Targeted Island

Formentera (shown in Figure 3-5), the smallest of the Balearic Islands, is located in the Mediterranean Sea, just south of Ibiza. Two underwater cables from Ibiza to Mallorca connect it: a more robust 132 kV double circuit cable to handle rising power demand and a 30 kV HVAC line. Although the island has a 2 MW solar capacity, seasonal demand sees variations from 7



Figure 3-5: Geographical Context of Formentera Island location

MW in winter to 18 MW in summer, which are usually met by these island links with considerable non-renewable energy capacity.

The selected case study is located west of Sant Francesc Xavier Village on the island. Figure 3-6 shows two different sites A and B that are approximately 600 meters away from each other. The community buildings are the council building of Formentera, two schools, a youth centre, a vehicle inspection station, a fire station and a slaughterhouse. The community buildings

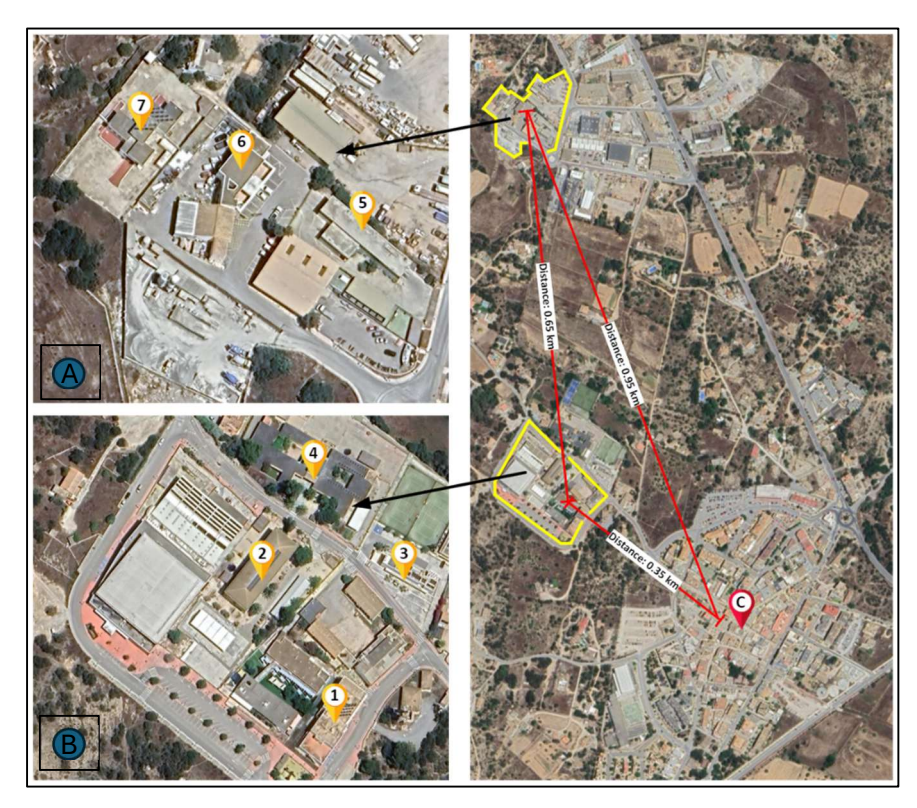


Figure 3-6: The geographical location of energy community buildings west of Sant Francesc Xavier capital of Formentera Island. Building 1: Culture Building electrical demand 44,995 kWh/year. Building 2: primary school with electrical demand 47,189 kWh/year. Building 3: Radio and Youth Centre with electrical demand 19,616 kWh/year. Building 4: Preschool with electrical demand 26,596 kWh/year. Building 5: Vehicle inspection station with electrical demand 11,486 kWh/year. Building 6: Fire station with electrical demand 23,584 kWh. Building 7: 29,437 kWh/year

exhibit different usages that would reflect a variety in the electrical demand during the day, at night and even during the weekends.

Figure 3-7 provides a visual summary of key input data used in this study. Subfigure 3-7a presents the historical hourly electricity consumption profile of the Formentera energy community in 2022. These real-world demand values were collected through the VPP4Islands<sup>4</sup> project and reflect aggregated load behaviour across public and residential buildings. The data was essential for initiating system planning and simulation under the VPP4Islands project. It was collected through collaborative efforts with the local DSO and project partners, using system-level measurements and non-invasive monitoring with clamp-type current transformers (CTs). The Formentera Council's Engineering Department cleaned and validated the dataset before distributing it to partners for modelling and use case development. The data capture clear seasonal variation, with elevated demand during the summer period, primarily due to increased cooling needs. The total annual demand amounts to 202,905 kWh, with a daily average of approximately 555.90 kWh and a peak demand of 67.91 kW.

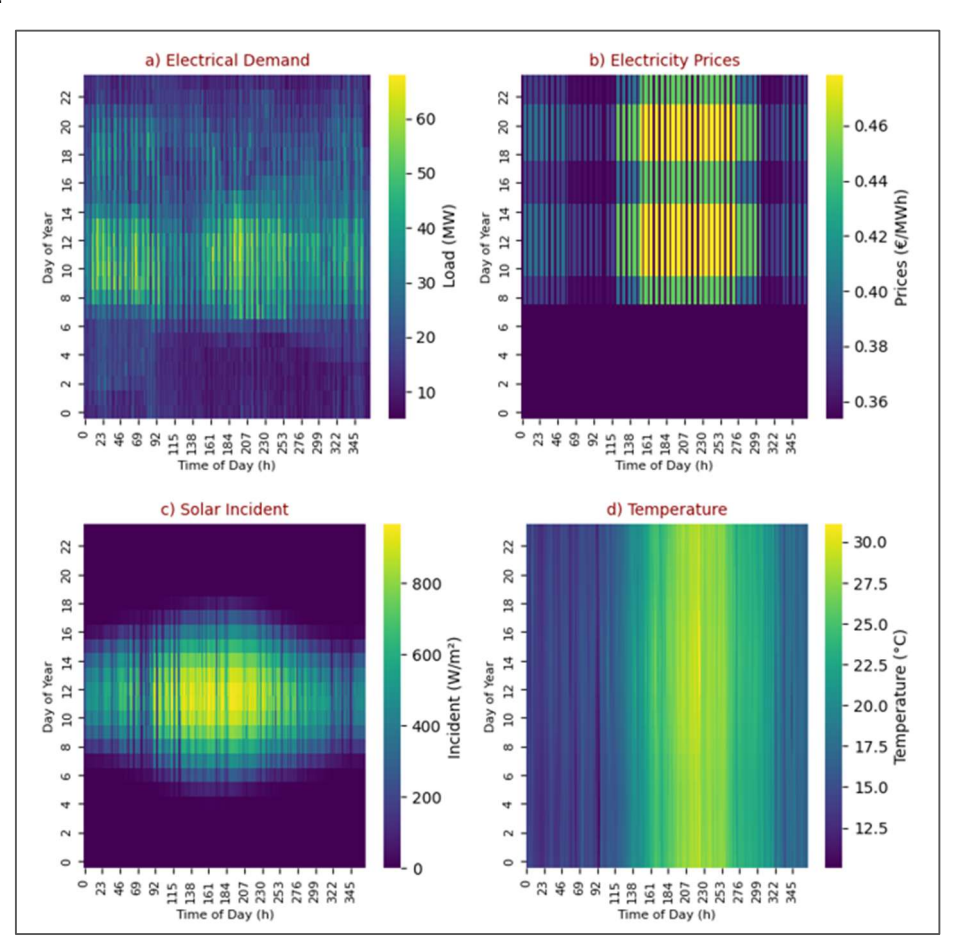


Figure 3-7: Data Input for Formentera case study

\_

<sup>4</sup> https://vpp4islands.eu/

Subfigure 3.7b illustrates the electricity pricing structure applied in the model. ToU tariff was derived from local partner inputs within the VPP4Islands project and reflects the six-period pricing scheme currently implemented on Formentera. The tariff data were used to model operational costs and guide energy dispatch optimisation, with further details on the tariff configuration provided in Section 3.3.3. For solar generation modelling, Subfigures 3.7c and 3.7d show the corresponding solar irradiance and ambient temperature profiles. These meteorological data were obtained from NASA's POWER database for the geographic coordinates of Formentera and cover the full year of 2022 [144]. The irradiance dataset was used to simulate PV energy yield, while temperature data informed thermal performance adjustments in the PV model.

#### 3.4.2 Grid Tariff Structure

The grid tariff model used in this study is based on Endesa's business tariff structure, which is currently applied to public buildings on the island of Formentera as shown in Figure 3-8 [145]. This structure was provided through local collaboration under the VPP4Islands project, where Formentera serves as a demonstration site. The tariff data were sourced from municipal infrastructure—specifically the Formentera Council buildings, and cross-validated with the applicable taxes, including the general electricity tax (5.11%) and value-added tax (VAT) at 21%. The feed-in (selling) price for exported electricity was set at 0.051 €/kWh, while the

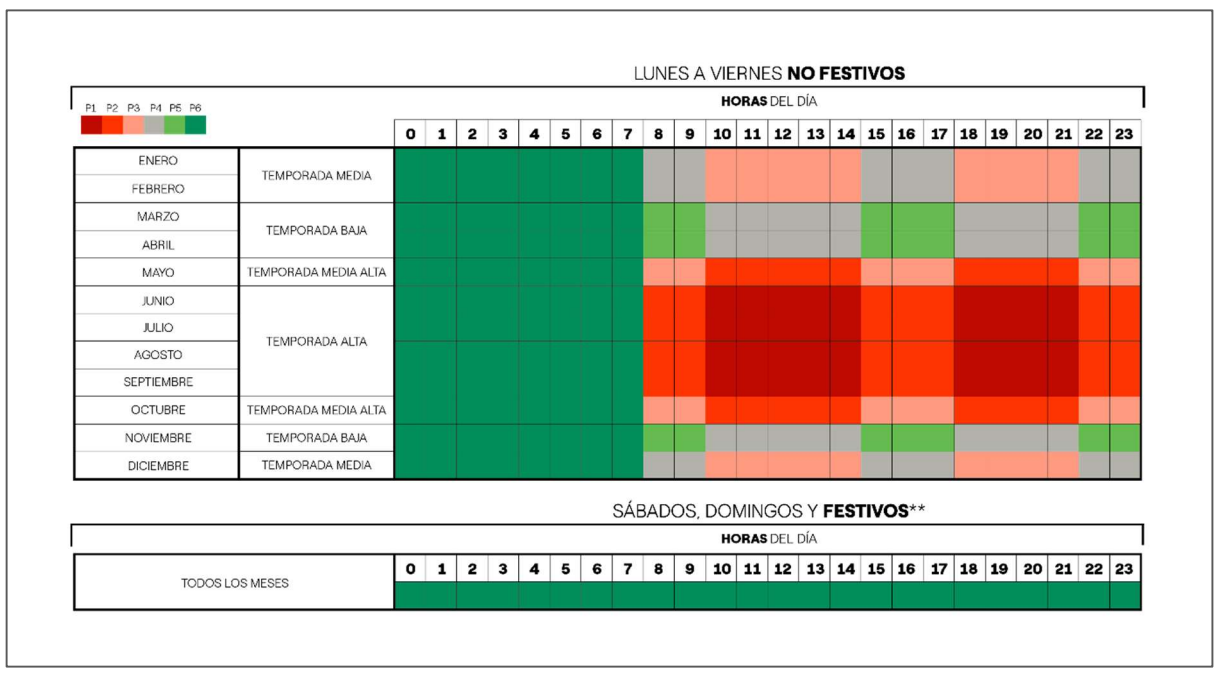


Figure 3-8: Endesa Grid Tariff structure adopted from [120]

average grid purchase price was 0.382 €/kWh, ranging from a minimum of 0.353 €/kWh to a maximum of 0.478 €/kWh. Electricity costs were observed to peak during the summer months (June to September), particularly across two high-demand time blocks: 10:00–14:00 and

18:00–21:00. Weekends and public holidays follow a reduced off-peak pricing schedule. The tariff model incorporates four distinct monthly charges to reflect commercial consumption patterns: the fixed contracted power charge  $F_{CP}$ , the electricity consumption charge  $E_{cc}$ , the peak power penalty charge  $F_{EP}$  and the selling back charge  $S_{BC}$ . These cost components are integrated into the financial model using the following formulations [128]:

$$F_{CP} = \sum_{p=1}^{P=i} Pc_P \cdot R_{t,p} \cdot D_{month}$$
(3-38)

$$E_{cc} = \sum_{t=1}^{T} \left( P_{grid, buy}[t] \cdot \pi_{buy}[t] \right)$$
(3-39)

$$F_{EP} = \sum_{p=1}^{P=i} t_p \times 2 \times (Pd_j - 1.05 \times Pc_P)$$
 (3-40)

$$S_{BC} = \sum_{t=1}^{T} \left( P_{grid, sell} [t] \cdot \pi_{sell} [t] \right)$$
(3-41)

The energy system's main breaker was configured to allow grid import and export flows up to 40% above the contracted power limit. However, penalty charges are applied whenever the instantaneous demand exceeds this contractual threshold, in accordance with the utility's pricing scheme. To account for long-term cost evolution, an annual electricity price escalation rate of 3% was applied over the 25-year project horizon, consistent with observed historical trends since 2007 [146].

# 3.4.3 Cost Assumptions and Sensitivity Analysis for Economic Inputs

The economic and performance inputs form a critical part of the optimisation model, influencing both system design and operational decision-making. These parameters directly affect the objective function of the MILP layer and the fitness evaluation in the GA loop, primarily through the calculation of NPC. The data presented in this section reflects a combination of sources, including manufacturer specifications, academic literature, and insights from the VPP4Islands demonstration activities in Formentera. The data used in this study were sourced from a combination of literature, direct communication with manufacturing companies, and project-specific insights from the VPP4Islands pilot activities in Formentera. The assumptions reflect current market trends and component availability relevant to island energy systems.

Table 3-4 summarises the key technical and economic input parameters for the main energy system components. All capital costs were directly obtained through the VPP4Islands project

for the Formentera Island case study and reflect supplier quotations or actual pilot project estimates. For example, the PV and battery costs were taken from site-specific procurement figures that incorporate not only equipment prices but also local installation, manpower, and system integration costs. Although the PV CAPEX (1,600 €/kW) is higher than typical values reported in literature, it was retained as it best represents the realistic deployment context of the case study. Battery cost (230 €/kWh) similarly reflects fully installed costs in the VPP4Islands<sup>5</sup> pilot. Inverter prices were also based on average supplier quotations relevant to the project. For hydrogen-related components, fuel cell, electrolyser, and H₂ tank, the cost inputs were likewise based on supplier quotations and design estimates used during the project's technical planning phase. This project-driven sourcing strategy ensures that the economic model remains rooted in real-world deployment conditions rather than theoretical assumptions that drive lifecycle cost evaluations over the 25-year planning horizon.

Table 3-4: Technical and Economic Data Inputs for the Modelling

Com-	Cost	O&M	Effi-	Lifetime	Ref / source	±Δ	±Δ
ponent	(unit)	(unit∙yr⁻¹)	ciency	Liletime	type	NPC	LCOE
PV .	1,600	10 €/kW	20%	25 yr	[147] Local pro-	4.00%	4.00%
panel	€/kW			,	ject cost		
Battery	230 €/kWh	10 €/kWh	95%	8,000 cy- cles	[148] Manufac- turer datasheet	3.00%	3.00%
Inverter	300 €/kW	10 €/kW	95%	20 yr	[147] Datasheet	0.49%	0.49%
Fuel cell	1,200 €/kW	0.02 €/kW·h	43%	15,000 h	[149], [150] Datasheet / study	0.14%	0.14%
Elec- trolyser	1,200 €/kW	0.05 €/kW·h	63%	35,000h	[151] Datasheet	0.13%	0.13%
H <sub>2</sub> tank	500 €/kg H <sub>2</sub>	10 €/kg	_	15 yr	[152] Datasheet	0.06%	0.06%

To validate the robustness of these selections, a ±10% sensitivity sweep was applied to each component's CAPEX while keeping all other parameters fixed. The resulting variations in Net Present Cost (NPC) and Levelised Cost of Energy (LCOE) are presented in the final two columns of Table 3-4. Results show that PV and battery CAPEX have the most significant influence on economic outcomes, causing changes of ±4.00% and ±3.00% in NPC and LCOE respectively. These technologies dominate the investment profile and are frequently dispatched in the optimised system. In contrast, hydrogen-related components exhibit marginal influence, typically below ±0.2%, reflecting their limited capacity sizing and lower utilisation under the model's cost-optimised regime.

<sup>&</sup>lt;sup>5</sup> https://vpp4islands.eu/

The component cost assumptions are based on real quotations and pilot study data from the Formentera case, ensuring alignment with site-specific conditions. Sensitivity analysis using ±10% CAPEX variation shows that resulting changes in NPC and LCOE remain below 5%, supporting the robustness of the economic model and highlighting the greater financial influence of PV and battery costs compared to other components.

In addition to technical inputs, financial modelling assumptions are summarised in Table 3-5. The nominal discount rate, varied between 6–10%, was the most influential parameter, causing changes of up to  $\pm 10\%$  in both metrics. Inflation and electricity price escalation, varied  $\pm 1\%$  from baseline, produced smaller effects in the range of  $\pm 4$ –6%. In contrast, statutory values such as Spain's general electricity tax (5.11%) and VAT (21%) were held fixed, as they are non-recoverable and set by regulation. These results confirm that the selected assumptions are reasonable and that model outcomes remain robust under expected financial variability in the 2025 Spanish context.

Table 3-5: Financial Parameters Used in Economic Assessment

Parameter	Value	Ref ΔNPC		ΔLCOE		Note	
Nominal discount rate	8	[152]	+9.61%	-7.21%	-10.05%	+10.87%	Low=6%, High=10%
Inflation rate	2	[153]	-4.10%	+4.68%	+5.72%	-5.38%	Low=1%, High=3%
Escalation rate	3	[146]	-3.98%	+5.27%	-3.98%	+5.27%	Low=1%, High=5%
General electricity tax rate	5.11	Statutory; non-recoverable; not swept					
VAT rate	21	Statutory; non-recoverable; not swept					

These input parameters collectively support a consistent and realistic techno-economic evaluation of hybrid energy system configurations. The following sections present results based on the application of these inputs within the GA-MILP framework.

### 3.5 Results

This section presents the comparative results of the proposed GA-MILP optimisation framework under two different energy management strategies, GA-Yearly Horizon and GA-Load Following, and benchmarks them against the established HOMER Pro software using its standard load-following approach. The optimisation problem was implemented using the PuLP library in Python to ensure consistency in solver syntax [154]. Gurobi 11.1.1 employed to solve the MILP-based lower operational layer for the GA-Yearly Horizon strategy [155]. Simulations were executed on a desktop computer equipped with an Intel(R) Core (TM) i7-11700 processor running at 2.50 GHz and 16 GB of RAM.

The results are structured into four main parts. Section 3.4.1 outlines the system sizing outcomes for each method, highlighting differences in component capacities, NPC, and LCOE.

Section 3.4.2 delves into the operational behaviour and energy flow dynamics, using representative winter and summer periods to analyse how each method allocates renewable generation, storage, and grid interaction. Section 3.4.3 shifts to a financial perspective, comparing capital, operational, and grid-related costs over the full project lifecycle, along with key financial metrics such as Internal Rate of Return (IRR) and payback period. Finally, Section 3.5 concludes with a summary of key insights.

### 3.5.1 System Sizing

The GA-Load Following and GA-Yearly Horizon approaches are benchmarked to highlight the differences in decision-making paradigms and their impact on system sizing and performance. The GA-Yearly Horizon method bases its decisions on knowledge of the entire year's horizon, optimizing capacities with a long-term view. On the other hand, the GA-Load Following method is more passive since it bases decisions on the available power at the present hour without considering future situations. Furthermore, HOMER is utilised as a validation tool to evaluate the dependability of the optimisation outputs and outcomes for identical input conditions.

Table 3-6 displays the size results for every method of energy allocation. By use of an 8-kilogram hydrogen tank, the GA-Yearly Horizon method balances intermittent renewable energy with storage, therefore optimizing 86 battery strings with a PV capacity of 156 kWp. Conversely, the GA-Load Following approach chooses reduced capacities of 124 kWp for PV and 58 battery strings, reflecting the trade-offs resulting from the lack of foresight in energy consumption. HOMER-based validation shows similar tendencies for system size, thus supporting these conclusions further.

Table 3-6: Comparison of the sizing outcomes for the three Benchmarking methods

Component	Units	GA Voorly Horizon	GA- Load Following	HOMER-	
Component	Units	GA- really Horizon	GA- Load Following	Load Following	
Solar PV	[kWp]	156	124	123	
Battery	[Strings]	86	58	58	
Inverter	[kW]	75	120	121	
Contracted Power	[kW]	52	78	77	
Fuel cell	[kW]	5	5	5	
Electrolyser	[kW]	6	5	5	
Tank	[Kg]	8	5	5	
NPC	[€]	625,776	665,236	661,677	
LCOE	[€/kWh]	0.228	0.243	0.241	

Likewise, the differences in system sizing are reflected in the Levelized Cost of Energy (LCOE) and Net Present Cost (NPC). Compared to the GA-Load Following technique's NPC of

€665,236 and LCOE of €0.243/kWh, the GA-Yearly Horizon method achieves a lower NPC of €625,776 and LCOE of €0.228/kWh. Moreover, HOMER's validation yields NPC and LCOE values (approximately €661,677 and €0.241/kWh, respectively) that closely align with GA-Load Following, reinforcing the dependability of the proposed framework and increasing confidence in these results.

Table 3-7 summarises the main performance indicators for GA-Yearly Horizon, GA-Load Following, and HOMER-Load Following. With its larger 156 kWp PV system, GA-Yearly Horizon generates the highest solar energy of 285,499.66 kWh compared to 226,935.63 kWh in GA-Load Following and 227,138.72 kWh in HOMER-Load Following. Although GA-Yearly Horizon achieves the highest absolute PV consumption by the load (123,924.70 kWh), covering 61.07% of the total load, its Renewable Self Consumption Rate of 43.40% is lower than the 52.45% in GA-Load Following and 51.65% in HOMER, illustrating how a larger system can boost total generation but yield a smaller on-site usage fraction.

Table 3-7: Performance metrics for benchmarking methods.

Metrics	Units	GA- Yearly	GA- Load	HOMER-	
Metrics	Units	Horizon	Following	Load Following	
PV Generated	kWh	285,499.66	226,935.63	227,138.72	
PV Directly Consumed	kWh	123,924.70	119,044.06	117,332.41	
PV Contribution to Load	%	61.07	56.24	57.82	
Renewable Self Consumption	%	43.40	52.45	51.65	
Battery Throughput	kWh	85,062.90	67,868.35	67,425.86	
Electrolyser Capacity Factor	%	15.61	9.63	10.94	
Fuel Cell Capacity Factor	%	5.17	2.25	2.54	
PV Excess Energy	kWh	169,088.38	107,891.57	109,806.31	
Electrolyser Usage	kWh	8,205.53	4,216.72	4,791.18	
Fuel Cell Usage	kWh	2,263.01	985.95	1,110.99	
Grid Dependence	%	7.21	14.62	15.63	
Grid Import	kWh	15,265.58	30,952.49	33,103.77	
Grid Export	kWh	61,686.44	30,224.30	28,060.84	

Likewise, GA-Yearly Horizon records 169,088.38 kWh of PV excess, substantially above the 107,891.57 kWh in GA-Load Following and 109,806.31 kWh in HOMER, highlighting the trade-off between maximising renewable production and managing higher surplus. Although none of the methods wastes renewable energy outright, GA-Yearly Horizon's long-term optimisation approach enables greater overall production and potentially more profitable export opportunities.

According to Table 3-7, GA-Yearly Horizon also experiences a higher battery throughput of 85,062.90 kWh, in contrast to 67,868.35 kWh in GA-Load Following and 67,425.86 kWh in HOMER. Assuming each battery string provides 14,400 kWh of total lifetime throughput, GA-Yearly Horizon (86 strings) offers a combined capacity of 1,238,400 kWh. At the current usage rate, this suggests a battery lifetime of about 15 years before replacement, leading to about one or two replacements over a 25-year span. Meanwhile, Load Following's 58 strings (835,200 kWh total capacity) and annual throughput of 67,868.35 kWh imply a shorter lifetime of approximately 12 years, increasing replacement frequency. These findings underscore the trade-offs: while Load Following reduces up-front battery costs, GA-Yearly Horizon's larger battery bank requires fewer replacements over the long run.

The Electrolyser and Fuel Cell Capacity Factors demonstrate GA-Yearly Horizon's further advantages. GA-Yearly Horizon attains a 15.61% electrolyser capacity factor (8,205.53 kWh/year) and a 5.17% fuel cell capacity factor (2,263.01 kWh/year), compared to 9.62% (4,216.72 kWh/year) and 2.38% (985.94 kWh/year) in Load Following. HOMER closely aligns with these, yielding capacity factors of 10.94% for the electrolyser (4,791.18 kWh/year) and 2.54% for the fuel cell (1,110.99 kWh/year). By strategically allocating surplus renewable power to hydrogen production and usage, GA-Yearly Horizon leverages foresight to enhance hydrogen storage integration, whereas Load Following's short-horizon approach limits component utilisation.

Despite the relatively small selected capacities for the electrolyser, fuel cell, and hydrogen tank, the GA-MILP optimiser made this choice based on a clear economic trade-off. The levelised cost of storage (LCOS) for the battery system was calculated at approximately 0.18 €/kWh, while the hydrogen system, based on the combined usage of the electrolyser and fuel cell, yielded an LCOS of over 0.80 €/kWh. This cost discrepancy stems not only from higher capital and replacement costs but also from significantly lower energy conversion efficiency. The battery system operated at an estimated round-trip efficiency of 95%, whereas the hydrogen subsystem, accounting for both the electrolyser (63%) and fuel cell (43%) efficiencies, achieved a combined round-trip efficiency of only 27%.

This stark performance gap, both in cost and energy efficiency, made it economically unfavourable to increase the hydrogen system's capacity. This explains why the GA-MILP optimiser selected a small hydrogen subsystem that it was economically suboptimal to expand it further. Nonetheless, hydrogen still contributed meaningfully to the overall system by absorbing excess PV generation during peak midday hours (approximately 8,205 kWh annually) and supporting grid independence during selected winter periods, as shown in the operational plots in Section 3.4.2. Its inclusion also aligns with the VPP4Islands project

requirement for hybrid battery regenerative hydrogen integration and supports seasonal storage, as discussed in Section 6.3. Furthermore, it contributes to broader sustainability goals related to EROI, which are further analysed in Chapter 5, Section 5.4.2. Therefore, even in modest quantities, hydrogen adds system-level value that extends beyond cost minimisation alone.

GA-Yearly Horizon method's grid dependence is 7.21%, well below Load Following's 14.62% and HOMER's 15.63%. Annually, GA-Yearly Horizon imports mainly 15,265.58 kWh from the grid, well below 30,952.48 kWh for Load Following and 33,103.77 kWh for HOMER. Meanwhile, GA-Yearly Horizon exports 61,686.44 kWh of surplus energy, more than the 30,224.30 kWh in Load Following or the 28,060.84 kWh in HOMER, thus generating additional revenue. If GA-Yearly Horizon's higher capacities were operated under Load Following rules, curtailment would rise markedly to 31,164.13 kWh, illustrating the drawbacks of short-horizon decision-making for large-scale renewable penetration.

This comparison highlights the trade-offs inherent in the three optimisation strategies. The GA-Yearly Horizon method is best interpreted as an optimistic benchmark, representing idealised energy allocation based on perfect foresight across the full year. In contrast, the GA-Load Following strategy serves as a conservative reference, constrained by real-time decision-making without anticipation of future states. HOMER further validates this short-horizon behaviour. To build on these insights, the next section investigates the energy dynamics across representative seasonal periods. This analysis focuses on the hourly operational decisions and their implications for system behaviour, resource utilisation, and overall performance under varying temporal and environmental conditions.

# 3.5.2 Energy Flow and Dynamics

# Winter Days Analysis:

Figure 3-9 shows the hourly operational decisions for GA-Yearly Horizon, GA-Load Following, and HOMER-Load Following during three typical winter days starting on the 13th day of the year. All techniques depend on grid imports in early morning hours (00:00–07:00) when PV generation is absent. Unlike the reactive decisions of HOMER and Load Following, Yearly Horizon regularly maintains a higher battery SOC%, indicating its foresight-driven approach.

From 08:00 to 10:00 Yearly Horizon minimises grid imports by efficiently using increased PV generating (124.14 kWh on Day 1, 77.99 kWh on Day 2, and 216.06 kWh on Day 3). Particularly on Day 2, where it imported 102.15 kWh against Yearly Horizon's 40.81 kWh, HOMER's dependence on synthetic solar data resulted in lower PV generation and higher imports.

Emphasising Yearly Horizon's cost-sensitive energy distribution, midday hours (11:00–15:00) charge batteries strategically to reduce grid reliance. For example, on Day 3 it produced 534.73 kWh and charged 343.37 kWh into its battery, surpassing HOMER and Load Following in both generation and storage measures.

Often lowering grid reliance (8.65 kWh on Day 2), Yearly Horizon shows in the evening (16:00–23:00) its strategic balancing of grid imports and battery discharges, so exporting surplus energy during low-tariff times. By comparison, Load Following shows strong reliance on grid imports (140.76 kWh on Day 2), and HOMER discharges notable battery energy (121.55 kWh on Day 3).

By using foresight to reduce grid reliance and operational expenses, GA-Yearly Horizon shows overall cost optimisation, improved PV use, and smart energy allocation. These approaches, however, are benchmarked as models of optimistic (Yearly Horizon) and pessimistic (Load Following and HOMER) scenarios of energy planning, therefore providing important new perspectives on the possibilities and constraints of hybrid energy systems under many paradigms of decision-making.

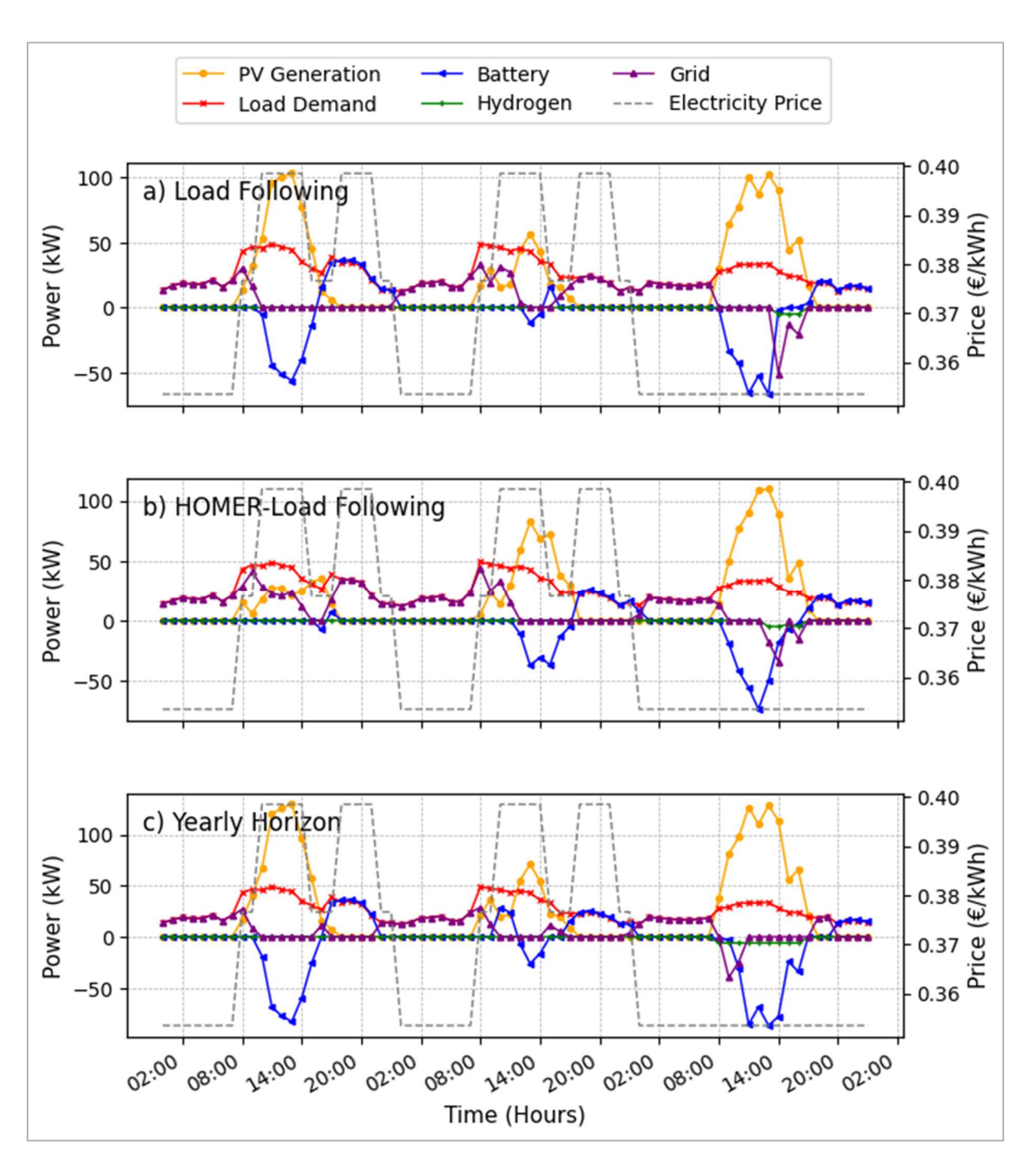


Figure 3-9: Winter Operational Dynamics for Load Following (a), HOMER - Load Following (b), and GA-Yealy Horizon (c). The positive values for hydrogen represent the fuel cell output in kW, and the negative values indicate electrolyser consumption. For the battery, positive values indicate discharge, and negative values indicate charging. Grid interactions show positive values for electricity purchases and negative values for sales.

# **Summer Days Analysis:**

Figure 3-10 presents the energy dynamics of GA-Yearly Horizon, GA-Load Following, and HOMER-Load Following during three typical summer days. While the winter analysis highlighted energy allocation strategies under minimal PV generation, the summer analysis looks at how these approaches handle periods of significant PV excess, with a focus on optimizing energy storage, grid exports, and demand satisfaction.

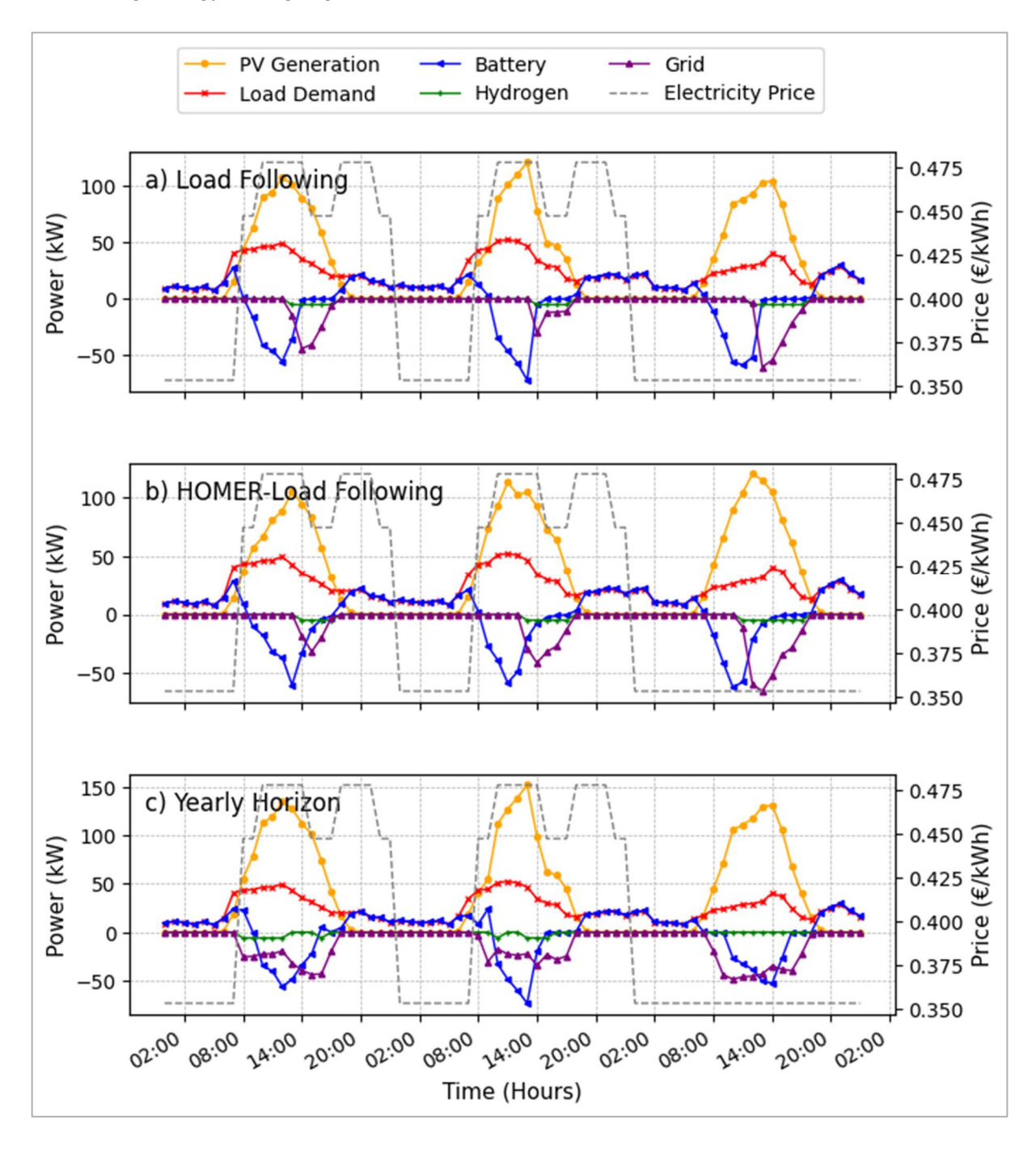


Figure 3-10: Summer Operational Dynamics for Load Following (a), HOMER - Load Following (b), and GA-Yealy Horizon (c). The positive values for hydrogen represent the fuel cell output in kW, and the negative values indicate electrolyser consumption. For the battery, positive values indicate discharge, and negative values indicate charging. Grid interactions show positive values for electricity purchases and negative values for sales.

All methods on the first summer day (Day 1) depend on grid imports in early hours (00:00–07:00) to satisfy a requirement of 110.77 kWh. While Yearly Horizon maintains its battery SOC% at 30.22%, giving future cost minimization top priority, HOMER and Load Following substantially discharge batteries with 101.54 kWh and 100.87 kWh respectively. Yearly Horizon uses the highest PV generating (248.23 kWh) between 08:00 and 10:00 to charge 34.98 kWh into its battery and export 73.02 kWh. Load Following charges 57.69 kWh from its PV production of 197.31 kWh while HOMER generates 159.96 kWh charging 28.22 kWh. Midday (11:00–15:00) shows the most significant PV output; Yearly Horizon generates 595.82 kWh and exports 156.99 kWh. HOMER generates 454.05 kWh, charges 173.71 kWh and exporting 50.31 kWh. From its 473.60 kWh generation, Load Following charges 136.87 kWh and exports 98.18 kWh. With just 6 kWh imported and 62.57 kWh exported vs HOMER's grid import of 22.70 kWh and Load Following's 30.98 kWh, evening hours (16:00–23:00) demonstrate Yearly Horizon's superior grid reliance minimizing.

The second and third days highlight Yearly Horizon's strategic energy consumption, always maximizing battery storage and grid exports. Day 3, Yearly Horizon exported 208.17 kWh noon, for example, compared to HOMER's 222.62 kWh, therefore demonstrating its cost-conscious focus. These results show that the foresight-driven technique of Yearly Horizon greatly improves operational efficiency and PV use over the reactive methods of Load Following and HOMER.

#### 3.5.3 Economic Analysis

A thorough financial assessment of hybrid energy systems is essential for understanding their long-term viability, particularly when evaluating different strategies for energy allocation and storage. In this section, three methods, GA-Yearly Horizon, GA-Load Following, and HOMER-Load Following, are compared as benchmarks to show how varying planning horizons and decision-making paradigms affect Net Present Cost, Levelized Cost of Energy, Internal Rate of Return, and Payback Period. Beyond these high-level indicators, a closer look at the detailed cost structure reveals how each approach balances capital investments, operational expenditures, and grid purchases over the system's lifetime. Figure 3-11 provides four perspectives on these costs: subplot (a) separates total expenditures into capital investments, O&M expenses, replacements, and salvage values; subplots (b) and (c) explore GA-Load Following and HOMER-Load Following in greater detail; and subplot (d) compares annualized costs across all three strategies.

From subplot (a), the most substantial capital spending occurs in PV panels (€249,600) and battery storage (€94,600). Although these outlays are considerable, they help reduce the system's reliance on the grid and can lower ongoing operational expenses. Even so, grid-

related O&M costs rise to €97,756, close to the battery replacement cost of €118,400, and notably higher than the annualized grid expense of €7,561 in GA-Yearly Horizon (subplot d). This highlights the delicate balance in storage utilization: excessive cycling drives up battery wear, but excessive dependence on the grid inflates day-to-day expenses.

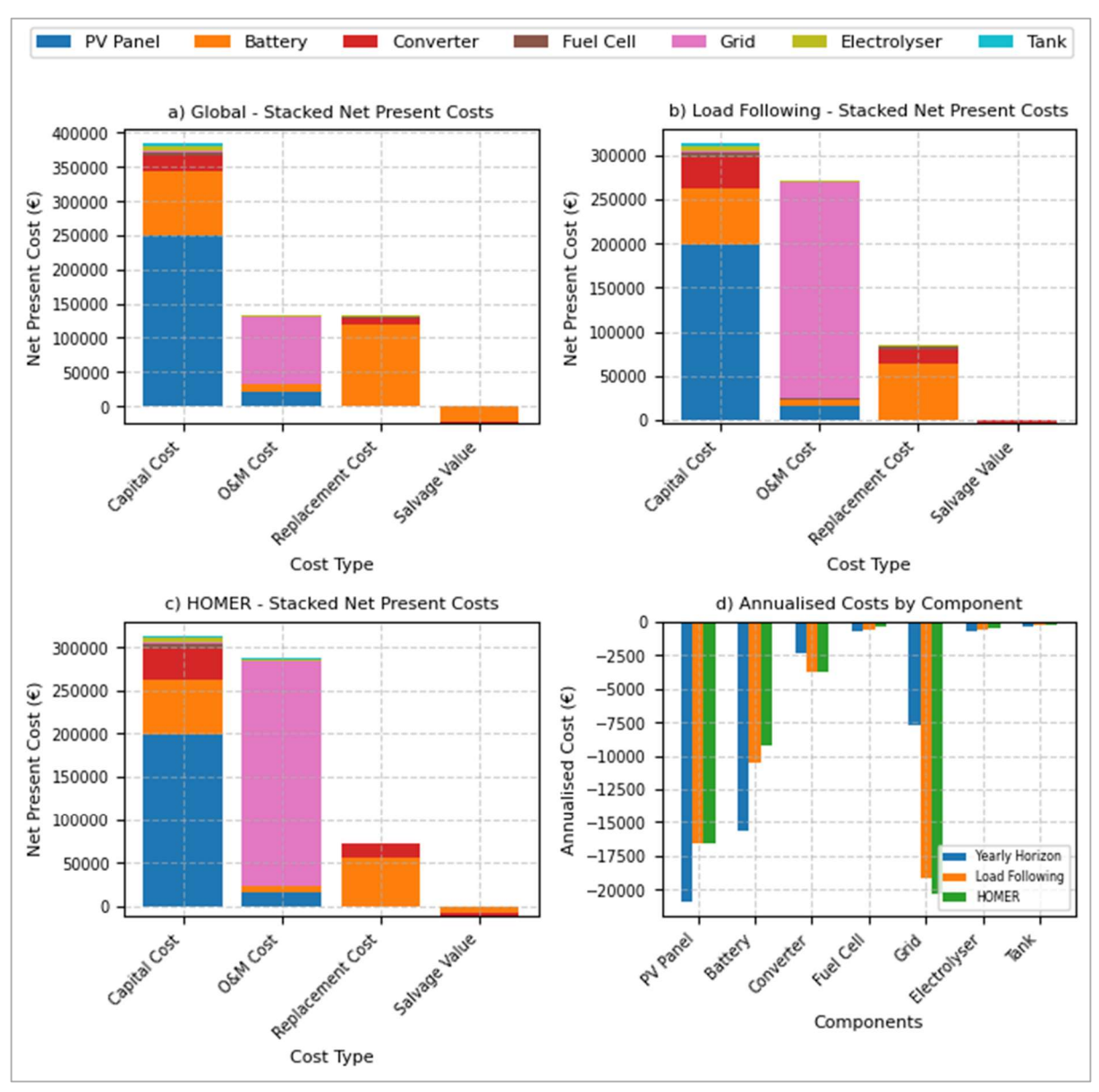


Figure 3-11: Breakdown of Net Present Costs and Annualized Expenditures. a) Total system costs by category, (b) GA-Load Following cost distribution, (c) HOMER-Load Following cost distribution, (d) Annualized costs by component across all strategies.

Turning to GA-Load Following in subplot (b), the capital investments for PV and batteries drop to €198,400 and €63,800, respectively, easing the immediate financial burden. However, the trade-off is higher O&M expenditures (€245,234) due to greater reliance on purchased electricity. This is reflected in GA-Load Following's grid import figure of 30,952.49 kWh, double the 15,265.58-kWh imported under GA-Yearly Horizon. Although GA-Load Following incurs a lower battery replacement cost (€64,148), this mainly stems from less battery usage rather

than more efficient dispatch. In fact, GA-Yearly Horizon's higher battery throughput (85,062.90 kWh compared to 67,868.35 kWh) illustrates how strategic cycling can yield fewer replacements over the full lifespan.

A similar pattern emerges in HOMER-Load Following (subplot c), where capital costs resemble GA-Load Following, yet O&M expenses reach €260,524. This increase likely arises from conservative scheduling based on synthetic solar data, evidenced by a 33,103.77-kWh grid import, again more than double that of GA-Yearly Horizon. While HOMER achieves the lowest battery replacement cost (€56,363), this advantage is cancelled out by the higher reliance on the grid.

Subplot (d) underscores GA-Yearly Horizon's advantage through its substantially lower annualized grid cost of €7,561, relative to GA-Load Following (€18,969) and HOMER-Load Following (€20,152). By operating with a broader planning horizon, GA-Yearly Horizon coordinates solar generation with battery dispatch more effectively, reducing day-to-day expenses and extending battery life. It's lower Net Present Cost (€625,776) offsets the initial delay even if it has a somewhat longer payback period (5.00 years instead of 4.48 for GA-Load Following). GA-Yearly Horizon also exports more surplus energy (61,686.44 kWh, compared to 30,224.30 kWh in GA-Load Following and 28,060.84 kWh in HOMER), hence highlighting its more efficient utilization of renewable output.

These results show the more fundamental difference between foresight-driven and near-term approaches. Although short-horizon approaches like GA-Load Following and HOMER call for lesser upfront budgets, they rely more on the grid and over time generate more running costs. By contrast, GA-Yearly Horizon's proactive method reduces total dependency on outside power by means of more consistent, long-term savings even when it raises initial expenditure. Although it represents a best-case benchmark assuming accurate forecasts and optimal dispatch, GA-Yearly Horizon's results highlight how strategic planning and efficient resource allocation can yield a more financially resilient system. By mapping out the strengths and limitations of each approach, this analysis lays the groundwork for introducing novel optimisation strategies, where these benchmarks will provide a valuable point of reference for enhanced system design.

Grid-related operating expenses and their monthly breakdown reveal clear differences among the GA-Yearly Horizon, HOMER, and GA-Load Following strategies as shown in Figure 3-12 (a) and (b). In January, GA-Yearly Horizon records a total monthly charge of €3,494.59 with 4,306 kWh purchased and 1,887 kWh sold, translating into a net import of 2,419 kWh.

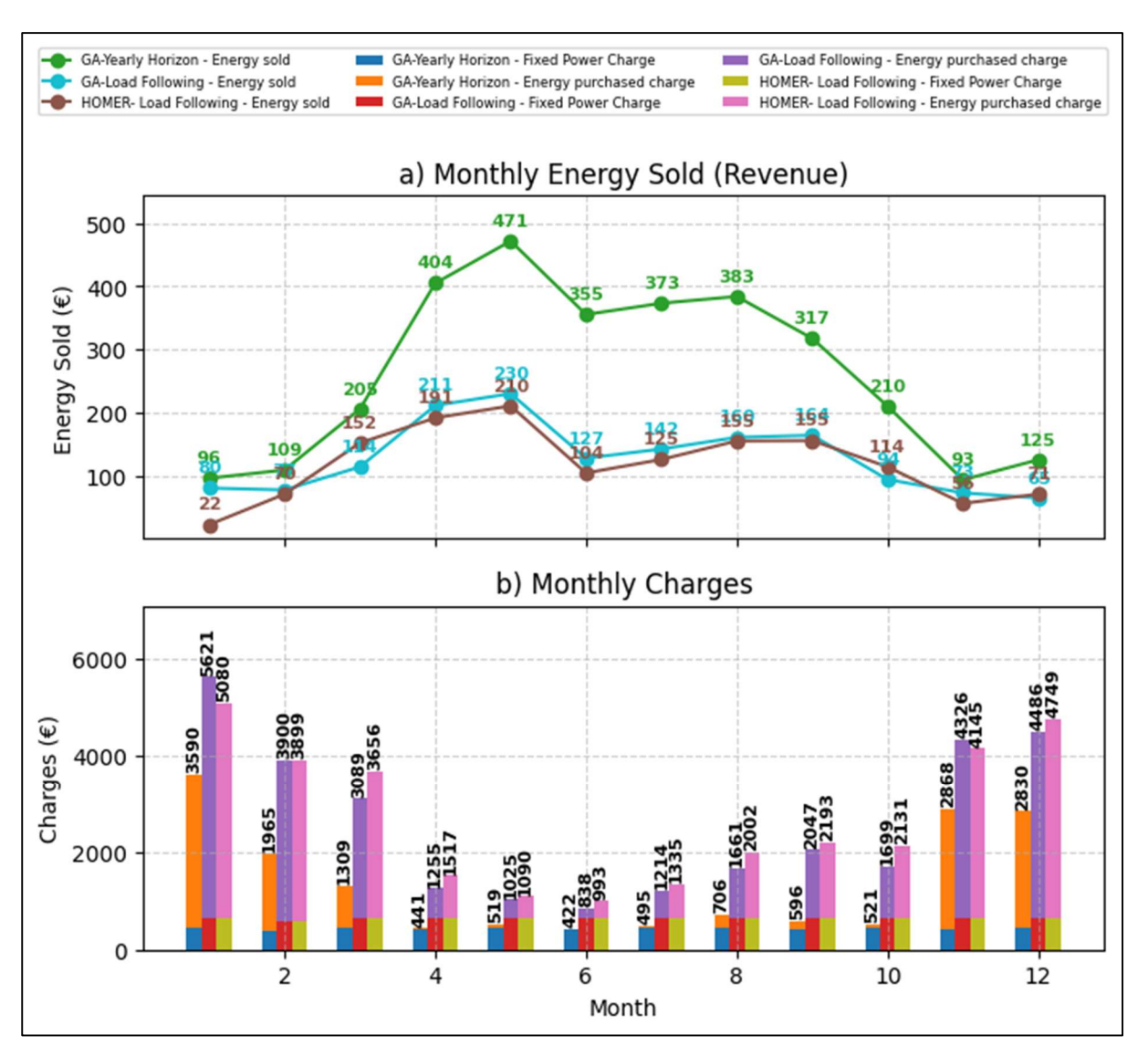


Figure 3-12: Benchmarking Methods Monthly Escalated Grid-Related Financial Performance. a) Monthly energy revenue from grid sales, (b) Monthly grid-related costs, including power purchases and fixed charges across GA-Yearly Horizon, GA-Load Following, and HOMER-Load Following.

Although the bought volume is relatively high, sales revenue mitigates much of the burden. HOMER, by contrast, posts a higher charge of €5,057.52 based on 5,914 kWh imported and only 446 kWh exported, while GA-Load Following peaks at €5,540.50, reflecting 6,587 kWh bought against 1,582 kWh sold. These stark discrepancies reflect the influence of planning horizons and the degree of coordination between storage dispatch and grid interactions.

February offers a further illustration of how closely matched import and export figures can lower costs. GA-Yearly Horizon's monthly total of €1,855.98 stems from 2,110 kWh purchased and 2,141 kWh sold, producing a slightly negative net purchase of –31 kWh. HOMER's charges reach €3,828.73, with 4,397 kWh imported and 1,392 kWh sold, whereas GA-Load Following records a similar total of €3,822.75, importing 4,379 kWh and exporting 1,523 kWh. March continues to highlight GA-Yearly Horizon's ability to run at an energy surplus. It holds monthly charges to €1,104.43 by buying just 1,214 kWh and exporting 4,030 kWh, achieving

a net negative purchase of –2,815 kWh. In comparison, HOMER sees €3,504.32 for the same period, after importing 4,090 kWh and selling 2,981 kWh, while GA-Load Following settles at €2,975.74 with 3,338 kWh in purchases and 2,237 kWh in exports. This pattern persists through the spring and summer months, where GA-Yearly Horizon's costs frequently drop well below €200 per month thanks to significant net negative purchases (–7,909 kWh in April, –9,129 kWh in May, and comparable figures in June through September) that are otherwise not replicated by HOMER or GA-Load Following.

April shows the importance of robust surplus production: GA-Yearly Horizon spends only €36.90 for buying 26 kWh and selling 7,935 kWh, highlighting how perfectly timed battery discharges and export decisions may drastically cut costs. Conversely, depending on at least several hundred thousand kilowatt-hours of monthly imports and less strong export management, HOMER and GA-Load each incur expenditures exceeding €1,000. May remains similarly revealing, with GA-Yearly Horizon's net negative purchase of −9,129 kWh dropping its total charge to about €47.91, while HOMER still spends €879.96 and GA-Load Following €795.56. Over the middle months of the year, GA-Yearly Horizon nearly always holds monthly costs between roughly €70 and €330 by strategically drawing from or sending energy to the grid at optimal times. HOMER and GA-Load Following rarely match this performance, and even in periods where they do export a respectable amount of solar energy, they still carry more substantial grid purchases.

Shifting toward autumn, an example emerges in October, when GA-Yearly Horizon's monthly charge grows to €311.34 due to a more modest net export of –3,889 kWh. Yet HOMER and GA-Load Following both surpass €1,600 that month, indicating how an increase in import requirements quickly drives up monthly bills. Similar outcomes appear in November and December as solar availability wanes, with GA-Yearly Horizon's costs climbing to €2,775.23 in November and €2,705.43 in December. HOMER, however, rises beyond €4,000 in both months, and GA-Load Following consistently hovers around that same level. Even in these higher-load conditions, the broad scheduling horizon of GA-Yearly Horizon still yields lower costs thanks to a more nuanced use of stored energy. In total, the GA-Load Following strategy accrues approximately €29,625 in annual grid-related charges, underscoring how limited foresight and passive dispatch compound costs over time, particularly in months of low solar availability and reduced export potential

From the monthly data, it is clear that the GA-Yearly Horizon approach systematically reduces grid reliance, captures higher revenues from surplus exports, and avoids steep peak-demand penalties through proactive scheduling. In contrast, HOMER and GA-Load Following, which operate with shorter planning windows, show significantly higher import volumes and less

precisely timed exports, causing their monthly costs to sometimes exceed €5,000. Over the course of a year, such differences accumulate into notably higher total charges for the short-horizon benchmarks, confirming that long-horizon optimisation can yield sustained financial benefits despite added complexity. These findings provide a valuable reference future practical novel methods, which aims to combine the strengths of extended foresight with the practical flexibility of load-following schemes.

Figure 3-13 depicts year-by-year evolution of cumulative present costs highlights how initial investments in PV and storage can ultimately yield substantial long-term savings when compared to a Grid-Only scenario. At the outset, GA-Yearly Horizon invests €384,200, while both HOMER and GA-Load Following spend about €313,000. Grid-Only's nominal entry cost of €2,500 looks appealing initially but escalates rapidly over time, culminating in a final net present cost of about €1,608,050 by Year 25. In contrast, GA-Yearly Horizon finishes with the lowest net present cost of €625,776, followed by HOMER at €661,677 and GA-Load Following at €665,236 as shown in Table 3-8.

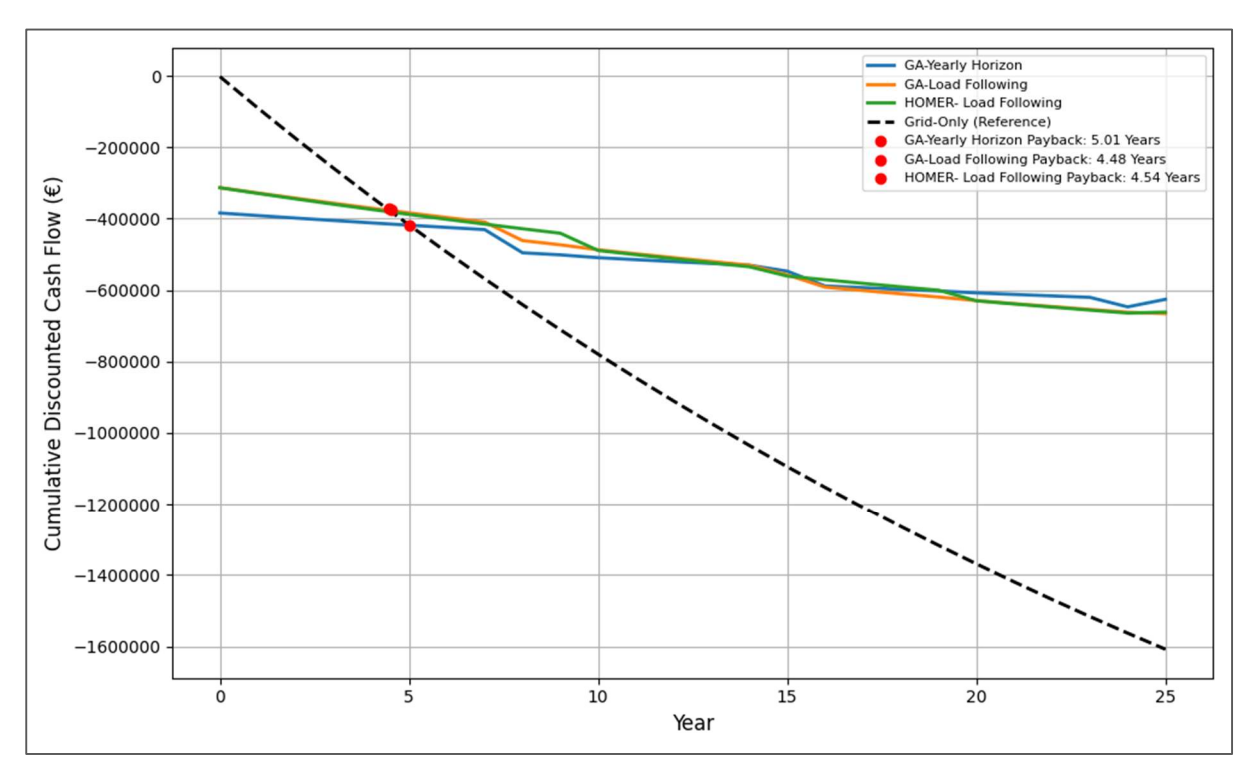


Figure 3-13: Cumulative Discounted Cash Flow Over a 25-Year Horizon for Different Energy Management

Table 3-8: Key Financial Metrics of Benchmarking Approaches

Financial Metric	Units	GA- Yearly Horizon	GA- Load Following	HOMER- Load Following
NPC	[€]	625,776	665,236	661,677
LCOE	[€/kWh]	0.228	0.243	0.241
IRR	[%]	17.05	19.68	19.74
Payback Period	[Years]	5.00	4.48	4.54

These end values reflect the compounding effect of operational savings, especially from reduced grid purchases and optimised surplus energy sales, which offset GA-Yearly Horizon's higher upfront outlay. The corresponding financial metrics reinforce the trade-offs in each approach. GA-Yearly Horizon achieves the lowest LCOE of €0.228/kWh yet has a moderately lower IRR of 17.05% and a slightly longer payback period of five years. Both HOMER and GA-Load Following realise higher IRRs of about 19.7% and slightly faster payback times around 4.5 years, but their LCOEs remain above €0.24/kWh, and their final net present costs exceed GA-Yearly Horizon's by roughly €35,000 to €40,000. These patterns confirm that longer-horizon planning can secure deeper lifetime cost reductions, albeit with more substantial upfront spending. Considering previous findings, which showed that GA-Yearly Horizon minimises month-to-month grid expenditures, the overall financial picture now confirms that strategic coordination of energy resources ultimately translates into lower lifetime expenses, even if the initial investment is higher and the return takes a little longer to materialise.

# 3.6 Summary

This chapter presented a comprehensive framework that brings together Genetic Algorithms (GA) and Mixed Integer Linear Programming (MILP) for both long-term planning and hourly dispatch of hybrid renewable energy systems. The GA scans a wide range of possible layouts, varying in photovoltaic, battery, and hydrogen capacities, seeking to minimise total project costs. Each candidate layout then goes through a MILP-based check to verify it can meet the full set of hourly demands across a calendar year. By packaging capacity decisions and operational constraints into a single, year-long optimisation, the proposed approach can uncover configurations that use resources more efficiently than simpler, short-horizon methods.

Nevertheless, this full-year optimisation operates under the assumption of perfect foresight. That assumption often improves the outcomes on paper but does not always mirror real-world conditions, where demand forecasts and renewable outputs evolve in shorter cycles. For that reason, the chapter concludes by comparing the GA–MILP approach with two alternatives that focus on more immediate decision-making: a rule-based load-following method and the HOMER Pro software. These analogies underline useful benefits and constraints of several temporal periods in system operation. The techno-economic results in this chapter are based on perfect foresight of hourly solar irradiance, load demand, and static time-of-use tariffs across a full deterministic year. Component efficiencies and financial inputs are treated as fixed, with no degradation modelling or multi-year uncertainty included in the optimisation.

Through an analysis of these opposing paradigms, the chapter clarifies how long-horizon optimisation might provide significant financial benefits yet depends on assumptions that might not always apply in operational settings. This investigation naturally emphasises the requirement of implementing realistic operational layer concepts such as rolling-horizon or Model Predictive Control (MPC) techniques with flexible load approaches, which more dynamically change schedules. Leveraging these ideas, the next chapter introduces MPC and flexible load-shifting strategies more realistically reflecting the daily reality of balancing renewable energy, storage, and end-user expectations.

# 4 Improving Renewable System Sizing Accuracy through Model Predictive Control Concept and Flexible Load Operation.

#### 4.1 Introduction

In Chapter 3, a nested GA–MILP approach was proposed and validated to determine optimal component sizes and an annual dispatch for a hybrid energy system, making use of a single, large-scale optimisation that assumed year-round knowledge of resources and loads. While that one-shot approach demonstrates how a system could theoretically minimise costs given perfect foresight, day-to-day operations in practice rarely enjoy such complete information. This chapter introduces an improved methodology intended to capture more realistic decision-making by dividing the year into smaller intervals and re-optimising repeatedly with partial forecasts. In addition, part of the electrical load is allowed to shift within each day described as flexible load in the coming sections, further enhancing operational efficiency. For the ease of modelling and to align with the real load from the Formentera case study, a selected water pump is modelled as flexible load.

## 4.2 Methodology

The novel framework keeps the familiar two-layer structure. The GA still handles long-term capacity choices, such as how large the battery bank or electrolyser should be, while the MILP determines an hourly dispatch. What changes is that the MILP is no longer solved over 8,760 consecutive hours at once; instead, it works in rolling windows of 24 hours. Only a subset of each solution (e.g., the first 12 hours of each 24-hour window) is "committed" to the final schedule, and then the process advances by half a day. By doing so, this approach more closely resembles a Model Predictive Control (MPC) scheme, where the horizon is gradually shifted as time progresses. The following sections detail the mathematical equations that are added or revised relative to Chapter 3's single-horizon MILP.

Figure 4-1 offers a schematic view of how the upper loop (GA) and local loop (rolling-horizon MILP) operate in unison. In each generation of the GA, an individual (i.e., a candidate set of capacities) is tested by running the MILP in sequential daily windows, each covering 24 hours. The MILP's solution for each window, complete with hour-by-hour decisions, yields an operating cost for that segment. These costs are aggregated across the full year, producing an annual operating profile that is then combined with capital costs, replacement schedules, and salvage values to compute the system's NPC. The GA's evolutionary operators, selection,

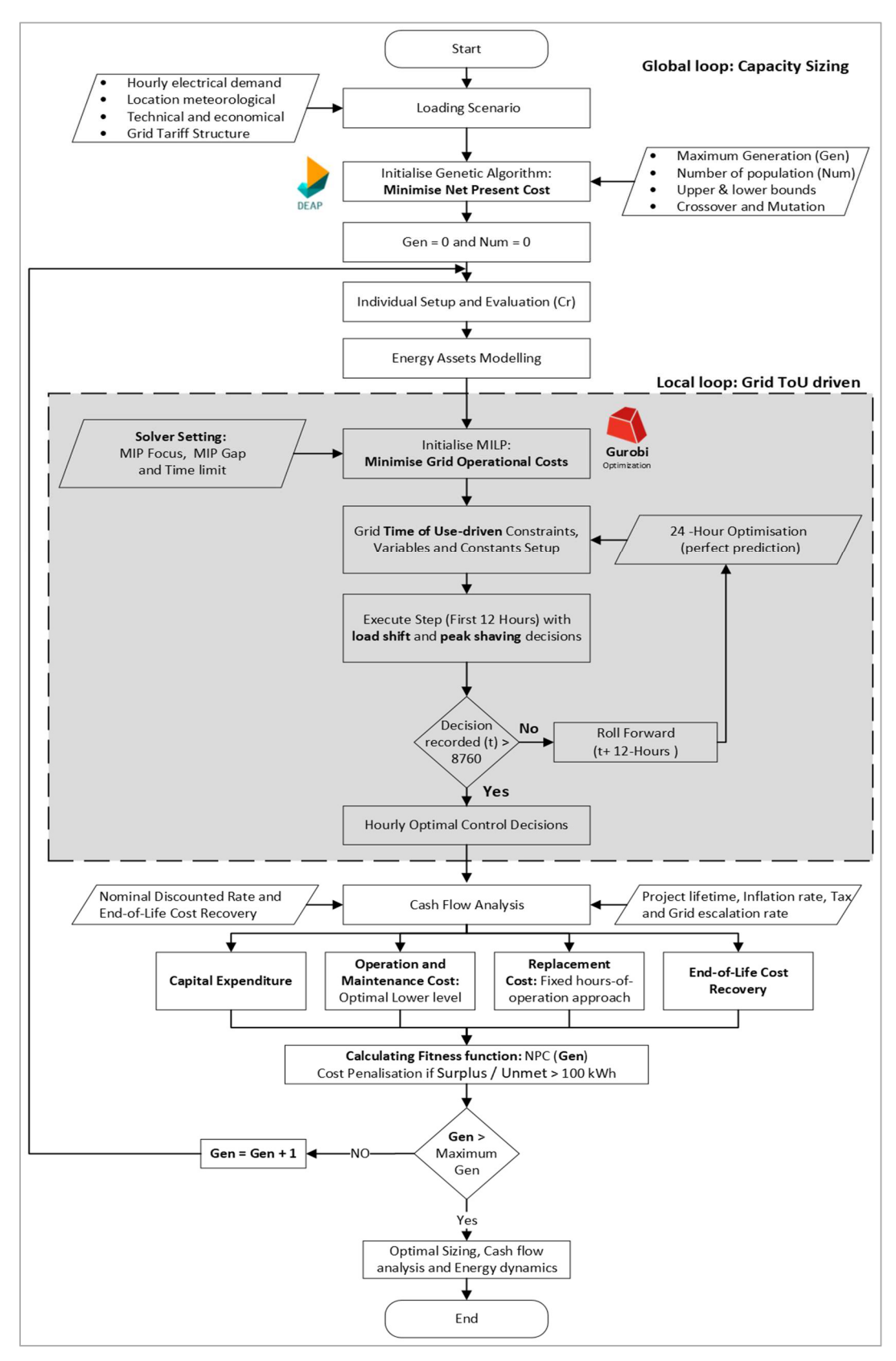


Figure 4-1: Proposed Novel GA-MILP-MPC Flexible Load Methodological for two layers Grid Time of Use driven Optimisation approach

crossover, and mutation, rely on this NPC value to guide the search toward more cost-effective designs.

The MILP solved in each 24-hour window is identical to the yearly MILP of Chapter 3: the same unmet- and excess-energy slack variables and the same per-kWh penalties (1 000 €/kWh unmet, 100 €/kWh excess) ensure that every window is feasible. The rolling horizon therefore produces 730 feasible sub-schedules, but after stitching the first 12 h of each window the GA receives one complete 8 760-hour schedule, exactly as in the GA-Yearly Horizon method. Solution quality is evaluated with the same annual indicators described in section 3.3.2.3 and the same fitness function (NPC plus the annual slack penalties) described in Section 3.3.2.2. No additional repair or replacement is required: if the stitched year still contains slack, the penalty already inflates NPC and the GA naturally pushes the population toward designs whose daily windows—and therefore the stitched year—drive both slacks to zero. In this way the rolling-horizon local loop inherits the feasibility guarantee and the evolutionary pressure of the Chapter 3 formulation while allowing limited-look-ahead operation. The next section, the detailed modelling is explained with focus on the rolling horizon with flexible load implementation.

#### 4.2.1 MPC-Flexible Load Formulation

Instead of solving for the entire year at once, the timeline is split into overlapping windows. Each window is set to 24 hours in length, though only the initial 12 hours of each solution are locked in before shifting to the next window. If a given window is indexed by w, its local hourly set is denoted by:

$$\mathcal{T} \in \{0,1,\dots,23\}. \tag{4-1}$$

In the global timeline of 8,760 hours, the starting hour of window w might be labeled h. Once the MILP determines a dispatch for hours h through h + 23, only the results for hours h to h + 11 become final, and the model moves on to the next window starting at h + 12. Within each 24-hour slice, the immediate goal is to minimise the operating cost:

$$\min_{\text{all variables}} \sum_{t \in \mathcal{T}} \left[ \pi_{\text{buy}}\left[t\right] \cdot P_{\text{grid,buy}}\left[t\right] - \pi_{\text{sell}}\left[t\right] \cdot P_{\text{grid,sell}}\left[t\right] + \text{ penalty }_{\text{unmet}} \cdot E_{\text{unmet}}\left[t\right] \right. \\ \left. + \text{ penalty }_{\text{excess}} E_{\text{excess}}\left[t\right] \right]$$

where  $\pi_{\text{buy}}[t]$  and  $\pi_{\text{sell}}[t]$  are the time-varying grid prices for purchasing and selling electricity, and  $E_{\text{unmet}}[t]$ ,  $E_{\text{excess}}[t]$  capture any shortfall or surplus energy at hour t. Since the overarching objective is to minimise total costs for the entire year, these 24 -hour solutions are ultimately pieced together, and their aggregated operational cost is added to the investment and maintenance costs in the GA's global net present cost (NPC) calculation.

Much like the formulation in Chapter 3, power flows on the DC side (where the battery and fuel cell reside) and the AC side (where the main load and grid connection are located) must balance each hour. If  $P_{ren,\ DC\ remaining}[t]$  is the portion of renewable power left on the DC bus after any direct usage represented by  $P_{ren,\ DC\ inverted}[t]$ , the DC node balance is:

$$\begin{split} P_{ren, \ DC \ inverted} \left[ t \right] + P_{ren, \ DC \ remaining} \left[ t \right] + P_{battery, \ discharge} \left[ t \right] + P_{fuel-cell} [t] \\ &- P_{battery, \ charge} \left[ t \right] - P_{inverter} \left[ t \right] \cdot \left( 1 + 1 - \eta_{DC/AC \ inverter} \right) \\ &- E_{\text{excess}} \left[ t \right] = 0, \qquad \forall t \in \mathcal{T} \end{split} \tag{4-3}$$

On the AC node, the inverter's output ( $P_{inverter}[t]$ ), any electricity bought from the grid ( $P_{grid\_buy}[t]$ ), and unmet load ( $E_{unmet}[t]$ ) are balanced with the main load, flexible load, any electrolyser usage, and any selling back to the grid  $P_{grid\_sell}[t]$ :

$$P_{\textit{inverter}}[t] + P_{\textit{grid\_buy}}[t] - P_{\textit{grid\_sell}}[t] - (P_{\textit{load}}[t] + P_{\textit{flexible}}[t]) - P_{\textit{electrolyser}}[t] + E_{\textit{unmet}}[t] = 0, \quad \forall t \in \mathcal{T}$$

$$(4-4)$$

Here,  $P_{\text{flexible}}[t]$  is a new term introduced in this chapter, reflecting that part of the load can be scheduled flexibly. A crucial difference from Chapter 3's single-shot solution is that each 24-hour window receives initial states for the battery and hydrogen tank from the final partial commitment of the previous window. The battery state of charge is redefined as following:

$$\operatorname{SoC}_{b}[t] = \begin{cases} \operatorname{SoC}_{\mathsf{init}}^{(w)}, & t = 0 \\ \operatorname{SoC}[t-1] + \frac{\eta_{\mathsf{b}} - N_{\mathsf{bt}} \cdot B_{\mathsf{m}}}{N_{\mathsf{bt}} \cdot B_{\mathsf{m}}} P_{\mathsf{battery}, \mathsf{charge}}[t] - \frac{P_{\mathsf{battery}, \mathsf{discharge}}[t]}{\eta_{\mathsf{b}+} \cdot N_{\mathsf{b}t} \cdot B_{\mathsf{m}}}, & t > 0 \end{cases}$$
(4-5)

The term  $SoC_{init}^{(w)}$  indicates that if window w begins at global hour h, its initial SoC for the battery equals the final SoC from the midpoint shift (h-12) of the previous window. The hydrogen tank Level of Hydrogen is redefined as following:

$$LoH[t] = \begin{cases} LoH_{\text{init}}^{(w)}, & t = 0\\ LoH[t-1] + \frac{\eta_{\text{el}}}{P_{HT} \times H_{LHV}} P_{\text{electrolyser}}[t] - \frac{P_{\text{fuel}-ce}[t]}{\eta_{fc} + x P_{HT} \times H_{LHV}}, & t > 0 \end{cases}$$
(4-6)

Here,  $LoH_{\rm init}^{(w)}$  is likewise set to the hydrogen tank level from the previously committed hours. At the end of each 24 -hour window's MILP, only the first 12 hours are appended to the final schedule, and the LoH values at hour t=12 become the initial states for the next window. To allow part of the load to be shifted for cost advantage, the model introduces a binary variable  $x_{\rm flexible,\ on/off}[t]$  and an associated power:

$$P_{\text{flexible}}[t] = P_{\text{flexible,rated}} \cdot x_{\text{flexible,on/off}}[t], \quad \forall t \in \mathcal{T}$$
 (4-7)

If  $P_{\text{flexible, rated}}$  is the rated power in kW and  $x_{\frac{\text{flexible, on off}}{\text{off}}}[t] = 1$  makes the load draw this power (kW) in hour t. The daily run-time requirement  $H_{\text{flexible, daily}}$  is enforced by summing the "on" hours across each calendar day:

$$\sum_{k \in T_d} x_{\text{flexible,on/off}} [k] = H_{\text{flexible,daily}}, \quad \forall d$$
 (4-8)

where  $T_d$  is the set of global hours belonging to day d. A complication arises because each rolling window might intersect multiple days. The code handles this by tracking how many flexible-load hours for each day were already used in a previous window. Let  $\phi_d^{(w-1)}$  be the flexible-load hours assigned to day d before window w. Then, if a window covers hours from day d, the MILP imposes:

$$\sum_{k \in T_d^{(w)}} x_{\text{flexible,on/off}}[k] + \phi_d^{(w-1)} = H_{\text{flexible,daily}}, \qquad \forall d$$
(4-9)

Thus, ensuring day d meets exactly the daily requirement by the time it finishes. The mutually exclusive constraints are applicable for this method for each window w, and it is given as following for the grid buy/sell exclusivity:

$$\begin{split} P_{\text{grid , buy}}\left(t\right) &\leq P_{gr}^{\max} \cdot \, x_{\text{grid}}\left(t\right), \\ P_{\text{grid,sell }}\left(t\right) &\leq P_{gr}^{\max} \cdot \left(1 - x_{\text{grid}}\left(t\right)\right), \qquad \forall t \in \mathcal{T} \end{split}$$

Battery Charge/Discharge exclusivity:

$$P_{\text{battery, charge}}\left(t\right) \leq P_{b}^{-\max}\left(1 - x_{\text{battery}}\left(t\right)\right), \tag{4-11}$$
 
$$P_{\text{battery, discharge}}\left(t\right) \leq P_{b}^{+\max}x_{\text{battery}}\left(t\right), \qquad \forall t \in \mathcal{T}$$

Electrolyser and Fuel Cell exclusivity:

$$\begin{split} P_{\text{electrolyser}}\left(t\right) &\leq P_{el}^{\max}\left(1 - x_{\text{hydrogen}}\left(t\right)\right), \\ P_{\text{fuel-cell}}\left(t\right) &\leq P_{fc}^{\max} x_{\text{hydrogen}}\left(t\right), \quad \forall t \in \mathcal{T} \end{split}$$

DC to AC limit and DC side constraints:

$$P_{\text{inverter}}\left(t\right) \leq P_{\text{inv}}^{\text{max}},$$

$$P_{\text{ren ,DC-inverted}}\left(t\right) + P_{\text{ren,DC-remaining}}\left(t\right) = P_{\text{ren-output}}\left(t\right),$$

$$P_{\text{ren, DC- remaining}}\left(t\right) = P_{\text{battery,charge}}\left(t\right) + E_{\text{exceess}}\left(t\right), \quad \forall t \in \mathcal{T}$$

Renewable availability to charge battery:

$$\begin{split} P_{ren, \ DC \ remaining} \left[ t \right] & \leq \left( M \cdot \ x_{ren-gen} \left[ t \right] \right) + \epsilon, \qquad \forall t \in \mathcal{T} \\ & \qquad \qquad P_{\text{ren,DC-remaining}} \left( t \right) \geq \epsilon x_{\text{ren-gen}} \left( t \right), \qquad \forall t \in \mathcal{T} \end{split} \tag{4-14}$$
 
$$P_{\text{battery,discharge}} \left( t \right) \leq \left( 1 - x_{\text{ren-gen}} \left( t \right) \right) \cdot P_{b+,max}, \qquad \forall t \in \mathcal{T}$$

All the mutual exclusivity constraints from Chapter 3, such as preventing simultaneous battery charging and discharging or blocking simultaneous buying and selling on the grid, and hydrogen remain valid in this rolling-horizon model. These physical and operational restrictions govern each 24-hour window w in the MPC-based framework. In other words, the method preserves all the prior constraints that define feasible operation at each hour, simply partitioning the year's timeline into segments and shifting states forward after every 12 hours of committed dispatch.

#### 4.2.2 Water Pump as a Flexible Load

In this work, we model the flexible load of a swimming pool water pump from the Formentera energy community. Essential for maintaining appropriate water circulation and filtration, the pump must run eight hours a day altogether. As long as the 8-hour daily run is attained, the exact timing of its operation is not constant and flexible; so, the model lets the start and stop times of the pump to be changed depending on renewable availability and grid prices signals. The active status of the pump is indicated by a binary decision variable, which guarantees that, on, it draws power at its rated value (3 kW). Table 4-1 offers a summary of the primary pump-related specs and input values.

Table 4-1:Flexible Load: Water Pump Specifications for the Formentera Energy Community

Parameter	Value	Units	Description
Rated Power  P <sub>flexible,rated</sub>	3	kW	Power draw when the pump is active.
Daily Operating  Requirement $H_{\text{flexible,daily}}$	8	hours	Minimum number of operating hours per day.
Pump Type	Swimming Pool	-	Non-critical load with flexible scheduling.
Operational Flexibility	Fully shiftable	-	Can be scheduled at any time, provided the 8-hour requirement is met.

The MPC framework incorporates this flexible scheduling, which lets the optimisation move the operation of the pump to times of more or less renewable availability or reduced grid charges. Such dynamic scheduling improves general system efficiency without endangering water quality criteria. Moreover, for better understanding, two scenarios of increased rated power of 4.35 and 5.8 kW were introduced to study the impact of an increased rated power of the flexible load.

While the community originally relies on a fixed 3 kW water pump, the present investigation assumes future expansions of similar load-sensitive equipment (for instance, additional pumps) to create larger flexible loads: 4.35 kW for MPC 6% and 5.8 kW for MPC 8%. These higher loads allow an expanded study into how adding flexibility influences both operating efficiency and overall economic returns. The scenarios are defined in Table 4-2.

Although the rated power of the current pump is modest (3 kW), the higher-rated scenarios (4.35 kW and 5.8 kW) allow the model to explore a meaningful flexible share of total daily energy use. In fact, in the MPC 6% and 8% scenarios, the flexible energy accounts for up to 6–8% of the community's average daily energy demand, which is significant from a system perspective. This supports a more robust evaluation of how load shifting affects capacity sizing, hydrogen utilisation, and economic outcomes.

Table 4-2: Scenarios defined for the flexibility investigation

Flexible load scenarios	Flexible load Power (kW)	Total non- flexible load (kWh)	Total Flexible energy (kWh)	Hours of the day	Compared to Fixed start (am)
GA- MILP - MPC 0%	0.00	211,665.3	0	0	08:00
GA- MILP - MPC 4%	3.00	202,905.3	8760	8	08:00
GA- MILP - MPC 6%	4.35	198,963.3	12,702	8	08:00
GA- MILP - MPC 8%	5.80	194,729.3	16,936	8	08:00

These higher loads allow an expanded study into how adding flexibility influences both operating efficiency and overall economic returns. The scenarios are defined in Table 4 2. These flexibility levels correspond to approximately 4%, 6%, and 8% of the community's average daily demand (≈579.9 kWh/day), with the highest case approaching 10%, a relatively high value compared with typical demand-side management studies.

#### 4.2.3 Summary

This rolling-horizon framework adds a realistic layer of adaptive control to the original GA–MILP model. By scheduling a flexible load within daily windows, the system can mitigate both unmet energy and renewable curtailment more effectively, taking advantage of near-term conditions rather than relying on year-long certainty. The next section will present numerical results comparing this rolling-horizon, flexible-load method to both the single-horizon solution from Chapter 3 and simpler rule-based dispatch algorithms. Through these comparisons, one can observe the distinct advantages when the model is made more dynamic.

#### 4.3 Results

This section presents the outcomes of the enhanced rolling-horizon MPC approach with flexible load integration, building on the methodology and findings of Chapter 3. Chapter 3 illustrated a full-year GA–MILP optimisation whereas the new method re-optimises in daily periods and allows dynamic load shifting. The results are arranged below: Section 4.3.1 describes system sizing and technical performance improvements; Section 4.3.2 investigates energy flows and dynamic behaviour; Section 4.3.3 addresses economic performance metrics; and Section 4.3.4 evaluates the effects of tuning both GA and MILP solver parameters. These results, put together, illustrate how a more realistic and adaptive optimisation framework benefits over the two benchmarking methods: the single-horizon technique and the short-horizon rule-based load-following approach.

#### 4.3.1 System Sizing

The results in Table 4-3 show how the newly deployed GA–MPC rolling-horizon method determines component capacities for flexibility levels of 0%, 4%, 6%, and 8%, in contrast to the single-horizon GA–MILP approach from Chapter 3 (Table 3-6). Previously, a year-long global optimisation with perfect foresight often led to higher photovoltaic (PV) capacity (156 kWp) and a large battery bank (86 strings), while simpler load-following strategies undersized both PV and batteries, boosting dependence on the grid. The rolling-horizon scheme, which re-optimises daily and, in some cases, allows part of the load to be rescheduled, avoids some of the oversizing observed with perfect foresight but still lowers grid imports more than do short-horizon heuristics.

Table 4-3: GA-MPC novel approach capacity sizing results.

Component	Units	GA-MILP -	GA-MILP -	GA-MILP -	GA-MILP -MPC
Component		MPC 0%	MPC 4%	MPC 6%	8%
Solar PV	[kWp]	155	152	154	150
Battery	[Strings]	76	74	76	80
Inverter	[kW]	77	75	75	72
Contracted	[kW]	41	40	39	37
Power	נעעען				
Fuel cell	[kW]	5	5	5	5
Electrolyser	[kW]	6	5	5	5
Tank	[Kg]	7	7	8	9
NPC	[€]	612,945	606,879	604,305	599,134
LCOE	[€/kWh]	0.224	0.221	0.221	0.218

At 0% flexibility, the GA–MPC solution selects a 155 kWp PV array, close to the 156 kWp from the annual optimisation but still far larger than the 124 kWp load-following benchmark. Even without load shifting, daily re-optimisation preserves most of the benefits of a year-long view. As flexibility rises from 0% to 8%, the PV rating declines slightly, reaching 150 kWp once a fraction of demand shifts to match solar production. Although the difference is only about 5 kWp, this shift highlights a design principle: nudging loads into midday hours eases pressure for extremely large PV arrays.

Battery sizing follows a subtler trend. The GA Yearly-horizon run selected 86 strings from Chapter 3, whereas rule-based load following chose around 58. Under GA–MPC, the system first adopts 76 strings at 0% flexibility, stays around 74–76 strings through 4%–6% flexibility, then jumps to 80 strings at 8%. Rolling-horizon scheduling plus limited load shifting avoids over-investment in battery storage at lower flexibility levels yet ultimately deploys a slightly bigger bank at 8%. Shifting demand toward daylight hours can diminish the need for excessive evening storage unless flexibility grows enough to justify adding more capacity to capture surplus solar power. Moving from 76 to 80 strings at the highest flexibility indicates that once shifting surpasses a threshold, a larger battery is advantageous for further minimising grid exchanges.

The contracted grid power and hydrogen elements show comparable patterns. While the single-horizon solution assigned up to 52 kW of contracted power, the new approach scales it back to 41 kW (0% flexibility), then to 37 kW (8%). Rolling-horizon control plus partial load shifting lowers grid peaks below either perfect foresight or purely reactive methods.

Meanwhile, the electrolyser rating moves from 6 kW to 5 kW as soon as any flexibility is introduced, reflecting reduced need to capture every midday surplus. The hydrogen tank, however, expands from 7 kg to 9 kg by 8% flexibility, signifying that fewer kilowatts of electrolyser capacity can be balanced by a slightly larger tank, which stores hydrogen for later use.

These capacity decisions translate directly into NPC differences. In Chapter 3, perfect foresight produced around €625,776 in NPC, while load-following solutions ranged from about €661,000 to €665,000. Under the rolling-horizon GA-MPC, even at 0% flexibility, the NPC drops below €613,000, reflecting that daily re-optimisation alone remedies certain inefficiencies of annual sizing. Moving to 8% flexibility brings the NPC down to €599,134, well below the Chapter 3 benchmarks, and reduces the Levelised Cost of Electricity to about €0.218/kWh. Breaking the year into 24-hour MPC windows and permitting modest flexible demand thus curbs oversizing, leverages local solar effectively, and delivers lower total project costs than either full-year or passive short-horizon methods. Table 4-4 compiles the principal performance indicators for the MPC-based method under four different levels of flexibility, providing a direct parallel to Table 3-7 in Chapter 3. In that earlier chapter, the GA-Yearly Horizon scheme yielded roughly 285 MWh of annual PV generation, covering approximately 61 percent of the electricity demand, while simpler load-following algorithms produced closer to 227 MWh but attained higher self-consumption percentages by virtue of smaller arrays. Under the present rolling-horizon technique, total PV output hovers at 280 MWh across all flexibility scenarios, and the share of load met directly by solar averages over 58%, marginally below the 61% recorded for the single-horizon approach. This little variation implies that MPCbased scheduling still efficiently uses solar resources even if it divides the year into daily windows.

Table 4-4 Performance metrics comparison for MPC approach with different flexibility %.

Metrics	Units	GA-MILP - GA-MILP -		GA-MILP -	GA-MILP -	
wietrics	Units	MPC 0%	MPC 4%	MPC 6%	MPC 8%	
PV Generated	kWh	283,669.53	278179.15	281600.73	274518.90	
PV Directly Consumed by load	kWh	123802.20	122563.30	122914.93	122328.25	
PV Contribution to Load	%	58.48	57.90	58.07	57.79	
Renewable Self Consumption	%	43.64	44.05	43.64	44.56	
Battery Throughput	kWh	83,739	84,303	84,840.85	85,201	
Electrolyser Capacity Factor	%	30.45	23.99	25.54	23.46	
Fuel Cell Capacity Factor	%	9.97	6.55	7.01	6.57	
PV Excess Energy	kWh	159,867.33	155615.9	158,686	152,190	
Electrolyser Usage	kWh	16,008.27	10,508.42	11,188.64	10,464.32	
Fuel Cell Usage	kWh	4,369.67	2,871.04	3,073.36	2,879.93	
Grid Dependence	%	9.47	10.14	9.96	10.5	
Grid Import	kWh	20,061.72	20,576.70	19825.76	20,459.23	
Grid Export	kWh	59,002.69	58,281.19	60,243.08	54,728.35	

Beyond the overall PV production, the most pronounced distinctions arise in the operational patterns of the electrolyser and fuel cell. In Chapter 3, the single-horizon optimisation often kept these hydrogen components running at modest capacity factors (around 15 % for the electrolyser and 5 % for the fuel cell). Now, as Table 4-3 reveals, the electrolyser capacity factor reaches approximately 30 percent even with no load flexibility, then falls to the midtwenties once partial demand shifting alleviates the midday surplus. A similar decline emerges in the fuel cell's capacity factor, dropping from almost 10 % under zero flexibility to about 6–7 percent when the load is partially rescheduled.

Battery throughput exceeds 80 MWh in each MPC scenario, aligning closely with the 85 MWh reported under the Yearly Horizon method. Meanwhile, the system's reliance on grid electricity settles around 9–10 percent, somewhat higher than the 7.21 % observed with perfect foresight, yet consistently below the 14–15 percent typical of load-following. Such results suggest that a rolling-horizon process, when combined with modest demand flexibility, can retain many of the advantages of long-term optimisation while offering improved responsiveness to short-term system variations.

#### 4.3.2 Energy Flow and Dynamics

#### Winter Days Analysis:

Figure 4-2 shows operational dynamics for the novel GA-MPC flexible approach. Three winter days (13–15 January 2022) closely follow the capacity sizing and performance work discussed in previous section. This section offers substantial perspectives on the performance of optimally configured GA-MPC approach under wintertime conditions marked by low photovoltaic (PV) generation. Such a close study proves particularly valuable before turning to the summer analysis, when PV output is likely to be much higher.

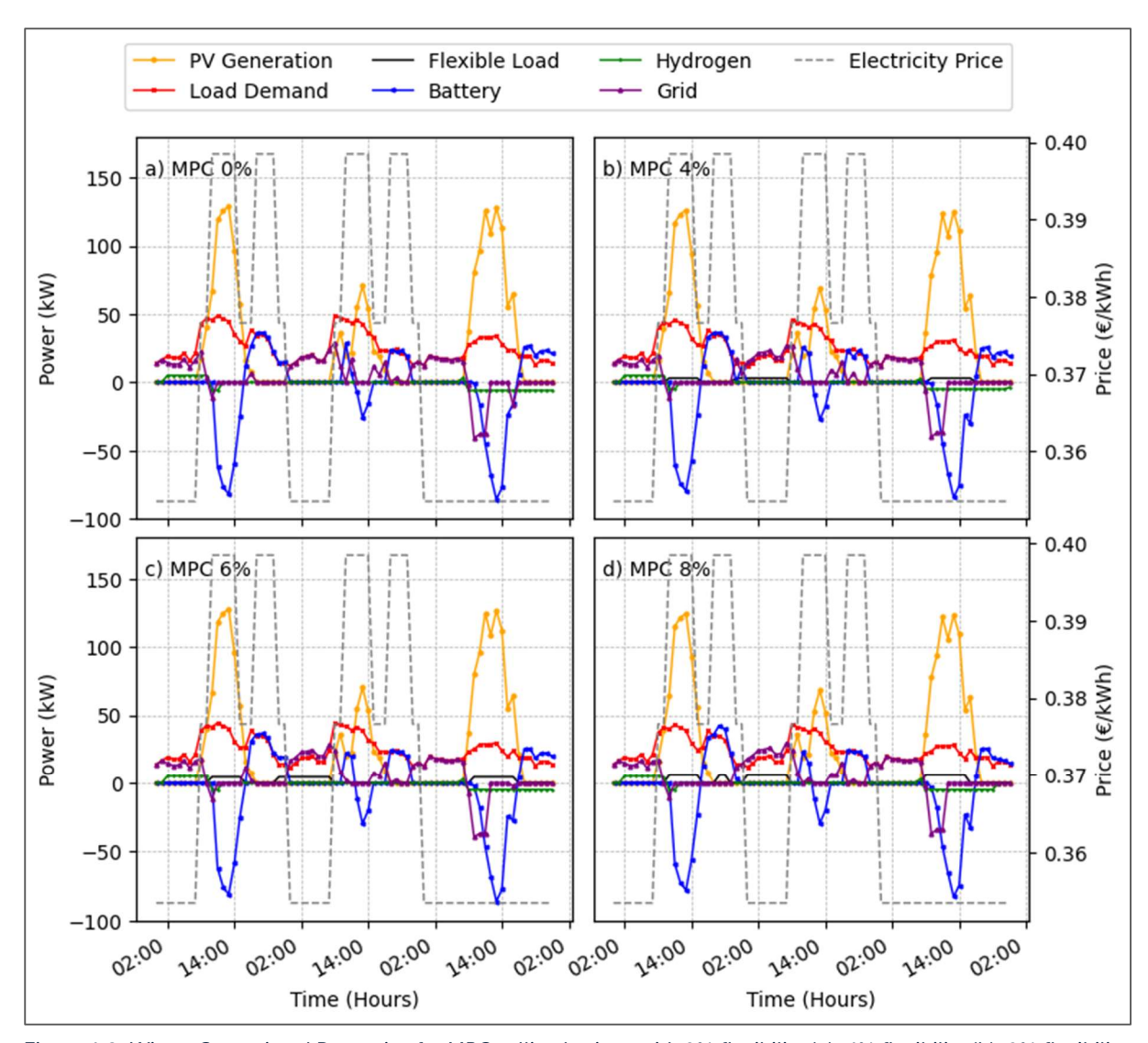


Figure 4-2: Winter Operational Dynamics for MPC rolling horizon with 0% flexibility (a), 4% flexibility (b), 6% flexibility (c), and 8% flexibility (d). The positive values for hydrogen represent the fuel cell output in kW, and the negative values indicate electrolyser consumption. For the battery, positive values indicate discharge, and negative values indicate charging. Grid interactions show positive values for electricity purchases and negative values for sales.

On 13 January (Day 1), hourly electricity rates ranged between €0.3535/kWh and €0.3985/kWh, thereby guiding how the GA–MPC scenarios (with 0%–8% flexibility) scheduled load and storage. Between 00:00 and 07:00, with no PV generation available, all scenarios

drew about 115 kWh from the grid, backed by steady fuel cell power of around 30 kWh. Because the overnight rate was €0.3535/kWh, the day's lowest, this choice effectively kept early-morning costs down. Later on (11:00–15:00), PV production varied between 510.12 kWh in MPC 8% and 527.12 kWh in MPC 0%. After satisfying the immediate load (11:00–15:00), these scenarios used the remaining solar surplus (roughly 289.39–305.34 kWh) to replenish batteries and drive electrolysers (5–6 kWh). Notably, systems with flexibility (0%–8% flexibility) shifted two hours of operation (08:00–10:00) for the pump load to night period (16:00–23:00), thus curtailing reliance on the grid during higher-priced daytime hours.

On 14 January (Day 2), similar pricing patterns prompted MPC 4%–MPC 8% to move significant portions of their pump demand (24–46.4 kWh) to early morning (00:00–07:00), when costs remained at €0.3535/kWh. Rolling short-horizon logic indicated times during the day that solar output would not meet the total load, matching up with pricier daytime tariffs, which led these flexible scenarios to shift usage earlier. Meanwhile, MPC 0%, lacking flexibility, imported 139.50 kWh overnight (00:00–07:00) at the same low rate. By midday (11:00–15:00), each scenario capitalised on about 219.88–224.22 kWh of PV energy to recharge batteries, holding midday grid imports to a modest 7.39–28.44 kWh. During the evening (16:00–23:00), approximately 85–90 kWh of stored battery energy was discharged, further cutting down the system's dependence on costlier grid electricity.

On 15 January (Day 3), a weekend day with a uniform charge of €0.3535/kWh throughout, there was no direct price-based incentive for shifting loads. Despite that, the GA–MPC approach still harnessed midday (11:00–15:00) solar surpluses (as high as 531.30 kWh for MPC 0%). Extensive battery charging (around 300 kWh) and hydrogen generation (up to 48 kWh in MPC 0%) allowed each scenario to operate independently of the grid from 08:00 onward. MPC 4%, MPC 6%, and MPC 8% likewise rescheduled parts of their pump use into midday hours, optimising the use of available solar, even without rate fluctuations.

These results taken together demonstrate the nimble approach of the GA–MPC system for managing variable loads in winter environments, where general solar availability is greatly reduced. Reacting dynamically to both electricity price structures and renewable availability, GA–MPC shows more flexibility than previously benchmarked methods (including GA–Yearly Horizon, GA–Load Following, and HOMER–Load Following, explored in Chapter 3), so improving operational efficiency in these low-sunlight winter scenarios.

#### **Summar Days Analysis:**

Extending the in-depth winter assessment, it is equally important to investigate how the GA–MPC method fares in the summer (Figure 4-3), when PV availability is greatly increased. Three illustrative summer days (18–20 August 2022) are thus reviewed to demonstrate the manner in which the previously sized hybrid capacities exploit excess solar energy, and how active load shifting influences operational efficiency.

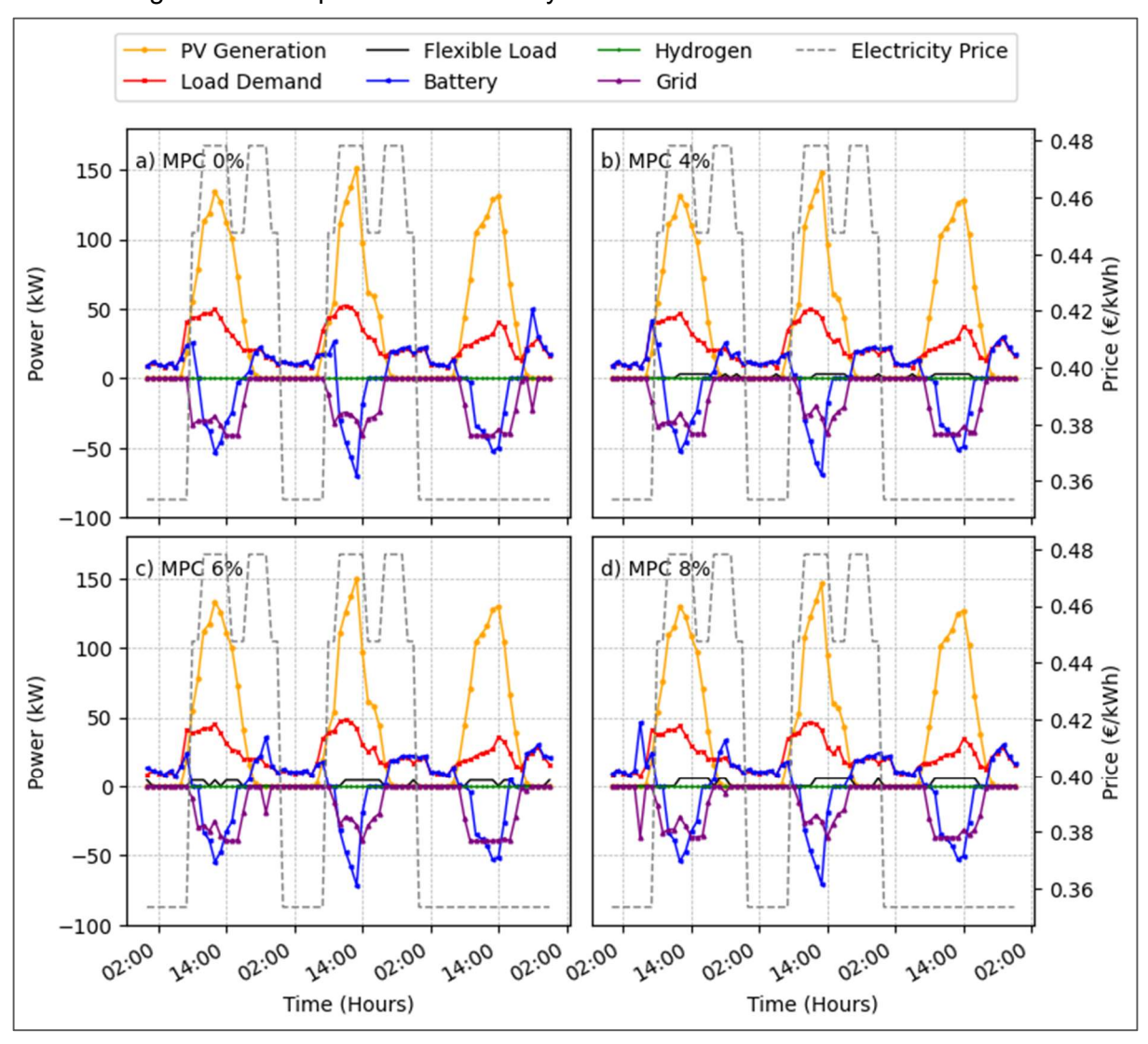


Figure 4-3: Summar Operational Dynamics for MPC rolling horizon with 0% flexibility (a), 4% flexibility (b), 6% flexibility (c), and 8% flexibility (d). The positive values for hydrogen represent the fuel cell output in kW, and the negative values indicate electrolyser consumption. For the battery, positive values indicate discharge, and negative values indicate charging. Grid interactions show positive values for electricity purchases and negative values for sales.

On 18 August (Day 1), which featured sizeable midday (11:00–15:00) solar yields about 572–591 kWh, the GA–MPC strategy fully capitalised on abundant renewable supplies. Between midnight and 07:00, all scenarios (0%–8% flexibility) satisfied load solely from stored battery power (96.64–136.13 kWh discharge), thus avoiding grid purchases at the €0.3535/kWh overnight rate. During the morning (08:00–10:00), MPC 4% and MPC 8% opted the same decisions by shifting these hours to operate at the evening window (16:00–23:00), avoiding

pricier grid tariffs. While the MPC 6% shifted flattened the flexible load, operating some of it at early morning hours (00:00–07:00) by 4.35 kWh and during evening hours (16:00–23:00) by 4.35 kWh, closely avoiding peak prices during midday hours. Substantial midday solar (11:00–15:00) enabled intensive battery charging (190–200 kWh) and exports of 155.9–173.6 kWh, thereby capitalising on peak PV for both economic and operational gain. In the evening (16:00–23:00), the battery (87.08–107.14 kWh discharge) adequately met the community's needs, preserving autonomy from the grid and permitting 52.8 – 76.8 kWh of further surplus exports.

On 19 August (Day 2), the GA–MPC scenarios managed variable tariffs again, €0.3535/kWh overnight and €0.4782/kWh at peak daytime. From midnight until 07:00, every scenario drew upon battery reserves (98–101 kWh) alone, eliminating the need for overnight grid imports. Between 08:00 and 10:00, MPC 0% sustained its non-shiftable 9 kWh load, while flexible scenarios (MPC 4%–MPC 8%) intentionally avoided heavy loads at that time, preserving more PV for export (67–98 kWh) and achieving moderate battery charging (30–32 kWh). By midday (11:00–15:00), the flexible load in MPC 6% and MPC 8% ramped up to 21.75 and 23.2 kWh, respectively, aligning with the robust solar output (571–556 kWh). This scheduling facilitated large-scale battery charging (191–211 kWh) and exports (142–200 kWh). In the evening (16:00–23:00), strategic discharges (100–106 kWh) again checked peak-hour imports, conserving sufficient battery headroom so that 38–52 kWh could be exported, thereby minimising reliance on higher-priced grid energy.

Finally, 20 August (Day 3) had a consistent €0.3535/kWh tariff, showcasing the GA–MPC framework's adaptive capabilities in the absence of differential pricing. During morning hours (08:00–10:00), MPC 6% and MPC 8% purposefully raised their flexible loads to 8.7 and 11.6 kWh, respectively, in tandem with ample PV (213–220 kWh). At midday (11:00–15:00), MPC8 utilised as much as 29 kWh of flex demand, optimising use of peak solar (572–592 kWh). Consequently, the battery was well charged (202–211 kWh), and surplus exports (178–200 kWh) were high. By late afternoon and evening (16:00–23:00), battery discharges of roughly 116–140 kWh ably met demands (164–174 kWh) while still producing 54–86 kWh for export, thereby sustaining a high degree of grid independence.

Diving deeper in the analysis, four days between winter and summer are selected for the analysis of method MPC-8%. Figure 4-4 illustrates the capability to strategically adjust and shift the loads in response to electricity prices and the availability of PV generation at each time step. For instance, on winter days, subplots a) and b), which are inherently limited in PV generation, the MPC-8% approach schedules most of the flexible load towards early morning hours. This tactic is clearly evident as the loads are scheduled between midnight and 07:00, taking advantage of the lower electricity tariffs of approximately €0.3535/kWh. Such scheduling reduces grid purchases when PV energy is insufficient to meet load demand during more expensive daytime hours. The MPC-8% approach reduces operating costs related to energy imports from the grid during low renewable generation by aggressively moving loads to periods of lower electricity prices.

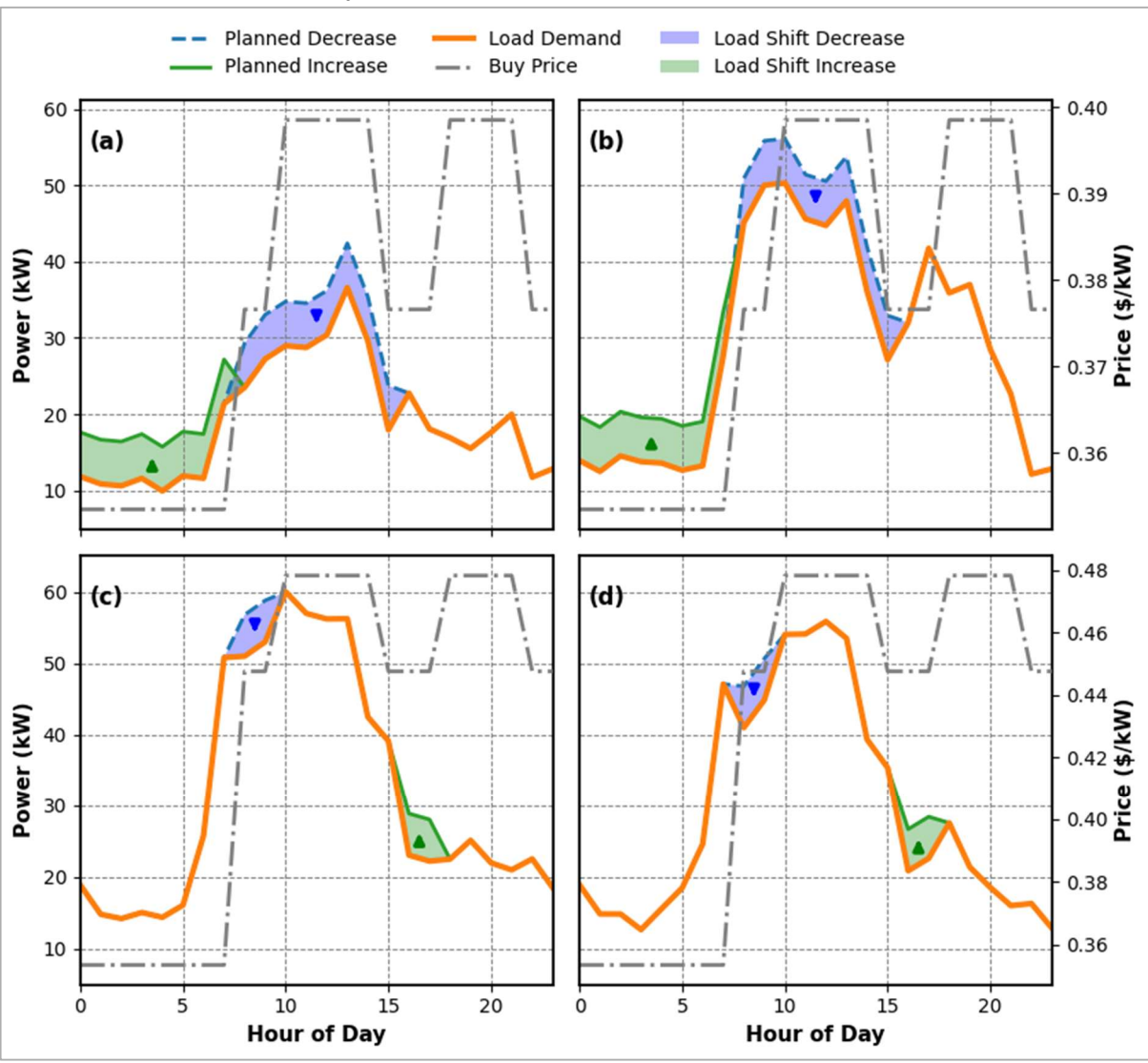


Figure 4-4: Hourly load profiles and pricing dynamics for MPC 8% flexible operation across four representative days: (a) 5<sup>th</sup> January 2022 and (b) 12<sup>th</sup> January 2022, representing winter days with low PV availability, whereas (c) 20<sup>th</sup> July 2022 and (d) 21<sup>st</sup> July 2022, reflecting summer days with abundant solar energy. Shaded regions indicate load shifts (green: increase, blue: decrease), highlighting MPC's adaptive strategy to minimize energy costs by aligning demand with low-tariff hours and PV generation windows. Dual-axis plots show both power demand (left y-axis) and electricity prices (right y-axis).

Contrastingly, on the summer days in subplots c) and d), a different behaviour is demonstrated, explained by the high PV generation and the availability of excess energy. The MPC-8% method is more selective and reduces the necessity for extensive use of electricity in the early morning as observed during the winter days. Instead, it only shifts loads when needed, specifically during hours between 8:00 and 10:00 in the morning, when demand is high, but PV generation is still insufficient to meet the load. This avoids peak price windows, thereby enhancing the utilisation of midday PV generation. Consequently, the summer operational profiles exhibit minimal reliance on grid imports during high-tariff periods, leveraging the full potential of abundant solar resources and storage solutions.

Comparative study during these summer and winter weeks highlights GA–MPC's improved operational responsiveness. Unlike earlier benchmark techniques, GA-Yearly Horizon, GA-Load Following, HOMER-Load Following, GA–MPC's short-horizon control realigns battery usage and flexible loads each hour according to solar output and tariff structures, achieving better cost savings and heightened renewable integration. Furthermore, the research underlines GA-MPC 8% as the assessment of selected days in both summer and winter confirms the effectiveness of the short-horizon MPC approach in dynamically modifying operational decisions to seasonal changes, so maximising cost efficiency and integration of renewable energy. This is followed by the next section, which examines how the capacities of solar, battery, and hydrogen systems relate to inverter sizing ratios, a crucial component in maximising the overall cost and efficiency of the system.

#### 4.3.3 Economic Analysis

Building on system sizing and operations, exploring in great depth how various load flexibility scenarios and short scheduling horizons can influence financial results. Using the same benchmarking approach (GA-Yearly Horizon, GA-Load Following), Figure 4-5 evaluate four MPC-based solutions, MPC 0% (subplot a), MPC 4% (subplot b), MPC 6% (subplot c), and MPC 8% (subplot d). Each scenario's cost components, including initial capital expenditure, operating and maintenance (O&M), replacements, and salvage values, are broken out to precisely estimate their financial effects.

The economic case for the community system is determined by how energy is traded with the grid and, more specifically, by the asymmetry between the retail import tariff and the feed-in price. Table 4-5 presents a Year-1 snapshot of grid-trading cash flows for all controllers considered in this study, including the baselines defined previously (Grid-Only, GA-Yearly horizon, GA-Load Following, and HOMER-Load Following) and the MPC cases with 0–8% flexible load. For each scenario the table separates exported energy and its income from imported energy and its cost and reports the resulting net grid cash-flow together with the

avoided import cost relative to Grid-Only. Because these figures are derived directly from hourly energy flows priced by the time-of-use schedule, with fixed contracted-power charges and excess-demand penalties applied explicitly, the results are fully auditable and comparable across controllers.

Table 4-5 Year-1 grid-trading cash-flow by scenario, separating export revenue from import costs and reporting net grid cash-flow and avoided import cost (Grid-Only – scenario)

Scenario	Exported kWh/year	Export rev- enue €/year	Imported kWh kWh/year	Import cost €/year	Net grid cash-flow €/year	Avoided import cost vs Grid-Only €/year
Grid-Only (reference)	-	-	211,665	83,198	86,946	-
GA-Yearly horizon	61,686	3,146	15,266	5,472	4,857	77,726
GA-Load Following	30,224	1,541	30,952	11,532	13,787	71,667
HOMER- Load Follow- ing	28,061	1,431	33,104	12,333	14,650	70,866
MPC 0 % flex.	58,932	3,006	20,094	7,295	6,285	75,904
MPC 4 % flex.	58,098	2,963	20,465	7,407	6,391	75,791
MPC 6 % flex.	60,243	3,072	19,826	7,160	5,988	76,038
MPC 8 % flex.	54,728	2,791	20,459	7,385	6,395	75,814

Taken together, the results show that export revenue is modest under all controllers because the feed-in price is far lower than the retail import tariff; the optimisation therefore prioritises self-consumption and temporal shifting over export. The principal source of economic value is the reduction in imported energy relative to Grid-Only, which appears clearly in the "Import cost" and "Avoided import cost" columns. Net grid cash-flow falls sharply for every optimised method, and the MPC cases deliver an additional reduction by shifting the flexible pump load into hours of higher on-site generation or lower retail price. Including GA-Yearly, GA-Load Following and HOMER-Load Following alongside MPC demonstrates that this conclusion is method-agnostic and rooted in the tariff structure rather than in a specific controller. Having established the composition of grid-trading cash flows in Year-1, the next paragraphs examine how flexibility reshapes the cost stack—CAPEX, O&M, replacements and salvage—for each MPC level and how this aligns with the monthly patterns shown in Figure 4-5 and Figure 4-6

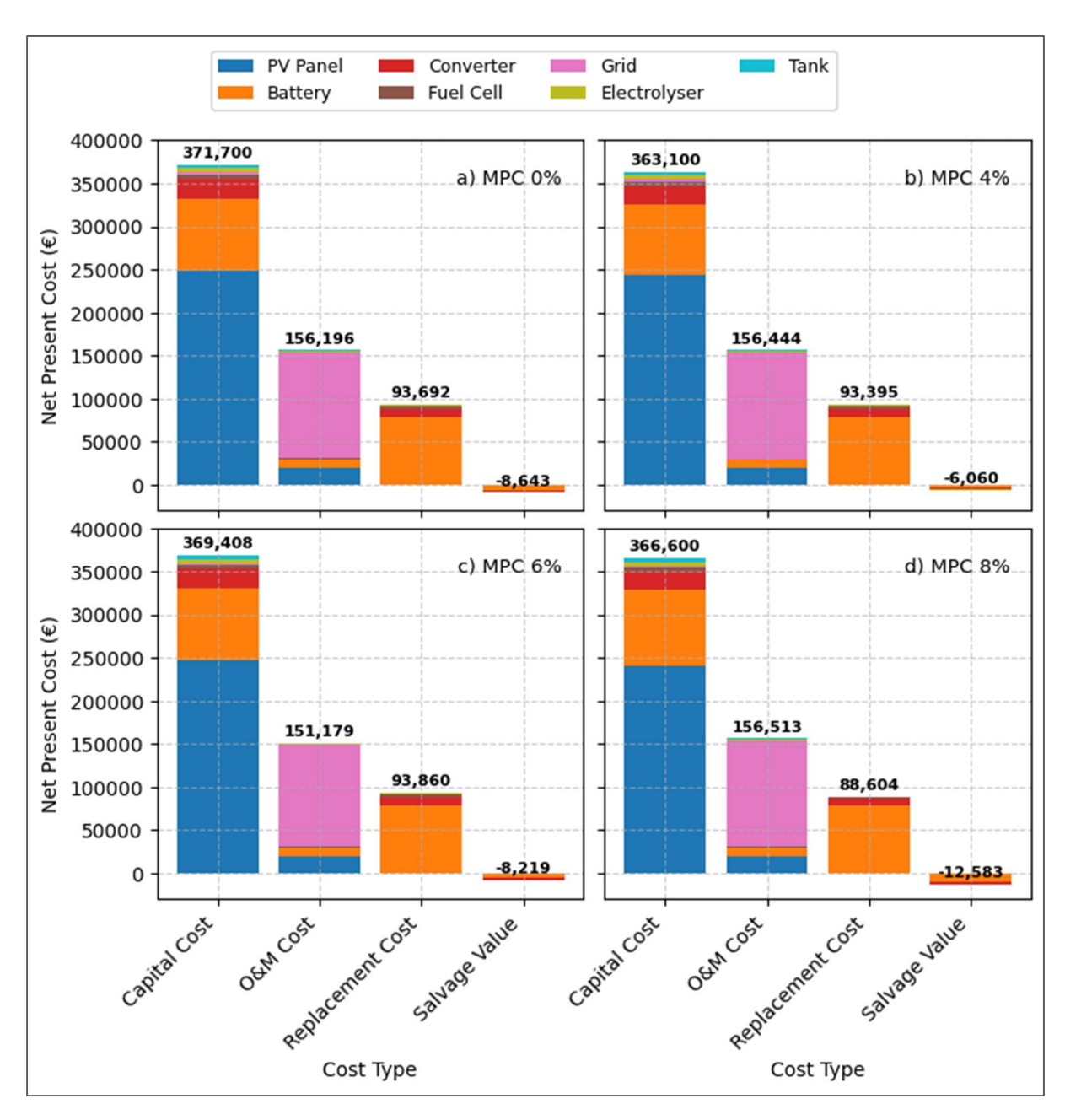


Figure 4-5: Breakdown of Net Present Costs for the total system costs by category for MPC rolling horizon with 0% flexibility (a), 4% flexibility (b), 6% flexibility (c), and 8% flexibility (d).

With no adjustable load, MPC 0% Scenario (subplot a) calls for the largest capital investments, €248,000 in PV panels and €83,600 in battery storage. This sizeable initial expense arises from the need to secure adequate renewable energy to offset higher grid dependence. Still, operational expenses are somewhat substantial even with these major upfront costs. Especially, O&M expenses for grid acquisitions alone come to €121,853, by far the biggest single component in the annualised expenses. Driven by heavy cycling and frequent partial-state operations, reflecting operational limits without flexible load shifting, battery replacement also adds major budgetary pressure (€77,958). Minimal salvage recovery (€6,278 from

batteries and €1,844 from inverters) points to quite high equipment wear brought on by frequent cycling and increased grid dependency.

Adding small load flexibility to the MPC 4% Scenario (subplot b) changes cost structures. PV capital investments drop somewhat to €240,000 while battery investment increases somewhat to €88,000. Most importantly, O&M costs for grid purchases remain high (€122,815), which reflects still significant dependence on grid energy, somewhat mitigated by better timing of flexible loads to lower tariff times. Though with less fuel cell replacements (€1,698), thanks to controlled hydrogen storage cycling, replacement prices for batteries remain similar (€77,742), emphasising continuous cycle demands. Salvage values also clearly improve (batteries €10,540, inverters €1,724), implying that more operating flexibility somewhat reduces equipment stress.

Increasing flexibility even more in the MPC 6% Scenario (subplot c). Although initial capital costs for PV (€246,191) and batteries (€84,060) remain in line with past scenarios, improved load scheduling notably reduces grid-related O&M costs to €117,390, so proving the financial advantage of moving a higher flexible load (4.35 kW) to periods when renewable energy is abundant, or electricity rates are low. Although replacement costs reflect higher battery throughput (€79,111), more regulated cycling greatly lowers running grid costs. Modest increases in inverter and electrolyser replacements (€9,518 and €1,697 respectively) indicate better total hydrogen cycle, hence optimising the use of renewable resources. Salvage values remain modest (€5,629 batteries, €1,791 inverters), showing the controlled battery and inverter use made possible by more operational flexibility.

Finally, the MPC 8% Scenario (subplot d) achieves the most refined balance between operational flexibility and financial prudence. Here, the capital investments for PV (€243,200) and battery storage (€81,400) slightly reduce, reflecting optimised capacity sizing from higher load flexibility. Despite high battery replacement costs (€78,619) due to slightly increased battery cycling (85,201 kWh annual throughput), strategic load shifting significantly mitigates operational costs, maintaining grid-related O&M at €123,513. This scenario shows that more frequent but shallower battery cycles, made feasible by flexibility, have continuous financial benefits by better controlling asset lifetimes, thereby attaining a considerable reduction in salvage values (€3,465 batteries, €1,497 inverters).

These MPC-based models clearly show a financial improvement over Chapter 3 benchmarks, such GA-Load Following, which suffered considerably greater NPC owing to increased annual grid imports and replacements. For instance, GA-Load Following registered grid purchases (O&M) of €245,234, more than double even the least flexible MPC scenario here (MPC 0%).

Similarly, MPC scenarios' carefully scheduled flexibility notably reduces battery replacements compared to GA-Load Following's €64,148 cost, despite comparable battery throughputs.

This assessment indicates that even modest enhancements in load flexibility substantially improve economic performance. Specifically, increasing flexibility from MPC 0% to MPC 4% and beyond systematically lowers grid-related operational expenditures and enhances renewable energy utilisation, despite moderately higher replacement costs. Among the evaluated methods, the MPC 8% scenario shows the highest overall economic performance, thereby amply illustrating the significant advantages obtained by carefully matching flexible loads with tariff variations and renewable generation.

Figure 4-6 presents a monthly breakdown of grid charges alongside the revenues gained from selling surplus energy for four GA-MPC flexibility scenarios: 0%, 4%, 6%, and 8%. This monthly perspective illustrates how short-term operational strategies shape both the system's economic results and its reliance on the grid throughout the calendar year.

In the 0% load flexibility scenario, the absence of shifting capabilities causes hefty grid charges during the colder months. January's costs, for instance, reach roughly €3,801, most of which arises from significant energy imports (€3,584.64) and fixed power fees (€344.55), with export earnings at a modest €128.18. By contrast, the summer sees robust photovoltaic (PV) generation and drastically reduced grid use. In June, imports dip to about €44.09 while export earnings climb to €320.27, leading to an overall monthly expense of just €57.25. Even so, the unavoidable winter reliance on grid power pushes the annual operational cost up to around €15,884, highlighting how a lack of flexibility exacerbates seasonal demand swings.

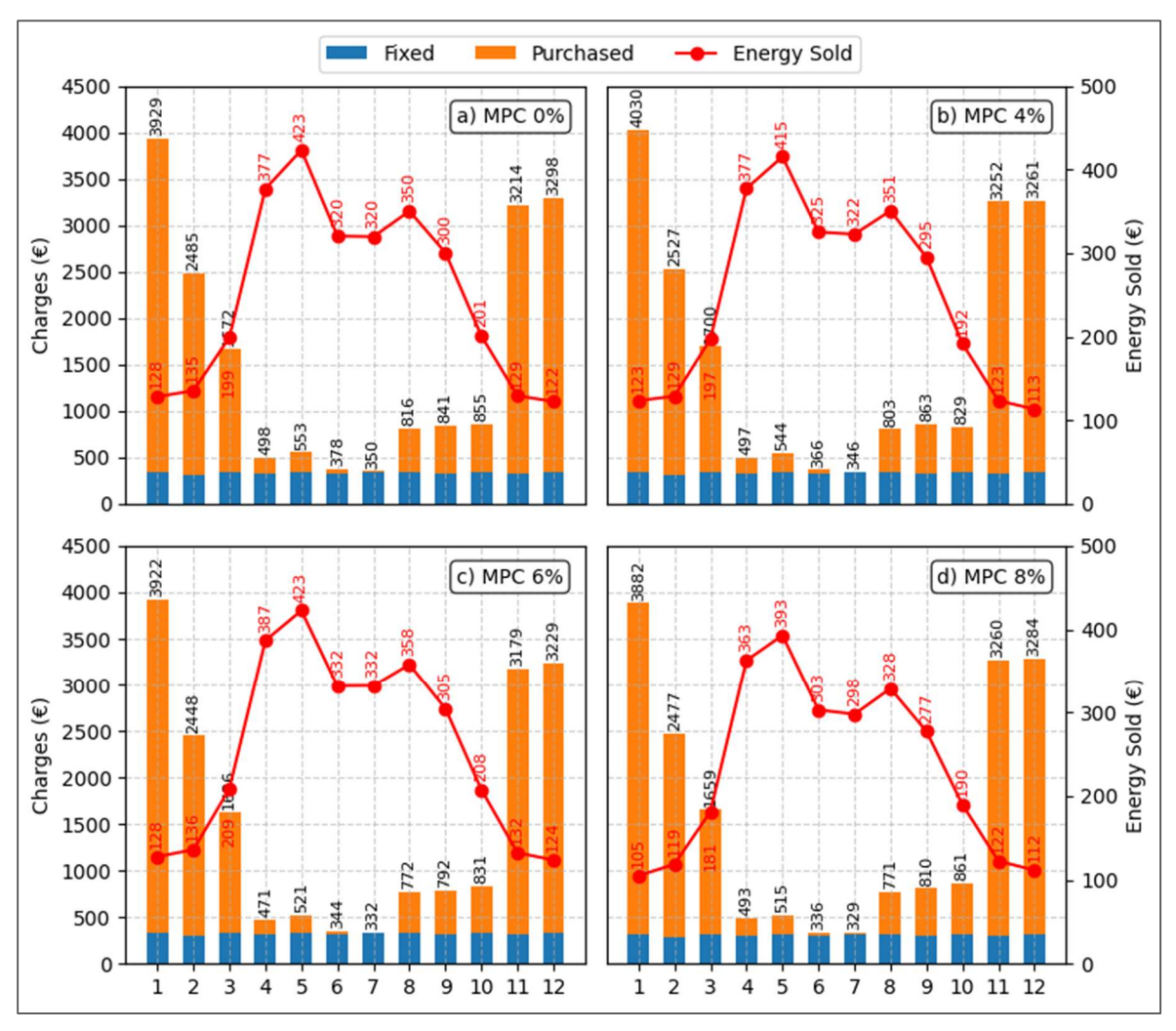


Figure 4-6: Monthly breakdown of grid escalated charges and revenues for MPC rolling horizon with 0% flexibility (a), 4% flexibility (b), 6% flexibility (c), and 8% flexibility (d).

Introducing 4% load flexibility adds a slight increase in battery expenses but creates new possibilities for capitalizing on cheaper tariff periods. Although January's monthly bill inches up to €3,907, with nighttime tariffs accounting for €3,694.21 of the import costs, the biggest gains become evident in the shoulder seasons. During April, the flexible 3 kW load is timed to maximize daytime exports, yielding €325.12 in export revenue and holding monthly grid fees to around €41.13. A similar improvement appears in May, where significant export revenue (€415.21) offsets import expenses (€208.13), pulling the overall monthly charge down to €129.06. As a result, total yearly grid costs land at €16,057, while renewable self-consumption improves significantly to 44.05%, demonstrating the value of even modest load-shifting.

Expanding the flexible load to 6% (4.35 kW) brings more pronounced financial benefits. January's grid costs fall slightly to €3,795 compared to the 4% scenario, thanks to more targeted scheduling of the 12,702-kWh annual flexible load. Export earnings of €331.91 greatly exceed the low imports (€23.05), so maintaining the net bill for June to be only €12.28. The

annual grid cost falls to €15,394 by maximising the usage of midday solar, the lowest amount among the four scenarios.

With 8% load flexibility, that is, 5.8 kW, or 16,936 kWh annually, the system maximises capacity to benefit from solar output. In months of plenty of sunlight, the financial effect is especially obvious. For example, exports in May bring €392.93 while imports come at €203.64, therefore producing a net charge of -€189.30. Strong export income (€302.91) and well-timed flexible loads help June follow a similar path whereby the month's grid bill of just €32.89 is maintained. While annual grid spending for the whole year reaches €15,886, equal to the 0% case, the 8% flexibility scenario boosts renewable self-consumption to 44.56% and generates considerable surplus energy exports (54,728 kWh/year), hence enhancing its financial resilience.

These MPC strategies show really good performance when compared with Chapter 3 benchmarks. Reflecting its less efficient alignment of renewable availability and load scheduling, GA-Load Following, for example, had a yearly grid cost of over €29,525.34, far higher than any MPC scenario. Although the GA-Yearly Horizon approach uses excellent long-term horizon, a very broad assumption, it delivers a lower yearly grid cost of €13,123. Focussing on short-horizon adaptability, the MPC approach provides a more realistic middle ground allowing variable loads to meet both solar generation and daily tariff adjustments while allowing sensible forecasting limits.

Figure 4-7 shows the cumulative discounted cash flows for the four MPC scenarios (0%, 4%, 6%, and 8%) over the project lifespan (25 years). This cash flow analysis distinctly highlights

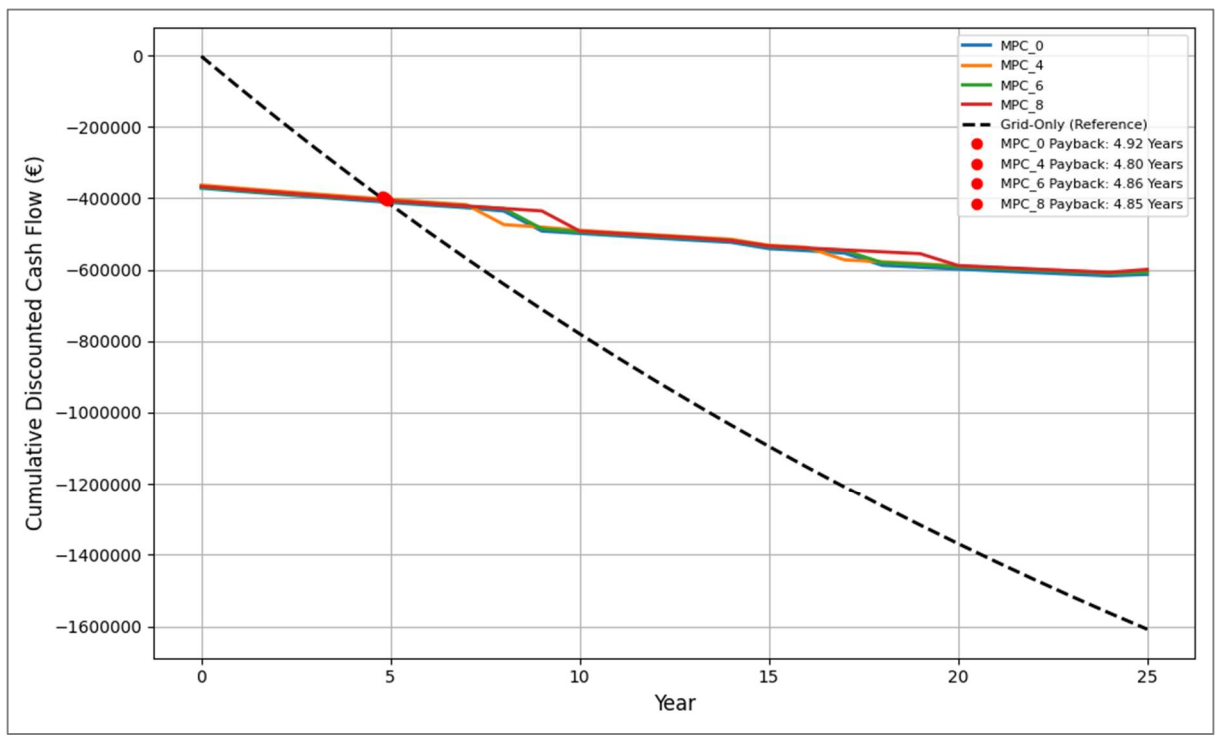


Figure 4-7: Discounted Cashflow for the GA-MPC approach with different flexibility scenarios

the internal rate of return (IRR) and payback period, providing a comprehensive perspective on investment viability and economic attractiveness for each flexibility scenario.

Analysing the MPC scenarios individually, MPC 0%, representing no load flexibility, exhibits the lowest IRR at 17.75% and the longest payback period of approximately 4.92 years, primarily due to higher initial capital outlays and operational grid costs resulting from inflexible load scheduling. For example, MPC 4%, allowing some flexibility, improves IRR to 18.15% and reduces the payback time to about 4.80 years. As already shown by lower monthly grid rates, this financial advantage results from the deliberate distribution of loads to more economically beneficial times.

Further allowing MPC 6% (17.98% IRR, 4.86 years repayment) and MPC 8% (18.22% IRR, 4.85 years payback) shows just slight variations as well. While MPC 8% has the greatest IRR across MPC scenarios at 18.22%, the variations from MPC 4% and MPC 6% are still small, showing a declining return on financial measures with increasing load flexibility beyond a certain threshold. However, these incremental improvements become significant when considering overall system reliability, renewable utilisation efficiency, and operational management of storage systems (Figure 4-6 and Figure 4-5).

Comparing these MPC scenarios to previously discussed Chapter 3 benchmarks, GA-Yearly Horizon (IRR: 17.05%, payback: 5.01 years), GA-Load Following (IRR: 19.69%, payback: 4.48 years), and HOMER-Load Following (IRR: 19.74%, payback: 4.54 years), yields insightful implications. Especially, the MPC approaches strike a good compromise. Although GA-Load Following and HOMER-Load Following methods show somewhat higher IRRs and shorter payback periods due to lower upfront investment and higher operational reliance on the grid, they incur significantly higher NPC values (€665,236 and €661,677, respectively) compared to MPC scenarios (ranging from approximately €625,776 for MPC 8% up to somewhat higher levels in lower-flexibility scenarios). The GA-Yearly Horizon approach, with its idealised long-term forecasting, achieves the lowest annual grid charges (€13,123), yet it still offers a longer payback period (5.01 years), reflecting higher initial investments.

Despite slightly higher annual grid costs than GA-Yearly Horizon, MPC scenarios strategically manage loads to reduce storage component stress, thus lowering replacement expenses and improving salvage values. These operational efficiencies translate into consistently competitive IRR and attractive payback periods, demonstrating the practical economic value of MPC-based load flexibility for hybrid renewable energy systems.

This analysis indicates the need to accurately estimate hybrid renewable energy costs. Still, optimisation parameters considerably impact economic results accuracy and efficiency. To enhance and testing the robustness of the GA-MPC optimisation approach, the following

section closely investigates the influence of adjusting solver settings. The section evaluates Mixed-Integer Linear Programming (MILP) parameters using the Gurobi solver and then explores crucial Genetic Algorithm (GA) parameter values to ensure a powerful and computationally effective optimisation method.

#### 4.3.4 GA and MILP Solvers parameter tunning

This section outlines the tuning process for critical solver parameters, with a particular focus on MIPGap and MIPFocus, to improve the stability and convergence efficiency of the MILP optimisation. By systematically exploring these settings through targeted grid searches, the aim was to enhance computational performance and reduce the Total Discounted Cost. Similarly, key GA parameters, including population size, crossover rate, and mutation probability, were also calibrated to identify a configuration that consistently delivers high-quality, near-optimal solutions within acceptable computation times.

#### 4.3.4.1 MILP Parameter tunning

Optimising solver settings is critical to ensure practical computational efficiency in the MILP framework implemented using Gurobi. The parameters varied in this analysis include MIPFocus, and MIPGap, each influencing the solver's precision and computational runtime. To reconcile runtime performance with solution quality, the grid search methodically investigated a spectrum of parameter values. MIPFocus was specifically examined across values 0 (default), 1, 2, and 3, thereby reflecting balanced, feasible-solution focus, optimality emphasis, and bound emphasis, respectively. The optimality tolerance (MIPGap) was adjusted from a tight 0.0001 up to a more relaxed 0.05, with the default being 0.0001. These parameter variations allowed systematic assessment of trade-offs between computational speed and solution accuracy.

Figure 4-8 reveals sensitivity of NPC's and computational length to the MIP Focus value. Setting the median Net Present Cost (NPC) to 1 (feasible-solution focus) exhibited more volatility (around €614,000–€616,000), therefore indicating less consistent solver performance. Conversely, the default setting (MIPFocus=0) and settings focused on optimality or bound tightening (MIPFocus=2,3) achieved more consistent results around €613,500–€614,500. Runtime analysis indicates that focusing on bound tightening (MIPFocus=3) significantly prolongs computation (~55 seconds median), whereas settings 1 and 2 notably

reduce computational time (median 35-40 seconds), albeit with marginally higher NPC variability.

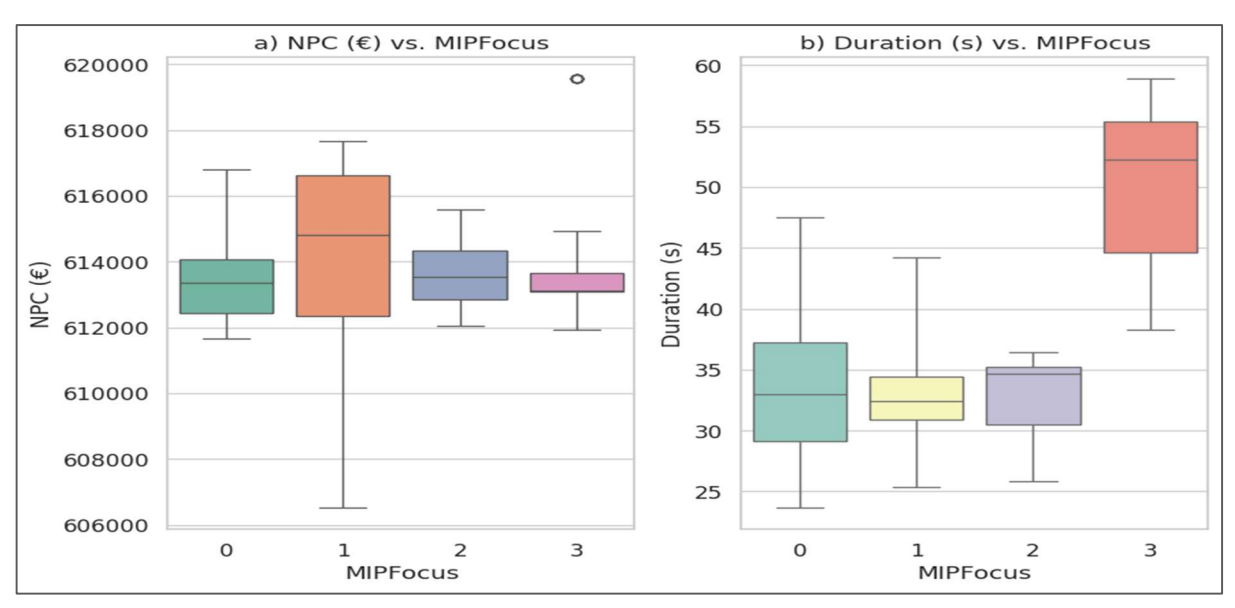


Figure 4-8: The influence of solver parameter tunning in Gurobi MIPFocus parameter

Analysing MIPGap (Figure 4-9) exposes even more these trade-offs. Although average computation time (~45 seconds) was raised by an exceptionally tight MIPGap (0.0001), NPC variability was lowest. On the other hand, at a small trade off in solution accuracy, decreasing the gap to 0.05 clearly reduced computational time (~30 seconds). Thus, depending on the value of accuracy over runtime in practical applications, properly balancing MIPFocus and

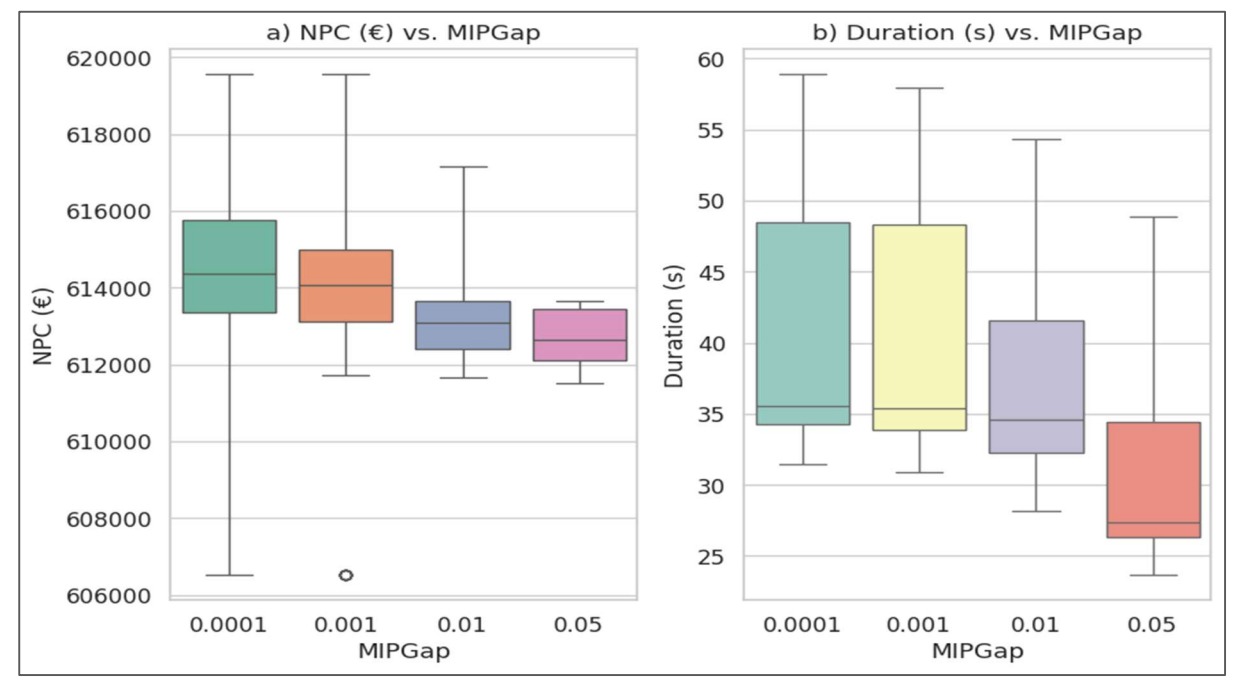


Figure 4-9: The Influence of MILPGap on accuracy and convergence speed

MIPGap parameters offers ideal solver configurations tuned either to speedier solutions or tighter economic precision.

#### 4.3.4.2 GA Parameter tunning

The convergence behaviour of the genetic algorithm (GA) across several crossover (CP) and mutation probability (MP) combinations, shown in the convergence plots and parameter heatmap, offers important new perspectives on the exploration-exploitation trade-off necessary for efficient parameter tuning in optimisation problems. Figure 4-10 shows the convergence plots for different mutation and crossover probability. Starting with subplot (b) from the convergence plot, high crossover probability (CP = 0.7–0.9) combined with low mutation probabilities (MP = 0.1–0.2) provide quick convergence, usually stabilising within less than 10 generations. These parameters clearly show convergence into local minima despite the apparent advantage of fast stabilisation; they prematurely converge at substandard net present cost (NPC) levels regularly above €625,000. For example, combinations such as CP = 0.7 with MP = 0.1 and CP = 0.9 with MP = 0.1 both illustrate swift but insufficient exploration,

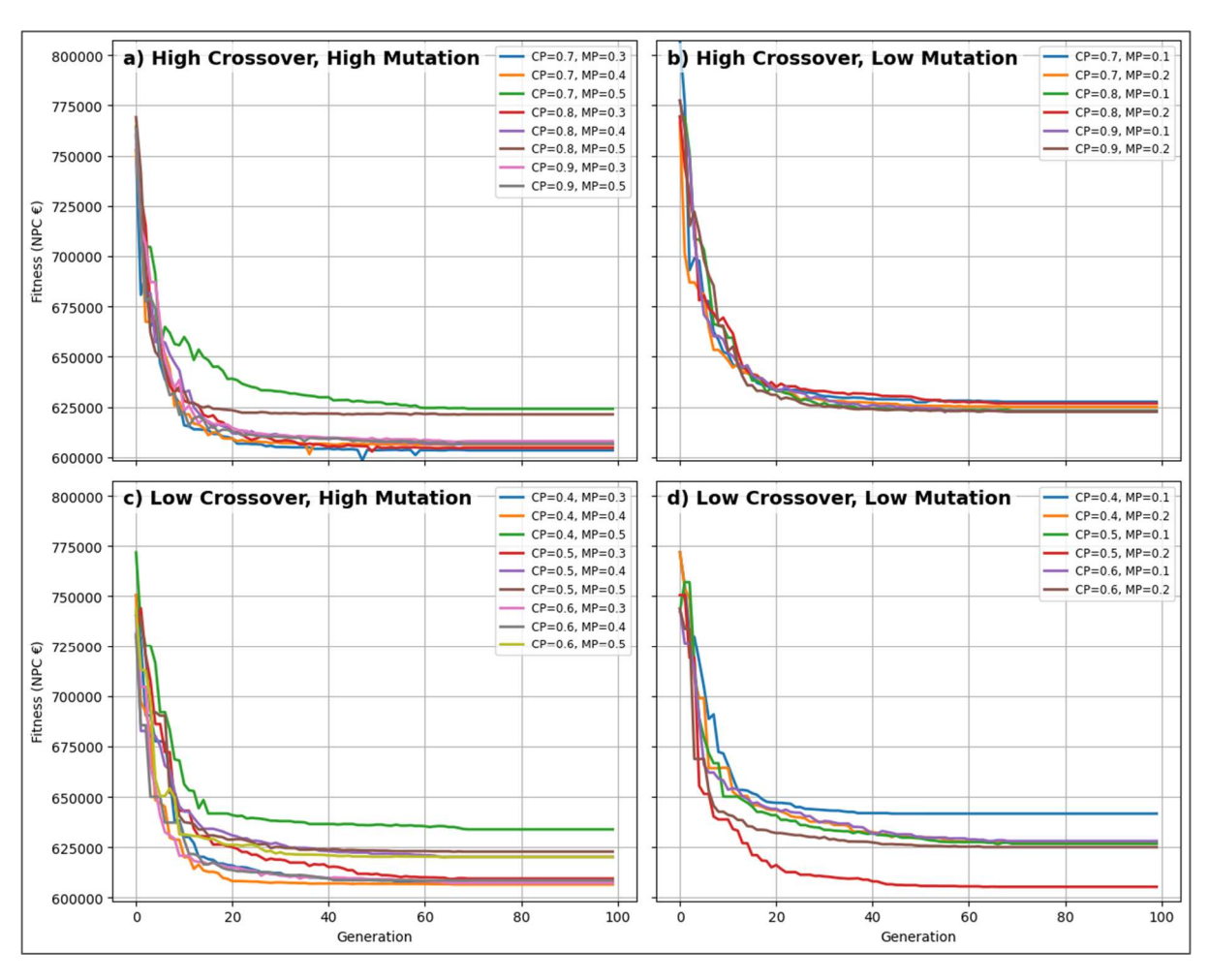


Figure 4-10: Convergence plots for different mutation and crossover mutation.

highlighting a critical limitation when mutation rates are insufficiently high to introduce necessary genetic diversity.

On the other hand, subplots (a) and (c) from the convergence plot stress, independent of crossover probability, the advantages of higher mutation probabilities (MP = 0.3–0.5). Particularly, subplot (c) shows a slower but rather much better convergence trend with lower crossover probability (CP = 0.4–0.6) associated with higher mutation rates (MP = 0.3–0.5. Reflecting their ability to maintain population diversity and thorough search space exploration, these designs get more ideal NPC values of roughly €606,000. Especially, the combination of CP = 0.4 and MP = 0.4 stands out; it always obtains the lowest NPC values at approximately €606,566, therefore exhibiting an excellent balance between extensive exploration and effective exploitation. Although high crossover rates cause somewhat less stability, same behaviour is also clearly shown in subplot (a), where high crossover rates (CP = 0.7–0.9) first show fluctuations but subsequently stabilise at favourable solutions between roughly €606,000–€627,000. Conversely, subplot (d), which shows low crossover and low mutation (CP = 0.4–0.6, MP = 0.1–0.2, exhibits first quick convergence but finally stagnates prematurely, obtaining inferior NPC values of approximately €608,000 to €621,000 due insufficient genetic variation.

The interaction plot in Figure 4-11 provides a detailed visualisation of how final fitness of NPC varies with crossover probability across different mutation rates ( $\mu$ ). This supports the convergence analysis by clearly illustrating the impact of GA parameter selection. The plot shows that the lowest NPC values are achieved in regions with moderate crossover

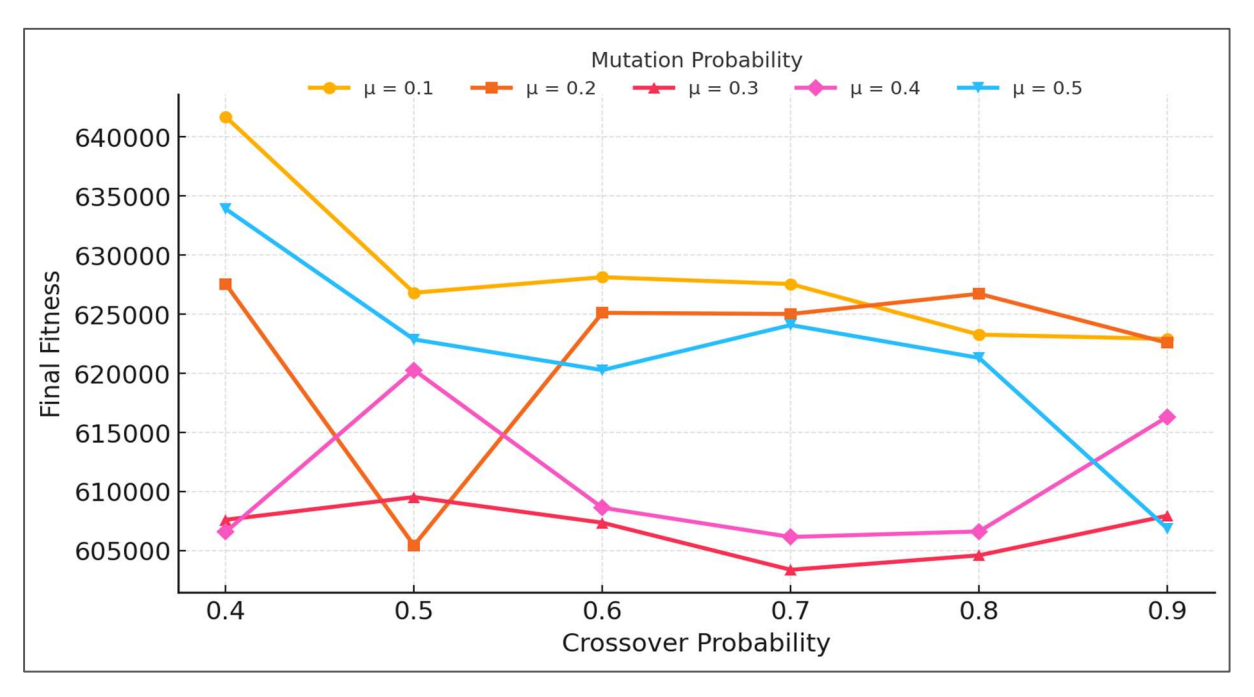


Figure 4-11: Interaction plot of final fitness versus crossover probability for different mutation rates ( $\mu$ ).

probabilities (CP = 0.4–0.5) combined with higher mutation rates ( $\mu$  = 0.3–0.4), with optimal solutions consistently falling in the range of €606,000–€607,000. Notably, the combination of CP = 0.4 and  $\mu$  = 0.4 yields one of the best-performing results, at €606,566.

In contrast, configurations with low mutation rates ( $\mu$  = 0.1–0.2) result in significantly higher NPC values, exceeding €620,000. This highlights the detrimental effects of limited genetic diversity, leading to premature convergence to local optima. The poorest-performing combination occurs at CP = 0.4 and  $\mu$  = 0.1, reaching a high NPC of €641,688.

These findings emphasise the critical role of mutation probability in avoiding early convergence and enabling a broader search of the solution space. While higher mutation rates may initially slow convergence, often stabilising only after 20–30 generations, they consistently yield better outcomes by maintaining genetic diversity. Conversely, faster convergence under low mutation rates, as seen in previous convergence plots, often leads to suboptimal solutions due to restricted exploration. Based on these results, the recommended GA parameter range for achieving minimal NPC includes moderate crossover probabilities (CP = 0.4–0.5) and relatively high mutation rates ( $\mu$  = 0.3–0.4). This interaction analysis not only validates the parameter choices used in this study but also provides evidence-based guidance for future GA-based optimisation of complex energy systems.

### 4.4 Summary

Adopting a rolling-horizon Genetic Algorithm–Mixed Integer Linear Programming (GA–MILP) framework with MPC and flexible load functionality significantly improves both the accuracy of component sizing and the operational flexibility of hybrid renewable systems. Unlike the single-horizon method from Chapter 3, which rests on a year's worth of perfect foresight, this updated strategy splits the year into sequential 24-hour windows, each overlapping by 12 hours, thus introducing short-term forecasts and fine-grained decision-making.

In addition, incorporating adjustable load demand (0%, 4%, 6%, 8% flexibility) further refines the balance between PV generation and energy storage, producing clearly improved system-level results. These flexibility levels correspond to approximately 4%, 6%, and 8% of the community's average daily demand (≈579.9 kWh/day), with the highest case approaching 10%, which is relatively high compared with typical demand-side management studies where 2–5% is common. Specifically, at 8% flexibility, the approach achieves the lowest NPC of nearly €599,134, compared to €612,945 under 0% flexibility, and it remains below the perfect-foresight benchmark of €625,776 in Chapter 3. Changes in PV capacity from 155 kWp at 0% flexibility to 150 kWp at 8% flexibility highlight the economic advantages of synchronising demand with peak solar output. Battery storage exhibits a similar adaptive trend: starting at

74–76 strings at lower flexibility and increasing to 80 strings at higher flexibility, thereby enabling more effective use of midday solar surpluses.

Detailed operational analyses for both winter and summer corroborate these advantages, with flexible loads consistently cut or shifted to lower-cost or high-supply hours. Winter daytime imports, for instance, shrink substantially (generally down to 7.39–28.44 kWh), while summer scheduling of flexible loads amplifies battery recharging (as much as 211 kWh per day) and boosts excess energy exports to above 200 kWh daily. This improved alignment lowers total annual grid charges, for example, from €15,884 at 0% flexibility to roughly €15,394 at 6% flexibility and raises renewable self-consumption to 44.56% at 8%. Solving solvers with tuned parameters strengthens the observed improvements: Genetic Algorithm convergence studies show that moderate crossover probability (0.4–0.5) and greater mutation rates (0.3–0.4) routinely provide strong solutions around €606,566, so balancing exploration breadth and solution quality. These results are derived under ideal forecast conditions, where 24-hour ahead predictions of PV output, load demand, and tariff levels are assumed to be perfectly accurate. Flexible loads are assumed to shift without any consumer discomfort, rebound effects, or minimum-up/minimum-down time constraints beyond those explicitly modelled. Combining demand flexibility with an MPC-based, short-horizon re-optimisation beats both full-year and totally reactive benchmarks, hence improving the battery and hydrogen storage systems. Such results confirm the feasibility of MPC frameworks for reasonable energy community scenarios and highlight the significant practical utility of implementing short-term forecasts and load scheduling in hybrid PV-storage projects.

# 5 Life-Cycle Energy Cost Analysis through a New Index for Hybrid Renewable-Fuel Cell Battery Storage Systems in Energy Communities.

#### 5.1 Introduction

In the framework of sustainable energy solutions and decarbonisation, the optimisation of energy systems during their life cycles has grown ever more important. Knowing the interaction between environmental and economic performance becomes essential as energy communities and grid-scale storage options grow. Combining upfront capital costs, operational expenses, and environmental impact measures, life-cycle energy cost analysis (LCECA) offers a complete framework for assessing energy systems and helps to provide understanding of long-term viability.

Traditional metrics such as Energy Stored on Invested (ESOI) and Energy Return on Investment (EROI) have been commonly used as performance measures for evaluating the energy efficiency of generating and storage technologies. The EROI compares the energy output of a generating plant to the principal energy needed for construction and operation. Similarly, the ESOI gauges the efficiency with which the energy spent constructing a storage device is utilised over its lifetime to provide useful energy back into the system. But historically, these measures have only been used to assess individual technologies; they have not sufficiently addressed the complexity brought forth by hybrid energy systems, which combine several generating and storage technologies under one operating platform. Particularly hybrid renewable-fuel cell-battery systems provide many energy paths, including direct use, storage, grid export, and curtailment. For example, Figure 5-1 presents normalised hourly data collected during the year 2022 from the Formentera Council building, including average solar output, electricity purchasing and selling prices, and average electricity demand. This statistic vividly illustrates the dynamic and complicated interactions in a hybrid renewable energy system, hence highlighting the need of comprehensive, all-encompassing measures to fairly evaluate and maximise system performance.

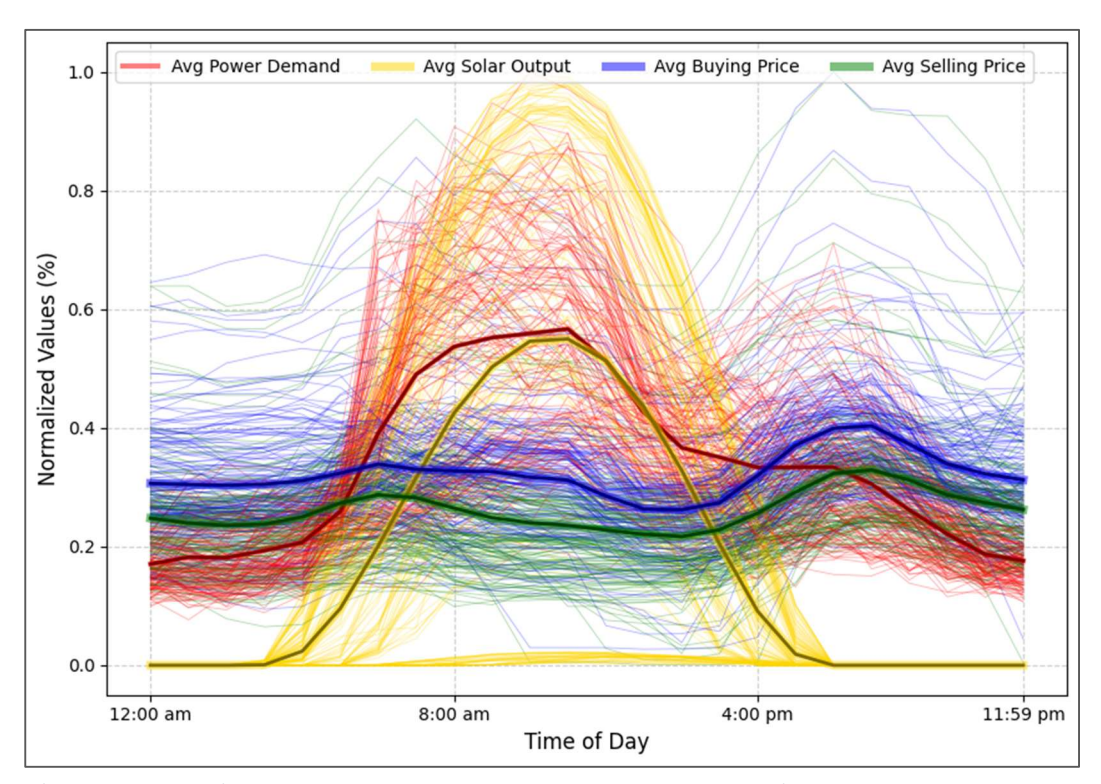


Figure 5-1: Normalised measured hourly data for whole year days and their average values for energy generation, prices and consumption.

Based on and greatly extending current EROI and ESOI frameworks, this chapter presents a new performance index especially intended for hybrid renewable energy systems within energy communities, therefore addressing this gap. Providing a practical, scalable, and more accurate method for life-cycle energy analysis in real-world energy communities, this new metric precisely incorporates the complexity and operational variety inherent in hybrid energy systems.

Devices for storing energy, such batteries or hydrogen systems, call for an initial manufacturing energy investment. These devices store and return energy several times over their working lifespan. The Energy Stored on Invested (ESOI) ratio measures the efficiency with which the energy spent creating the storage device is used to provide the system with useable energy:

$$ESOI = \frac{E_{\text{out,st}}}{E_{\text{emb,st}}}$$
 5-1)

Where the  $E_{\rm out,st}$  is the total energy dispatched from storage over its lifetime, measured in megajoules (MJ).  $E_{\rm emb\,,st}$  is the embodied energy required for manufacturing the storage system, also in MJ. The ESOI ratio is dimensionless measured in terms of electrical-equivalent energy, and a higher ESOI indicates an energetically beneficial storage system since the device returns more units of energy over its lifetime for every unit of energy invested in its construction.

A well-known energy index, the Energy Return on Investment (EROI) links the total primary (or embodied) energy needed to build a generation facility to the entire energy production of that facility throughout its lifetime. For a generation facility (e.g., photovoltaic panels and wind turbine), if  $E_{gen}$  is the total lifetime energy generated and  $E_{emb,gen}$  is the embodied energy of the generation facility, then:

$$EROI_{gen} = \frac{E_{gen}}{E_{emb,gen}}$$
 5-2)

Where the  $E_{\rm gen}$  is the total lifetime generated energy, in MJ.  $E_{\rm emb,gen}$  is the embodied energy for constructing and operating the generation facility, in MJ. A high EROI means that the generation technology improves the net energy benefit to the system by being rather effective in transforming invested energy into supplied energy.

The next parts provide a thorough derivation of the conventional formulations of the current EROI and ESOI measurements, therefore exploring their theoretical foundations. It then highlights the need of customised metrics for hybrid systems and the justification for the suggested changes. The study ends in a look at how these changes might support major uses such energy community initiatives and grid-scale storage.

## 5.2 Novel Index for Energy Systems in Communities

Figure 5-2, subplot (A) illustrates the foundational energy return framework often used for grid-scale analysis, originally proposed by [113] and extended in similar works by [55]. This approach assumes a single generation source with a fixed lifetime energy output, from which a fraction  $\phi$  is either dispatched directly or routed through a storage pathway. Each route carries distinct energy implications: direct dispatch incurs no losses, while storage paths are penalised by round-trip efficiency and the embodied energy cost of the storage device itself. This model enables the computation of an effective system-wide EROI that accounts for these trade-offs and has become a widely accepted benchmark for comparing the energy performance of storage technologies at scale. However, it remains limited to systems with a single storage route and no direct representation of curtailment, multi-path interactions, or community-based demand structures. The complete derivation of this formulation is provided in Appendix 9.4 for transparency.

To overcome these limitations and reflect the operational realities of distributed hybrid energy communities, Figure 5-2, subplot (B) extends this framework to include multiple storage pathways and energy flow options. The following derivation formalises this expanded

approach. First, as shown in subplot (B), we redefine the lifetime energy generation presented  $E_{gen}$  in the foundational framework (equation 9-4)) as split into multiple different energy paths:

- $\phi_{pv load}$ : Fraction of generation delivered directly to the load.
- $\phi_{bat}$ : Fraction of generation routed into battery storage.
- $\phi_{H_2}$ : Fraction of generation routed into hydrogen storage.
- $\phi_{pv_{arid}}$ : Fraction of generation is being exported to the grid.
- $\phi_{curt}$ : Fraction of generation is being curtailed.

#### By definition:

$$\phi_{\text{pv\_load}} + \phi_{\text{bat}} + \phi_{H_2} + \phi_{pv_{grid}} + \phi_{curt} = 1$$
5-3)

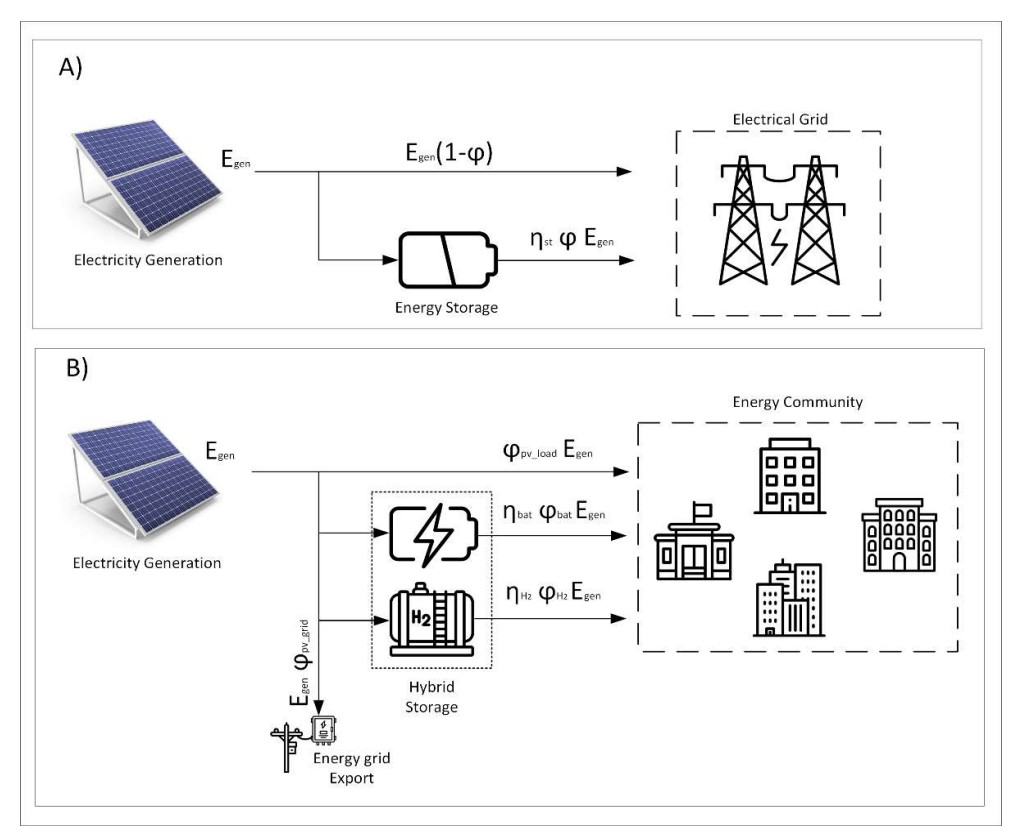


Figure 5-2: Energy flow comparison between (A) a simple grid-connected system with single storage and (B) a hybrid energy community with multiple storage paths and direct load consumption, highlighting the need for an extended EROI metric.

Each storage technology i (where  $i \in \{\text{battery, hydrogen}\}\)$  has its own round-trip efficiency  $\eta_i$ , and  $[ESOI]_i$ . The energy does not suffer storage efficiency losses when it is directly consumed within the community or exported to the grid. Therefore, the total dispatched energy  $E_{\text{disp,total}}$ 

is redefined from equation 9-5) over the lifetime consist of contributions from all possible pathways as follows:

$$E_{\text{disp,total}} = E_{\text{gen}} \left( \phi_{\text{pv\_load}} + \phi_{pv_{grid}} + \phi_{\text{bat}} \eta_{\text{bat}} + \phi_{\text{H}_2} \eta_{H_2} + \phi_{curt} \right)$$
 5-4)

Where  $E_{\text{disp,total}}$  is in megajoules (MJ). Embodied energy consists of the generation subsystem plus the embodied energy of each storage subsystem.

$$E_{emb,gen} = \frac{E_{gen}}{[EROI]_{gen}}$$
 5-5)

For each storage technology i, the total delivered energy from storage is  $\phi_i E_{gen} \eta_i$ . Then the  $E_{emb,i}$  is given by:

$$E_{emb,i} = \frac{\phi_i E_{gen} \eta_i}{[ESOI]_i}$$
 5-6)

Summing over the generation and the two storages (battery and hydrogen):

$$E_{\text{emb, total}} = \frac{E_{\text{gen}}}{[\text{EROI}]_{\text{gen}}} + \frac{\phi_{\text{bat}} \eta_{\text{bat}} E_{\text{gen}}}{[\text{ESOI}]_{\text{bat}}} + \frac{\phi_{\text{H}_2} \eta_{\text{H}_2} E_{\text{gen}}}{[\text{ESOI}]_{H_2}}$$
5-7)

Factor out  $E_{gen}$ :

$$E_{\text{emb,total}} = E_{\text{gen}} \left( \frac{1}{[\text{EROI}]_{gen}} + \frac{\phi_{\text{bat}} \eta_{\text{bat}}}{[\text{ESOI}]_{bat}} + \frac{\phi_{H_2} \eta_{H_2}}{[\text{ESOI}]_{H_2}} \right)$$
 5-8)

The aggregate EROI of the extended system (entire configuration to a community load) is defined as:

$$[EROI]_{system} = \frac{E_{disp,total}}{E_{emb,total}}$$
 5-9)

Substitute Equations 5-4) and 5-8):

$$[EROI]_{community} = \frac{E_{gen} \left(\phi_{pv\_load} + \phi_{pv_{grid}} + \phi_{bat} \eta_{bat} + \phi_{H_2} \eta_{H_2} + \phi_{curt}\right)}{E_{gen} \left(\frac{1}{[EROI]_{gen}} + \frac{\phi_{bat} \eta_{bat}}{[ESOI]_{bat}} + \frac{\phi_{H_2} \eta_{H_2}}{[ESOI]_{H_2}}\right)}$$
5-10)

Cancelling  $E_{qen}$ :

$$[EROI]_{community} = \frac{\phi_{pv\_load} + \phi_{pv_{grid}} + \phi_{bat} \, \eta_{bat} + \phi_{H_2} \eta_{H_2} + \phi_{curt}}{\frac{1}{[EROI]_{gen}} + \frac{\phi_{bat} \, \eta_{bat}}{[ESOI]_{bat}} + \frac{\phi_{H_2} \eta_{H_2}}{[ESOI]_{H_2}}}$$
 5-11)

This equation offers a novel and all-around measure specifically for hybrid renewable energy systems in local surroundings. This index precisely characterises the intricate relationship of direct usage, storage inefficiencies, and embodied energy requirements and explicitly analyses numerous simultaneous storage alternatives. By means of such extensive evaluations, energy planners and system designers can acquire greater understanding of operational efficiencies, pinpoint appropriate technology configurations, and so increase both environmental and financial sustainability inside energy communities. To position the proposed index within the wider body of energy-return metrics, Table 5-1 compares it with the most frequently cited alternatives in the literature, highlighting differences in system boundary, information captured and practical usefulness for community-scale hybrids.

Table 5-1: Comparison of life-cycle energy-return metrics and their suitability for community hybrid systems

Metric	System scope & flows captured	Key strengths	Main limitations	Suitability for community HRES
Classic EROI	Generation asset only	Simple; widely used	Ignores stor- age, curtail- ment, demand diversity	Low
ESOI	Individual storage technology	Highlights embodied en- ergy of storage	Detached from generation and load	Partial
EROI ± ESOI inequality (Barnhart 2013)	PV/Wind plus one stor- age route	Energetic viability thresh- old	Assumes single storage path; no demand structure	Moderate
EROI_grid (Pellow 2015)	Grid over-generation with one storage loop	Includes round-trip losses & curtailment	Still single stor- age; no spatial demand hetero- geneity	Moderate
Proposed EROI_com- munity	Multi-vector hybrid (PV-battery-H₂-grid) with hourly demand, curtailment & export, embodied energies for all assets	Integrates simultaneous storage paths; directly uses MILP hourly dis- patch; mirrors community import/export rules	Higher data re- quirement	High

The comparison confirms that existing metrics either treat generation and storage in isolation or assume a single-path storage loop. In contrast, [EROI]<sub>community</sub> captures multiple storage pathways, curtailment, direct load supply and grid exchanges within a single life-cycle boundary, leveraging the hourly dispatch outputs already generated in Chapters 3 and 4. This integrated perspective is essential for energy-community planners who must balance investment in batteries, hydrogen, grid contracts and renewable capacity simultaneously. The remainder of this section therefore reports and interprets [EROI]<sub>community</sub> values for the Formentera case study, alongside the financial results presented earlier.

# 5.3 Applying the EROI Community Metric: Sensitivity and Scaling Analysis

Following the derivation of our new index in Section 5.2, designed specifically to capture the energy life-cycle performance of hybrid renewable—hydrogen—battery systems in community settings, a hierarchical methodological approach is adopted. Figure 5-3 presents a structured flow chart illustrating the two-stage methodological framework employed in this study to evaluate the life-cycle energy performance of a hybrid renewable—battery—hydrogen system using the derived EROI-based metric. The process is divided into Step 1: Parametric Sensitivity Analysis with Fixed Capacities, and Step 2: Capacity Scaling and Mapping Analysis.

In Step 1, a set of pre-optimised system capacities, obtained from the GA-MILP sizing framework introduced in Chapter 4, is held constant while key technical parameters are independently varied. These include component round-trip efficiencies, operational lifespans (durability), and embodied energy intensities. For each parameter variation, the MILP-based operational dispatch is executed to derive annual energy flows and component usage, from which operational pathway fractions and total operating hours are calculated. These outputs are then used to compute the proposed life-cycle energy return metric. This procedure is iteratively repeated until all scenarios are exhausted, with results used to generate sensitivity plots that highlight the impact of each parameter on overall energy performance.

In Step 2, the analysis shifts from technical parameter variation to capacity scaling. Here, uniform scaling factors are applied to the base component capacities (e.g., PV, battery, electrolyser, fuel cell, and hydrogen tank), ranging from 0.1× to 2.0× of their original sizes. Technical parameters remain fixed at their nominal values, and the MILP dispatch model is rerun for each scaled configuration. The resulting energy flows and system usage are used to compute the same set of performance metrics (EROI, NPC, unmet and excess energy). These results are then used to train surrogate models via third-degree polynomial regression, enabling the interpolation and smoothing of performance across the design space. Results are visualised through heatmaps, facilitating exploration of trade-offs across multiple performance dimensions. This two-part framework provides both a parameter-level understanding of energy-system behaviour and a design-space mapping to support planning decisions, particularly relevant for energy communities deploying hybrid storage configurations.

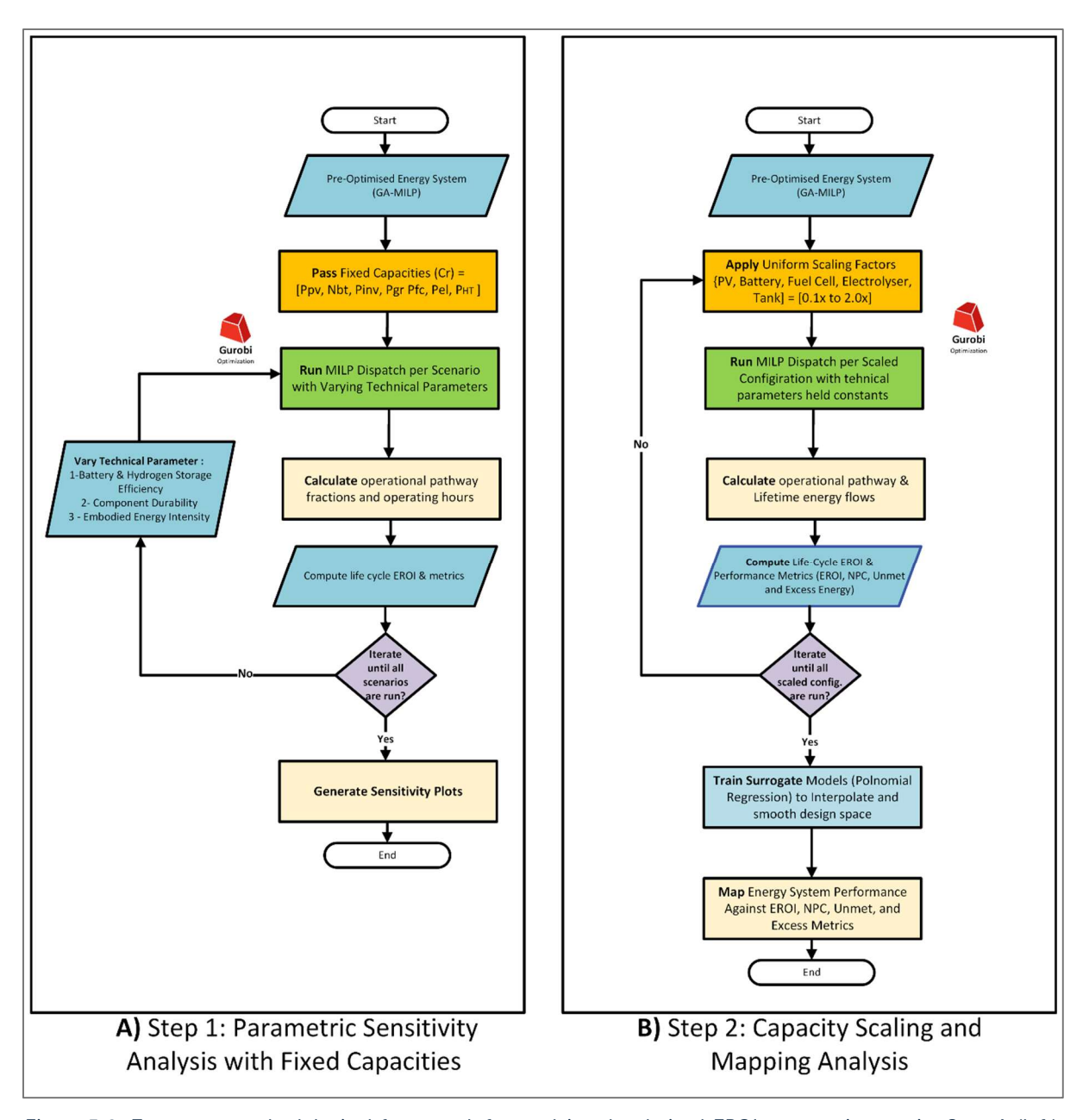


Figure 5-3: Two-stage methodological framework for applying the derived EROI-community metric. Step A (left) conducts parametric sensitivity analysis using fixed, optimised system capacities while varying key technical parameters, efficiency, durability, and embodied energy. Step B (right) applies uniform scaling to system capacities to assess the impact of system size on performance. Both steps use rolling-horizon MILP dispatch to extract operational metrics, which are then used to compute and analyse the life cycle EROI and associated sustainability indicators.

To implement Step 1 of the methodology, three main classes of technical parameters were independently varied while holding the system capacity fixed. These represent commonly cited sources of uncertainty and improvement in hybrid system deployment:

- Round-trip efficiency: The efficiency of the battery subsystem (charging-discharging) and the hydrogen subsystem (electrolyser-fuel cell) are adjusted.
- **Durability:** The lifespans of the battery, electrolyser, and fuel cell are shifted, thereby altering replacement schedules.

• **Embodied energy intensity:** The megajoule-per-unit-of-capacity values for each technology are modified, reflecting possible improvements or variations in manufacturing processes.

Table 5-2 summarises the nominal values used as baselines, together with illustrative lower and upper bounds. These moderate parameter variations allow direct comparison of how, for example, battery round-trip efficiency influences the final life-cycle metric, while holding capacity fixed.

Table 5-2: Sample Parameter Ranges for Efficiency, Durability, and Embodied Energy Sensitivity Studies

Doromotor [vof]	Units	Nominal	Lower	Upper	Resolution
Parameter [ref]		Value	Bound	Bound	Kesolution
Battery Efficiency $(\eta_{b+}$ and $\eta_{b-})$	%	82.5	0.7	0.95	10
Electrolyser Efficiency $(\eta_{el-})$	%	55	40	70	10
Fuel Cell Efficiency $(\eta_{fc+})$	%	45	30	60	10
Battery Durability $( au_{bat})$	kWh	14,400	7,200	21,600	16
Electrolyser Durability $( au_{el})$	hours	46,250	17,500	75,000	16
Fuel Cell Durability $( au_{fc})$	hours	9,500	4,000	15,000	16
Embodied Energy – PV $(\varepsilon_{pv})$ [156]	MJ/kWp	12000	10000	14000	5
Embodied Energy – Battery $(\varepsilon_{bat})$ [157]	MJ/kWh	1000	800	1,200	5
Embodied Energy – Fuel Cell $(\varepsilon_{fc})$ [55]	MJ/kW	1,150	1000	1,300	5
Embodied Energy – Electrolyser $(\varepsilon_{el})$ [55]	MJ/kW	1,150	1000	1,300	5
Embodied Energy – Tank $(\varepsilon_{st})$ [55]	MJ/Kg	1,000	800	1,200	5

By running this sequence of simulations, a clear sense is obtained of how the system's life-cycle performance responds to distinct engineering improvements or manufacturing optimisations (life cycle stages). This study highlights which parameter modifications provide the most meaningful gain for energy communities in both cost and environmental terms.

Consequently, as discussed in step 2 of this methodology, whereby uniform scaling factors are applied to the capacities of major components, PV, battery, electrolyser, fuel cell, and hydrogen tank, as shown in Table 5-3. Each scaled configuration is subjected to the same rolling-horizon dispatch and life-cycle index calculation, but without any additional global capacity optimisation.

Table 5-3: Illustrative Capacity Variations Relative to the MPC-4% Baseline

Parameter	Units	Baseline (GA-	Lower Bound	Upper Bound
. u.uo.		MILP-MPC)	(x 0.1)	(x 2)
PV Array Rating	kW	152	15.2	304
Battery Strings	Strings	76	7.6	152
Electrolyser Rating	kW	5	0.5	10
Fuel Cell Rating	kW	5	0.5	10
Hydrogen Tank Capacity	kg	7	0.7	14

Exploring these alternative capacities provides a broader perspective on how baseline technology parameters perform when the system is scaled up or down from the MPC-4% design point. Unlike the first set of runs, where efficiency, durability, and embodied energy were individually varied, second stage keeps those parameters fixed at their nominal values, modifying only the component capacities through uniform scaling between 0.1 and 2.0. These optimisation data sweeps are collected with all results metrics (EROI, NPC, Unmet and Excess) and used to train and fit regression models.

Surrogate models are commonly used in renewable energy optimisation to predict either component sizes or performance metrics (e.g., cost or sustainability) for given configurations. Authors [158] built second-order polynomial regression models showing how climatic and geographic factors, such as temperature and irradiance, influence the PV system size and visualised these relationships using contour and surface plots. Other authors [159], [160], [161], [162] have demonstrated that polynomial regression models can match the predictive power of advanced machine learning models while requiring less data and being faster to train. These studies typically present their findings through heatmap-style visualisations (2D or 3D), which improve interpretability and allow for more thorough performance exploration.

In this work, a third-degree polynomial surrogate model was constructed for each performance metric using the five scaling factors-PV, battery, tank, fuel cell, and electrolyser scales -as input variables. Let  $X \in \mathbb{R}^{N \times 5}$  be the matrix containing design configurations, where each row represents a candidate solution, and each column corresponds to one of the scaling factors. The surrogate models approximate a target metric of NPC, EROI, unmet load, or excess energy as a polynomial function, expressed as:

$$f(\mathbf{x}) = \beta_0 + \sum_{a_1=1}^5 \beta_{a_1} x_{a_1} + \sum_{a_1=1}^5 \sum_{a_2=a_1}^5 \beta_{a_1 a_2} x_{a_1} x_{a_2} + \sum_{a_1=1}^5 \sum_{a_2=a_1}^5 \sum_{a_3=a_2}^5 \beta_{a_1 a_2 a_3} x_{a_1} x_{a_2} x_{a_3}$$
 5-12)

To ensure that the surrogate model generalizes well and is not overfitting the training data, we employ 10-fold cross-validation-a widely used best practice for model evaluation [163], [164]. In 10-fold cross-validation, the dataset is partitioned into 10 equally sized folds. For each fold, the model is trained on the remaining 9 folds ( 90% of the data) and then evaluated on the held-out fold (10% of the data). This process yields 10 independent estimates of the model's performance.

The following metrics are computed for each fold, starting with the coefficient of determination  $(R^2)$ :

$$R^{2} = 1 - \frac{\sum_{n=1}^{N} (y^{(n)} - \hat{y}^{(n)})^{2}}{\sum_{n=1}^{N} (y^{(n)} - \bar{y})^{2}}$$
 5-13)

Which indicates the fraction of variance explained by the model, later the Mean Absolute Error (MAE) is calculated using this equation:

MAE = 
$$\frac{1}{N} \sum_{n=1}^{N} |y^{(n)} - \hat{y}^{(n)}|$$
 5-14)

This analyses the average absolute error between predictions and observed data. Finally, the Mean Squared Error (MSE) is calculated using:

MSE = 
$$\frac{1}{N} \sum_{n=1}^{N} (y^{(n)} - \hat{y}^{(n)})^2$$
 5-15)

These metrics are then averaged over 10 folds to give a robust estimate of the surrogate model's predictive accuracy. High average  $R^2$  values (close to 1) alongside low MAE and MSE indicate that the model effectively interpolates between the simulation data points.

Once validated, the four surrogate models (targeted outputs: EROI, NPC, Unmet and Excess) are retrained on the entire dataset. A grid of input values is generated (e.g., 100 points linearly spaced between 0.1 and 2.0 for each dimension) to evaluate the surrogate model over continuous ranges of two selected variables, while holding the others constant. The predictions are then used to produce smooth contour plots (heatmaps) of the performance metrics. These smoothed heatmaps enable a clear visual representation of trends and tradeoffs, such as between NPC and EROI, that might be obscured in the raw, scattered simulation data.

In the results that follow, the effect of each parameter change on novel energy life-cycle metric under fixed capacities is first presented. Subsequently, an analysis is presented on how scaling the system size, with parameters held at their baseline values, influences overall performance. This two-pronged approach clarifies whether the improvements identified in the

first step remain beneficial under specific capacity settings, and it also assists energy communities in balancing technological upgrades and system sizing in planning. Throughout this methodological framework, the economic dimension, represented by Net Present Cost (NPC) is maintained to complement the novel technical sustainability indicator (EROI system), in addition to unmet and excess energy figures (in MWh/year). This combined approach ensures balanced decision-support metrics that clearly reflect the economic and energetic trade-offs.

#### 5.4 Results

To introduce the results, this subsection begins by illustrating the annual energy allocation in the MPC-4% scenario (base line), which provides a visual baseline for all subsequent analyses. The community load uses roughly 44.2% of the PV power directly; about 30.9% goes into the battery. At less than 0.03%, curtailment contributes very little to the remaining power, which is divided between hydrogen generation (2.6%) and grid export (19.6%).

This division reveals that over three-quarters of the energy is stored or serves the local need right now. The significant share of direct load consumption is a result of efficient generation and demand matching, which is the result of the MPC-based scheduling. The battery's notable 30.9% slice highlights its application in diurnal smoothing and short-term energy arbitrage; the smaller hydrogen branch (2.6%) implies this circuit largely controls longer-duration or overflow conditions. The 19.6% sent to the grid shows timeframes when neither local use nor storage offered a more affordable option. Finally, the near-zero curtailment underscores that the dispatch strategy rarely discards available renewable energy.

In subsequent sections, the resilience of this flow distribution to variations in efficiency, durability, and embodied energy parameters will be examined. The study is advanced to how these flows are affected if overall capacities are scaled. This annual energy fraction overview offers a first starting point for grasping the operational balance of the system under the MPC-4% setup. Managing the renewable generation across daily and seasonal cycles is done via direct consumption, battery storage, hydrogen use, and grid exports, each of which plays unique role and causes little curtailment. Once this baseline is set, the following section looks at how important performance criteria, efficiency, durability, and embodied energy, may change these distributions and affect the life-cycle measurements of the system.

#### 5.4.1 Parametric Sensitivity Analysis with Fixed Capacities

#### 5.4.1.1 Impact of Round-Trip Efficiency in Battery and Hydrogen Systems

Expanding on the baseline of energy flow allocations set earlier, Figure 5-4 investigates in detail how variations in round-trip efficiencies for battery and hydrogen storage individually

affect the system's energy performance and the corresponding net present cost (NPC). The four subplots analyse the relationships between the round-trip efficiencies of battery and hydrogen subsystems against both system-level Energy Return on Investment (EROI) and storage-specific Energy Stored on Investment (ESOI), with each data point coloured according to the resulting NPC value.

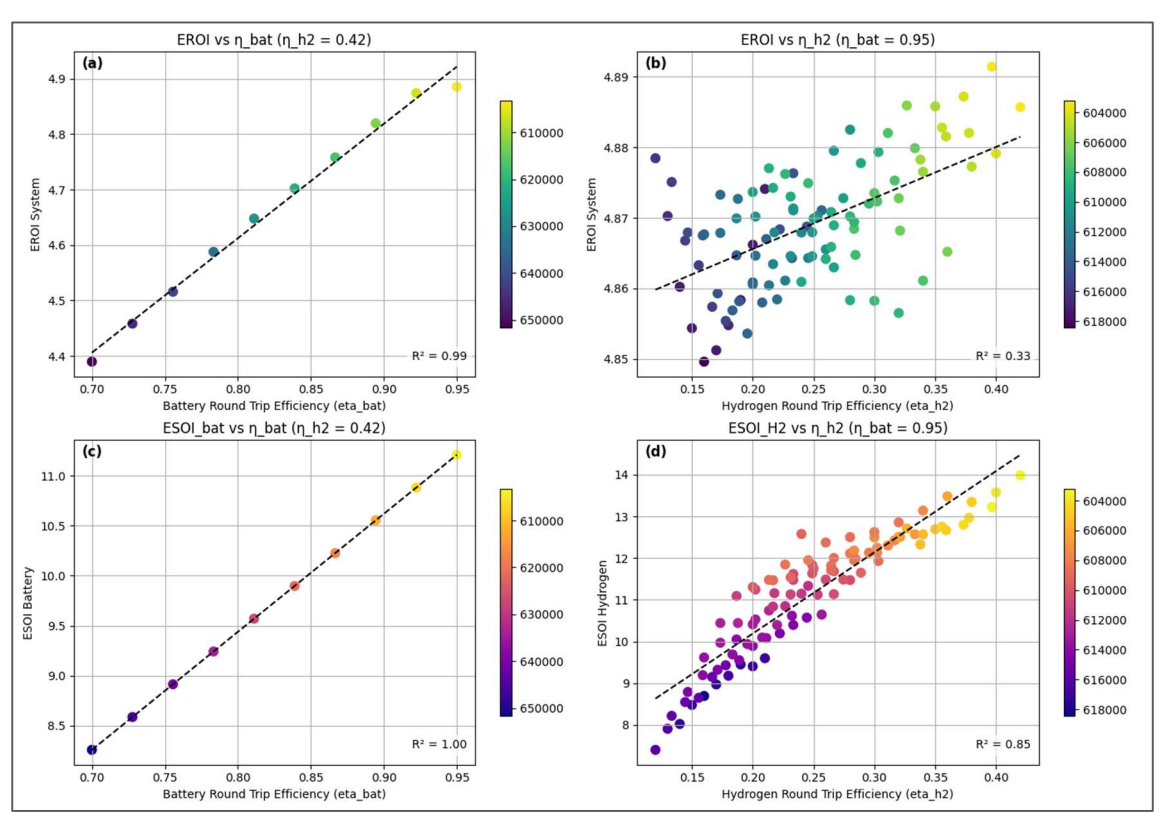


Figure 5-4: Sensitivity of system EROI and storage ESOI to variations in round-trip efficiency. The four subplots show that battery efficiency ( $R^2$  = 0.99 for EROI and 1.00 for ESOI) has a stronger impact than hydrogen efficiency ( $R^2$  = 0.33 for EROI and 0.85 for ESOI), with each point coloured by NPC.

In subplot (a), a strong linear correlation (R² = 0.99) is observed between battery round-trip efficiency and system-level EROI, with EROI increasing from approximately 4.4 at 70 % efficiency to nearly 4.9 at 95 % efficiency. This pronounced sensitivity results from the substantial fraction (around 30.9%) of total generated energy routed through the battery. Consequently, improvements in battery efficiency significantly enhance overall system EROI and reduce NPC, with NPC values decreasing from approximately €650,000 at lower efficiency to around €610,000 at higher efficiency (as depicted by the colour gradient).

Similarly, subplot (c) reveals an essentially perfect linear relationship (R<sup>2</sup> = 1.00) between battery efficiency and battery-specific ESOI, rising notably from approximately 8.5 to 11.0 across the same efficiency range. These ESOI changes directly relate to a noticeable drop in NPC given the battery's significant share in energy storage, hence stressing the economic advantage of improved battery performance.

On the other hand, subplot (b) shows a quite low connection (R² = 0.33) between system-level EROI and hydrogen round-trip efficiency, with little EROI increases (from around 4.85 to 4.89) despite hydrogen efficiency gains from about 15% to 40%. This limited sensitivity is directly explained by the small fraction (~2.6%) of total energy passing through hydrogen storage. Correspondingly, NPC values show only modest reductions, from around €618,000 at lower hydrogen efficiencies to about €604,000 at higher efficiencies, indicating a secondary economic influence. Subplot (d) exhibits a more evident relationship between hydrogen efficiency and hydrogen-specific ESOI (R² = 0.85), increasing from about 8.0 to nearly 14.0. However, because the hydrogen fraction of total PV generation is minimal (2.6%), improvements in hydrogen ESOI have only marginal impacts on overall system economics and performance, confirming its secondary role compared to battery storage.

These findings closely correspond to Equation (5-11), which indicates that storage-specific ESOI values are weighted by their corresponding energy flow fractions within the general system EROI computation. Improvements in battery efficiency and ESOI have far more impact than hydrogen efficiency changes as the battery channel controls the storage route (about 30.9% of PV generation). With the role of efficiency variations clarified, the next part applies this parametric sensitivity study to component durability, hence assessing how the energy and economic criteria of the system are affected by battery and hydrogen storage lifespan.

#### 5.4.1.2 Influence of Component Durability (Battery, Fuel Cell, Electrolyser)

In continuation of the parametric sensitivity analysis for in-depth understanding, Figure 5-5 examines how altering the operational lifetimes (durabilities) of key storage components influences the overall system EROI and component-specific ESOI. This durability analysis provides deeper insights by directly linking component longevity and replacement frequency to economic and energetic outcomes, indicated by the net present cost (NPC) shown by the colour gradient in each subplot.

Battery durability (subplots a and b), varied between approximately 7,200 and 21,600 hours, demonstrates a clear and robust influence on both system-level EROI and battery-specific ESOI. The overall system EROI significantly rises from about 4.3 to nearly 5.0 (R² = 0.94), whereas the battery ESOI exhibits an even stronger linear response, increasing from roughly 6 to 15 (R² = 1.00). These pronounced improvements stem from the battery's substantial contribution (approximately 30.9 % of PV generation) as extended battery lifetimes reduce replacement cycles, thus decreasing both embodied energy requirements and economic costs. Correspondingly, NPC values decrease substantially from around €660,000 at shorter battery lifetimes to approximately €610,000 at extended durability.

On the system-level EROI, however, the effect of fuel cell lifetime (subplots c and d, ranging between around 4,000 and 15,000 hours) is somewhat low; it only rises from around 4.86 to 4.88 ( $R^2 = 0.88$ ). The hydrogen-specific ESOI, on the other hand, is significantly influenced by

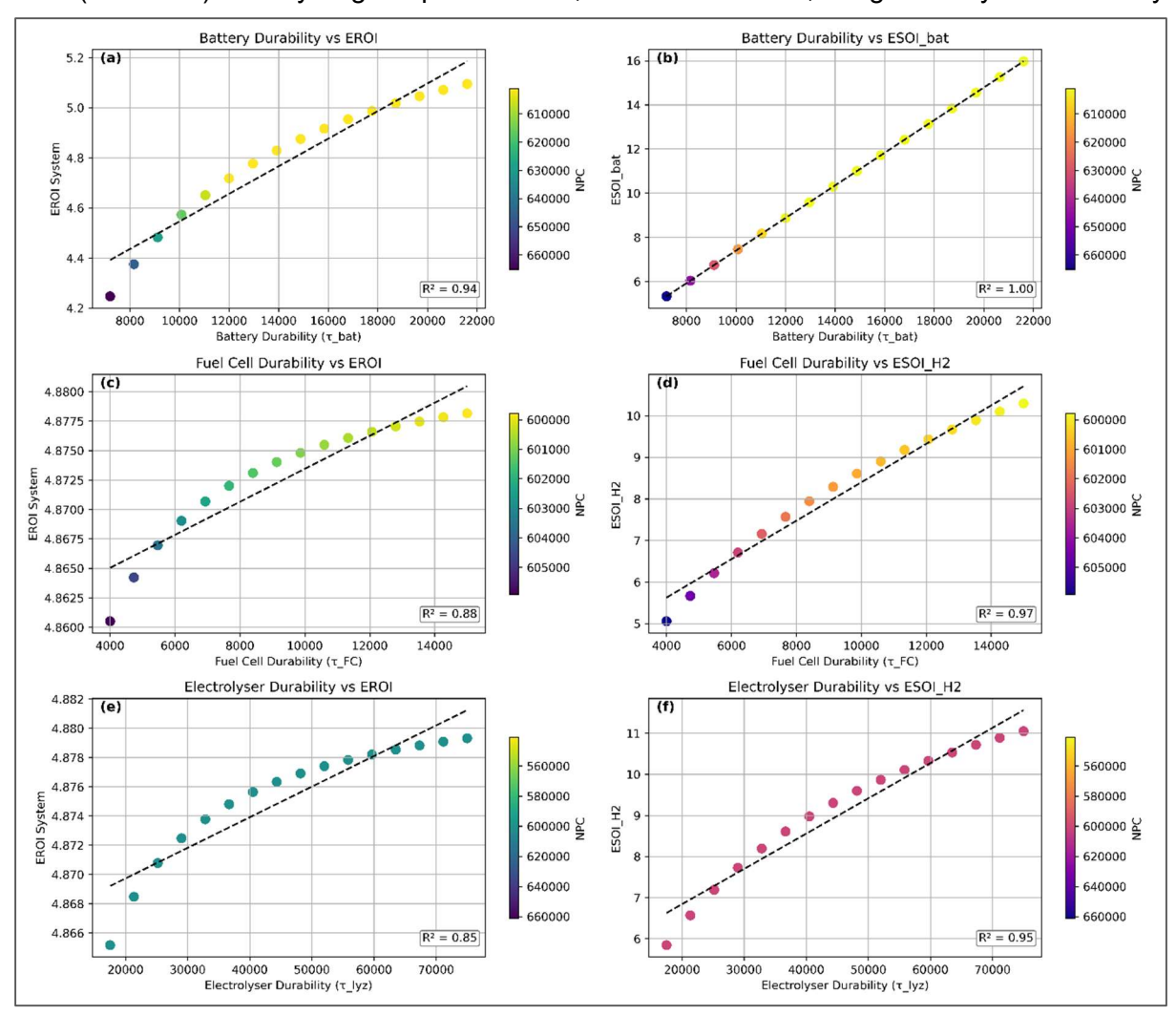


Figure 5-5: Sensitivity of system-level EROI and component-specific ESOI to variations in component durability (battery, fuel cell, electrolyser). Data points are coloured according to net present cost (NPC), illustrating economic impacts associated with differing durability levels.

fuel cell durability; from roughly 5.5 to 10.0 (R²=0.97), it shows a clear linear improvement. This contrast highlights the limited fraction (~2.6 %) of PV energy passing through the hydrogen pathway. Although the direct impact on the overall EROI is minor, extending fuel cell lifetimes meaningfully enhances hydrogen subsystem viability, with noticeable yet moderate NPC reductions (from approximately €615,000 to €605,000).

Subplots e and f show electrolyser durability's influence (varied between about 17,500 and 75,000 hours). While a noticeable yet moderate improvement in system EROI from about 4.865 to 4.880 ( $R^2 = 0.85$ ) is evident, the hydrogen-specific ESOI clearly benefits, increasing from roughly 6.5 to nearly 11 ( $R^2 = 0.95$ ). However, the NPC colour gradient remains notably consistent across durability levels, suggesting that electrolyser lifetime alone has a limited

effect on reducing overall costs. Nonetheless, because the electrolyser and fuel cell function jointly within the hydrogen cycle, simultaneous improvements in durability across both hydrogen components can collectively generate more substantial reductions in NPC and embodied energy impacts, even though each individually appears to offer modest improvements.

Taken together, these durability sensitivities highlight that extending battery lifetimes significantly enhances both economic viability and life-cycle energy performance due to the battery's large share of energy throughput. Unlike efficiency variations, durability changes do not substantially alter the operational energy fractions; hence, the numerator in Equation 5-11) remains nearly constant. Instead, durability directly impacts component replacements and thus the denominator of the equation (through the ESOI terms). Shorter component lifetimes necessitate more frequent replacements, increasing embodied energy demands and consequently inflating the ESOI denominator, which negatively affects the overall system EROI and raises the NPC. Contrarily, improvements in fuel cell and electrolyser durability, although individually modest in their system-level impact, collectively enhance the viability and cost-effectiveness of the hydrogen storage pathway. These observations emphasise that component-level ESOI improvements influence system-level EROI proportionally to each component's fraction of energy throughput. Having addressed both efficiency and durability impacts, the subsequent subsection 5.4.1.3 explores the sensitivity related to embodied energy intensity, evaluating how changes in manufacturing energy inputs for each component affect the overall life-cycle performance and economics of the system.

#### 5.4.1.3 Effects of Embodied Energy Intensity on Life-Cycle Metrics

At this subsection, following the evaluation of efficiency and durability with the baseline optimised capacities, this analysis addresses the sensitivity of the system-level EROI and storage-specific ESOI to variations in embodied energy intensities of major system

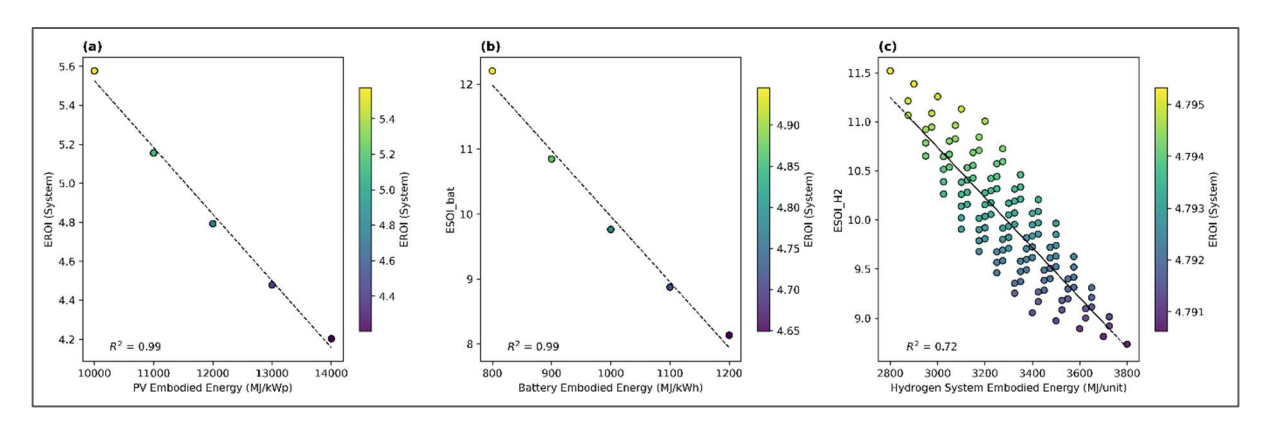


Figure 5-6: Sensitivity of system-level EROI and storage-specific ESOI to variations in embodied energy intensity for PV, battery, and hydrogen storage components. Points are coloured by the corresponding system-level EROI, illustrating how manufacturing energy inputs influence overall energy life-cycle metrics.

components. Figure 5-6 explores how modifications in the embodied energy intensity, representing variations in manufacturing energy inputs per unit capacity, affect the system's life-cycle metrics. Each subplot provides quantitative evidence of the direct correlation between embodied energy intensity and corresponding performance indicators, further complemented by the EROI colour scale, thus giving a nuanced perspective of system energy performance shifts.

In subplot (a), photovoltaic (PV) embodied energy intensity is varied between approximately 10,000 and 14,000 MJ/kWp. A highly linear and inverse relationship with the system-level EROI emerges (R² = 0.99), clearly indicating the considerable sensitivity of EROI to the PV's manufacturing energy footprint. Specifically, as PV embodied energy intensity increases from 10,000 MJ/kWp to 14,000 MJ/kWp, system-level EROI sharply decreases from about 5.6 down to nearly 4.2. This substantial drop emphasizes the pivotal role that PV manufacturing efficiency plays, given the PV's central role in overall system energy throughput and its proportionally high influence on the denominator of Equation 5-11).

Subplot (b) similarly illustrates the impact of battery embodied energy intensity, ranging from approximately 800 to 1,200 MJ/kWh. The battery-specific ESOI displays a robust inverse linear correlation (R² = 0.99), declining from about 12 to 8. This tendency underscores the strong dependency of battery ESOI on manufacturing energy demands, which in turn significantly impacts the overall system EROI due to the battery's sizeable contribution to the storage energy fraction. Increased battery embodied energy directly increases the ESOI denominator, thus negatively influencing the overall system performance and intensifying economic costs over the project's lifetime.

Subplot (c) addresses the embodied energy sensitivity for the hydrogen storage pathway (combined fuel cell and electrolyser), varied broadly between approximately 2,800 and 3,800 MJ per unit. The observed relationship between hydrogen subsystem embodied energy and hydrogen ESOI (R² = 0.72) reveals moderate linearity, yet with notable scatter. ESOI decreases from roughly 11.5 to about 8.5 over the examined range, reflecting a more variable but clear downward trend as embodied energy increases. Despite this variability, the influence on overall system-level EROI is limited, ranging from approximately 4.79 to 4.791. This constrained impact aligns with the relatively small fraction of total energy PV generation managed by the hydrogen storage subsystem. Thus, although increased hydrogen subsystem embodied energy negatively impacts hydrogen ESOI, its broader impact on the overall system's energy performance is modest.

Collectively, these findings underscore the crucial influence of embodied energy intensities on system life-cycle energy index. PV and battery manufacturing energies exert substantial impacts, both economically and energetically, due to their central roles in total energy throughput. On the other hand, the hydrogen subsystem, while revealing obvious sensitivity at the subsystem storage level, barely slightly affects the general system EROI as it manages smaller portion of energy. These studies support the idea that significant increases in general life-cycle performance requires giving PV and battery embodied energy intensities top priority. With these insights clearly established, the subsequent analysis moves beyond fixed capacities and examines how systematic scaling of the optimised MPC capacities impacts the established relationships.

#### 5.4.2 Capacity Scaling and Generalisation Framework

The previous subsections provided an isolated parametric sensitivity analysis, examining the effect of altering key system parameters, efficiency, durability, and embodied energy intensity, under fixed, optimised system capacities. However, real-world energy community planners frequently face scenarios that necessitate adjusting the scale of system components from initial optimised recommendations. Consequently, a generalisation framework introduced in this subsection provides critical insights into how variations in component capacities influence system sustainability and economics. By applying uniform scaling to the baseline capacities established in the MPC-4% scenario, the resulting heatmaps with EROI contours superimposed over NPC gradients offer a visual analytical tool that captures both economic performance and energy sustainability. This method helps energy communities plan choices, so allowing them to properly balance their sustainability enhancements and investment.

Figure 5-7 shows the 10-fold cross-validation approach which has thoroughly evaluated the accuracy of the generated surrogate models, predicting the energy system performance metrics, NPC, EROI, unmet load, and extra energy. With a Mean Absolute Error (MAE) of €6,715.55, a Mean Squared Error (MSE) of €124,329,111, and an average coefficient of determination (R²) of 0.9957, the NPC surrogate shows exceptionally remarkable accuracy. The EROI model reveals analogous remarkable predictive potential by showing its dependability for accurately capturing the energy efficiency dynamics of the system with a R² of 0.9879, a very low MAE of 0.0791, and an MSE of 0.0193.

The excess energy surrogate model also presents excellent predictive performance, with an R² value of 0.9784, MAE of 98.20 MWh/year, and MSE of 18,183.16 MWh²/year², signifying accurate forecasting of excess generation. The unmet load model, while demonstrating a comparatively lower R² of 0.8448, still provides acceptable accuracy with an MAE of 0.2814 MWh/year and an MSE of 0.2708 MWh²/year², reflecting the inherent difficulty in precisely modelling unmet demand due to its higher variability.

These validation results indicate that the polynomial surrogate models regularly interpolate the performance of energy systems inside the examined design space. Thus, by generating comprehensive heatmaps, these models offer a solid foundation that obviously shows the slight trade-offs between economic and energetic performance criteria.

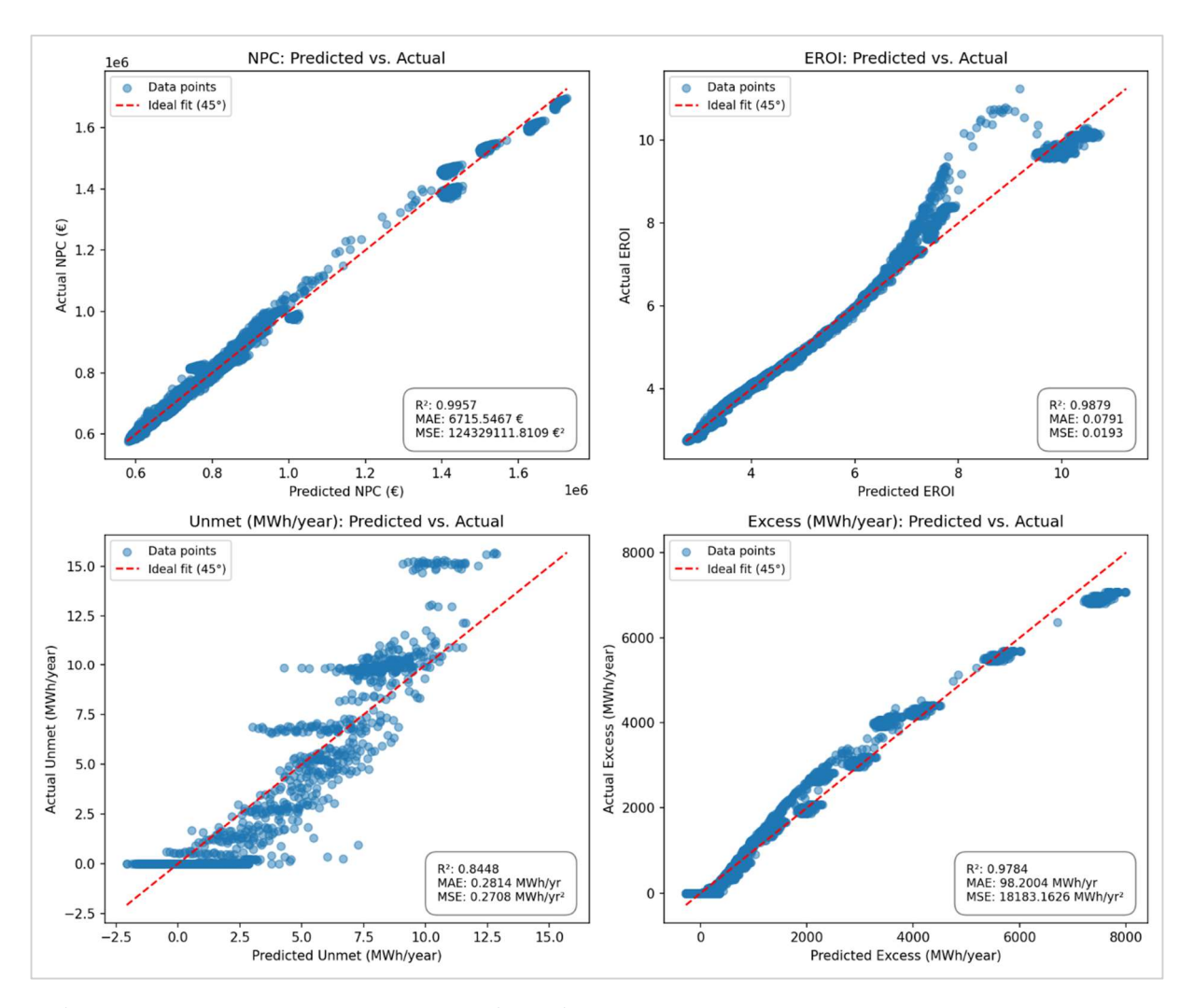


Figure 5-7: Surrogate model accuracy shown via predicted vs. actual plots for NPC, EROI, Unmet, and Excess energy (10-fold cross-validation)

#### 5.4.2.1 PV Sizing Relative to Storage Configuration

Presenting the heatmap for PV and battery capacity scales, Figure 5-8 shows how system EROI and the NPC interactively react to changes in capacity. At lower PV capacities (around 0.25 to 0.5 scale factor) coupled with small to moderate battery scales (0.5 to 1.0), the system attains high EROI system values between approximately 7.23 − 8.71, signifying strong energy performance. However, these configurations entail prohibitively high NPC values, typically ranging from about € 847,603 − €1,199,751, with minimal unmet load (1–4 MWh/year) and almost no excess energy. Conversely, configurations with substantially larger PV capacities (scale factor around 1.5 to 1.7) and moderate battery sizing (around 0.8–1.0) slightly increases NPC, typically reaching values close to or marginally between € 631,554 − €675,363, yet at

the expense of lower EROI system outcomes, falling to approximately 3.18-3.52. Although these configurations reduce unmet demand to near-zero, they cause a large increase in excess energy generation, reaching up to 2,429 MWh/year, indicating underutilised PV resources. This substantial numerical trade-off underscores the inherent tension between economic affordability and energy sustainability.

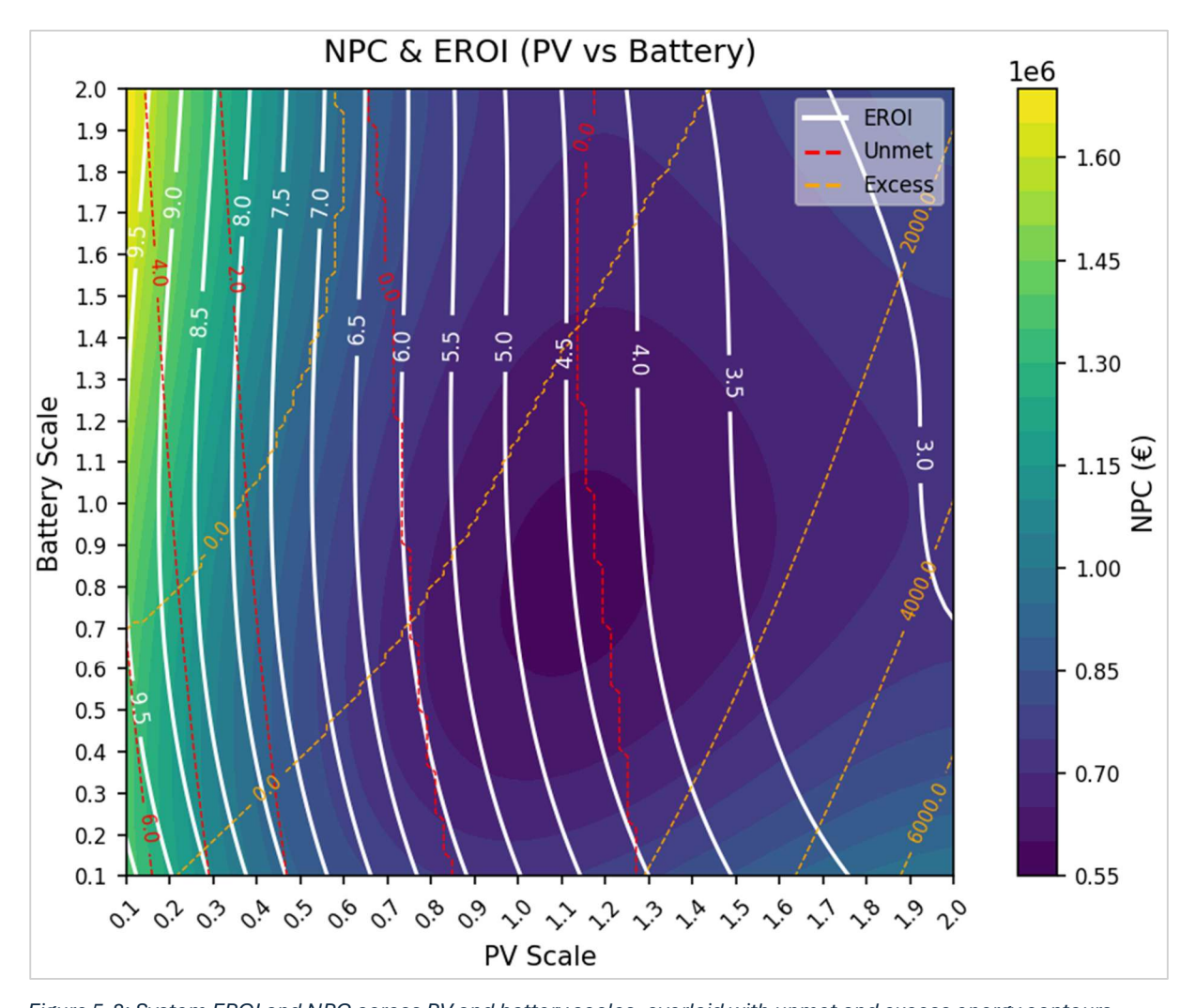


Figure 5-8: System EROI and NPC across PV and battery scales, overlaid with unmet and excess energy contours (MWh/year), highlighting trade-offs between cost, sustainability, and energy utilisation.

From a deeper analysis, an optimal performance region clearly emerges, forming a circular heat light colouring around the baseline scenario (PV ~1.0, Battery ~1.0). Interestingly, this optimal region subtly shifts towards slightly larger PV and smaller battery scales (approximately PV ~1.1 and Battery ~0.8), corresponding to an NPC of around €586,437 − €586,766 and an EROI system of about 4.53 − 4.60. Reaching 0% unmet demand indicates this area's efficient balance between cost and sustainability under moderate excess generation (323–375 MWh/year). These results highlight how relaxing surplus energy constraints would allow better trade-offs and how they might be a useful road map for adding hydrogen storage or other flexible options to the system.

Figure 5-9 heatmap shows PV and hydrogen tank scales, revealing a markedly different sensitivity pattern compared to the battery storage system. At hydrogen tank capacities (0.2–1.6 scale), increasing PV capacity (1.1–1.3 scale) substantially increases the NPC to approximately €590,018 – €607,552, while the system EROI correspondingly decreases to values between 3.97 – 4.60. This suggests a little trade-off, somewhat greater system costs accompany modest gains in sustainability (EROI). The increase in EROI is therefore somewhat small, implying that its economic effect decreases with more PV growth in this region. Conversely, lowering PV capacities below the baseline scenario (around 0.4–0.6 scale), even at relatively large hydrogen tank scales (1.3–1.6), significantly raises NPC, approaching €792,241 – €991,294, while providing only marginal improvements in EROI (around 6.65 – 7.69). The trade-off between NPC and EROI in the hydrogen tank scenario is therefore less pronounced than with battery storage, indicating lower sensitivity of hydrogen storage sizing to both economic and energy-life cycle metrics. Rather than forming a sharp optimal pocket, a broader, more diffuse optimal band appears around PV scales of 1.0–1.1

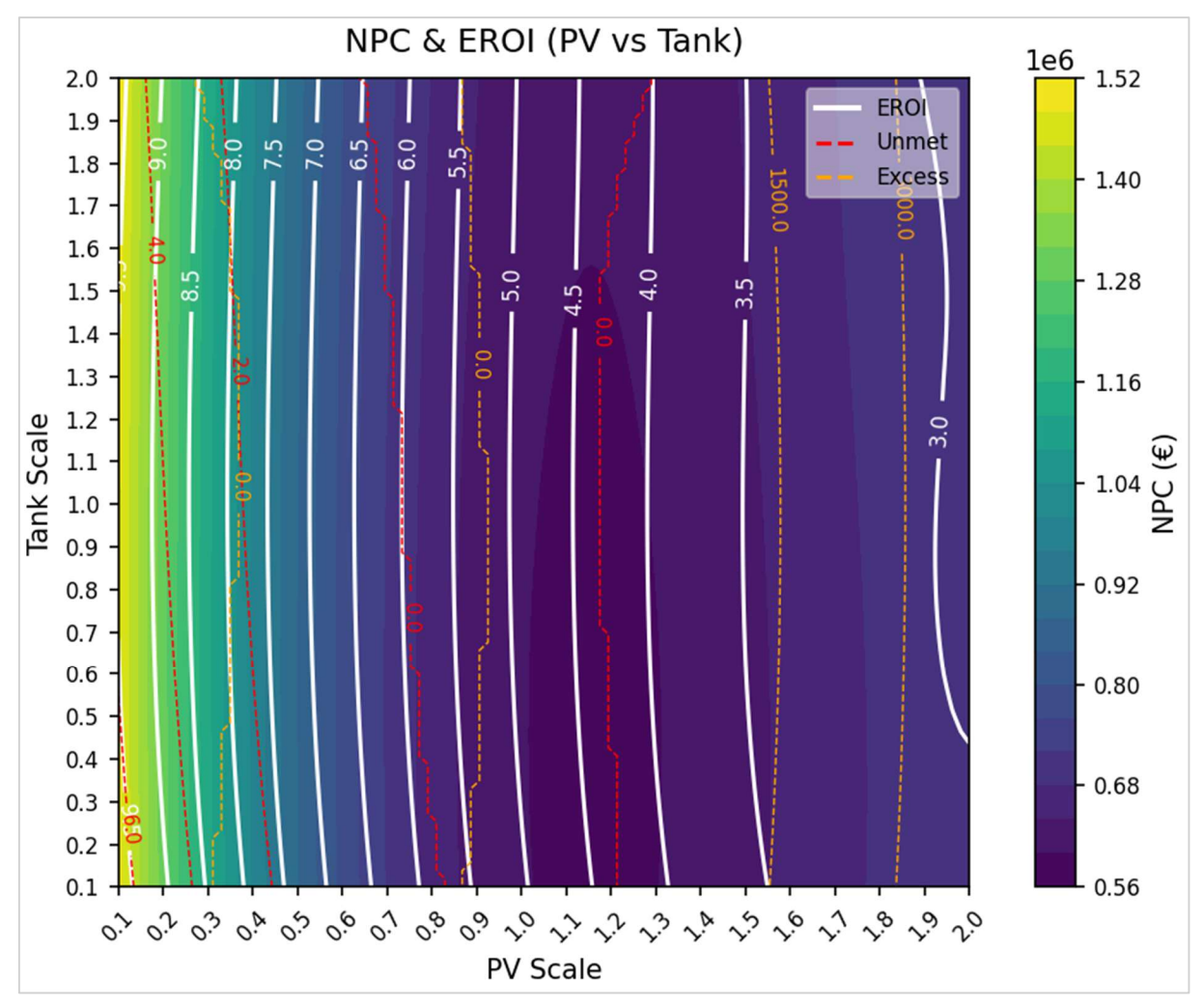


Figure 5-9: System EROI and NPC across PV and hydrogen tank capacity scales, overlaid with unmet and excess energy contours (MWh/year), illustrating the diffuse trade-offs between cost, sustainability, and renewable energy utilisation in hydrogen-based storage configurations.

and tank scales of 0.8–1.0. Within this region, the system achieves moderate EROI values between 4.56 and 4.90, and NPC values ranging from €593,006 to €604,513, with no unmet load and only moderate excess generation (64–182 MWh/year). This flexibility makes the hydrogen storage scenario appealing for energy communities seeking a balance between investment efficiency and energy resilience.

Figure 5-10 expands the capacity-scaling investigation presented earlier, showing how varying PV and fuel cell capacities influence both economic costs and energy sustainability. The contour map shows three principal performance zones based on system-level EROI and NPC. The high EROI-high NPC region (PV scales roughly 0.10–0.35 and fuel cell scales 0.10–2.00) yields EROI values of 8.00–9.61 at a considerable economic burden, with NPC up to €1.50 million and an unmet load range of 1.44–8.95 MWh/year. Conversely, the low EROI-low NPC region (PV scales approximately 1.29–1.92 and fuel cell scales 0.10–2.00) reduces NPC to about €598,388–€699,981 but lowers EROI to 3.01–3.99, accompanied by sizable excess energy (546–3,630 MWh/year). Between these extremes lies a moderate trade-off region (PV scales around 0.85–1.12 and fuel cell scales 0.10–0.20), where EROI holds at 4.50–5.50 and

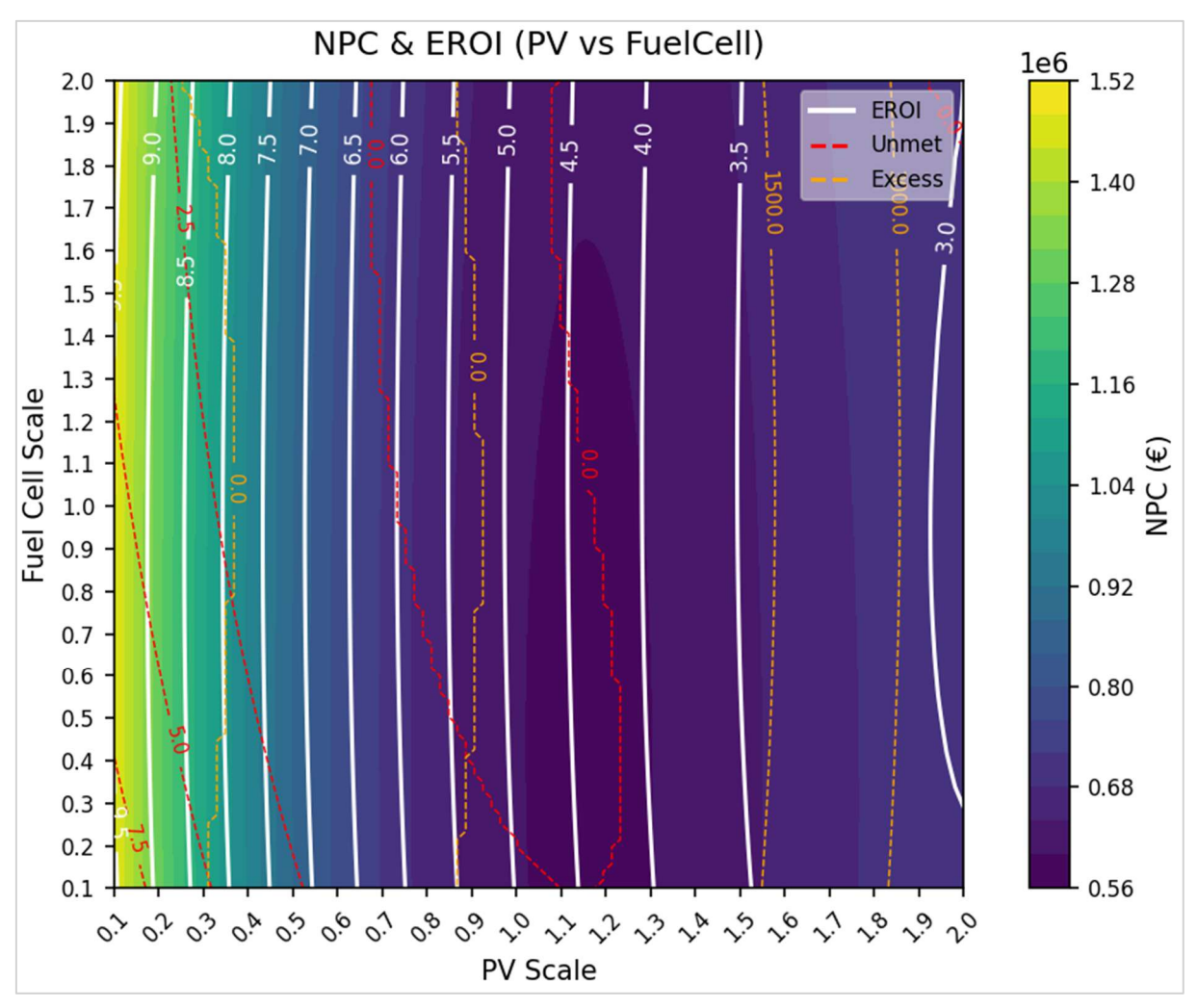


Figure 5-10: Capacity scaling analysis of PV and fuel cell systems showing trade-offs between system EROI and NPC.

NPC stands near €600,019–€649,974, while surplus energy lies in the 0–270 MWh/year range and unmet demand remains minimal. Though NPC increases to around €619,201–€649,974 as EROI moves higher (5.18–5.50), a narrower sub-region further tightens PV (0.85–0.93) and raises fuel cell capacity (0.41–1.92) to eliminate both unmet load and curtailment. Oversizing the fuel cell beyond 1.5 rarely boosts EROI but raises cost; minor PV trim reduction eliminates wasted generation without significantly affecting general system viability. These results show once again that EROI-based sustainability and cost efficiency seldom coincide precisely, hence stressing the need of careful capacity tuning depending on local energy needs and financial objectives.

Figure 5-11 broadens the capacity-scaling investigation by focusing on how varying PV and electrolyser dimensions can shift both NPC and EROI. The resulting contour map separates into three main performance zones, revealing how system designs can pivot between cost and sustainability goals. In the high EROI–high NPC region (PV scale 0.10–0.37, electrolyser scale 0.10–2.00), EROI reaches up to 9.64, but NPC can exceed €1 million, with unmet loads

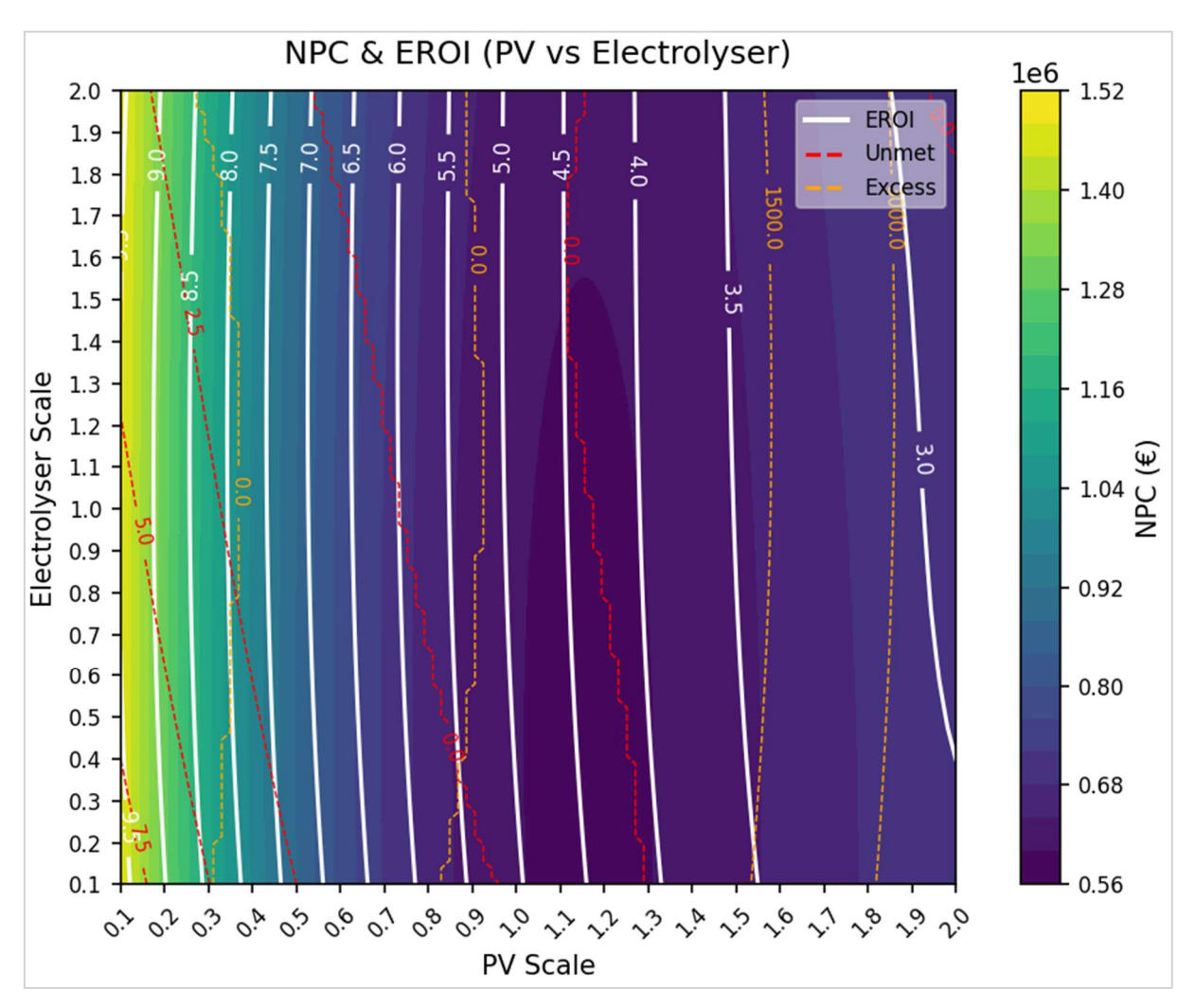


Figure 5-11: Capacity scaling analysis of PV–electrolyser systems, illustrating trade-offs between economic cost and energy sustainability.

of 0.92–8.74 MWh/year, indicating strong sustainability with a considerable financial burden and operational risks from undersized PV. Conversely, the low EROI–low NPC area (PV scale 1.27–1.96, electrolyser scale 0.10–2.00) pushes costs down toward €600 k yet drops EROI to 3.01–4.00, accompanied by substantial curtailment (520–4,019 MWh/year). While cheaper in absolute terms, these configurations compromise long-term energy efficiency by oversizing PV relative to the electrolyser capacity. A moderate trade-off area (PV scale 0.85–1.10, electrolyser scale 0.10–2.00) finds a more harmonic equilibrium with EROI values spanning from 4.53 to 5.50 and NPC clustering around €600k–€650k. Minimal excess and unmet demand in this range improve dependability as well as price stability. Within that moderate zone, a narrower subset (PV 0.85–0.93, electrolyser 0.41–2.00) achieves zero unmet and zero excess, at slightly higher costs but with EROI rising to 5.17–5.50. These nuanced capacity-scaling outcomes underscore the need to harmonise local load, financial constraints, and desired sustainability targets when deciding on optimal PV–electrolyser configurations.

#### 5.4.2.2 Scaling Battery, Fuel Cell, Electrolyser, and Hydrogen Tank Capacities

Emphasizing four separate areas that underline the natural trade-offs in hybrid energy system design, Figure 5-12 offers a complex mapping of the interaction between battery and hydrogen tank capacity and their combined influence on system-level performance. The system reaches EROI levels between 8.00 and 9.61 in the High EROI–High NPC area, where battery scales vary from 0.10 to 0.25 and tank scales from 0.10 to 0.60. Reducing embodied energy suggests that reducing component sizes might greatly improve energy efficiency; nonetheless, the related net current costs surpass €1 million, which emphasizes the great financial load of such drastic downsizing. The Moderate Trade-off area offers a balanced outcome with intermediate scales (battery and tank both around 0.85–1.15), where EROI ranges from 4.53 to 5.50 and NPC stabilizes between €600,000 and €650,000 while sustaining low unmet demand and moderate excess energy. Especially interesting is a very appealing cluster with battery scales of 0.75–0.80 and tank scales of 0.40–0.70 that produces the lowest NPC (around €591,600) and a fair EROI just around 5. These results offer important direction for maximizing component size to balance financial limits with sustainable energy performance.

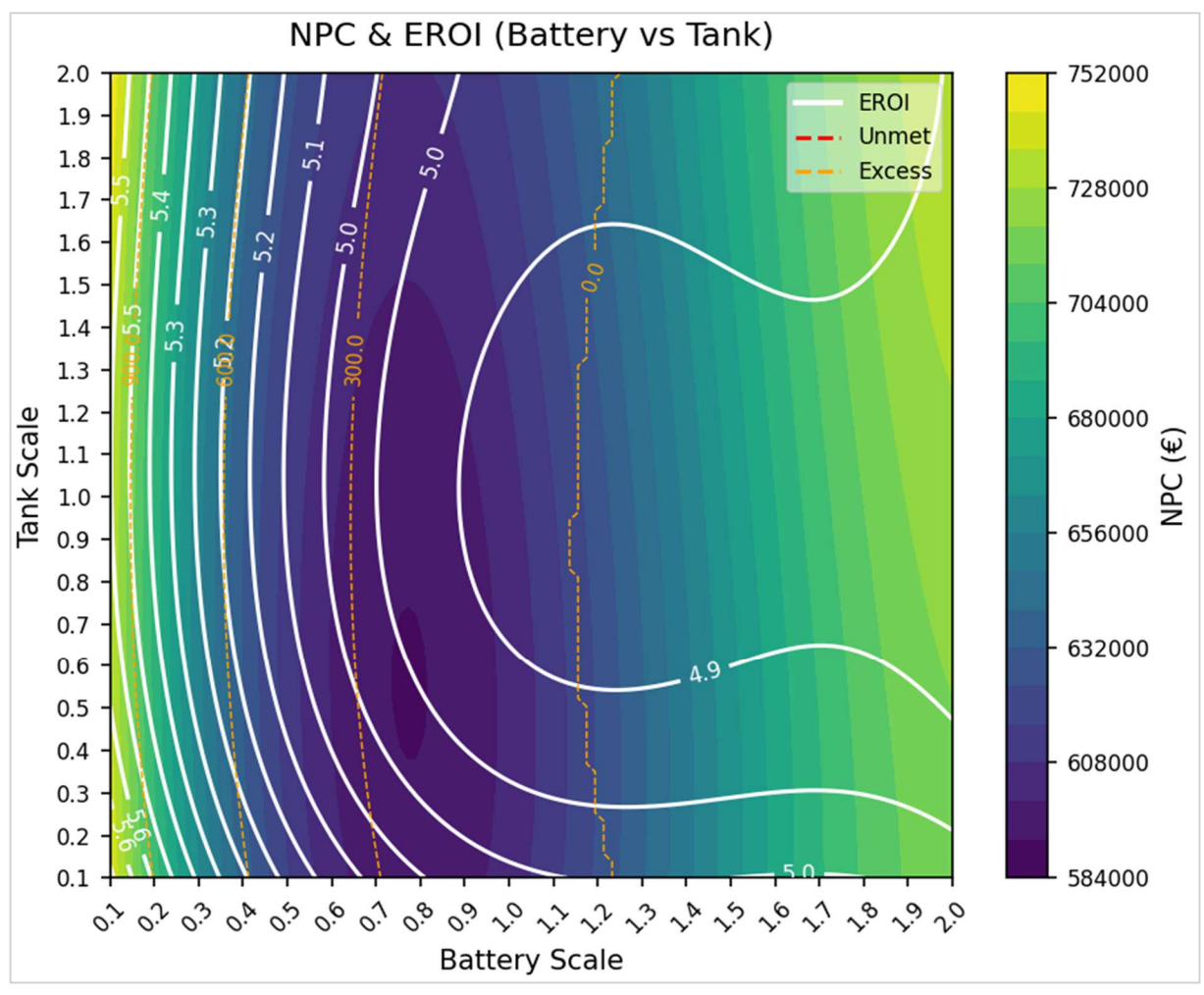


Figure 5-12: Battery and hydrogen tank capacity scaling analysis showing four performance regions that capture the trade-offs between system-level EROI and NPC.

Figure 5-13 illustrates the intricate trade-offs encountered in hybrid energy system design by jointly varying battery and fuel cell capacities and examining their impact on system-level EROI and NPC. In our analysis, the data reveal that a central configuration, where battery and fuel cell scales fall between 0.81–1.10 and 0.81–1.29 respectively, consistently delivers the lowest NPC (approximately €593,061–€617,948) while achieving zero unmet demand and only modest excess energy (around 16.5-178.2 MWh/year). Though modest, its sustainability performance (EROI = 4.89-4.95) is fair, hence this "sweet spot" is a cost-optimal choice. By contrast, a nearby region with somewhat higher EROI (up to 5.27) and even lower NPC values (down to €594,593) is countered by notable excess generation (up to 614.4 MWh/year). suggesting possible inefficiencies from under sizing. In the upper-right sector, where battery capacity is minimised (0.10-0.29) and fuel cell capacity is considerably over scaled (1.71-2.00), the system achieves peak EROI values (5.30-5.56) but at the expense of markedly higher NPC (exceeding €670,000) and excessive energy wastage (over 1,000 MWh/year). Notably, further increasing both battery and fuel cell capacities beyond 1.4 eliminates all unmet and excess energy, confirming technical robustness; however, this comes at a cost, with EROI falling to 4.88–4.93 and NPC rising to approximately €732,620. These results underscore my

contention that, while storage scaling can refine system performance, the overall EROI is far more sensitive to PV sizing, highlighting the need for a judicious balance between economic and energy sustainability in practical hybrid system design.

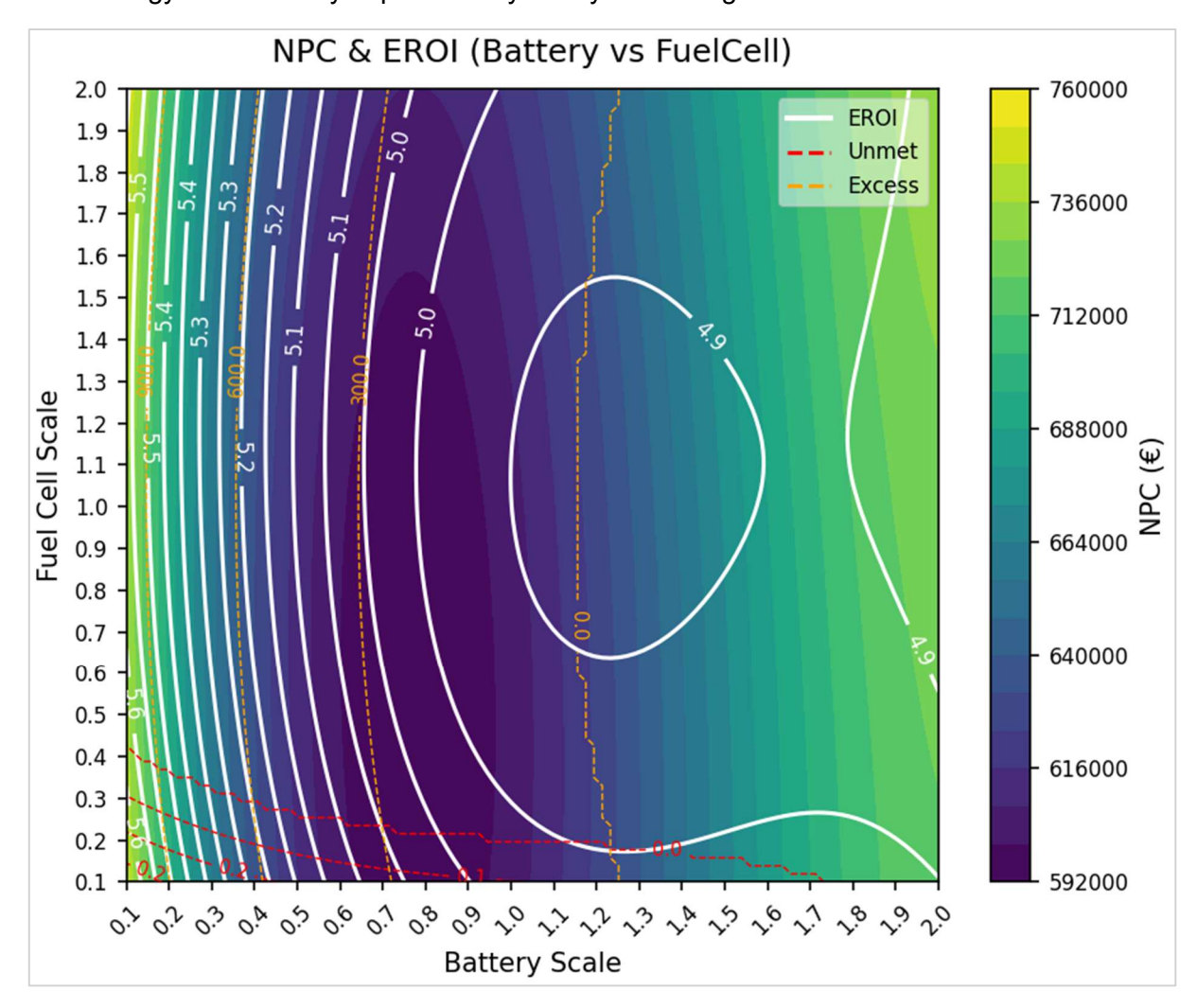


Figure 5-13: Battery–Fuel Cell capacity scaling delineates four distinct regions of trade-off between lifecycle energy efficiency (EROI) and economic cost (NPC), underscoring the importance of balanced storage sizing for sustainable hybrid systems.

Figure 5-14 presents a comprehensive analysis of the trade-offs inherent in storage sizing considering how battery and electrolyser capacity scaling affects energy sustainability as well as economic cost. The figure shows six distinguished regions. Though with modest excess energy (about 145–246 MWh/year), the system in Region A achieves the lowest NPC (about €591,868–€594,739) with a reasonable EROI close to 5.0, where battery scales range from around 0.75 to 0.89 and electrolyser scales from 0.50 to 0.60. In contrast, Region B, characterized by very low battery (0.10–0.29) and electrolyser (0.10–0.20) scales, attains higher EROI values (up to 5.78) but incurs significantly higher NPC (up to €744,223) and substantial excess generation (approximately 787–1117 MWh/year), highlighting the pitfalls of under sizing. Defined by large components (battery and electrolyser scales over 1.62), Region C presents poorer sustainability (EROI about 4.86–4.89) despite no surplus; NPC climbs to

between €697,038 and €734,261. Operating with no unmet and excess energy but at approximately greater cost, Region D features moderate battery scaling (1.31–2.00) and a wide electrolyser range. While Region F, the balanced trade-off (battery scale ~1.00–1.10 and electrolyser scale ~0.71–0.98), finds an optimal convergence with NPC between €603,221 and €615,086 and EROI around 4.89–4.93 with minimal excess, Region E provides configurations with large excess yet low NPC and high EROI. These results taken together highlight that a moderate, balanced strategy offers the greatest compromise between cost and energy efficiency while both forceful downsizing and oversizing can negatively affect system performance.

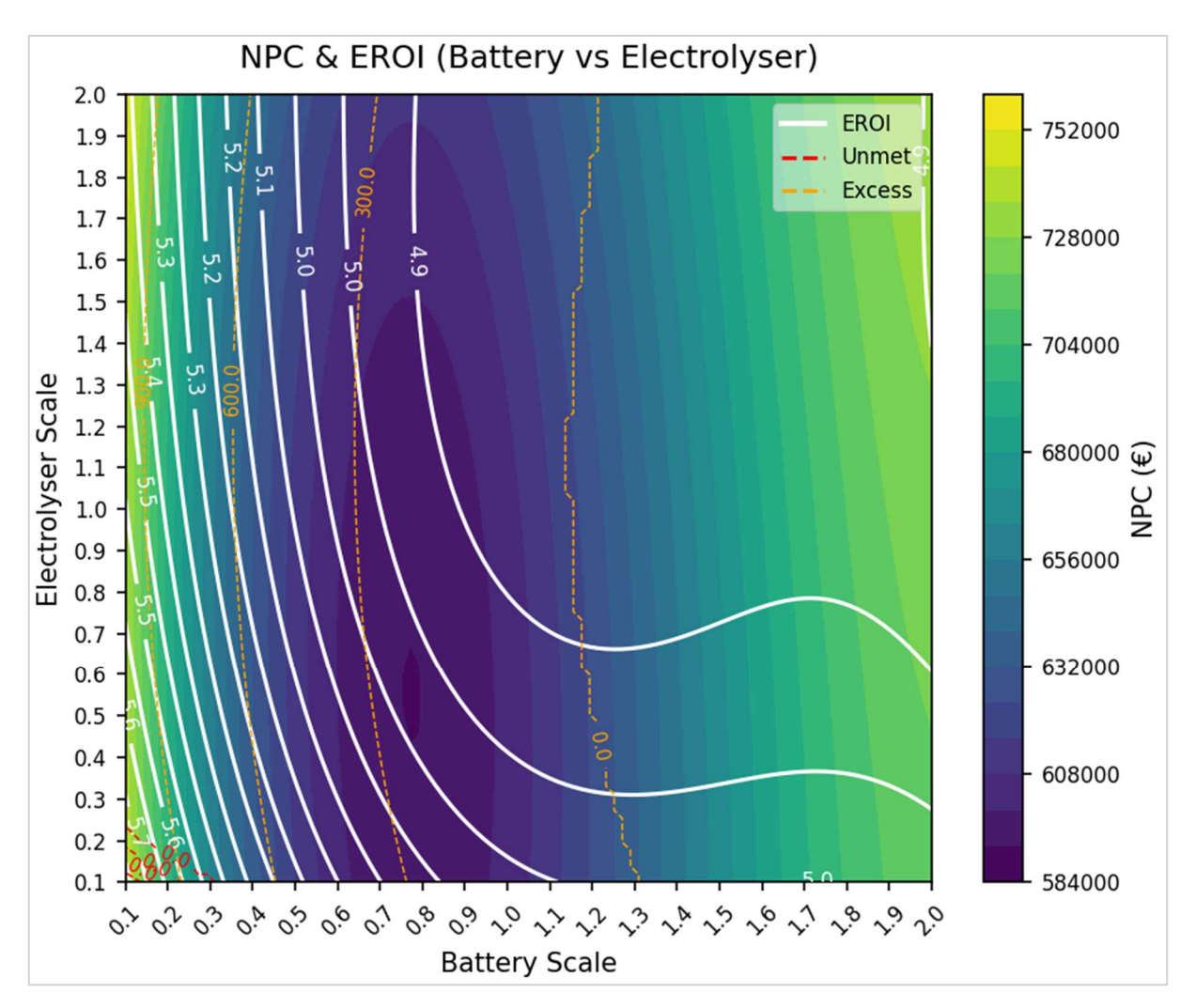


Figure 5-14: Battery–Electrolyser capacity scaling analysis showing how moderate storage configurations yield optimal trade-offs between system-level EROI and NPC.

Figure 5-15 illustrates the impact of hydrogen tank and fuel cell capacity scaling on system-level economic and sustainability metrics. It is observed that when tank scales are maintained between approximately 0.2 and 0.8 and fuel cell scales vary from about 0.15 to 0.9, the system achieves the most cost-effective performance, with NPC values ranging from roughly €600,311 to €602,511 and an EROI between 4.91 and 5.06. In this region, unmet demand is

consistently zero, while excess energy remains moderate, between 63.1 and 138.0 MWh/year, indicating an efficient balance between investment and renewable utilisation. In contrast, configurations cantered around tank and fuel cell scales near unity, approximately 0.96 to 1.04, exhibit similarly balanced performance, with NPC values between €604,390 and €605,728 and a nearly constant EROI of 4.90; notably, excess energy in these scenarios is further reduced to a narrow range of 62.0 to 63.0 MWh/year, signifying a finely tuned operational equilibrium. But when both tank and fuel cell capacities are raised to a scale of 1.4, performance clearly deteriorates: NPC rises to between €712,000 and €736,000 and EROI falls somewhat to about 4.88–4.93. These results highlight that while both under sizing and oversizing of hydrogen components create inefficiencies that degrade general system

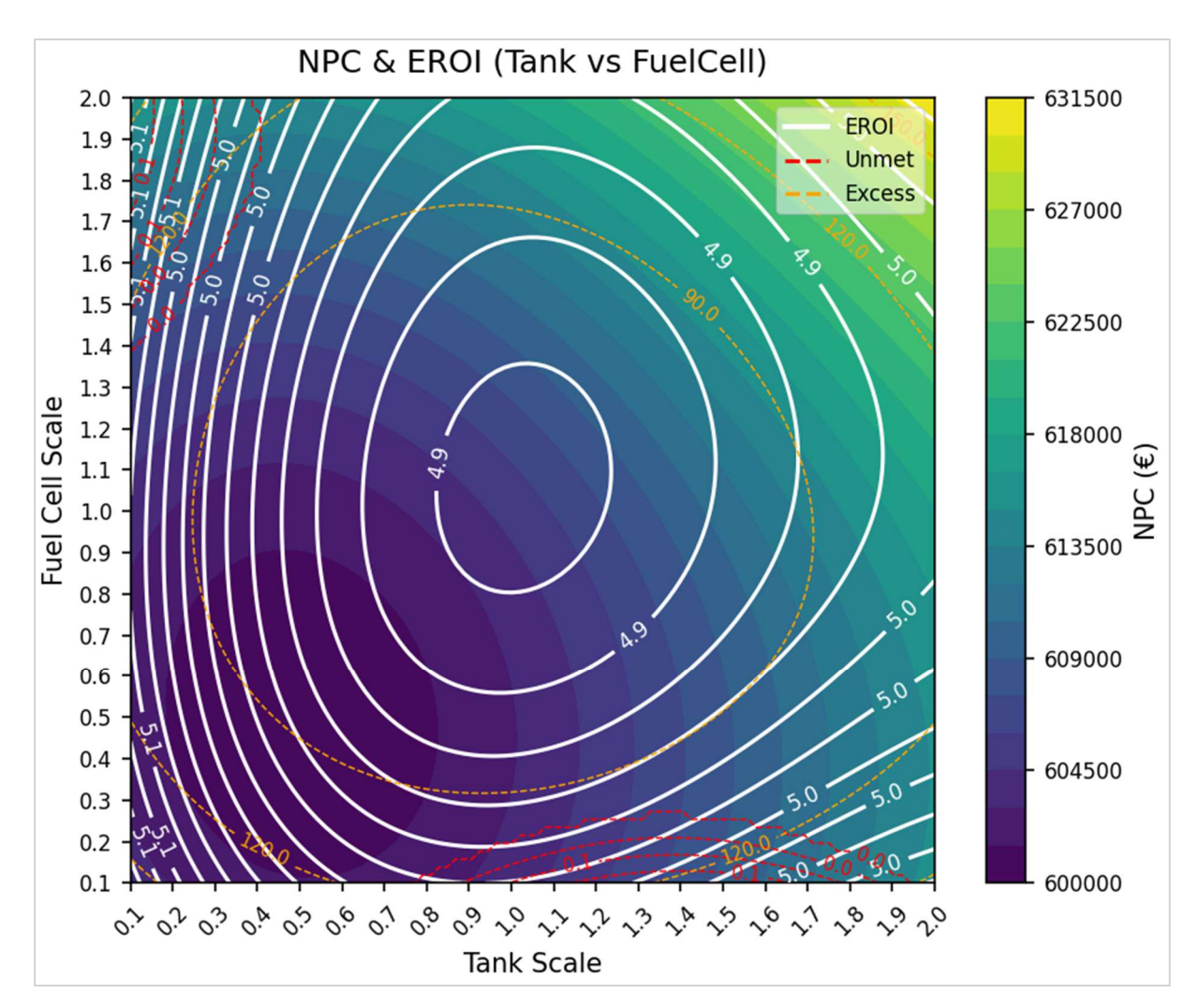


Figure 5-15: Tank and fuel cell scaling reveals optimal cost—sustainability trade-offs near baseline configurations, with under sizing or oversizing degrading performance.

performance, moderate, near-baseline scaling produces the strongest trade-off between cost, sustainability, and operational reliability.

Figure 5-16 illustrates how varying hydrogen tank and electrolyser capacities affects overall system performance, revealing a complex interplay between cost and energy return. Configurations with moderate tank and electrolyser scales, roughly in the 0.7–1.1 range, consistently yield some of the lowest NPC values, around €600,000–€607,000, while maintaining a balanced EROI of approximately 4.89–4.94 with minimal excess energy (near 61–74 MWh/year) and zero unmet demand. By contrast, setups with very small tank sizes (roughly 0.1–0.3) combined with bigger electrolyser scales (about 1.5–2.0) tend to produce somewhat higher EROI values (about 4.99–5.08) but at the cost of higher NPC (approximately €608,000–€618,000) and moderate excess levels (roughly 94–144 MWh/year). A particularly notable configuration emerges in the central region (tank scale 0.42–0.60 and electrolyser scale 0.35–0.55), where NPC drops to as low as €599,875 with EROI values narrowly distributed between 4.97 and 5.02. These solutions maintain unmet load at zero and excess energy below 116 MWh/year, reinforcing this as the most cost-optimal and technically reliable area in the design space. Exhibiting a strong trade-off with NPC values between €602,700

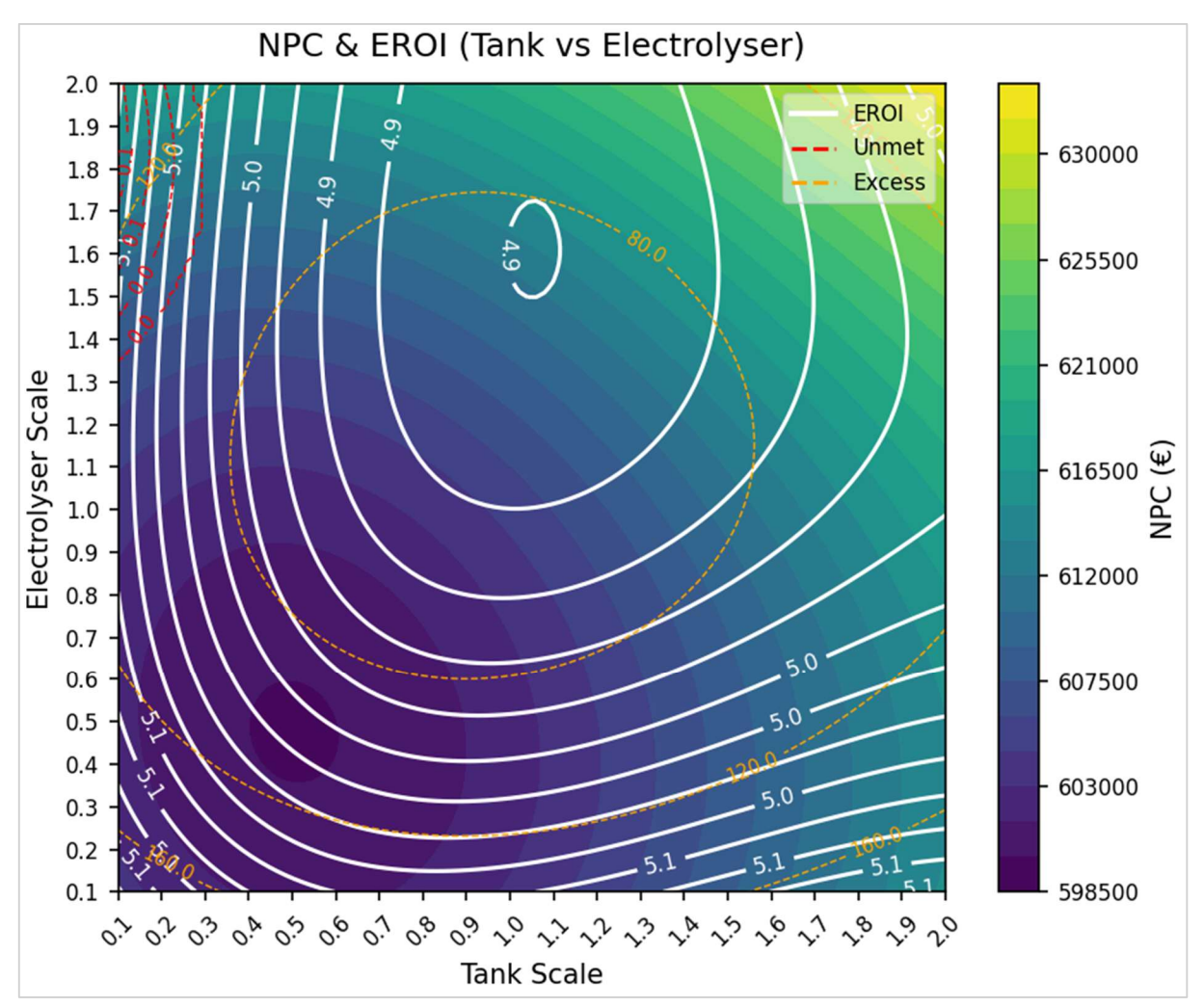


Figure 5-16: System EROI and NPC response to hydrogen tank and electrolyser capacity scaling, highlighting costoptimal and energy-efficient regions.

and €612,800 and closely regulated excess energy (about 61–79 MWh/year), a unique cluster showing low excess, where tank scales range from around 0.91 to 1.39 and electrolyser scales from 0.81 to 1.29. Extreme oversizing, with both tank and electrolyser scales above roughly 1.62, leads to higher NPC values (around €620,700–€632,600) and somewhat lower EROI (4.91–4.97) together with substantial excess (94–140 MWh/year). These results show, then, that while variations toward under sizing or oversizing create operational inefficiencies, moderate, near-baseline settings offer the greatest balanced economic and energy performance.

Figure 5-17 explores how system performance changes with fuel cell and electrolyser capacity scaling, revealing nuanced trade-offs between economic cost and energy efficiency. Analysis shows that although maintaining zero unmet load and moderate excess energy, configurations with fuel cell scales of about 0.27–0.77 and electrolyser scales of 0.23–0.71, representing the most cost-effective zone, produce NPC values closely grouped around €600,776–€602,010 and an EROI ranging from about 4.93 to 5.06. In contrast, designs featuring very small fuel cell and electrolyser capacities (scales roughly 0.10–0.29) exhibit marginally higher EROI (up

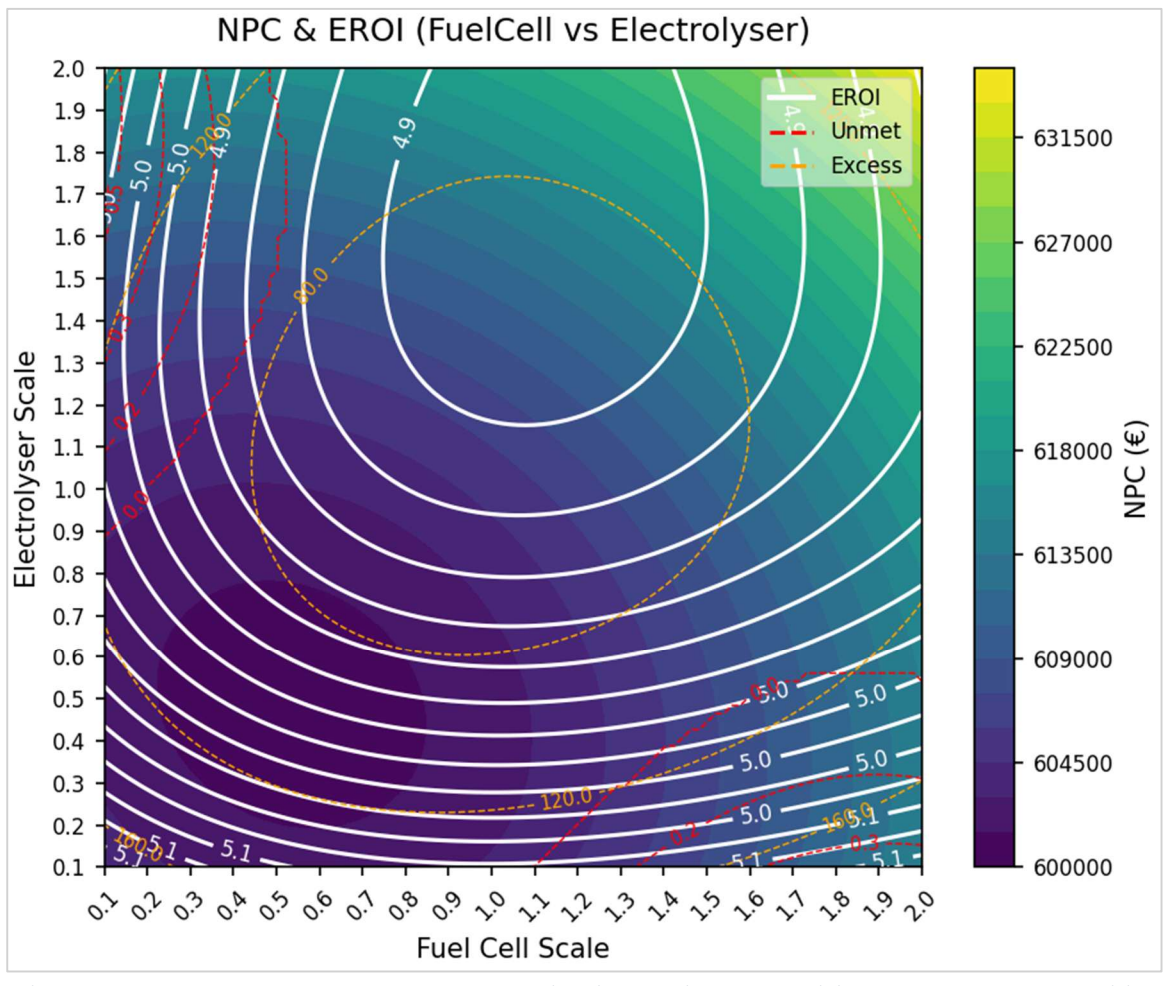


Figure 5-17: Balanced fuel cell and electrolyser scaling yields optimal cost–efficiency trade-offs; extreme sizing degrades performance.

to 5.11) but are burdened by increased excess energy, sometimes approaching 174 MWh/year, even though their NPC remains similar. When one component is significantly oversized relative to the other, a pronounced mismatch emerges, with NPC values rising to between €607,116 and €617,225 and excess energy increasing up to 191 MWh/year, highlighting the adverse effects of imbalance. A finely balanced system, where both fuel cell and electrolyser scales are around unity (approximately 0.91–1.10), shows a practically invariant EROI around 4.90 and NPC values in the narrow region of €603,590–€606,756 with little excess. Oversizing both components beyond 1.5 eventually results in far greater costs (NPC up to €633,668) with little additional EROI benefit. These findings show that whereas extreme under sizing or oversizing exacerbates operational inefficiencies, sensible, well-balanced scaling of fuel cell and electrolyser capacities generates the best strong performance.

#### 5.5 Summary

This study introduces a new life-cycle energy index that holistically incorporates multiple energy flows, including direct consumption, storage via battery and hydrogen, and grid export, while accounting for the embodied energy of each subsystem. A detailed parametric analysis demonstrates that battery storage dominates system-wide effects, as it often channels over 30 % of total PV generation. For instance, improving battery round-trip efficiency from 70 % to 95 % raises the extended EROI from around 4.4 to nearly 4.9, while also lowering the NPC by over 6 %. In contrast, hydrogen storage typically handles only about 2.6 % of PV output, so even raising electrolyser—fuel cell efficiency from 15 % to 40 % yields a relatively modest EROI increment, underscoring the secondary role of hydrogen unless it is significantly upsized. The chapter further shows that PV manufacturing energy intensity exerts a substantial influence on overall results: increasing the embodied energy from 10,000 MJ/kWp to 14,000 MJ/kWp cuts system EROI by nearly a quarter, from approximately 5.6 down to 4.2.

In addition, capacity-scaling studies reveal that both under sizing and oversizing can undermine cost-effectiveness or lifecycle efficiency. Systematically investigating hundreds of scaled configurations shows a surrogate model trained using polynomial regression and validated by 10-fold cross-validation with coefficients of determination (R²) over 0.98. By creating heatmaps of EROI, NPC, unmet load, and curtailment, the model pinpoints "sweet-spot" capacity ranges, often around a 1.0–1.1 scale of the baseline design, that achieve EROI near 5.0 while holding NPC below €610,000 and curtailment under 200 MWh/year.

Examining scaling decisions more closely, the study finds that PV capacity creates the most design potential by far by imposing the most cost and environmental load. Though a little rise above scale = 1 results shows only small trade-offs, then bigger expansions, especially

beyond 1.8 or 2.0, often result in oversizing, when both the EROI and NPC suffer and aligns. Conversely, scaling down tends to raise EROI but also escalates specific costs, indicating a clear tension at smaller sizes. These observations are explained by constrained fixed inverter and grid-contract limits, which throttle surplus generation for oversized systems and thus align economic and energy performance trends in higher PV capacities. These findings rest on a set of simplifying assumptions. The extended EROI and ESOI calculations treat system operation as steady state (The annual dispatch pattern is assumed to repeat identically every year), using a single representative year without accounting for degradation (linear degradation assumed), and recycling benefits. Component round-trip efficiencies and embodied energy intensities are held constant, while dynamic environmental impacts such as extreme weather, multi-year wear are excluded from the lifecycle boundary. As whole, these heatmaps become a vital decision-support tool for energy communities trying to strike environmental performance with techno-economic limits, thereby directing planners toward strong, data-driven design decisions that maximize energy returns as well as cost.

# 6 Integrated Analysis of Sizing, Operation, and Life-Cycle Performance

Chapter 6 brings the thesis full circle by weaving together the discrete, yet complementary insights derived in Chapters 3, 4 and 5 into a single narrative. It integrates techno-economic sizing, operational control, and life-cycle sustainability into a unified performance analysis of the hybrid PV-battery-hydrogen system. Chapter 3 established the techno-economic "blueprint", using a GA-MILP framework to co-optimise long-term sizing and hourly dispatch under realistic grid-tariff constraints. Chapter 4 then demonstrated how rolling-horizon MPC, augmented by a modest approach of flexible load setting, can translate that blueprint into day-to-day operation while shaving peaks, curtailment and costs. Chapter 5 introduced a the life-cycle lens through an extended EROI/ESOI index that quantifies how each storage path, direct PV, short-duration battery, long-duration hydrogen, contributes to both economic return and net-energy pay-back.

The purpose of this chapter is therefore threefold: first, to demonstrate how the sizing ratios shaped by GA–MILP are reshaped, though not undone, by MPC and flexible demand strategies; second, to interpret the integrated techno-economic and environmental performance of the system under various scenarios; and third, to position these findings in the context of real-world planning constraints such as contracted-power limits and control logic. Importantly, this chapter focuses entirely on presenting the original contributions and results of this thesis. Comparative benchmarking with existing literature is deliberately deferred to Section 6.6, allowing the novel framework's internal performance to be presented without interruption or external influence.

### 6.1 Main Findings from Integrated System Design

The effect of integrated MPC design on component sizing is captured in Figure 6.1, which contrasts the Load-Following baseline with four MPC strategies enabling 0% to 8% load flexibility. The baseline maintains a conservative solar-to-inverter ratio (SIR) of 1.03, closely aligned with traditional 1:1 DC/AC matching. This conventional approach, while simple, restricts inverter utilisation and offers limited flexibility in managing surplus PV generation.

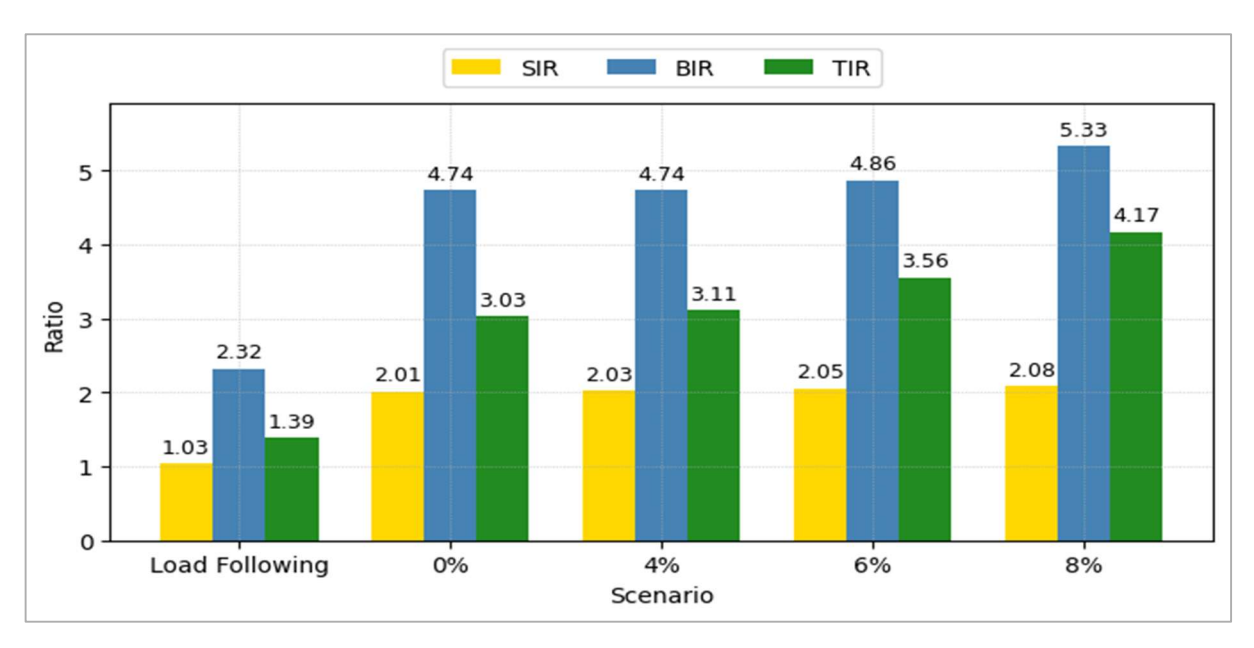


Figure 6-1: Comparison of solar-to-inverter (SIR), battery-to-inverter (BIR), and tank-to-inverter (TIR) sizing ratios for the Load-Following baseline and MPC strategies with 0 %, 4 %, 6 %, and 8 % load-shifting.

Figure 6-1 summarises the evolution of key sizing ratios across the Load-Following baseline and four MPC-based operational strategies with varying degrees of load flexibility. Three metrics are examined: the solar-to-inverter ratio (SIR), battery-to-inverter ratio (BIR), and tank-to-inverter ratio (TIR). The baseline system maintains conservative sizing across all metrics, particularly with an SIR of 1.03 and BIR of 2.32, reflecting a traditional DC/AC matching and limited storage duration. However, the MPC-based designs adopt a markedly different architecture. As load flexibility increases from 0% to 8%, the system progressively shifts towards higher inverter utilisation and longer storage durations. SIR stabilises around 2.0, indicating deliberate PV oversizing across all MPC variants. Meanwhile, BIR rises steadily from 4.74 to 5.33, enabling the battery to provide extended discharge coverage, particularly in response to diurnal demand shifts. Notably, TIR also escalates, from 3.03 to 4.17, demonstrating that hydrogen storage is increasingly employed for long-duration energy balancing. These results confirm that the joint optimisation of sizing and flexible control not only reduces curtailment and inverter idling but also rebalances storage responsibilities across short and long timescales.

The impact of these revised sizing ratios is best understood by examining the system's hourly operational dynamics. Figure 6-2 offers a year-round view of how each scenario converts solar generation into usable output while managing storage state-of-charge. The figure illustrates the annual power and storage dynamics under three supervisory strategies: Load-Following, MPC 0%, and MPC 8%. In the Load-Following case, the 120-kW inverter is frequently saturated during peak PV periods, resulting in noticeable clipping losses, while the battery operates around mid-capacity (46.4%) and hydrogen storage remains underutilised at 23.0% average SoC. By contrast, the MPC 0% scenario reduces inverter size to 77 kW yet achieves comparable AC output by deliberately overbuilding the PV array and maintaining the battery near 33.3% SoC. This mid-empty strategy enables the battery to absorb midday surpluses more effectively, shifting energy to evening loads. Hydrogen storage in this case steps up significantly, with its average SoC rising to 55.2%, suggesting a clear seasonal balancing role. The MPC 8% scenario further reinforces this trend: inverter size drops to 72 kW while storage states remain well-managed, with average battery and hydrogen SoC at 33.5% and 51.1%, respectively. The added flexibility allows modest load shifting to improve PV utilisation, smooth out inverter excursions, and defer seasonal energy through the hydrogen subsystem. Together, these patterns confirm that integrated control and flexible demand enable substantial inverter downsizing without compromising system output, while actively partitioning storage roles across daily and seasonal cycles.

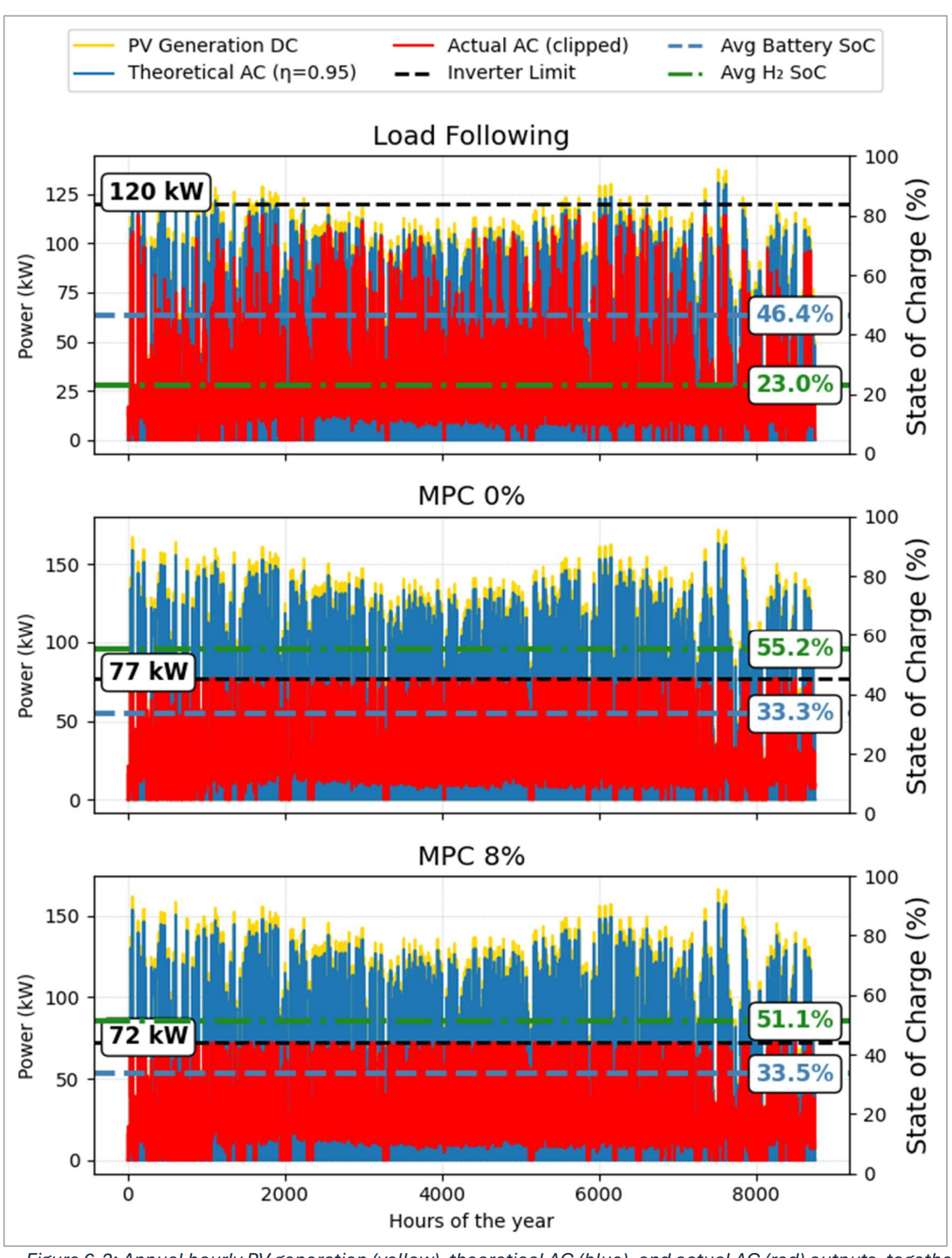


Figure 6-2: Annual hourly PV generation (yellow), theoretical AC (blue), and actual AC (red) outputs, together with average battery (dashed blue) and hydrogen tank (dashed green) SoC, for (a) Load-Following with a 120 kW inverter (Battery  $\approx$  46 %,  $H_2 \approx$  23 %), (b) MPC 0 % with a 77 kW inverter (Battery  $\approx$  33 %,  $H_2 \approx$  55 %), and (c) MPC 8 % with a 72 kW inverter and 8 % load shifting (Battery  $\approx$  34 %,  $H_2 \approx$  51 %).

This enhanced operational coordination also translates into improved utilisation of contracted grid capacity, as shown in Figure 6-3. The figure presents the evolution of contracted-power-normalised ratios for solar (SPR), battery (BPR), and hydrogen tank (TPR) components. The Load-Following strategy remains modest across all three metrics, with limited storage capacity relative to grid import/export constraints. However, once MPC control is introduced, even with zero load flexibility, both BPR and TPR sharply increase, reflecting a deliberate shift towards storage-dominant infrastructure. As the flexibility rises to 8%, BPR and TPR reach 10.38 and 8.11 respectively, illustrating a system increasingly oriented around autonomous operation and seasonal energy balancing. The gradual rise in SPR, from 1.59 to 4.05, demonstrates that solar oversizing also scales in parallel with storage capacity, reinforcing the system's ability to meet demand internally. Collectively, these trends underscore the central thesis contribution: MPC-based hybrid systems can maximise renewable utilisation and minimise grid dependency not only through control logic but also through co-optimised sizing decisions anchored to contracted power availability.

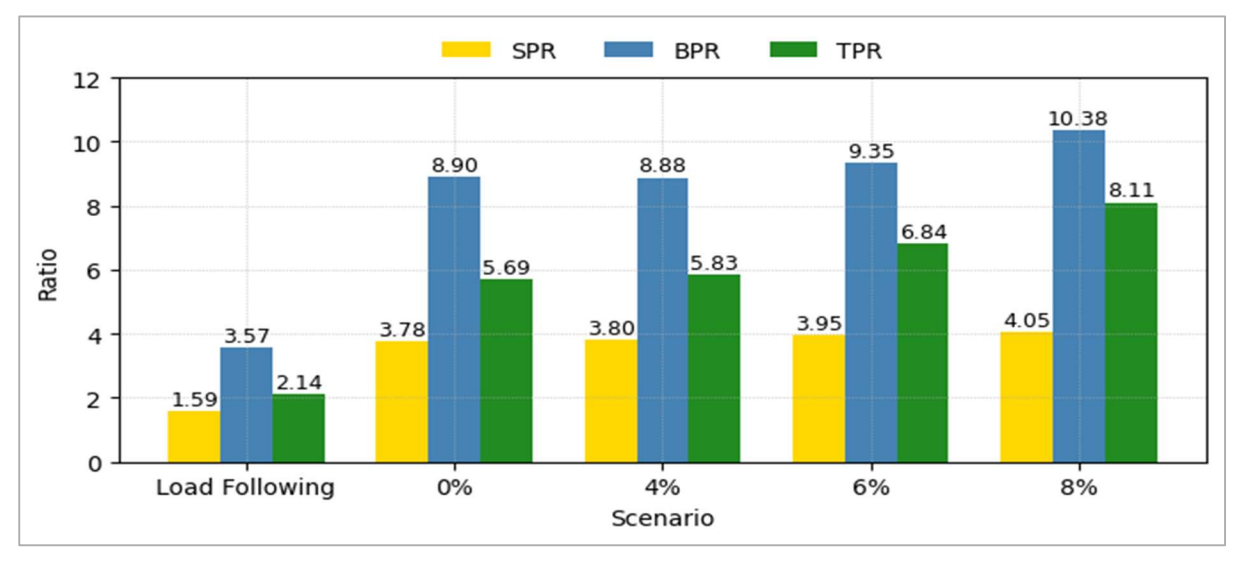


Figure 6-3: Contracted-power ratios (SPR, BPR, TPR) for Load-Following vs. MPC (0–8 %); MPC greatly boosts storage versus grid capacity, enabling higher PV capture and seasonal balancing.

This strategic shift towards storage-dominated infrastructure has a direct impact on the nature and frequency of grid interactions. Figure 6-4 illustrates how grid imports and exports are shaped under Load-Following and MPC 8% scenarios, plotted against instantaneous PV generation. In the Load-Following configuration, the system relies on a ±78 kW contracted grid envelope. Despite high PV availability, there are significant occurrences of both import and export events, with grid interactions constrained more by inverter size than by energy availability. Notably, the system avoids grid imports 77% of the time, but only manages complete independence—i.e., zero grid exchange, for 66% of hours annually. This indicates

suboptimal internal balancing, with surplus energy frequently exported and occasional reliance on the grid to meet evening or cloudy-day loads.

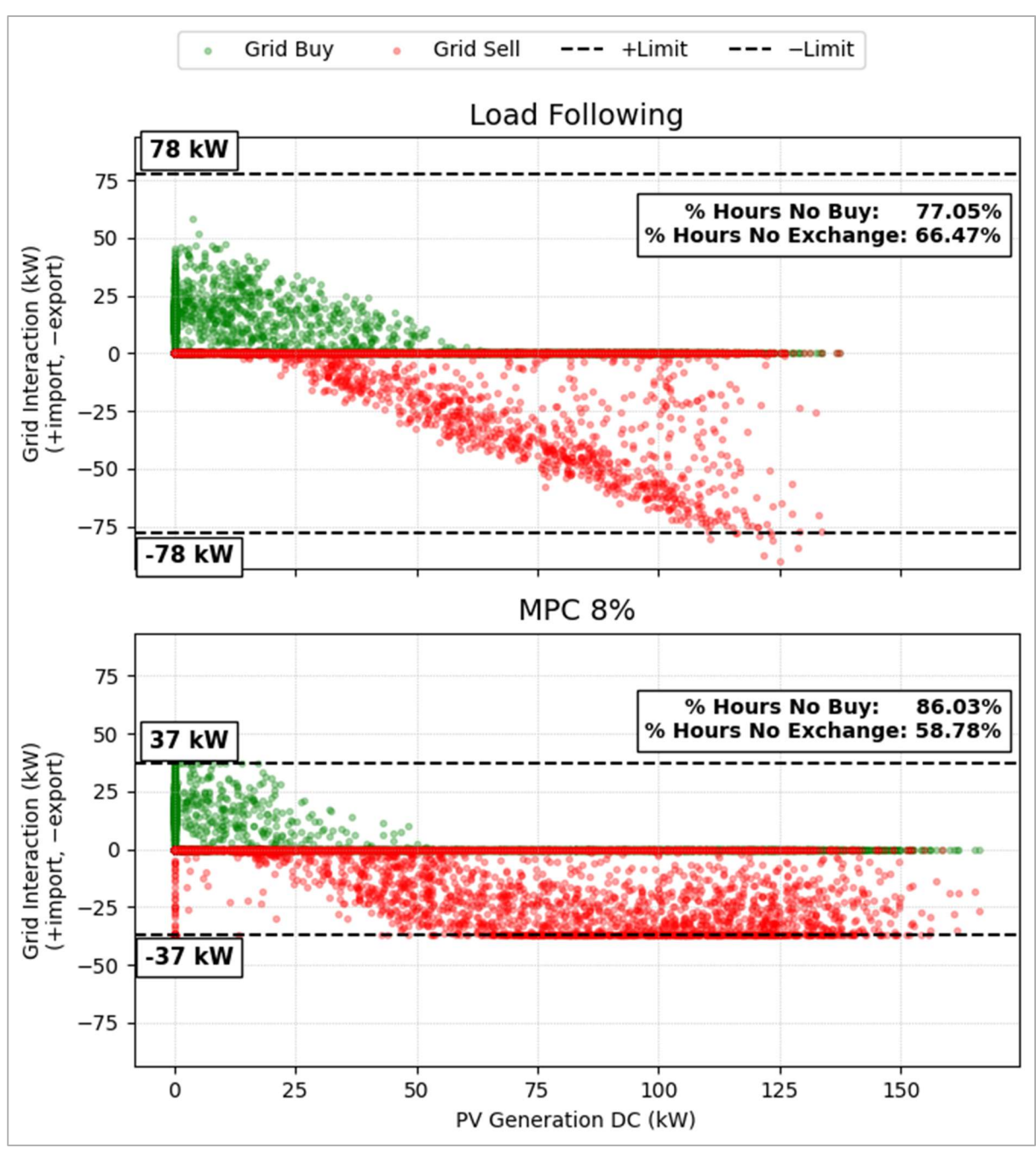


Figure 6-4: PV vs. grid import/export for Load-Following (±78 kW) and MPC 8 % (±37 kW): MPC achieves import-free operation 86 % of hours and uses storage discharge at zero PV, flattening grid exchanges.

In contrast, the MPC 8% design operates within a much narrower ±37 kW contracted power range yet demonstrates superior autonomy. Grid imports are avoided during 86% of the year, and complete self-sufficiency (no exchange) is achieved in nearly 59% of hours. This performance is achieved not by simply increasing system size, but through the coordinated discharge of storage assets during low-PV periods and intelligent load shifting during high-PV availability. The figure also reveals a flattening of the import/export envelope, reflecting

smoother and more controlled grid interactions. This outcome highlights the value of coupling flexible control with precise sizing: the system effectively decouples from the grid by using energy where and when it is most valuable, without exceeding contracted limits or over relying on the external network.

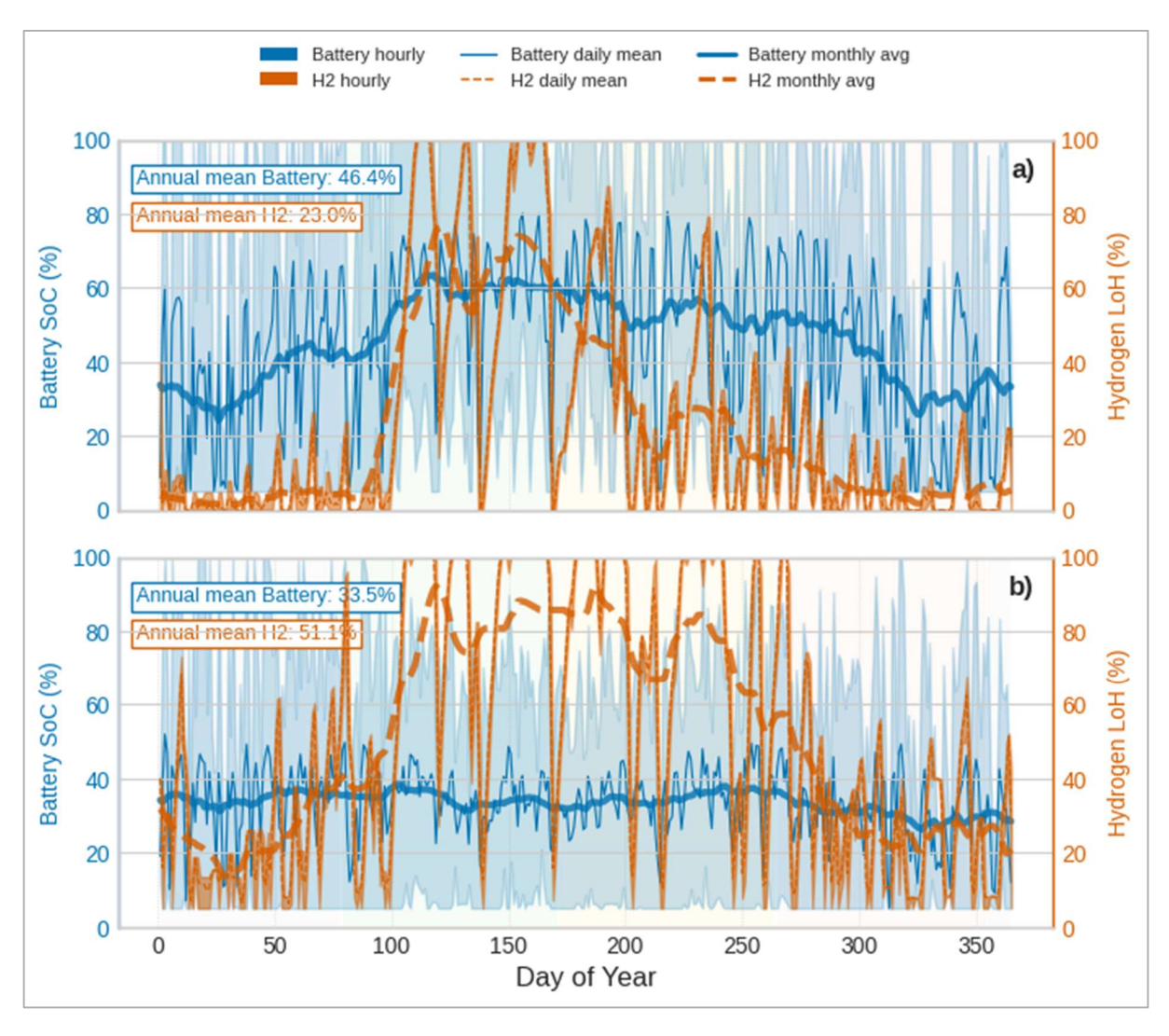


Figure 6-5: Annual dynamics of Battery SoC and Hydrogen LoH for (a) Load Following and (b) MPC 8%. Each subplot shows hourly values (faded), daily means, and 30-day rolling averages. MPC 8% maintains the battery at a lower SoC set point with reduced daily fluctuation while using hydrogen for long-term seasonal storage, in contrast to Load Following which underutilises hydrogen and experiences frequent battery saturation.

The internal balancing mechanisms enabling such controlled grid interaction are best illustrated through the seasonal storage dynamics in Figure 6-5. This final figure compares the hourly, daily, and monthly behaviour of battery SoC and LoH under Load-Following and MPC 8% configurations. In the Load-Following scenario, the battery hovers near mid-capacity with an annual mean SoC of 46.4%, exhibiting strong daily fluctuations and frequent saturation. The hydrogen system, by contrast, remains largely underutilised with an annual average LoH of only 23.0%, and no clear seasonal pattern. This operational profile indicates poor long-term

storage integration: the battery is routinely tasked with covering both diurnal and seasonal mismatches, which exceeds its optimal duty cycle and leads to curtailed surplus energy.

Under MPC 8%, however, the control strategy explicitly separates the roles of short- and long-duration storage. The battery is maintained at a consistently lower set point, averaging 33.5% SoC, with noticeably reduced daily cycling range. This creates headroom for absorbing midday surpluses and enables higher flexibility for short-term balancing. More importantly, hydrogen storage becomes the principal vector for inter-seasonal energy shifting. Its average LoH rises sharply to 51.1%, and its dynamics reveal a distinct charging trend during summer and discharging in winter. The smoother and broader seasonal LoH profile confirms that hydrogen is not just an auxiliary buffer but a fully integrated component of the energy management strategy. This functional separation enhances the lifecycle performance of both storage technologies and is a hallmark of an optimally coordinated hybrid system.

# 6.2 Robustness Under Economic and Environmental Variability

While favourable results under nominal conditions are promising, they do not alone ensure broader applicability under variable real-world contexts. To explore the robustness of the proposed framework, a sensitivity analysis is conducted, drawing on the structure outlined by [165]. This coming analysis systematically investigates how variations of  $\pm 10\%$  in equipment prices, grid capacity, and solar irradiance affect the proposed nested GA-MILP-MPC framework's techno-economic outcome in terms of NPC and LCOE. Table 6-1 encapsulates the system's re-optimised capacities and resultant techno-economic indices across six scenarios. In every case, the model maintained annual unmet and excess energy below 100 kWh, reflecting the dispatch strategy's robustness in aligning production and demand without compromising economic viability.

Under escalated equipment prices, the NPC rose to €643,297 with a corresponding LCOE of €0.235/kWh, accompanied by mostly modest capacity adjustments. On the other hand, when component costs dropped, the system found it advantageous to enlarge the PV array to 167 kW and bolster battery storage, driving the NPC down to €574,537 and the LCOE to €0.210/kWh. This contrast suggests that more affordable hardware encourages heavier reliance on self-generated power and stored energy, thereby reducing dependence on the grid over the system's lifetime.

Table 6-1: Sensitivity Analysis of System Components under External Variations (MPC-4% selected)

Description	PV (kW)	Battery (strings)	Inverter (kW)	Grid (kW)	Fuel Cell (kW)	Electrolyser (kW)	Tank (kg)	NPC (€)	LCOE (€//kWh)
Base Scenario	152	74	75	40	5	5	7	606,879	0.221
Scenario 1: +10% Equipment Price	152	75	75	41	5	5	7	643,297	0.235
Scenario 2: -10% Equipment Price	167	79	87	52	5	5	8	574,537	0.21
Scenario 3: +10% Grid Price	161	74	89	46	5	5	8	612,298	0.224
Scenario 4: -10% Grid Price	163	79	84	50	5	5	9	612,133	0.224
Scenario 5: +10% Solar Irradiance	137	78	106	36	5	5	6	592,206	0.216
Scenario 6: -10% Solar Irradiance	177	77	86	48	5	5	7	642,447	0.235

Moderate changes in grid tariffs similarly triggered recalibrations in plant sizing. A 10% tariff uptick led to additional PV (161 kW) and inverter capacity (89 kW), raising the NPC to €612,298 and the LCOE to €0.224/kWh; when grid electricity was cheaper, the model still opted for a moderate PV and storage increase, settling at an NPC of €612,133 with an LCOE of €0.224/kWh. These findings imply that high tariffs incentivize an expanded local generation portfolio, whereas low tariffs, although less punitive, do not necessarily diminish the value of storage, particularly over a 25-year project planning where operational savings can offset capital outlays.

In scenarios of elevated solar irradiance (+10%), the model could curtail PV capacity to 137 kW while assigning a larger inverter (106 kW) to handle higher midday outputs, reducing the NPC to €592,206 and the LCOE to €0.216/kWh. Conversely, less irradiance drove the system to boost PV capacity up to 177 kW, with the NPC climbing to €642,447 and the LCOE to €0.235/kWh. Despite such divergent solar resource profiles, the optimisation reliably preserved sufficient battery and hydrogen storage to supply the load without resorting to excessive grid imports.

Collectively, these outcomes underscore that the nested MPC-Flexible Load approach retains both cost-effectiveness and operational reliability across a variety of environmental and financial inputs, consistently capping any unmet or dumped energy at fewer than 100 kWh per annum. By dynamically reallocating PV, battery, and hydrogen capacities in response to fluctuating costs and irradiance, the system achieves stable NPC within ±6% figures and

consistently low LCOE fluctuations limited to ±6.3%. Such resilience affirms the suitability of this framework for island microgrids and remote communities, where both economic conditions and solar resources can experience wide swings over the project's lifespan.

# 6.3 Design Decision Support Using EROI–NPC Trade-offs

As discussed in the preceding comparison section, the GA-MILP-MPC layout shows favourable performance relative to the recent peer-reviewed studies in terms of both NPC and LCOE. The ±10% sensitivity sweep (Table 6-2) demonstrated that these savings hold up even when there are reasonable changes in equipment cost, tariffs, and solar yield. The last step is to determine whether the design also overcomes a lifecycle-energy hurdle that is significant to planners who must justify projects on grounds other than cost alone, after economic superiority and parameter robustness have been established.

Figure 6-6 presents the new interactive NPC-vs-EROI dashboard at the calibrated optimum. Colour shades Net-Present-Cost, white contours trace *EROI* community, and dashed lines show unmet and excess energy. One glance tells decision-makers that the reference mix (PV = 152 kW, battery ≈ 365 kWh, tank = 7 kg) sits inside the darkest-purple cost basin (~€0.60 M), straddles the EROI = 4.8 iso-line, and keeps unmet load below the policy ceiling (< 0.1 MWh yr<sup>-1</sup>). Because the basin is broad and the EROI ridge is flat nearby, engineers can reassure councils that modest procurement slippage will not jeopardise either affordability or sustainability, an insight that static tables struggle to convey.

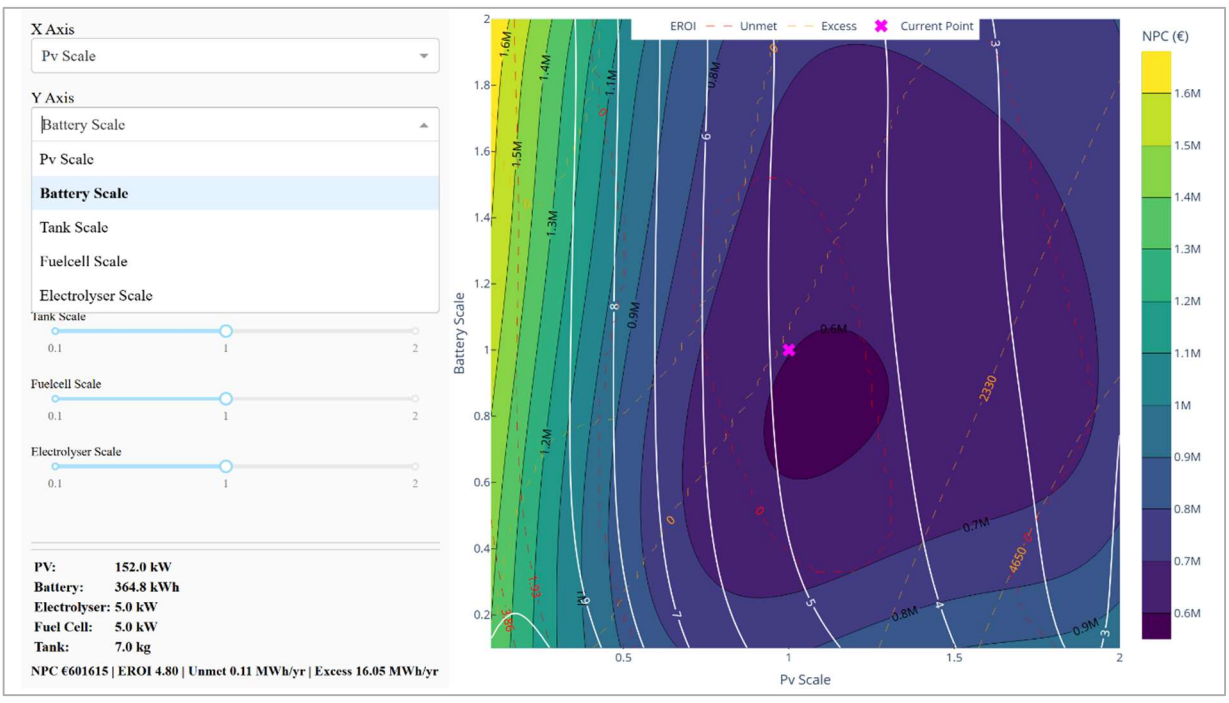


Figure 6-6: Interactive Cost–EROI dashboard. Baseline optimal mix with ability to compare different equipment sizes

Figure 6-7 illustrates how the same tool guides negotiations. Sliding the PV scale to 1.44 × (while leaving storage untouched) moves the magenta star onto a higher-PV/lower-battery lobe: NPC rises to ~€0.66 M and the EROI contour falls to 3.8. Unmet energy stays within

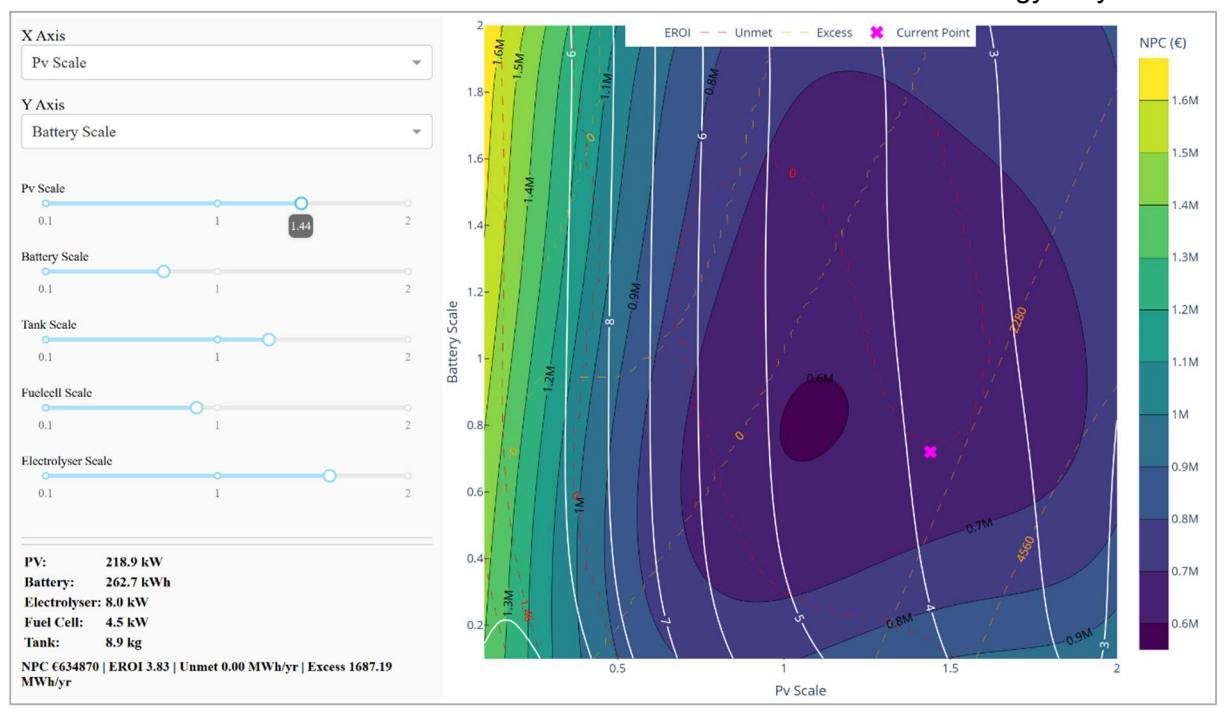


Figure 6-7: Interactive Cost-EROI dashboard, PV-heavy what-if scenario

limits, so the plant is still technically feasible, yet the EROI drop below the 4.0, threshold warns stakeholders that the extra PV has become energetically counter-productive. No fresh optimisation run is required; the dashboard translates the complex GA–MILP–MPC surrogate into an immediate visual trade-off. Planners can therefore explore budget caps, sustainability mandates or export-limit rules in real time, turning the holistic community EROI metric into a practical steering wheel rather than a static footnote.

# 6.4 Comparative Benchmarking with Literature

The following benchmark analysis compares the proposed GA–MILP–MPC optimisation framework against relevant peer-reviewed studies as summarised in Table 6-2. The comparative analysis explicitly addresses each method's key features, highlighting concrete numerical outcomes and methodological reasons behind their results, and systematically contrasts them against the specific findings of the novel proposed approach.

The discussion opens with [166], who couples a particle-swarm sizer to a 72-h rolling dispatcher that honours electrolyser and fuel-cell transients. Relative to HOMER's cycle-charging baseline, LCOE falls from 0.3976 to 0.3695 £/kWh (-7.1 %). Because inverter rating, maximum contracted power and load-shifting remain fixed inputs, the economic upside stops

at transient optimisation. By contrast, the GA–MILP–MPC platform co-optimises those three additional levers and achieves a 9 % NPC saving; about two percentage points come from right-sizing the inverter and cutting the contracted power limit, dimensions untouched in the researcher's formulation [166].

Moving from hydrogen-centric design to isolated rural microgrids, [167] applied PSO with ε-constraints in an islanded PV-diesel-battery hybrid system, delivering 0.37 \$/kWh versus HOMER's 0.40 \$/kWh (-7.5 % LCOE). Dispatch is a single deterministic year with static diesel price (0.26 \$/L) and no forecast layer, so diesel start—stop penalties or weather uncertainty are not explored. Although the study is off-grid, it highlights the value of capacity-mix optimisation; our GA–MILP–MPC addresses the complementary operational dimension in a grid-connected scenario, cutting annual grid charges 46 % (€29 625 to €15 886) against a load-following benchmark by anticipating low-tariff hours also reduction in LCOE of 10%. The results show that static sizing and static dispatch each leave sizeable savings untapped.

Study from [105] bring the conversation closer to this thesis novel framework by integrating GA-based battery sizing with an MPC dispatcher that runs once per day using a 72-h prediction window. Annualised NPC drops 19 % (1.08 to 0.87 M JPY) and operating cost alone plunges 44.4 % versus a day-ahead rule, principally by clipping evening peaks. Because the controller re-optimises only daily, it still cannot track intra-day tariff swings in real time. This thesis novel approach GA–MILP–MPC uses a 24-hour prediction horizon (shorter horizon assumption of 24h/12h) but executes only the first 12 hours of that plan before shifting the window forward by 12 hours and re-optimising. This twice-daily receding-horizon cycle, combined with a second storage vector (hydrogen), delivers a 46 % reduction in grid charges on the same load profile, slightly higher than the 44.4 % achieved by Tamashiro's once-daily (72 h/24 h) MPC [105].

From urban flexibility, we pivot to utility-scale design. The study from [98] introduced realistic grid tariffs and applied sensitivity in lowering the contracted power from 30, 24, and 18KW all by using deterministic MILP, resulting in an 18% NPC and 12% LCOE reduction. Despite these impressive results, their static approach lacked adaptability of the AC/DC conversion breakdown and omitted free optimisation of grids limits, and optimised the operation decision on the knowledge of 8760 full year data, over estimating the results [98]. This thesis nested optimisation approach explicitly uses a balanced realistic day ahead with intraday decision making (12h/24), dynamically balancing between battery and hydrogen storage systems without over inflating results. This method demonstrated substantial cost reductions (around 10% NPC) by optimally utilising hourly decisions, achieving peak shaving demand with inverter and contracted power optimised limits.

The study [43] also utilise MILP, but in a hybrid PV-battery-H<sub>2</sub> islanded microgrid. They apply a single-layer MILP with an internal TOU-based demand-response scheme to an off-grid PV-

battery-H<sub>2</sub> micro-grid, cutting LCOE 11 % relative to a GA + rule-based baseline; however, the optimisation still relies on a deterministic year-long horizon with perfect foresight, no rolling reoptimisation or multi-year uncertainty, so the resulting dispatch strategy may overestimate real-world savings [43]. This thesis GA–MILP–MPC approach explicitly considers detailed TOU tariff structures and predictive load management, dynamically adjusting operational strategies in response to daily and seasonal variations. This strategy directly reduces operational LCOE by approximately 10.3% compared to static dispatch methods, clearly improving overall economic outcomes and system reliability.

Expanding the source mix, this study in [168] implemented PSO optimisation in a complex PV-wind-biomass system, achieving substantial (24%) LCOE reductions compared to traditional rule-based methods. However, their method operated within HOMER's limited dispatch framework, neglecting inverter clipping, and grid-contracted power optimisation [168]. In contrast, our method explicitly integrates inverter clipping management, alongside dynamically optimised grid power constraints. This comprehensive optimisation significantly enhances economic performance, particularly through reduced storage replacement costs and optimal inverter sizing, achieving consistent and verifiable cost reductions of about 9–10% compared to HOMER-based approaches.

Researchers in [169] used NSGA-II for tariff-aware PV-BES sizing, realising a 12% annualised cost improvement. Nevertheless, their static dispatch methodology lacked dynamic optimisation and omitted hydrogen storage, thus restricting their achievable operational savings [169]. Our nested framework strategically incorporates hydrogen storage and predictive dispatch, significantly reducing grid dependency and achieving NPC of approximately 10%. This method explicitly optimises inverter sizing and grid interactions, consistently outperforming static dispatch approaches and enhancing overall system efficiency.

Table 6-2: Comparison of optimisation studies, showing grid/island context, cost reductions ( $\Delta$  NPC,  $\Delta$  LCOE) against each paper's benchmark, and which advanced features are implemented; shortcuts: GS = meta-heuristic sizing, DO = Dispatch Optimisation, RH = rolling-horizon/MPC, SH = static-hourly assumption, LS = load-shifting, CG = contracted-grid optimisation, IC = inverter-capacity optimisation, AD = detailed AC/DC buses, TO = time-of-use tariffs, PS = peak-shaving.

Ref	Study	Grid / Island	Method	Bench- mark	ΔNPC	Δ LCOE	G S	D O	R H	S H	L S	C G	I C	A D	T O	P S
[166]	Atteya & Ali 2024	Grid	Dynamic-component PSO sizes PV-H <sub>2</sub> ; 72 h rolling dispatch tracks FC/EL transients	HOMER	_	<b>-7</b> %	✓	Х	✓	Х	Х	Х	Χ	X	<b>√</b>	<b>√</b>
[167]	Fodhil et al. 2019	Island	PSO sizes PV-Diesel-Battery under ε-constraints; HOMER hourly simulation	HOMER	_	-8 %	✓	X	Х	✓	Х	X	Χ	X	Х	X
[105]	Tamashiro et al. 2023	Grid	GA sizing + 24 MPC dispatch for smart apartments over 72 horizons	Day- ahead rule	<b>–19</b> %	_	<b>√</b>	✓	✓	Х	✓	Х	Χ	X	X	<b>√</b>
[98]	Agha Kassab et al. 2024	Grid	MILP co-optimises PV-BES & contracted power with peak-shave penalty	Flat-rate tariff	<b>–18</b> %	<b>–12</b> %	X	✓	X	✓	X	<b>&gt;</b>	X	X	<b>✓</b>	<b>√</b>
[43]	Marocco et al. 2021	Island	MILP vs GA for PV-Battery-H <sub>2</sub> campus; flexible-load model	GA baseline	_	<b>–11</b> %	X	✓	X	✓	✓	X	<b>√</b>	X	X	X
[168]	Firdouse & Reddy 2023	Island	PSO vs GA for islanded PV-Wind-Biomass-BES	HOMER / GA	_	-24 %	<b>✓</b>	X	X	✓	X	X	Χ	X	X	X
[169]	Niveditha & Singaravel 2022	Grid	NSGA-II adds tariff-aware objective to PV-BES sizing	2-objec- tive GA	-12 % (ACS)	_	✓	X	X	✓	✓	Х	X	X	✓	X
[170]	Hossain et al. 2023	Grid	PSO retrofit PV-BES; cuts TOU bill & demand charge	Grid- only bill	_	_	<b>✓</b>	X	Х	✓	<b>√</b>	X	X	X	<b>✓</b>	<b>✓</b>
[171]	Kaewnukul- torn et al. 2024	Grid	MILP sizes PV-BES & tilt under TOU; US residence	Flat tariff	_	_	X	<b>√</b>	Х	<b>✓</b>	✓	Х	X	X	<	X
This v	vork (8% load shift)	Grid	GA with day-ahead MILP and 12 hours decision MPC; full AC/DC, TOU & peak-shave and load shifting	HOMER + GA	<b>–10</b> %	-10.3 %	<b>✓</b>	<b>√</b>	<b>✓</b>	<b>✓</b>	✓	<b>√</b>	✓	✓	<b>✓</b>	<b>✓</b>

Expanding on the previous study, [170] optimised a campus-scale PV-BES retrofit using heuristic PSO dispatch, achieving notable electricity bill reductions. However, their heuristic dispatch lacked formal optimisation, predictive capabilities, and inverter tuning, severely limiting potential saving opportunities. This thesis method of rolling MPC dispatch explicitly times renewable utilisation, manages storage strategically, and optimises inverter capacity dynamically, clearly reducing contracted grid demand and maximising renewable energy capture. This strategy directly reduces operational grid charges by approximately half (44.6%) annually compared to heuristic dispatch, providing demonstrable financial advantages.

Finally, [171] optimised residential-scale PV-BES systems under US TOU tariffs using MILP, effectively modelling inverter clipping and battery replacement. Their absence of dynamic dispatch strategies and hydrogen storage limited their operational flexibility and seasonal adaptability. In contrast, our GA–MILP–MPC framework explicitly integrates hydrogen storage and predictive dispatch, strategically balancing between short-term battery storage and long-term hydrogen buffering. This approach significantly improves economic and operational performance, reducing operational grid charges consistently by around 44.6%, particularly through better inverter sizing and seasonal hydrogen storage utilisation [171].

In summary, each of the reviewed studies either operated with static full-year horizons or limited predictive dispatch capabilities, implicitly assuming perfect foresight or simple heuristic logic. Our GA–MILP–MPC framework explicitly avoids these limitations by employing a rolling 24-hour horizon with a practical 12-hour execution window. This approach balances predictive accuracy with operational flexibility, achieving robust, verifiable NPC and LCOE reductions around 10%, explicitly through optimised inverter sizing, contracted power management, predictive load scheduling, and effective battery-hydrogen storage utilisation. This detailed analysis distinctly illustrates why this methodology consistently outperforms the reviewed optimisation strategies, presenting a replicable and economically robust pathway for hybrid renewable energy system design. To reinforce the comparative benchmarking in Section 6.4, the following three subsections (6.4.1 to 6.4.3) examine system sizing, operational dynamics, and storage integration in detail, positioning the proposed approach relative to established strategies in the literature

# 6.4.1 Sizing Ratios and Operational Load Matching

The four MPC designs that gradually shift 0% to 8% of the demand are contrasted with the benchmark Load-Following controller's sizing ratios in Figure 6-1. The figure captures on how far the MPC approach, can stretch an inverter's usefulness. The benchmark Load-Following design embraces a SIR of 1.03, a near-textbook 1:1 DC/AC match. While that seems prudent, it contradicts almost two decades of field evidence that high-insolation sites can safely push the ratio well above unity without damaging energy yield. A study quantified this ceiling in a

100 MW-AC Texas plant, showing that a DC/AC of approximately 2.0 maximised exported energy once a DC-side battery soaked up clipping losses [172]. Even more recent studies confirmed with a 5-kW bifacial test bed that bifacial PV coupled to lithium-ion storage moves the "sweet spot" from 1.2 (PV-only) to 1.4–1.6 under Arizona sunshine [171]. Large-sample monitoring of 93 U.S. residential arrays echoes that conclusion, annual yield gains flatten beyond ILR about 1.25, yet no performance penalty appears until around 1.4 [173]. Taken together, these studies bracket 1.6–2.0 as a realistic upper bound for stand-alone PV plants in bright climates. It is therefore encouraging that every MPC instance gravitates towards SIR approximately 2.0, filling the gap between conservative practice (1.0) and empirically proven limits (2.0).

The economic motive for that shift is equally strong. Researchers found that, under Ontario's three-tier TOU tariff, profit, not LCOE, peaks at an array-to-inverter ratio of 2.0 and remains flat out to about 2.4, after which clipping losses dominate [174]. Parallel modelling for the Iberian market shows that every 20 % fall in Li-ion capex or 5 % rise in round-trip efficiency roughly doubles arbitrage NPV, further nudging investors toward high DC/AC ratios [175]. By choosing SIR about 2 our MPC designs effectively tap the lowest-cost segment of the profit curve while keeping within the physical ceiling.

That same logic extends to storage. Authors define BIR as the ratio of battery power capacity to inverter capacity and then fix the battery's duration at 4 h, so a BIR of 1.0 corresponds to 4 h of discharge at full inverter power [176]. Researchers show that at this BIR = 1.0 level (i.e. 4 h), coupled PV and battery systems hit the breakeven point where both energy- and capacity-value benefits justify higher PV oversizing [176]. Yet, grid planners start to treat a hybrid plant as a reliable peak-shaving resource only once its storage can sustain approximately 3.3 hours at full power [177]. The Load-Following design, limited to 2.32 h, just clears the arbitrage threshold but falls short of the grid-service mark. In contrast, every MPC layout lifts BIR above 4.7 h, bridging that policy gap and aligning the system with the "moderate-duration" class now favoured in capacity-market qualification rules.

Work in [178] use rain-flow analysis to show that once a PV plant's DC/AC ratio exceeds around 1.4, the minimum battery capacity needed to guarantee a 10-year life rises superlinearly driven by the volume of clipped energy. In their 1 MW-AC case study the required BESS steps from a few-hundred kWh at DC/AC = 1.4 to over 500 kWh at DC/AC = 2.0, highlighting how aggressive PV oversizing rapidly balloons storage needs. Hydrogen shows a similar, but longer-tail, pattern. Increasing the TIR from 1.39 h in the baseline to 4.17 h in the MPC-8 % case may appear extravagant at first glance, yet without it the battery would be forced to time-shift seasonal surpluses, a task to which high-cycle lithium-ion packs are poorly

suited both energetically and economically which will be demonstrated later in this discussion. Notably, while there's a growing literature on optimal BIR for PV hybrids (e.g. [178], [176]), very few studies to date have simultaneously examined the analogous TIR for power-to-gas or hydrogen-augmented systems. Before we turn to our analysis of hydrogen storage sizing, it's worth highlighting this lack of dual-storage guidance in the published work. The progressive rise in both BIR and TIR from the 0% to the 8% scenario reflects the need for more overnight storage capacity to absorb shifted load and shave daytime peaks. Accordingly, the optimiser relies on a mix of short and long-duration assets to meet that load-shifting requirement.

The effect of inverter ratios is noticed in the overall yearly data simulated. Figure 6-2 provides more insight into the operational effects of the sizing ratios discussed earlier by displaying annual hourly PV generation next to the theoretical and actual outputs of the inverter under several energy management strategies for the three methods of Load Following, MPC 0%, and MPC 8%. The figure summarises hour-by-hour how each supervisory strategy converts raw PV production (yellow) into usable AC power (red), while concurrently managing the average State-of-Charge (SoC) of both battery (blue dashed bar) and hydrogen storage (green dashed bar).

In the Load-Following scenario the 120-kW inverter is oversized relative to the seasonal low in PV output; during winter mornings the plant idles near 20 % capacity, yet at noon in May and June the PV array repeatedly slams the inverter limit, hence the tell-tale horizontal plateaus in the red AC-output trace. In comparison to literature, researchers in [66] with 2.5 kW inverter 0.74 kWp site, observe essentially zero clipping at SIR = 1.0, but already by SIR = 1.2 the AC output flattens at mid-day, and clipping grows further at SIR = 1.3, underscoring how even modest PV oversizing rapidly induces energy losses without storage . Also, [179] site-specific study find clipped hours under 2 % at SIR  $\simeq$  1.4, rising more rapidly at higher SIR, suggesting that beyond SIR  $\simeq 1.6$  the risk of significant clipping grows in many locations [179]. Load following, since the battery's state of charge averages 46.4 %, neither full nor empty, there is little headroom to absorb those noon spikes, but still with less renewable penetration to avoid clipping. The first MPC variant (0 % load flexibility) downsizes the inverter to 77 kW but deliberately oversized both PV and battery. Two moves make this viable. First, the controller holds the battery mid-empty, around 33 % SoC, creating a 35 kWh "spare tank" that automatically catches mid-day clipping. Second, it allows PV to overbuild to drive SIR to 2.0: the array hits the 77 kW AC ceiling far more often, but now the excess is stored rather than curtailed. The net effect is identical annual AC yield with a 36 % smaller inverter. For rooftop projects without storage, a calibrated Malaysian study finds the LCOE minimum at SIR around 1.19, underscoring that modest inverter under sizing pays even before batteries enter the picture [66].

Adding 8 % load flexibility compounds that advantage. Because pool pumps, or similar non-essential demand can be shifted up to four hours without compromise, the MPC pushes 8 % of consumption towards daylight when available. PV utilisation rises, PV-to-battery charge rates smooth out, and inverter excursions become even flatter. Despite a further reduction in name-plate power to 72 kW, the system now records fewer clipped hours than the 120-kW baseline and boosts self-sufficiency from 71 % to 84 %. Hydrogen's role emerges in the background. In both MPC runs its average SoC doubles (around 50 %) relative to 23 % in Load-Following, a clear sign that surplus summer energy is being captured for winter release. By outsourcing seasonal balancing to H<sub>2</sub>, the battery stays in its low-cycle, high-efficiency comfort zone, and the inverter is spared the need to honour simultaneous high-power charge and discharge requests.

## 6.4.2 Grid Dependency and Storage Utilisation Trends

Figure 6-3 highlights significant differences between the Load Following controller and the MPC strategies (0% to 8% scenarios) regarding the Contracted Power Ratios for solar (SPR), battery (BPR), and hydrogen tank (TPR). In the Load-Following case, SPR is modest (1.59), closely aligning the PV size with the contracted grid power, which indicates minimal reliance on grid flexibility or storage-driven arbitrage. In all MPC scenarios, this ratio consistently climbs above 3.7, suggesting a sizing for higher renewable penetration and major storage dependence to balance and smooth solar variability and lower grid interaction. This trend is reinforced by empirical evidence from [180], whose grid-connected HRES case study illustrates the implications of fixed contracted power limits. Their system, sized with a 26 kW PV array and 100 kW wind capacity against a 110-kW grid cap, achieves a renewable-tocontracted power ratio of only around 1.15. Despite the installed capacity, roughly 90% of the system's total energy demand is still met by grid imports, and storage utilisation remains low. Critically, the grid cap in the studied EMS formulation is static, highlighting how pre-set grid constraints, if not dynamically optimised, can limit the effective use of renewables and storage. This underscores the importance of letting the optimisation framework treat contracted power as a tuneable parameter, responsive to techno-economic trade-offs rather than rigid planning assumptions [180].

The pattern continues with storage. There is also a more obvious increase in the Battery-to-Contracted Power Ratio (BPR), which climbs from 3.57 in the Load-Following scenario to as high as 10.38 in the MPC 8% scenario. This substantial rise underscores MPC's shift towards longer-duration storage and greater storage-driven grid services, enabling substantial peak shaving and significant grid power curtailment. Researchers in [181] support this interpretation in a Malaysian context, demonstrating how short term load control with BESS reduced peak demand charges by 8.4% daily, emphasizing the economic and operational benefits of

storage-enabled flexibility during high-demand periods. Furthermore, the Hydrogen Tank-to-Contracted Power Ratio (TPR), which rises from 2.14 to over 8.0 across the MPC scenarios, also implies a greater focus on seasonal energy shifting. The increase of self-consumption and aiding long-term grid balancing depend on hydrogen storage. Without much depending on grid exchanges, this high TPR lets MPC systems absorb excess solar energy during long periods of high solar irradiance and redistribute it during energy-deficit times. This aligns with [182], where static export constraints, such as capping grid export from PV output to 67% (or as low as 35% when paired with storage), can significantly enhance hosting capacity and promote decentralized energy balancing through self-consumption and local storage [182]. The work demonstrates that even within constrained export frameworks, storage-centric designs can support deeper renewable integration and operational resilience.

The structural shift is easiest to visualise in Figure 6-4, to analyse the grid dependency and contracted power optimal sizing, grid interaction for Load following and GA-MPC 8% is compared. The figure illustrates the detailed grid interaction profiles of the Load-Following and MPC 8% strategies as scattered plot. Load-Following maintains higher grid interaction limits (±78 kW), resulting in frequent, substantial energy exchanges, indicative of relatively limited reliance on internal storage capabilities. The percentage of hours without grid purchases (77.05%) is moderately high, however, the hours without any grid exchange (66.47%) remain lower, reflecting constant reliance on grid resources to manage the system's surplus and deficit conditions and this well observed in analysed metrics tables in Table 3-7 and Table 4-4.

Contrastingly, MPC 8% demonstrates a markedly improved operational profile despite its reduced contracted grid capacity (±37 kW). This scenario achieves superior self-sufficiency, with a remarkable 86.03% of hours free from grid imports, despite the lower grid limit. Although overall hours without grid exchange (58.78%) slightly decrease due to tighter constraints on export and import capacity, the scatter clearly shows strategic battery utilisation: when PV generation is low or zero, energy stored in batteries and hydrogen is actively dispatched back to the grid, creating a distinctive "negative" power pattern, meaning the storage systems actively support grid stability during demand peaks. This strategic dispatch of stored energy to the grid is notably absent in Load Following. Thus, MPC clearly achieves demand-peak shaving by strategically deploying storage assets, especially during periods of zero PV production, demonstrating advanced operational flexibility compared to the traditional Load Following approach.

## 6.4.3 Seasonal Energy Balancing and Storage Role Separation

Figure 6-5 translates the sizing logic into storage behaviour over an entire year. Under Load Following (subplot (a)) the battery acts as the primary buffer: its daily mean SoC tracks the solar cycle, climbing above 55 % in midsummer and falling below 35 % in winter, with a standard deviation of roughly 15 %. Over sixty summer days the battery exceeds 80 % SoC, crowding out additional PV harvest and explaining the inverter clipping seen earlier. Hydrogen remains largely dormant, its daily mean hovers around 23 %, hardly surpassing 40 %, so the system lacks any genuine seasonal reservoir. High-frequency cycling is therefore concentrated in the battery, limiting renewable utilisation.

This storage hierarchy is fundamentally restructured under the MPC 8% scenario. The controller pins the battery near one-third full throughout the year, cutting its daily variability to 9 % and eliminating episodes above 80 % SoC. Surplus spring and summer energy is channelled into hydrogen: the LoH monthly average rises steeply to 80–100 % between June and August, then is drawn down to support winter loads. Hydrogen's standard deviation a factor of four relative to the baseline, confirming its new role as the long-duration store, while the battery is relegated to short-term balancing. This division of labour maximises PV capture and allows the inverter to be downsized without loss of service.

These results echo and are reinforced by recent studies. Researchers in [183] demonstrate that in PV-battery-hydrogen hybrids, effective SoC management requires batteries to operate around mid-range levels to handle daily variability, while a minimum hydrogen reserve is necessary for seasonal smoothing. Failure to coordinate these roles leads to excessive battery cycling and curtailed energy. Further studies such as [184] shows that when optimally dispatched, batteries and hydrogen in hybrid systems self-organize into distinct timescale functions, batteries absorb intra-day volatility while hydrogen buffers seasonal mismatches, precisely the operational stratification observed under MPC-8%. The study from [185] confirm this behaviour quantitatively, finding that hybrid storage architectures outperform battery-only or hydrogen-only systems across both temperate and tropical climates. The separation of short- and long-duration functions not only boosts efficiency but also extends component lifespan and enhances renewable integration.

Having established the internal operational benefits of our MPC-enhanced strategy, including its ability to reshape inverter loading, smooth state-of-charge dynamics, and balance seasonal energy using dual-storage architecture, the discussion is being broadened to position these findings within the wider optimisation literature. The following comparative benchmark examines recent studies to assess how their methods and assumptions stack up against our framework, particularly in terms of realism, cost-effectiveness, and replicability.

## 6.5 Summary

The discussion now concludes by connecting deeper insights from the main optimisation chapters (3 and 4) into a coherent Better-Robust-Sustainable arc. Firstly, Chapter 6 validated that the GA-MILP-MPC hybrid design achieves superior performance, surpassing benchmarked state-of-the-art studies on both NPC and LCOE. Secondly, a ±10% parameter sensitivity analysis confirmed these economic advantages hold firm under realistic market and climate variability, reinforcing the robustness of the framework. Lastly, by integrating Net-Present-Cost, unmet-energy constraints, and the novel community EROI sustainability metric into a dynamic, slider-driven dashboard, the thesis introduced a holistic decision-making tool. Planners can immediately visualise the impact of capacity adjustments, observing how shifts affect both cost and lifecycle energy payback, and swiftly verifying if designs surpass the crucial two-year net-energy threshold (EROI ≥ 4). The calibrated baseline system comfortably resides within the optimal €0.60 M cost and EROI 4.8 zone, whereas increasing PV sizing by 1.44× noticeably elevates costs and reduces EROI, offering a visual caution against imbalanced sizing. Consequently, this thesis not only delivers a superior and resilient optimisation strategy but also provides a practical, transparent, and intuitive interface, empowering energy communities to confidently transform complex technical analyses into clear investment decisions.

## 7 Conclusion

This thesis improves the capacity planning of hybrid renewable energy systems by means of a proposed and profoundly integrated optimisation framework combining long-term planning with short-term operational realism. The framework tackles three general objectives by means of a combination of Genetic Algorithms (GA), Mixed Integer Linear Programming (MILP), and Model Predictive Control (MPC): minimising lifecycle cost, enhancing renewable energy autonomy still linked to the grid in community configuration, and improving energy return efficiency through improved performance indices. The first major contribution is the development of a nested GA–MILP model for the year-long sizing and dispatch of PV–battery–hydrogen microgrids. This deterministic approach co-optimises component capacities and hourly dispatch strategies using a full-year dataset of load, irradiance, and tariff signals. It outperforms established methods such as HOMER Pro and reactive rule-based systems, achieving verifiable reductions in Net Present Cost (NPC) of 5.9% and Levelised Cost of Energy (LCOE) of approximately 6.2%. These improvements result not only from better sizing of PV and storage, but also from the novel AC/DC nodal representation, co-optimisation of inverter limits and contracted grid capacity, dimensions often overlooked in prior studies.

However, this full-year optimisation assumes perfect foresight and fixed performance metrics, which can result in overly optimistic cost predictions and underrepresentation of operational flexibility. To bridge this gap, Chapter 4 introduces a rolling-horizon MPC module that executes every 12 hours using a 24-hour forecast. By embedding this MPC engine within the larger GA–MILP structure, the system gains predictive adaptability to dynamic conditions. Additionally, the inclusion of flexible load scheduling, ranging from 0% to 8%, enables fine-tuned demand shaping in response to variable solar supply and tariff cycles. This more granular control results in significant operational advantages: total annual grid charges decline from €29,625 under load-following operation to just €15,886 at 8% flexibility (reduction of 46%), while self-consumption increases to 44.56%. Moreover, the MPC 8 % scenario delivers approximately a 10 % reduction in NPC and a 10.3 % reduction in LCOE compared to the load-following benchmark. These gains demonstrate the economic and technical value of embedding short-term foresight and demand flexibility into hybrid energy systems.

The third key innovation lies in the introduction of an extended Energy Return on Investment (EROI) and Energy Stored on Invested (ESOI) metric suite, designed specifically for community-scale hybrid systems. Unlike traditional EROI calculations, which typically only account for primary energy generation and a single storage loop, this extended framework captures all major energy pathways, including curtailment losses, battery and hydrogen flows, and grid exports, and compares them against embodied energy in PV modules, batteries, fuel cells, and hydrogen tanks. Through detailed parametric analysis, the results reveal that battery efficiency improvements have the most significant impact on system-wide energy returns. Raising battery round-trip efficiency from 70% to 95% increases extended EROI from 4.4 to 4.9, while improving electrolyser–fuel cell efficiency from 15% to 40% yields only marginal gains due to hydrogen's relatively small energy throughput. These findings underscore the necessity of prioritising battery performance and sizing in systems where daily balancing dominates over seasonal shifting.

In addition to parametric evaluations of the novel EROI community, the thesis introduces a generalised framework for exploring how system performance evolves under capacity variation, using polynomial-regression-based surrogate models to generate smooth heatmaps across scaled configurations. These heatmaps, constructed for Net Present Cost (NPC), EROI, unmet load, and excess energy, offer community planners an intuitive, visually rich decision-support tool. The analysis identifies clear "sweet spot" ranges—typically at 1.0–1.1 times the baseline capacities—where both cost and lifecycle energy efficiency are jointly optimised. Specifically, these zones yield EROI values near 5.0 while holding NPC below €610,000 and excess generation under control. More extreme scaling, particularly oversizing PV beyond 1.8×, increases curtailment and reduces EROI despite marginal cost gains, while

downsizing elevates energy return but at the cost of affordability and unmet demand. This dual-parameter sensitivity, visually conveyed via NPC–EROI contour plots, provides a practical, evidence-driven pathway for right-sizing infrastructure, and highlights the intricate trade-offs between economic feasibility and environmental sustainability.

Across these dimensions, long-horizon planning, short-horizon re-optimisation, and life-cycle sustainability, the thesis proposes a new design logic for hybrid energy systems. It shows that performance should not be judged purely on static costs or capacity metrics, but on dynamic control responsiveness and presented later with energy circularity edge. This is made possible by the modular nesting of GA for layout optimisation, MILP for high-resolution dispatch feasibility, and MPC responsiveness approach. Each layer feeds into the next, forming a continuous feedback loop that mirrors how real systems must operate: planning ahead, reacting quickly, and balancing costs with resilience. The short-horizon MPC particularly addresses a central challenge in real-world deployments, how to handle weather variability, shifting demand, and changing market tariffs without incurring excess cost or grid dependency. The flexibility offered by even modest demand shifting (e.g., 8%) yields material financial benefits, with annual grid-related charges significantly reduced compared to load-following baselines. This responsiveness, embedded in the MPC logic, bridges the planning-execution gap and enables systems that are economically efficient and operationally viable.

In addition to economic metrics, the extended EROI and ESOI indices offer meaningful energy benchmarks for sustainable system design. Unlike pure cost metrics, these indicators reflect embedded environmental impact of system components. The life-cycle analysis reveals clear patterns: hydrogen remains a niche but necessary long-duration storage option, with limited EROI impact unless its share of energy throughput is significantly increased. Batteries, in contrast, serve as the dominant modulator of energy returns, and their embodied energy and efficiency should be carefully managed to maintain overall system sustainability. These insights help shift the conversation from purely financial design toward multi-dimensional optimisation, where economic, operational, and environmental performance are considered in the planning.

From a practical standpoint, the thesis delivers clear implications for community energy planners, especially in islanded or weak-grid settings. The MPC-based framework offers a model that can be adapted to simulate real community conditions, including time-varying loads, tariff structures, and weather patterns. The optimisation of contracted grid power, typically a static assumption in most studies, is shown to be a powerful lever for cost savings. By tuning the contracted limit in tandem with inverter and storage sizes, the framework avoids over-design while still ensuring adequate supply security and peak demand management. This

dimension of the optimisation aligns with regulatory trends in many regions where demand charges or power-based tariffs are becoming more prevalent. The insights gained from this thesis can directly inform tariff policy, incentive design, and capacity market participation strategies for distributed energy providers.

Despite the comprehensive design proposed in the work, several limitations are acknowledged. The assumption of perfect short-horizon forecasts in the MPC layer does not reflect the stochastic nature of real-time solar and load data. Future iterations should incorporate probabilistic forecasts or robust optimisation techniques to quantify and mitigate uncertainty. Equipment replacements are considered depending on hourly operational limits, but degradation and system failure modes are also not modelled; incorporating battery ageing, and inverter reliability would provide a fuller picture of lifecycle performance. Additionally, thermal energy demand and sector coupling are not represented in this study, which limits its immediate application to systems with significant heating or cooling loads. Integrating cogeneration, heat pumps, or demand-side thermal storage could broaden the model's scope. Social and behavioural factors are also outside the current modelling framework. Future work could include surveys or behavioural models to better understand user responses to flexible load incentives or energy storage deployment. While the model outputs optimised schedules, it remains silent on whether households or facility operators would accept such schedules in practice, especially if they affect comfort, convenience, or economic risk. Addressing this would add important realism to the model's predictions.

# 8 Future Work and Research Directions Work

The methodological and modelling novelty presented in this thesis offer a strong foundation for future research and application. Several extensions are envisioned to enhance the technical robustness, real-world applicability, and policy relevance of the proposed GA–MILP–MPC framework.

#### **Technical and Control Enhancements**

- Forecasting and Uncertainty Integration: Incorporating demand and generation forecasting models that explicitly simulate forecast error, particularly as a function of horizon length, can strengthen the robustness of the dispatch strategy into sizing and planning context.
- Linearised Degradation Models: Current models assume fixed component lifespans.
   Including degradation-dependent performance loss (e.g., battery fade, fuel cell efficiency drops) would improve sizing realism and replacement strategies with balance inclusion into the objective function.

## **Environmental and Policy Coupling**

 Translating EROI to Environmental Indicators: Mapping embodied energy (from the EROI formulation) into CO<sub>2</sub>-equivalent emissions enables dual evaluation of energy efficiency and carbon mitigation.

#### **Generalisation and Real-World Validation**

 Multi-Year, Multi-Region Simulation: Extending the analysis across multiple years and climatic zones would increase model generalisability and policy relevance.

#### **Community-Level Modelling and Sectoral Integration**

- Stakeholder Granularity and Revenue Modelling: Introducing individual agents (households, SMEs) with varied loads, ownership, and investment logic enables modelling of energy sharing, peer trading, and new revenue streams.
- Hybrid Configuration and Sector Coupling: Expanding to wind, EVs, heating/cooling, or water sectors supports cross-sector planning and decarbonisation in rural or isolated communities.

# 9 Appendices

### 9.1 Literature Table Nomenclature

 $P_{RES}(t)$ : Renewable generation (e.g., PV, wind) at time t

 $P_{\mathrm{BT,dc}}(t)$ : Battery discharge to DC bus at time t

 $P_{\rm FC}(t)$ : Fuel cell electrical output at time t

 $P_{\rm NS}(t)$ : Net supply to system at time t

 $P_{\mathrm{LD}}(t)$ : Load demand at time t

 $P_{\rm BT,ch}(t)$ : Battery charging power at time t

 $P_{\mathrm{BL}}(t)$ : Electrolyser electrical consumption at time t

 $P_{\rm CT}(t)$ : Curtailment losses at time t

 $P_{PV}(t)$ : PV array electrical production at time t

 $P_{\rm WT}(t)$ : Wind turbine electrical production at time t

 $P_{o, \text{ bat }}(t), P_{i, \text{ bat }}(t)$ : Battery output/input power

 $P_{o,H}(t)$ ,  $P_{i,H}(t)$ : Hydrogen system output/input power

 $P_{\text{inv}}(t)$ : Inverter output power at time t

 $E_{\text{dis}}(t)$ : Dispatchable energy losses at time t

 $U_{i,i,t}$ : Grid imports for energy carrier j by device i at time t

 $P_{j,i,t}$ : On-site generation or storage discharge for carrier j

 $V_{i,i,t}$ : Grid exports for energy carrier j

 $F_{i,i,t}$ : Fuel input to device i for carrier j

 $L_{j,t}$ : Demand for energy carrier j at time t

 $y_i$ : Binary: 1 if PV option i is selected, 0 otherwise

 $A_i$ : Area of PV option i

GHI<sub>h</sub>: Global horizontal irradiance in year h

 $P_{i,n}^{FG}$ : Power from PV *i* to Grid (DC before inversion)

 $P_{i,n}^{PL}$ : Power from PV *i* to Load (DC before inversion)

 $P_{ij,p}^{PB}$ : Power from PV i to Battery j (DC)

 $P_p$ : Total load demand at time p (AC)

 $P_n^{GL}$ : Power from Grid to Load at p (AC)

 $h_{\text{PV inv}}$ : Inverter efficiency (PV/DC  $\rightarrow$  AC)

 $P_{i,p}^{BL}$ : Power from Battery j to Load at p (AC)

 $P_{GT}$ : Total power from dispatchable gas turbines (including the spare)

 $P_{PV}$ : photovoltaic generation

 $P_{B,\,\mathrm{dis}}$  ,  $P_{B,\,\mathrm{ch}}$  : battery discharge and charge

 $P_{\rm curt}$ : curtailed renewable energy

 $P_{\text{load}}$ : electrical demand

*I*: Number of PV sizing options

J: Number of battery sizing options

 $p_{\text{bus}}(t_i)$ : Net DC bus balance at time step  $t_i$ 

 $p_{DL}(t_i)$ : Load demand at time step  $t_i$ 

 $\gamma_{coPPV}$ ,  $\gamma_{co}$  b,  $\gamma_{cog}$ : Inverter efficiencies (PV, battery, grid)

 $\mu_c, \mu_d$ : Battery charge/discharge efficiencies

 $p_{cb}(t_i)$ ,  $p_{db}(t_i)$ : Battery charging/discharging power at t

 $p_{qs}(t_i)$ ,  $p_{qin}(t_i)$ : Grid export/import power"

 $E_i(t)$ : Stored energy in storage unit i (LiB or  $H_2$  tank) at t

 $P_{qd}(t)$ ,  $P_{qd, exp}(t)$ : Grid import/export power

 $P_{\rm nv}(t)$ ,  $P_{\rm wt}(t)$ : PV and wind generation in Diabate et al.

 $P_{\mathrm{bat}}^{\mathrm{char}}\left(t\right)$ ,  $P_{\mathrm{bat}}^{\mathrm{disch}}\left(t\right)$ : Battery charge/discharge powers

 $P_{\rm el}(t)$ : Electrolyser power consumption

 $P_{fc}(t)$ : Fuel cell power generation

 $P_{\rm BS,dc}(t)$ ,  $P_{\rm BS,ch}(t)$ : Battery discharge/charge to/from DC bus

 $P_{PV.BS}(t)$ : PV export to battery subsystem

 $P_{\mathrm{GR,buy}}(t)$ ,  $P_{\mathrm{GR,\,sell}}\left(t\right)$  : Grid buy/sell powers (AC side)

 $P_{\mathsf{EL,in}}\left(t\right)$ ,  $P_{\mathsf{EL\,,out}}\left(t\right)$  : Electrolyser input/output powers

 $P_{\mathrm{HS,dc}}(t)$ ,  $P_{\mathrm{HS,ch}}(t)$ :  $\mathrm{H_2}$  storage discharge/charge power

 $P_{\mathsf{LD},\mathsf{H}}\left(t
ight)$  : Hydrogen load demand

## 9.2 Algorithmic Setup and Implementation (Python)

## 9.2.1 Genetic Algorithm (GA) Implementation (DEAP)

A Genetic Algorithm (GA) is a metaheuristic search algorithm that mimics the process of natural selection, a fundamental concept of biological evolution. Genetic Algorithm, which are part of the Evolutionary Algorithms (EA), are population-based solution that evolve through generation toward an optimal global solution avoiding local minima. They are often favoured above single-based solution metaheuristic algorithms, such as simulated Annealing (SA). Population based-solution metaheuristics are used widely to solve real-life sophisticated problems from fields such as engineering and energy system optimisation [186].

When the optimisation problem comprises many variables with complicated interdependencies, which makes conventional techniques like gradient-based approaches less effective, GA is particularly useful. In this work, distributed evolutionary algorithm in Python DEAP module is deployed to build the GA for hybrid energy system optimisation [187]. DEAP is an open-source, adaptable framework that helps to create evolutionary algorithms and lets us modify the GA implementation to fit the needs of the nested layered optimisation method. While the modular architecture of the library provides the flexibility needed for developing hybrid energy systems, DEAP helps effective management of large search areas and decision factors related with system size.

The upcoming sections cover the theoretical part of GA and bridge the use of the DEAP library in formulating the GA components, including chromosome representation, fitness function, selection criteria, crossover, and mutation probabilities. These sections are designed to fit these parameters within the broader context of the nested optimisation framework proposed in this chapter, where the GA performs the global optimisation search for system capacity sizing, and MILP handles the local operation dispatch optimisation. Each fundamental feature of GA as used in this work will be discussed in the following subsections, showing how the DEAP library was used to provide a customised optimising environment.

#### 1- Chromosome Representation

In GA, Potential solutions are expressed as chromosomes, basically vectors encoding choice variables. Every gene found in a chromosome function as a decision variable influencing the general performance of the system. In the framework of energy system optimisation, for instance, the chromosome encodes factors including the rated power of renewable energy components of hybrid systems as was formulated before:

Photovoltaic (PV) capacity (kW)

- Battery storage size (number of battery modules)
- Inverter capacity (kW)
- Grid-contracted power (kW)
- Fuel cell size (kW)
- Electrolyser size (kW)
- Hydrogen tank size (kg)

Candidate information is stored explicitly as a 7-gene real-valued vector  $C_r = [P_{PV}, N_{bt}, P_{inv}, P_{gr}, P_{fc}, P_{el}, P_{HT}]$  with admissible bounds. Tournament selection (k=3) copies short, well-performing "building blocks" into the next generation; blend crossover preserves parental mid-points while exploring a  $\pm 50\%$  envelope around them, which is well-suited to continuous capacities; Gaussian mutation (  $\mu=0,\sigma=1$ , indpb = 0.2) injects small, independent perturbations to prevent premature convergence. In combination, these operators retain useful substructures (e.g., PV-inverter-grid ratios that the MILP evaluates favorably) and diffuse them across the population, so dispatch-feasible, low-NPC patterns become more frequent generation by generation.

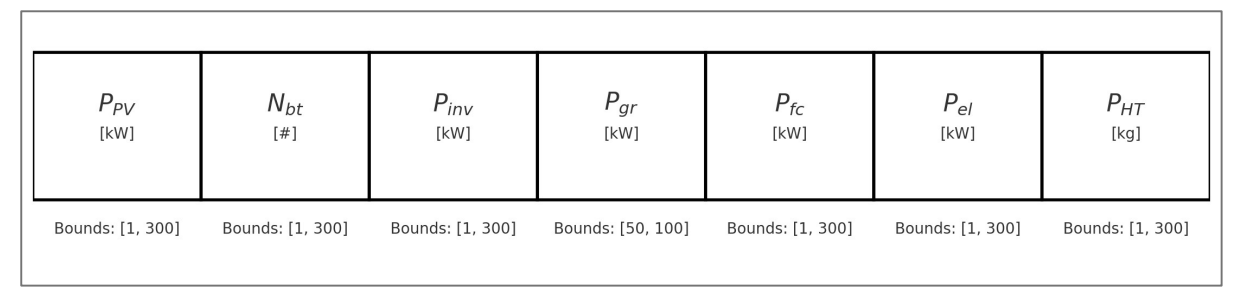


Figure 9-1: Chromosome layout for capacity sizing showing the decision variables: PV capacity, number of battery units, inverter rating, contracted grid limit, fuel cell power, electrolyser power, and hydrogen tank capacity. The bounds of each variable are indicated below the corresponding gene.

In the DEAP framework, these decision variables are expressed as toolbox attributes registered in the toolkit. Figure 9-2 shows the code snippet used in DEAP syntax illustrating initialisation of these variables:

Figure 9-2: DEAP initialisation of decision variables

#### 2- Population Size

A GA begins with an initial population of randomly produced chromosomes, each is a possible solution. The size of this population may affect the search space exploration; a larger population result in a more varied collection of starting solutions. The population changes over many generations while the method aims to improve the fitness of the solutions. Practically, the initial population's decision variables are produced within established upper and lower boundaries, thereby guaranteeing that all solutions are physically practical in the framework of system restrictions, such as the maximum allowed PV capacity or storage sizes. In this study, the population size is set in DEAP as follows in Figure 9-3.

```
# Create the initial population
population = toolbox.population(n=POPULATION_SIZE)
```

Figure 9-3: Population size setup in DEAP framework

#### 3- Fitness Function

In a GA, the fitness function is essential as it assesses every chromosome and decides the optimum or "fit" nature of a solution. For energy system as it was reviewed in previous chapters before, there are different fitness functions that are indeed attracted the researcher community as well the industry. The main indices can be economical, environmental, reliability and social. This work aims to minimise the Net Present Cost (NPC) of the hybrid energy system by means of fitness function. This feature guarantees that, in spite of all technological restrictions, the optimisation process favours configurations that reduce total lifetime costs. In DEAP, this is implemented as follows in Figure 9-4.

```
def evaluate(individual):
    PV_size, Battery_size, Inverter_capacity, Grid_power, Fuel_cell,
Electrolyser, Tank_size = individual
    .
    .
    # Calculate NPC based on full fitness function
    .
    .
    return (NPC,)
```

Figure 9-4: DEAP setup for the NPC fitness function

#### 4- Selection

GAs run by choosing the best chromosomes for reproduction in next generations. Higher-fitness solutions are ranked using selection techniques such as tournament selection, therefore preserving variation. This technique allows well-performing solutions to contribute more genetic material to the next generation, essentially simulating survival of the fittest. For the DEAP setup, the tournament method was implemented and the selected numbers of individuals are 3 as balanced choice as described by [188]. The code snippet in Figure 9-5 shows the tournament method selected for DEAP configuration.

```
# Select method and tournament size
toolbox.register("select", tools.selTournament, tournsize=3)
```

Figure 9-5: Tournament setup for the DEAP library

#### 5- Crossover

The process by which two parent chromosomes are mixed to generate offspring is known as recombination or crossover. Through mixing traits from both parents, this process brings fresh solutions into the population. Blend crossover lets parents smoothly exchange genetic material, therefore enabling the GA to investigate other areas of the solution space. Blend Crossover (cxBlend) is well suitable in continuous-variable situations like the one in your optimisation framework, in which the decision variables such as PV size, inverter capacity are continuous rather than discrete. The final optimisation results are then rounded up to the nearest real-life capacity for realistic impact, allowing the algorithm to sieve smoothly the search space. The range that the offspring are from the parents are within 50%, this is achieved by setting up alpha to 0.5, defining how far the offspring can differ from the parents. This lets the algorithm to explore the search space in balance.

Furthermore, guiding the frequency of crossover in the algorithm is crossover probability (CXPB). For example, if a balanced value of CXPB=0.6, 60% of the time two parents from the population would crossover to generate offspring; 40% of the time the offspring will be mere copies of the parents. This preserves diversity in the population and yet lets new solutions emerge, as shown in Figure 9-6.

```
# Crossover method: Blend crossover for continuous variables
toolbox.register("mate", tools.cxBlend, alpha=0.5)

# Crossover Probability: 60% chance that crossover is applied to parents
CXPB = 0.6
```

Figure 9-6: Crossover method selection and setup range of offsprings

#### 6- Mutation

Mutation guarantees genetic variation by introducing random changes to just a small portion of an individual's genes, therefore preventing the algorithm from settling too rapidly on a suboptimal answer. The mutation in DEAP is carried out utilising the Gaussian distribution depicted in Figure 9-7.

```
# Mutation method: Gaussian mutation for continuous variables
toolbox.register("mutate", tools.mutGaussian, mu=0, sigma=1, indpb=0.2)
# Mutation Probability: 10% chance that mutation is applied
MUTPB = 0.1
```

Figure 9-7: Mutation method selection and setup on DEAP

mu=0 in the figure guarantees the mutation generates only minor changes by cantering the mutation around the present gene value. Using sigma=1 preserves variability by controlling the distribution of these changes. Indpb=0.2 guarantees that, in every person, 20% of the genes are modified, thereby balancing exploration of the search space without excess randomisation. This configuration promotes a broad search, therefore preventing early convergence and preserving significant exploration.

Furthermore, regulating the possibility that every individual will undergo mutation after crossover is mutation probability (MUTPB). Ten percent of the population are exposed to mutation with MUTPB=0.1, enabling fresh variants to arise in the population and hence avoiding the algorithm from being caught in local optima.

In the next, section, the MILP implementation using pulp python library and the final integration between the two algorithms will be discussed and the operational reliability indicators that are passed from the Unit commitment are utilised by the GA penalty function to guide the optimiser.

### 9.2.2 MILP Implementation (PULP)

In this section, PuLP library and the Gurobi solver implementation in python environment is explained. This arrangement aims to minimise grid operating expenses over an annual horizon of 8760 hours by effectively solving the unit commitment problem. Key libraries listed below help to build up the Python environment:

- PULP: Designed for both mixed-integer linear programming (MILP) and linear programming (LP)
- Gurobi: Designed to tackle the formulated MILP problem, gurobi is a high-performance solver that is used for both, industrial and academic works.

The execution and implementation consist of the following key steps:

1. **Model Definition:** Pulp's LpProblem class is used to construct the MILP problem, with a minimisation aim described here. Minimising the overall operating cost, which includes grid energy buying expenses, income from grid sales, and penalties that range for both unmet and surplus energy, is the target function as shown in Figure 9-8.

```
# Initialise the optimisation problem
prob = LpProblem("Minimise_Operating_Costs", LpMinimize)
```

Figure 9-8: Pulp initialisation of the problem

2. Decision Variables: The MILP formulated problem consist of two distinguished decision variables of continuous and binary variables. Where the binary decision variables act as a switch which as if real life energy management system to decide which asset to respond to the load or which asset sells/charge for this problem the core is whether its grid, battery storage or hydrogen storage. On the other hand, the continuous variables are deemed to decide how much of energy should be exchanged at each time step. Table 9-1 shows the type of decision variables formulated and the way it was implemented in python environment using PULP library syntax.

Table 9-1: Type of variables and with pulp syntax example

Variable Type	Variable Name	PuLP Syntax Example				
Binary Variables	battery_decision(t)	<pre>battery_decision = {t:</pre>				
	grid_interaction(t)	<pre>LpVariable(f"battery_decision_{t}",</pre>				
	Hydrogen_decision(t)	<pre>cat='Binary') for t in T}</pre>				
Continuous	battery_charge_power(t)					
Variables	battery_discharge_power(t)					
	SoC(t)					
	grid_buy(t)					
	grid_sell(t)					
	unmet_energy(t)	<pre>battery_charge_power = {t:</pre>				
	excess_energy(t)	<pre>LpVariable(f"battery_charge_power_{t}"</pre>				
	PV_self_consumed(t)	<pre>0, P_b_minus_max) for t in T}</pre>				
	PV_power_remain(t)					
	Electrolyser_power(t)					
	Fuelcell_power(t)					
	SoC_H(t)					

3. Objective function: The objective function minimises the operational grid costs over the entire year horizon by summing up the hourly purchasing from grid and subtracting the hourly revenues from energy exports. To encourage the system to decrease wastage and excess for optimal operational decisions, penalties are applied. Figure below shows the way how the objective function was initialised in PULP syntax in python environment as shown in Figure 9-9.

```
# Initialise the problem objective
prob += lpSum([(grid_buy[t] * pi_grid_minus[t] - grid_sell[t] *
pi_grid_plus[t] + unmet_energy[t] * penalty_unmet + excess_energy[t] *
penalty_excess) for t in T])
```

Figure 9-9: Objective problem method of implementation

4. Constraints: A set of constraints guarantees that the system meets energy demand at every time step and runs within its physical limitations. The PULP library in the Python environment implements these constraints by appending "+=" to the problem formulation. The full constraints list was discussed before, but here in Figure 9-10 is the implementation example of how this was passed through Python environment as a method.

```
# grid constraint example:
prob += grid_buy[t] <= P_grid_max * grid_interaction[t]
prob += grid_sell[t] <= P_grid_max * (1 - grid_interaction[t])</pre>
```

Figure 9-10: Grid Constraint method of application

5. Solver Configuration: One of the reasons why PULP was selected in this study, because of its adaptability in solving mixed-integer linear programming (MILP) and linear programming (LP). PuLP's main benefit is that it provides an interface for a great range of solvers such commercial (Gurobi and CPLEX) and open source (CBC default for PULP) alike. This lets academics move between many solvers without changing the underlying optimisation approach. In the nested optimisation approach, this adaptability is very essential as it allows the comparison of many solver performance criteria (e.g., speed, optimality gap, and feasibility) without vendor lock-in.

#### 9.2.3 MILP Decision Variables

Variable Type	Variable Name	Description	PuLP Syntax
Binary			
Variables			
variables	battery decision(t)	Controls whether the battery is charging	battery decision = {t: LpVariable(f"battery deci-
	battery_decision(t)	(0) or discharging (1) at time ttt.	sion_{t}", cat='Binary') for t in T}
	i-l :t(4)		
	grid_interaction(t)	Controls whether energy is being bought	grid_interaction = {t: LpVariable(f"grid_interaction_{t}",
		(1) or sold (0) from the grid at time ttt.	cat='Binary') for t in T}
	Hydrogen_decision(t)	Controls whether the electrolyzer is	Hydrogen_decision = {t: LpVariable(f"Hydrogen_deci-
		charging hydrogen (0) or the fuel cell is	sion_{t}", cat='Binary') for t in T}
		discharging hydrogen (1).	
Continu-			
ous Varia-			
bles			
	bat-	Power charged into the battery at time ttt	battery_charge_power = {t: LpVariable(f"bat-
	tery_charge_power(t)	(in kW).	tery_charge_power_{t}", 0, P_b_minus_max) for t in
			T}
	battery_dis-	Power discharged from the battery at time	battery_discharge_power = {t: LpVariable(f"bat-
	charge_power(t)	ttt (in kW).	tery_discharge_power_{t}", 0, P_b_plus_max) for t in
			T}
	SoC(t)	State of charge of the battery at time ttt	SoC = {t: LpVariable(f"SoC {t}", SoC min, SoC max)
	.,	(as a percentage).	for t in T}
	grid buy(t)	Power bought from the grid at time ttt (in	grid_buy = {t: LpVariable(f"grid_buy_{t}", 0,
	9~ / (.)	kW).	P grid max) for t in T}
	grid sell(t)	Power sold to the grid at time ttt (in kW).	grid sell = {t: LpVariable(f"grid sell {t}", 0,
	3.14_3011(t)	i one cold to the grid at time th (iii kw).	P grid max) for t in T}
	upmot operav(t)	Unmet energy demand at time ttt (in kW).	unmet energy = {t: LpVariable(f"unmet energy {t}",
	unmet_energy(t)	Onniet energy demand at time tit (in kw).	= 0, , , , = 0,=,,
	40		0, None) for t in T}
	excess_energy(t)	Excess energy at time ttt (in kW).	excess_energy = {t: LpVariable(f"excess_energy_{t}",
			0, None) for t in T}
	PV_self_consumed(t)	PV power self-consumed at time ttt (in	PV_self_consumed = {t: LpVariable(f"PV_self_con-
		kW).	sumed_{t}", 0, PV_power[t], cat='Continuous') for t in
			T}

PV_power_remain(t)	Remaining PV power after self-consump-	PV_power_remain = {t: LpVariable(f"PV_power_re-
	tion at time ttt (in kW).	main_{t}", 0, None, cat='Continuous') for t in T}
Electrolyser_power(t)	Power consumed by the electrolyzer at	Electrolyser_power = {t: LpVariable(f"Electro-
	time ttt (in kW).	lyser_power_{t}", 0, P_el_minus_max) for t in T}
Fuelcell_power(t)	Power produced by the fuel cell at time ttt	Fuelcell_power = {t: LpVariable(f"Fuelcell_power_{t}",
	(in kW).	0, P_fc_plus_max) for t in T}
SoC_H(t)	State of charge of the hydrogen tank at	SoC_H = {t: LpVariable(f"SoC_H_{t}",
	time ttt (as a percentage).	SoC_hydorgen_min, SoC_hydorgen_max) for t in T}

## 9.3 Rule-Based Load Following

The load-following energy management technique processes from 1 to 3 shown in Figure 9-11, starts with initialising necessary system inputs that provide the basis for further computations. These inputs include hourly electricity demand, accessible renewable resources, and thorough technical and financial specifications for every system component. This starting point, which corresponds to Process 1, helps the model to dynamically react to changes in supply and demand, therefore guaranteeing a balanced approach to energy allocation that reduces grid reliance and manages renewable energy surpluses and shortages properly.

In Process 2, the model compiles three key datasets: technical and financial data for every

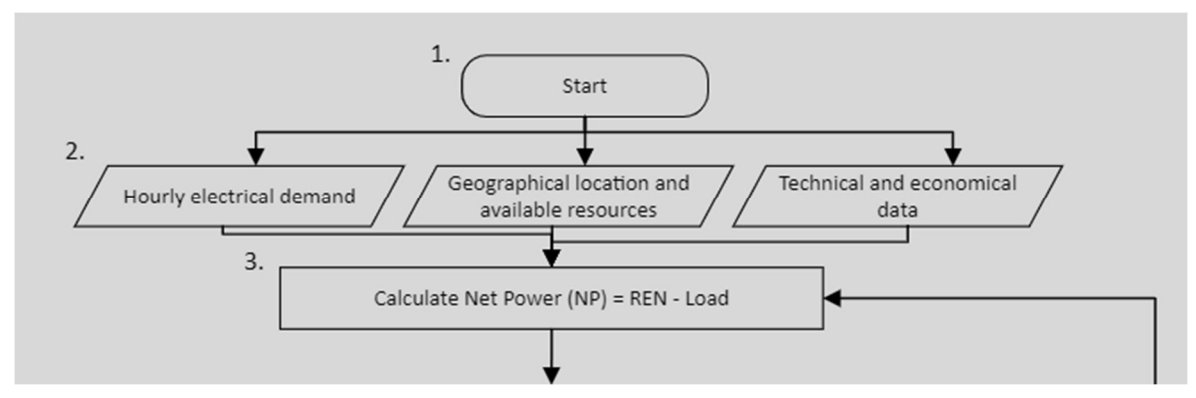


Figure 9-11: Focused snippet Between Process 1-3

system component, geographic data influencing the availability of renewable resources, and hourly electricity consumption. The hourly demand data shows the community's energy needs hourly throughout the year, therefore guiding the baseline for energy balancing at every time interval. Geographical data including sun irradiation and ambient temperature guides the generating potential for renewable energy, therefore enabling the model to modify its energy distribution depending on historic resource availability. Technical and financial criteria for parts including photovoltaic panels, wind turbines, batteries, fuel cells, electrolysers, and grid tariffs give the model necessary performance, capacity, and cost constraints, so guiding wise use of the resources at hand.

The model computes the net power (NP) at every time step by deducting the electrical load from the renewable energy production (NP = REN - Load), as Process 3 explains. This net power computation is crucial as it guides the next actions of the model: either allocating energy to storage, transforming it to hydrogen, or depending on grid imports to satisfy the demand. A positive NP denotes surplus renewable energy; a negative NP indicates a power scarcity. Therefore, the sign of NP defines the direction the model uses for energy allocation.

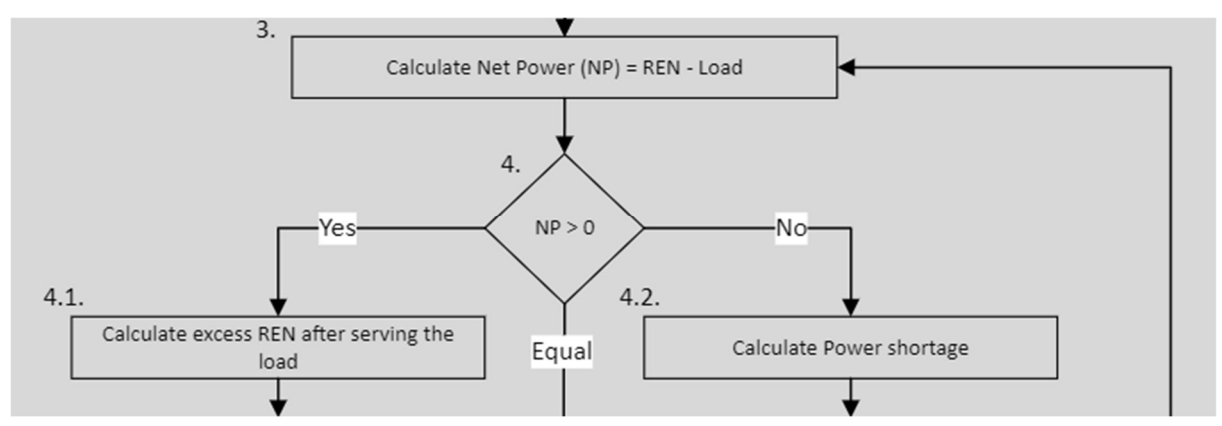


Figure 9-12: Focused snippet Process 4 and its two main decisions 4.1 and 4.2

Process 4's decision point is when the model assesses the sign of NP to ascertain the suitable allocation route as shown in Figure 9-12. The model follows the route described in Process 4.1 when NP is positive, meaning an excess of renewable energy. Examining the battery's state of charge (SOC) comes first along this road (Process 4.1.1). Should the battery be not completely charged (SOC < 100%), the model uses the surplus energy to charge the battery

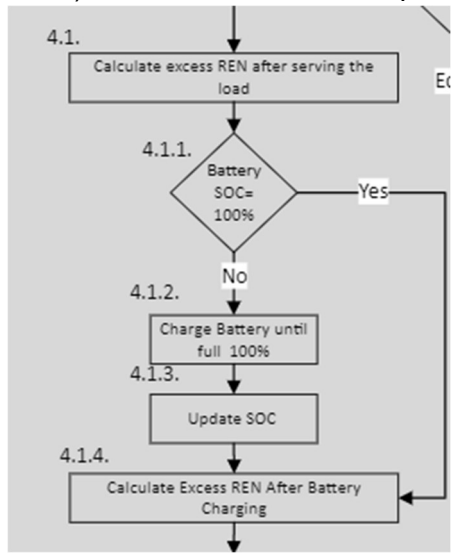


Figure 9-13: Focused on Decision Branches from 4.1 to 4.1.4

(as described in Process 4.1.2), therefore conserving the excess renewable energy for usage when demand could surpass generation. Following every charging cycle, the model updates

the battery SOC (Process 4.1.3), therefore preserving a precise record of accessible storage capacity as shown in Figure 9-13.

The model computes the extra energy after battery charging (Process 4.1.4) should the battery reach its maximum SOC and still have surplus energy. Should more renewable energy still be available, the system assesses conditions for running the electrolyser, per Process 4.1.5 and 4.1.6. The model specifically confirms that the operating limitations of the inverter are not exceeded and examines the SOC of the hydrogen tank to guarantee enough storage capacity. Should these requirements be satisfied, the model turns on the electrolyser (Process 4.1.7), transforming the residual surplus energy into hydrogen, which finds residence in the hydrogen tank. Level of hydrogen (LoH) of the hydrogen tank is changed to correspond with the new hydrogen storage (Process 4.1.8) as shown in Figure 9-15.

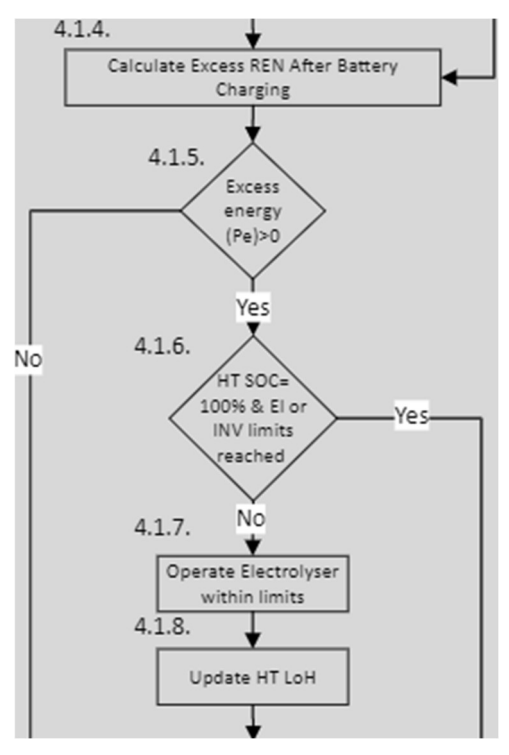


Figure 9-15: Focused on Decision Branch es from 4.1.4 to 4.1.8

Should extra energy remain after electrolyser operation, the model investigates as demonstrated in Figure 9-14, in Process 4.1.9 and 4.1.10, the viability of exporting energy to the grid. Examining if the grid connection and inverter stay within stipulated restrictions comes in this phase. Should grid export be possible, the model saves this surplus for further study (Process 4.1.12) and exports the extra energy within these constraints (Process 4.1.11). The information on surplus energy sent to the grid shows the capacity of the system to optimise the usage of renewable energy as well as hints on possible income from energy sales.

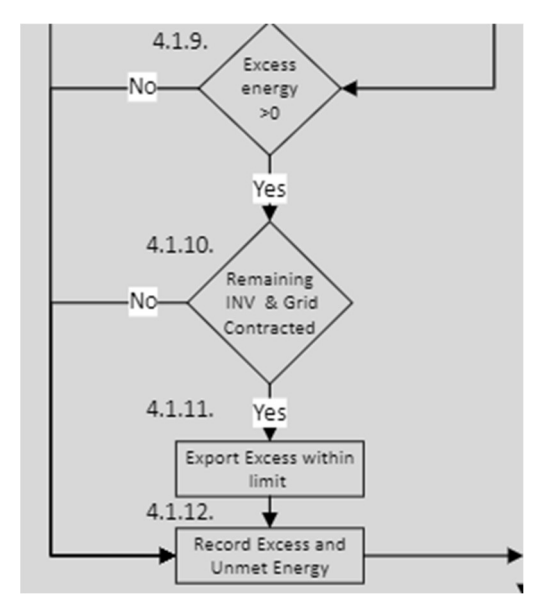


Figure 9-14: Focused on Decision Branch es from 4.1.8 to 4.1.12

Should NP be negative, indicating a power shortfall, the model uses the alternate route described in Process 4.2. Examining the battery SOC first on this road (Process 4.2.1) will help one to determine if sufficient stored energy exists to meet the demand. Should the SOC above the minimum five percent barrier, the battery releases energy to balance the shortfall (Process 4.2.2). Careful regulation of this discharge process helps to prevent draining the battery below the minimal SOC, therefore extending the lifetime of the battery and guaranteeing a reserve of energy for future shortages. Following each discharge cycle (Process 4.2.3), the model changes the battery SOC while accurately documenting the accessible stored energy.

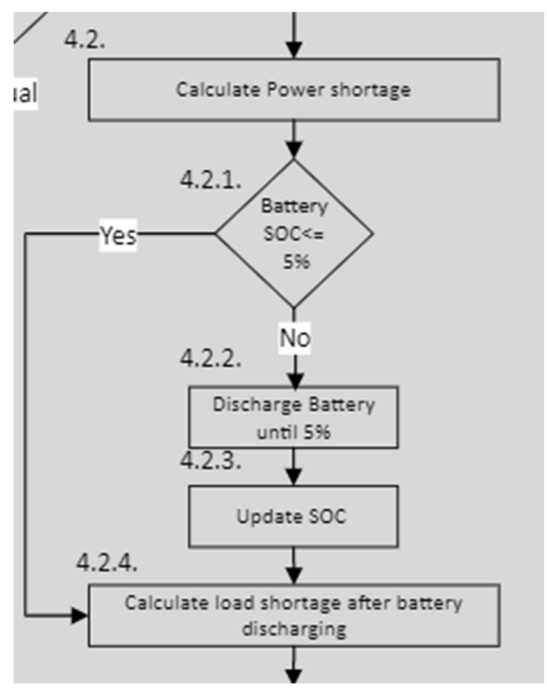


Figure 9-16: Focused on Decision Branches from 4.2 to 4.2.4

As described in Process 4.2.5 as shown in Figure 9-17, the model evaluates the likelihood of employing the fuel cell to provide extra power should a power shortfall persist beyond battery exhaustion. As Process 4.2.6 explains, the fuel cell activation depends on the operating limitations of the inverter and the SOC of the hydrogen tank. While the hydrogen tank's LoH is updated to reflect the lowered hydrogen storage, the fuel cell uses stored hydrogen back into electricity to fulfil the residual demand when both requirements are met (Process 4.2.7). This conversion technique maximizes hydrogen use while honouring the capacity limitations of the fuel cell.

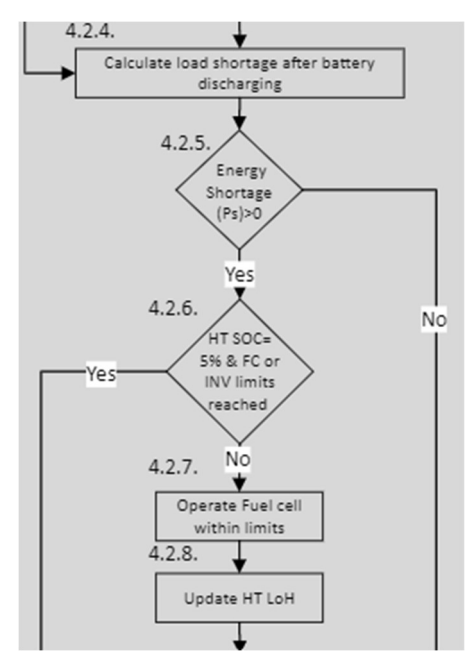


Figure 9-17: Focused on Decision Branches from 4.2.4 to 4.2.8

Should a power shortfall still exist after battery and fuel cell use, the model takes grid importation into account, as Process 4.2.9 and 4.2.10 indicate. The contracted grid capacity restricts grid imports so that they guarantee system compliance with allowed import limitations. Should grid energy be within these limitations, the model imports the energy to meet the unmet demand (Process 4.2.11) and notes this residual shortfall for further examination. Examining the system's dependency on grid power during shortages relies on this unmet demand data, which also highlights areas where increased renewable or storage capacity may reduce this need.

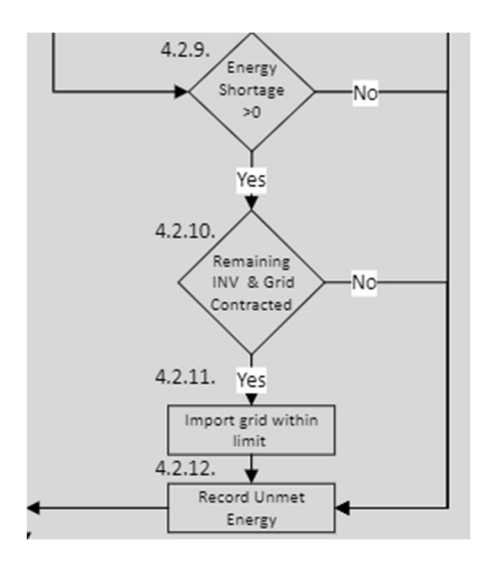


Figure 9-18: Focused on Decision Branch es from 4.2.8 to 4.2.12

Figure 9-19 shows the final process check (Process 5.). After every hourly time step, the model advances to the next hour (procedure 5.1), hence repeating the energy distribution process across the complete simulation length. Over every hour of the year, the model compiles data on grid interactions, battery and hydrogen SOC changes, and excess and unmet energy iteratively. Process 5.2 helps the model to gather the entire unmet and excess energy at the end of the simulation, therefore providing a complete picture of the performance and efficiency of the system all year long. This overview covers significant numbers like the Net Present Cost (NPC), general unmet demand, and energy delivered to the grid. These calculations provide perceptive insight on the balance between demand and renewable generation of load-following energy management system.

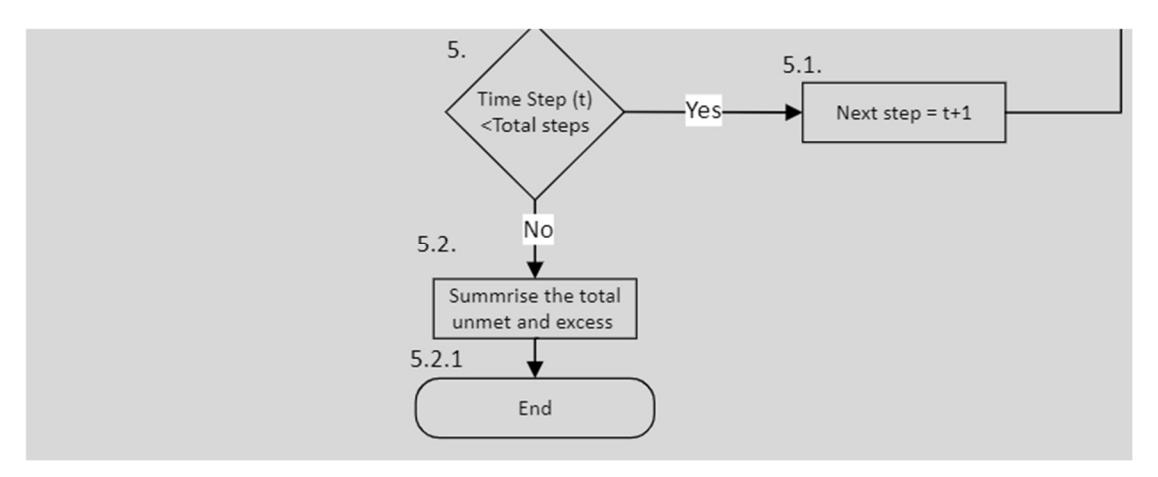


Figure 9-19: Focused on Decision Branch es from 5. to 5.2.1 and 5. To 5.1.

## .

## 9.4 The Foundational Theoretical Framework

In the simplest scenario described by [55], [113], the derived  $[ESOI]_{grid}$  targets energy generation and storage system comparison at grid scale. It assumes a single generation source with lifetime generation  $E_{gen}$  and a fraction  $\varphi$  of that generation either curtailed or routed through storage. The embodied energy of the generation facility is:

$$E_{emb,gen} = E_{gen} \cdot \varepsilon_{gen}$$
 9-1)

where  $\varepsilon_{gen} = 1/EROI_{gen}$  is the energy intensity of generation (MJ of manufacturing per MJ generated). If a fraction  $\varphi$  of  $E_{gen}$  is diverted into storage, the embodied energy of the storage system is related to the storage ESOI<sub>e</sub> by:

$$E_{emb,st} = E_{gen} \cdot \varphi \cdot \varepsilon_{st}$$
 9-2)

where  $\varepsilon_{st} = 1/\text{ESOI}_e$  is the energy intensity of the storage (MJ of manufacturing per MJ delivered from storage). The total embodied energy of the generation-plus-storage configuration is given as follows:

$$E_{emb,total} = E_{emb,gen} + E_{emb,st} = E_{gen} (\varepsilon_{gen} + \varphi \varepsilon_{st})$$
9-3)

The total dispatched energy from the system  $E_{emb,total}$  consists of energy directly delivered from generation  $E_{disp,gen}$  and energy delivered from storage  $E_{disp,st}$ , and the  $\eta_{st}$  as the round-trip efficiency of the storage system.

$$E_{disp,gen} = (1 - \varphi)E_{gen}$$

$$E_{disp,st} = \eta_{st} \varphi E_{gen}$$
9-4)

Thus:

$$E_{\text{disp,total}} = E_{gen}[(1 - \varphi) + \eta_{st}\varphi]$$
 9-5)

Now, applying the definition of EROI to the combined system (grid scale):

$$[EROI]_{grid} = \frac{E_{disp,total}}{E_{emb,total}}$$
 9-6)

From equations 9-3) and 9-5),  $[EROI]_{grid}$ :

$$[EROI]_{grid} = \frac{E_{gen}[(1-\varphi) + \eta_{st}\varphi]}{E_{gen}(\varepsilon_{gen} + \varphi\varepsilon_{st})}$$
9-7)

Cancelling  $E_{gen}$ :

$$[EROI]_{grid} = \frac{(1 - \varphi) + \varphi \eta_{st}}{\varepsilon_{gen} + \varphi \varepsilon_{st}}$$
9-8)

Since  $\varepsilon_{gen} = 1/EROI_{gen}$  and  $\varepsilon_{st} = 1/ESOI_e$ , we rewrite:

$$[EROI]_{grid} = \frac{(1-\varphi) + \varphi \eta_{st}}{\frac{1}{EROI_{gen}} + \frac{\varphi}{ESOI_e}}$$
9-9)

This final equation shows how the overall EROI of the grid system changes when a fraction  $\varphi$  of the generation is routed through a storage device characterised by a certain ESOI and efficiency.

## 10 Reference

- [1] UNFCCC, 'COP 28: What Was Achieved and What Happens Next?' Accessed: Sept. 02, 2024. [Online]. Available: https://unfccc.int/cop28/5-key-takeaways#end-of-fossil-fuels
- [2] 'BP Energy Outlook 2022', BP. Accessed: June 15, 2022. [Online]. Available: https://www.bp.com/content/dam/bp/business-sites/en/global/corporate/pdfs/energy-economics/energy-outlook/bp-energy-outlook-2022.pdf
- [3] K. Riahi *et al.*, 'The Shared Socioeconomic Pathways and their energy, land use, and greenhouse gas emissions implications: An overview', *Global Environmental Change*, vol. 42, pp. 153–168, Jan. 2017, doi: 10.1016/j.gloenvcha.2016.05.009.
- [4] M. Crippa *et al.*, 'GHG emissions of all world countries', 2024. doi: 10.2760/4002897.
- [5] A. Gambhir, J. Rogelj, G. Luderer, S. Few, and T. Napp, 'Energy system changes in 1.5 °C, well below 2 °C and 2 °C scenarios', *Energy Strategy Reviews*, vol. 23, pp. 69–80, Jan. 2019, doi: 10.1016/j.esr.2018.12.006.
- [6] Energy Institute, 'Resources and data downloads', Statistical review of world energy. Accessed: Sept. 02, 2024. [Online]. Available: https://www.energyinst.org/statistical-review/resources-and-data-downloads
- [7] IEA, 'Buildings Energy System', IEA. Accessed: Sept. 03, 2024. [Online]. Available: https://www.iea.org/energy-system/buildings
- [8] European Commission, 'The European Green Deal'. Accessed: Sept. 03, 2024. [Online]. Available: https://commission.europa.eu/strategy-and-policy/priorities-2019-2024/european-green-deal en
- [9] EPBD, 'Energy Performance of Buildings Directive'. Accessed: Sept. 03, 2024. [Online]. Available: https://energy.ec.europa.eu/topics/energy-efficiency/energy-efficient-buildings/energy-performance-buildings-directive\_en
- [10] Eurostat, 'Renewable energy statistics'. Accessed: Sept. 04, 2024. [Online]. Available: https://ec.europa.eu/eurostat/statistics-explained/index.php?title=Renewable energy statistics
- [11] Eurostat, 'Energy consumption in households'. Accessed: Sept. 04, 2024. [Online]. Available: https://ec.europa.eu/eurostat/statistics-explained/index.php?title=Energy consumption in households
- [12] Odyssee Mure, 'Appliances & Lighting | Energy consumption per dwelling'. Accessed: Oct. 04, 2024. [Online]. Available: https://www.odyssee-mure.eu/publications/efficiency-by-sector/households/electrical-appliances.html
- [13] L. Childs, G. Bennett, S. Watson, and G. Wilson, 'Predicting the heat pump readiness of existing heating systems in the UK using diagnostic boiler data', *Building Services Engineering Research & Technology*, vol. 46, no. 2, pp. 157–175, Mar. 2025, doi: 10.1177/01436244241306591.
- [14] European Commission, 'In focus: Reducing the EU's dependence on imported fossil fuels', Brussels, 2022. Accessed: Oct. 04, 2024. [Online]. Available: https://commission.europa.eu/news/focus-reducing-eus-dependence-imported-fossil-fuels-2022-04-20\_en
- [15] E. Bertoli, Silvia Laera, and F. van Dedem, 'Islands need resilient power systems more than ever. Clean energy can deliver'. Accessed: Sept. 04, 2024. [Online]. Available: https://www.iea.org/commentaries/islands-need-resilient-power-systems-more-than-ever-clean-energy-can-deliver
- [16] R. Sauter, P. ten Brink, S. Withana, and L. Mazza, 'Impacts of climate change on European islands', IEEP AISBL. Accessed: Sept. 04, 2024. [Online]. Available: https://ieep.eu/publications/impacts-of-climate-change-on-european-islands/
- [17] European Commission, 'Even at 1.5°C warming, small island developing states risk flooding from sea level rise European Commission'. Accessed: Oct. 04, 2024. [Online]. Available: https://joint-research-centre.ec.europa.eu/jrc-news-and-updates/even-

- 15degc-warming-small-island-developing-states-risk-flooding-sea-level-rise-2023-12-05 en
- [18] Directorate-General for Energy, 'In focus: EU islands and the clean energy transition', Brussels, July 15, 2021. Accessed: June 21, 2023. [Online]. Available: https://commission.europa.eu/news/focus-eu-islands-and-clean-energy-transition-2021-07-15 en
- [19] G. Kallis, P. Stephanides, E. Bailey, P. Devine-Wright, K. Chalvatzis, and I. Bailey, 'The challenges of engaging island communities: Lessons on renewable energy from a review of 17 case studies', *Energy Research & Social Science*, vol. 81, p. 102257, Nov. 2021, doi: 10.1016/j.erss.2021.102257.
- [20] Eurostat, 'Tourism peak months differ across EU regions'. Accessed: Sept. 04, 2024. [Online]. Available: https://ec.europa.eu/eurostat/web/products-eurostat-news/w/ddn-20231130-2
- [21] R. D. Prasad, D. A. Chand, S. S. S. L. Lata, and R. S. Kumar, 'Beyond Energy Access: How Renewable Energy Fosters Resilience in Island Communities', *Resources*, vol. 14, no. 2, Art. no. 2, Feb. 2025, doi: 10.3390/resources14020020.
- [22] W. Zhu, S. Wen, Q. Zhao, B. Zhang, Y. Huang, and M. Zhu, 'Deep Reinforcement Learning Based Optimal Operation of Low-Carbon Island Microgrid with High Renewables and Hybrid Hydrogen–Energy Storage System', *Journal of Marine Science and Engineering*, vol. 13, no. 2, Art. no. 2, Feb. 2025, doi: 10.3390/jmse13020225.
- [23] Giorgio Bonvicini *et al.*, 'EU geographical islands as leaders of green energy transition [version 1; peer review: 1 approved, 1 approved with reservations]', *Open Research Europe*, vol. 4, no. 258, 2024, doi: 10.12688/openreseurope.18856.1.
- [24] P. Blechinger, R. Seguin, C. Cader, P. Bertheau, and Ch. Breyer, 'Assessment of the Global Potential for Renewable Energy Storage Systems on Small Islands', *Energy Procedia*, vol. 46, pp. 294–300, Jan. 2014, doi: 10.1016/j.egypro.2014.01.185.
- [25] M. Noussan, P. P. Raimondi, R. Scita, and M. Hafner, 'The Role of Green and Blue Hydrogen in the Energy Transition—A Technological and Geopolitical Perspective', *Sustainability*, vol. 13, no. 1, Art. no. 1, Jan. 2021, doi: 10.3390/su13010298.
- [26] K. Kwon, H.-B. Lee, N. Kim, S. Park, and S. R. Joshua, 'Integrated Battery and Hydrogen Energy Storage for Enhanced Grid Power Savings and Green Hydrogen Utilization', *Applied Sciences*, vol. 14, no. 17, Art. no. 17, Jan. 2024, doi: 10.3390/app14177631.
- [27] Y. Zeng, T. Zhou, T. Wang, M. Zhang, S. Zhang, and H. Yang, 'Long-Duration Energy Storage: A Critical Enabler for Renewable Integration and Decarbonization', *Energies*, vol. 18, no. 3, Art. no. 3, Jan. 2025, doi: 10.3390/en18030466.
- [28] IEA, 'Global Hydrogen Review 2021', IEA, Paris, 2021. [Online]. Available: https://www.iea.org/reports/global-hydrogen-review-2021
- [29] IEA, 'The Future of Hydrogen', IEA, Paris, 2019. [Online]. Available: https://www.iea.org/reports/the-future-of-hydrogen
- [30] Office of Energy Efficiency & Renewable Energy, 'Hydrogen Production', Energy.gov. Accessed: Mar. 31, 2022. [Online]. Available: https://www.energy.gov/eere/fuelcells/hydrogen-production
- [31] Hydrogen Council, 'Hydrogen for Net-Zero A critical cost-competitive energy vector', Hydrogen Council, 2021. [Online]. Available: https://hydrogencouncil.com/en/hydrogenfor-net-zero/
- [32] J. P. Barton and D. G. Infield, 'Energy storage and its use with intermittent renewable energy', *IEEE Transactions on Energy Conversion*, vol. 19, no. 2, pp. 441–448, June 2004, doi: 10.1109/TEC.2003.822305.
- [33] A. G. Olabi, C. Onumaegbu, T. Wilberforce, M. Ramadan, M. A. Abdelkareem, and A. H. Al Alami, 'Critical review of energy storage systems', *Energy*, vol. 214, p. 118987, Jan. 2021, doi: 10.1016/j.energy.2020.118987.
- [34] S. Ould Amrouche, D. Rekioua, T. Rekioua, and S. Bacha, 'Overview of energy storage in renewable energy systems', *International Journal of Hydrogen Energy*, vol. 41, no. 45, pp. 20914–20927, Dec. 2016, doi: 10.1016/j.ijhydene.2016.06.243.

- [35] G. Jansen, Z. Dehouche, and H. Corrigan, 'Cost-effective sizing of a hybrid Regenerative Hydrogen Fuel Cell energy storage system for remote & off-grid telecom towers', *International Journal of Hydrogen Energy*, vol. 46, no. 35, pp. 18153–18166, May 2021, doi: 10.1016/j.ijhydene.2021.02.205.
- [36] P. Taylor, R. Bolton, D. Stone, X.-P. Zhang, C. Martin, and P. Upham, 'Pathways for Energy Storage in the UK', Report for the Centre for Low Carbon Futures, York, Mar. 2012, Accessed: Nov. 03, 2021. [Online]. Available: http://www.lowcarbonfutures.org/sites/default/files/Pathways%20for%20Energy%20St orage%20in%20the%20UK.pdf
- [37] M. S. Okundamiya, 'Size optimization of a hybrid photovoltaic/fuel cell grid connected power system including hydrogen storage', *International Journal of Hydrogen Energy*, vol. 46, no. 59, pp. 30539–30546, Aug. 2021, doi: 10.1016/j.ijhydene.2020.11.185.
- [38] Z. Huang, H. Yu, Z. Peng, and Y. Feng, 'Planning community energy system in the industry 4.0 era: Achievements, challenges and a potential solution', *Renewable and Sustainable Energy Reviews*, vol. 78, pp. 710–721, Oct. 2017, doi: 10.1016/j.rser.2017.04.004.
- [39] G. Walker and N. Simcock, 'Community Energy Systems', in *International Encyclopedia of Housing and Home*, S. J. Smith, Ed., San Diego: Elsevier, 2012, pp. 194–198. doi: 10.1016/B978-0-08-047163-1.00598-1.
- [40] M. G. Gebreslassie and C. Cuvilas, 'The role of community energy systems to facilitate energy transitions in Ethiopia and Mozambique', *Energy Syst*, Nov. 2023, doi: 10.1007/s12667-023-00640-w.
- [41] A. C. Lazaroiu, M. Roscia, G. C. Lazaroiu, and P. Siano, 'Review of Energy Communities: Definitions, Regulations, Topologies, and Technologies', *Smart Cities*, vol. 8, no. 1, Art. no. 1, Feb. 2025, doi: 10.3390/smartcities8010008.
- [42] R. Garner and Z. Dehouche, 'Optimal Design and Analysis of a Hybrid Hydrogen Energy Storage System for an Island-Based Renewable Energy Community', *Energies*, vol. 16, no. 21, Art. no. 21, Jan. 2023, doi: 10.3390/en16217363.
- [43] P. Marocco, D. Ferrero, E. Martelli, M. Santarelli, and A. Lanzini, 'An MILP approach for the optimal design of renewable battery-hydrogen energy systems for off-grid insular communities', *Energy Conversion and Management*, vol. 245, p. 114564, Oct. 2021, doi: 10.1016/j.enconman.2021.114564.
- [44] M. Wirtz, M. Hahn, T. Schreiber, and D. Müller, 'Design optimization of multi-energy systems using mixed-integer linear programming: Which model complexity and level of detail is sufficient?', *Energy Conversion and Management*, vol. 240, p. 114249, July 2021, doi: 10.1016/j.enconman.2021.114249.
- [45] C. Mokhtara, B. Negrou, N. Settou, A. Bouferrouk, and Y. Yao, 'Design optimization of grid-connected PV-Hydrogen for energy prosumers considering sector-coupling paradigm: Case study of a university building in Algeria', *International Journal of Hydrogen Energy*, vol. 46, no. 75, pp. 37564–37582, Oct. 2021, doi: 10.1016/j.ijhydene.2020.10.069.
- [46] P. Nagapurkar and J. D. Smith, 'Techno-economic optimization and environmental Life Cycle Assessment (LCA) of microgrids located in the US using genetic algorithm', *Energy Conversion and Management*, vol. 181, pp. 272–291, Feb. 2019, doi: 10.1016/j.enconman.2018.11.072.
- [47] Y. Zhang, P. E. Campana, A. Lundblad, and J. Yan, 'Comparative study of hydrogen storage and battery storage in grid connected photovoltaic system: Storage sizing and rule-based operation', *Applied Energy*, vol. 201, pp. 397–411, Sept. 2017, doi: 10.1016/j.apenergy.2017.03.123.
- [48] Mhd. W. Chamout, A. Perl, E. J. Hengeveld, and J. Aué, 'Simulation and analysis of hybrid hydrogen-battery renewable energy storage for off-electric-grid Dutch household system', *International Journal of Hydrogen Energy*, vol. 70, pp. 170–182, June 2024, doi: 10.1016/j.ijhydene.2024.05.106.
- [49] G. Jansen, Z. Dehouche, and H. Corrigan, 'Cost-effective sizing of a hybrid Regenerative Hydrogen Fuel Cell energy storage system for remote & off-grid telecom

- towers', *International Journal of Hydrogen Energy*, vol. 46, no. 35, pp. 18153–18166, May 2021, doi: 10.1016/j.ijhydene.2021.02.205.
- [50] L. Jesus, R. Castro, and A. S. Lopes, 'Hydrogen-based solutions to help the electrical grid management: Application to the Terceira Island case', *International Journal of Hydrogen Energy*, vol. 48, no. 4, pp. 1514–1532, Jan. 2023, doi: 10.1016/j.ijhydene.2022.10.048.
- [51] R. Babaei, D. S.-K. Ting, and R. Carriveau, 'Optimization of hydrogen-producing sustainable island microgrids', *International Journal of Hydrogen Energy*, vol. 47, no. 32, pp. 14375–14392, Apr. 2022, doi: 10.1016/j.ijhydene.2022.02.187.
- [52] A. Arsalis, P. Papanastasiou, and G. E. Georghiou, 'A comparative review of lithium-ion battery and regenerative hydrogen fuel cell technologies for integration with photovoltaic applications', *Renewable Energy*, vol. 191, pp. 943–960, May 2022, doi: 10.1016/j.renene.2022.04.075.
- [53] L. P. Van, K. D. Chi, and T. N. Duc, 'Review of hydrogen technologies based microgrid: Energy management systems, challenges and future recommendations', *International Journal of Hydrogen Energy*, vol. 48, no. 38, pp. 14127–14148, May 2023, doi: 10.1016/j.iihydene.2022.12.345.
- [54] Y. He, S. Guo, P. Dong, Y. Zhang, J. Huang, and J. Zhou, 'A state-of-the-art review and bibliometric analysis on the sizing optimization of off-grid hybrid renewable energy systems', *Renewable and Sustainable Energy Reviews*, vol. 183, p. 113476, Sept. 2023, doi: 10.1016/j.rser.2023.113476.
- [55] M. A. Pellow, C. J. M. Emmott, C. J. Barnhart, and S. M. Benson, 'Hydrogen or batteries for grid storage? A net energy analysis', *Energy & Environmental Science*, vol. 8, no. 7, pp. 1938–1952, 2015, doi: 10.1039/C4EE04041D.
- [56] K. Anoune, M. Bouya, A. Astito, and A. B. Abdellah, 'Sizing methods and optimization techniques for PV-wind based hybrid renewable energy system: A review', *Renewable and Sustainable Energy Reviews*, vol. 93, pp. 652–673, Oct. 2018, doi: 10.1016/j.rser.2018.05.032.
- [57] M. F. Roslan, M. A. Hannan, P. J. Ker, and M. N. Uddin, 'Microgrid control methods toward achieving sustainable energy management', *Applied Energy*, vol. 240, pp. 583–607, Apr. 2019, doi: 10.1016/j.apenergy.2019.02.070.
- [58] A. Chauhan and R. P. Saini, 'A review on Integrated Renewable Energy System based power generation for stand-alone applications: Configurations, storage options, sizing methodologies and control', *Renewable and Sustainable Energy Reviews*, vol. 38, pp. 99–120, Oct. 2014, doi: 10.1016/j.rser.2014.05.079.
- [59] B. Modu, M. P. Abdullah, A. L. Bukar, and M. F. Hamza, 'A systematic review of hybrid renewable energy systems with hydrogen storage: Sizing, optimization, and energy management strategy', *International Journal of Hydrogen Energy*, vol. 48, no. 97, Art. no. 97, Dec. 2023, doi: 10.1016/j.ijhydene.2023.06.126.
- [60] E. L. V. Eriksson and E. MacA. Gray, 'Optimization and integration of hybrid renewable energy hydrogen fuel cell energy systems A critical review', *Applied Energy*, vol. 202, pp. 348–364, Sept. 2017, doi: 10.1016/j.apenergy.2017.03.132.
- [61] T. S. Le, T. N. Nguyen, D.-K. Bui, and T. D. Ngo, 'Optimal sizing of renewable energy storage: A techno-economic analysis of hydrogen, battery and hybrid systems considering degradation and seasonal storage', *Applied Energy*, vol. 336, p. 120817, Apr. 2023, doi: 10.1016/j.apenergy.2023.120817.
- [62] R. Babaei, D. S.-K. Ting, and R. Carriveau, 'Optimization of hydrogen-producing sustainable island microgrids', *International Journal of Hydrogen Energy*, vol. 47, no. 32, pp. 14375–14392, Apr. 2022, doi: 10.1016/j.ijhydene.2022.02.187.
- [63] O. Farhat, M. Khaled, J. Faraj, F. Hachem, R. Taher, and C. Castelain, 'A short recent review on hybrid energy systems: Critical analysis and recommendations', *Energy Reports*, vol. 8, pp. 792–802, Nov. 2022, doi: 10.1016/j.egyr.2022.07.091.
- [64] D. Neves, C. A. Silva, and S. Connors, 'Design and implementation of hybrid renewable energy systems on micro-communities: A review on case studies', *Renewable and*

- Sustainable Energy Reviews, vol. 31, pp. 935–946, Mar. 2014, doi: 10.1016/j.rser.2013.12.047.
- [65] T. Jeyaraj, A. Ponnusamy, and D. Selvaraj, 'Hybrid renewable energy systems stability analysis through future advancement technique: A review', *Applied Energy*, vol. 383, p. 125355, Apr. 2025, doi: 10.1016/j.apenergy.2025.125355.
- [66] H. Imad Hazim, K. Azmi Baharin, C. Kim Gan, and A. H. Sabry, 'Techno-economic optimization of photovoltaic (PV)-inverter power sizing ratio for grid-connected PV systems', *Results in Engineering*, vol. 23, p. 102580, Sept. 2024, doi: 10.1016/j.rineng.2024.102580.
- [67] L. P. Van, K. D. Chi, and T. N. Duc, 'Review of hydrogen technologies based microgrid: Energy management systems, challenges and future recommendations', *International Journal of Hydrogen Energy*, vol. 48, no. 38, pp. 14127–14148, May 2023, doi: 10.1016/j.iihydene.2022.12.345.
- [68] A. Naderipour *et al.*, 'Comparative evaluation of hybrid photovoltaic, wind, tidal and fuel cell clean system design for different regions with remote application considering cost', *Journal of Cleaner Production*, vol. 283, p. 124207, Feb. 2021, doi: 10.1016/j.jclepro.2020.124207.
- [69] M. S. Okundamiya, 'Size optimization of a hybrid photovoltaic/fuel cell grid connected power system including hydrogen storage', *International Journal of Hydrogen Energy*, vol. 46, no. 59, pp. 30539–30546, Aug. 2021, doi: 10.1016/j.ijhydene.2020.11.185.
- [70] Á. Ordóñez, E. Sánchez, J. Carlos Solano, and J. Parra-Domínguez, 'Demand charges reduction with photovoltaics in industry', *Heliyon*, vol. 10, no. 1, Art. no. 1, Jan. 2024, doi: 10.1016/j.heliyon.2023.e23404.
- [71] World Population Review, 'How Many Islands are There in the World 2024'. Accessed: Aug. 19, 2024. [Online]. Available: https://worldpopulationreview.com/metrics/how-many-islands-are-there-in-the-world
- [72] Directorate-General for Energy, 'In focus: EU islands and the clean energy transition'. Accessed: May 17, 2023. [Online]. Available: https://clean-energy-islands.ec.europa.eu/about
- [73] L. Ge *et al.*, 'A review of hydrogen generation, storage, and applications in power system', *Journal of Energy Storage*, vol. 75, p. 109307, Jan. 2024, doi: 10.1016/j.est.2023.109307.
- [74] A. S. Sánchez, E. P. Junior, B. M. Gontijo, P. de Jong, and I. B. dos Reis Nogueira, 'Replacing fossil fuels with renewable energy in islands of high ecological value: The cases of Galápagos, Fernando de Noronha, and Príncipe', *Renewable and Sustainable Energy Reviews*, vol. 183, p. 113527, Sept. 2023, doi: 10.1016/j.rser.2023.113527.
- [75] O. A. Odetoye, P. K. Olulope, O. M. Olanrewaju, A. O. Alimi, and O. G. Igbinosa, 'Multi-year techno-economic assessment of proposed zero-emission hybrid community microgrid in Nigeria using HOMER', *Heliyon*, vol. 9, no. 9, p. e19189, Sept. 2023, doi: 10.1016/j.heliyon.2023.e19189.
- [76] W. Zhu, S. Wen, Q. Zhao, B. Zhang, Y. Huang, and M. Zhu, 'Deep Reinforcement Learning Based Optimal Operation of Low-Carbon Island Microgrid with High Renewables and Hybrid Hydrogen–Energy Storage System', *Journal of Marine Science and Engineering*, vol. 13, no. 2, Art. no. 2, Feb. 2025, doi: 10.3390/jmse13020225.
- [77] A. J. Handique, R. A. M. Peer, and J. Haas, 'Understanding the Challenges for Modelling Islands' Energy Systems and How to Solve Them', *Curr Sustainable Renewable Energy Rep*, vol. 11, no. 4, pp. 95–104, Dec. 2024, doi: 10.1007/s40518-024-00243-8.
- [78] 'Orkney's Energy Orkney Renewable Energy Forum (OREF)'. Accessed: Aug. 04, 2025. [Online]. Available: https://www.oref.co.uk/orkneys-energy/
- [79] 'Orkney-wide energy audit 2014: Energy Sources and Uses', Aquatera Ltd, Dec. 2014. Accessed: Aug. 04, 2025. [Online]. Available: https://www.oref.co.uk/wp-content/uploads/2015/05/Orkney-wide-energy-audit-2014-Energy-Sources-and-Uses.pdf
- [80] 'Board Minutes/AGM', Shapinsay. Accessed: Aug. 04, 2025. [Online]. Available: https://shapinsay.org.uk/sdt/board-minutes-agm/

- [81] EMEC, 'Press release: BIG HIT hydrogen to power Orkney transport and heating: EMEC: European Marine Energy Centre'. Accessed: Aug. 04, 2025. [Online]. Available: https://www.emec.org.uk/press-release-big-hit-hydrogen-to-power-orkney-transport-and-heating/
- [82] A. Barney, H. Polatidis, M. Jelić, N. Tomašević, G. Pillai, and D. Haralambopoulos, 'Transition towards decarbonisation for islands: Development of an integrated energy planning platform and application', *Sustainable Energy Technologies and Assessments*, vol. 47, p. 101501, Oct. 2021, doi: 10.1016/j.seta.2021.101501.
- [83] A. Barney, H. Polatidis, and D. Haralambopoulos, 'Decarbonisation of islands: A multi-criteria decision analysis platform and application', *Sustainable Energy Technologies and Assessments*, vol. 52, p. 102115, Aug. 2022, doi: 10.1016/j.seta.2022.102115.
- [84] M. Thirunavukkarasu, Y. Sawle, and H. Lala, 'A comprehensive review on optimization of hybrid renewable energy systems using various optimization techniques', *Renewable and Sustainable Energy Reviews*, vol. 176, p. 113192, Apr. 2023, doi: 10.1016/j.rser.2023.113192.
- [85] R. Siddaiah and R. P. Saini, 'A review on planning, configurations, modeling and optimization techniques of hybrid renewable energy systems for off grid applications', *Renewable and Sustainable Energy Reviews*, vol. 58, pp. 376–396, May 2016, doi: 10.1016/j.rser.2015.12.281.
- [86] Y. Zhang, P. E. Campana, A. Lundblad, and J. Yan, 'Comparative study of hydrogen storage and battery storage in grid connected photovoltaic system: Storage sizing and rule-based operation', *Applied Energy*, vol. 201, pp. 397–411, Sept. 2017, doi: 10.1016/j.apenergy.2017.03.123.
- [87] S. Singh, P. Chauhan, and N. Singh, 'Capacity optimization of grid connected solar/fuel cell energy system using hybrid ABC-PSO algorithm', *International Journal of Hydrogen Energy*, vol. 45, no. 16, pp. 10070–10088, Mar. 2020, doi: 10.1016/j.ijhydene.2020.02.018.
- [88] T. S. Le, T. N. Nguyen, D.-K. Bui, and T. D. Ngo, 'Optimal sizing of renewable energy storage: A techno-economic analysis of hydrogen, battery and hybrid systems considering degradation and seasonal storage', *Applied Energy*, vol. 336, p. 120817, Apr. 2023, doi: 10.1016/j.apenergy.2023.120817.
- [89] H. HassanzadehFard, F. Tooryan, V. Dargahi, and S. Jin, 'A cost-efficient sizing of gridtied hybrid renewable energy system with different types of demands', *Sustainable Cities and Society*, vol. 73, p. 103080, Oct. 2021, doi: 10.1016/j.scs.2021.103080.
- [90] B. Modu, M. P. Abdullah, A. Alkassem, A. L. Bukar, and N. H. Zainal, 'Operational Strategy of a Hybrid Renewable Energy System With Hydrogen-Battery Storage for Optimal Performance Using Levy Flight Algorithm', in 2023 IEEE Conference on Energy Conversion (CENCON), Oct. 2023, pp. 35–40. doi: 10.1109/CENCON58932.2023.10369217.
- [91] D. A. Pérez Uc, S. E. de León Aldaco, and J. Aguayo Alquicira, 'Trends in Hybrid Renewable Energy System (HRES) Applications: A Review', *Energies*, vol. 17, no. 11, Art. no. 11, Jan. 2024, doi: 10.3390/en17112578.
- [92] A. Akter *et al.*, 'A review on microgrid optimization with meta-heuristic techniques: Scopes, trends and recommendation', *Energy Strategy Reviews*, vol. 51, p. 101298, Jan. 2024, doi: 10.1016/j.esr.2024.101298.
- [93] S. Ahmad, M. Shafiullah, C. B. Ahmed, and M. Alowaifeer, 'A Review of Microgrid Energy Management and Control Strategies', *IEEE Access*, vol. 11, pp. 21729–21757, 2023, doi: 10.1109/ACCESS.2023.3248511.
- [94] M. Shadoul, R. Al Abri, H. Yousef, and A. Al Shereiqi, 'Designing a Dispatch Engine for Hybrid Renewable Power Stations Using a Mixed-Integer Linear Programming Technique', *Energies*, vol. 17, no. 13, Art. no. 13, Jan. 2024, doi: 10.3390/en17133281.
- [95] T. Khan, M. Yu, and M. Waseem, 'Review on recent optimization strategies for hybrid renewable energy system with hydrogen technologies: State of the art, trends and future directions', *International Journal of Hydrogen Energy*, vol. 47, no. 60, Art. no. 60, July 2022, doi: 10.1016/j.ijhydene.2022.05.263.

- [96] Y. Zhang, Q. S. Hua, L. Sun, and Q. Liu, 'Life Cycle Optimization of Renewable Energy Systems Configuration with Hybrid Battery/Hydrogen Storage: A Comparative Study', *Journal of Energy Storage*, vol. 30, p. 101470, Aug. 2020, doi: 10.1016/j.est.2020.101470.
- [97] P. Gabrielli, M. Gazzani, E. Martelli, and M. Mazzotti, 'Optimal design of multi-energy systems with seasonal storage', *Applied Energy*, vol. 219, pp. 408–424, June 2018, doi: 10.1016/j.apenergy.2017.07.142.
- [98] F. A. Kassab, B. Celik, F. Locment, M. Sechilariu, S. Liaquat, and T. M. Hansen, 'Optimal sizing and energy management of a microgrid: A joint MILP approach for minimization of energy cost and carbon emission', *Renewable Energy*, vol. 224, p. 120186, Apr. 2024, doi: 10.1016/j.renene.2024.120186.
- [99] M. A. Giovanniello and X.-Y. Wu, 'Hybrid lithium-ion battery and hydrogen energy storage systems for a wind-supplied microgrid', *Applied Energy*, vol. 345, p. 121311, Sept. 2023, doi: 10.1016/j.apenergy.2023.121311.
- [100] A. Zelaschi, L. Pliotti, G. Betti, G. Tonno, D. Sgrò, and E. Martelli, 'An effective MILP model for the optimal design of microgrids with high-reliability requirements', *Applied Energy*, vol. 383, p. 125359, Apr. 2025, doi: 10.1016/j.apenergy.2025.125359.
- [101] O. Talent and H. Du, 'Optimal sizing and energy scheduling of photovoltaic-battery systems under different tariff structures', *Renewable Energy*, vol. 129, pp. 513–526, Dec. 2018, doi: 10.1016/j.renene.2018.06.016.
- [102] F. A. Kassab, B. Celik, F. Locment, M. Sechilariu, and T. M. Hansen, 'Combined Optimal Sizing and Energy Management of a DC Microgrid using MILP', in *2023 IEEE Belgrade PowerTech*, June 2023, pp. 1–6. doi: 10.1109/PowerTech55446.2023.10202939.
- [103] P. Marocco, M. Gandiglio, and M. Santarelli, 'Optimal design of PV-based grid-connected hydrogen production systems', *Journal of Cleaner Production*, vol. 434, p. 140007, Jan. 2024, doi: 10.1016/j.jclepro.2023.140007.
- [104] P. Rullo, L. Braccia, P. Luppi, D. Zumoffen, and D. Feroldi, 'Integration of sizing and energy management based on economic predictive control for standalone hybrid renewable energy systems', *Renewable Energy*, vol. 140, pp. 436–451, Sept. 2019, doi: 10.1016/j.renene.2019.03.074.
- [105] K. Tamashiro, E. Omine, N. Krishnan, A. Mikhaylov, A. M. Hemeida, and T. Senjyu, 'Optimal components capacity based multi-objective optimization and optimal scheduling based MPC-optimization algorithm in smart apartment buildings', *Energy and Buildings*, vol. 278, p. 112616, Jan. 2023, doi: 10.1016/j.enbuild.2022.112616.
- [106] B. Li, R. Roche, and A. Miraoui, 'Microgrid sizing with combined evolutionary algorithm and MILP unit commitment', *Applied Energy*, vol. 188, pp. 547–562, Feb. 2017, doi: 10.1016/j.apenergy.2016.12.038.
- [107] B. Li, R. Roche, D. Paire, and A. Miraoui, 'Sizing of a stand-alone microgrid considering electric power, cooling/heating, hydrogen loads and hydrogen storage degradation', *Applied Energy*, vol. 205, pp. 1244–1259, Nov. 2017, doi: 10.1016/j.apenergy.2017.08.142.
- [108] Y. Pu *et al.*, 'Optimal sizing for an integrated energy system considering degradation and seasonal hydrogen storage', *Applied Energy*, vol. 302, p. 117542, Nov. 2021, doi: 10.1016/j.apenergy.2021.117542.
- [109] A. Al-Quraan and B. Al-Mhairat, 'Sizing and energy management of grid-connected hybrid renewable energy systems based on techno-economic predictive technique', *Renewable Energy*, vol. 228, p. 120639, July 2024, doi: 10.1016/j.renene.2024.120639.
- [110] A. M. Eltamaly and Z. A. Almutairi, 'Nested Optimization Algorithms for Accurately Sizing a Clean Energy Smart Grid System, Considering Uncertainties and Demand Response', *Sustainability*, vol. 17, no. 6, Art. no. 6, Jan. 2025, doi: 10.3390/su17062744.
- [111] S. Mohseni and A. C. Brent, 'A Metaheuristic-Based Micro-Grid Sizing Model with Integrated Arbitrage-Aware Multi-Day Battery Dispatching', *Sustainability*, vol. 14, no. 19, Art. no. 19, Jan. 2022, doi: 10.3390/su141912941.

- [112] C. J. Barnhart and S. M. Benson, 'On the importance of reducing the energetic and material demands of electrical energy storage', *Energy Environ. Sci.*, vol. 6, no. 4, Art. no. 4, Mar. 2013, doi: 10.1039/C3EE24040A.
- [113] C. J. Barnhart, M. Dale, A. R. Brandt, and S. M. Benson, 'The energetic implications of curtailing versus storing solar- and wind-generated electricity', *Energy Environ. Sci.*, vol. 6, no. 10, pp. 2804–2810, Sept. 2013, doi: 10.1039/C3EE41973H.
- [114] S. D. Kurland and S. M. Benson, 'The energetic implications of introducing lithium-ion batteries into distributed photovoltaic systems', *Sustainable Energy Fuels*, vol. 3, no. 5, pp. 1182–1190, Apr. 2019, doi: 10.1039/C9SE00127A.
- [115] Y. Ghiassi-Farrokhfal, S. Keshav, and C. Rosenberg, 'An EROI-based analysis of renewable energy farms with storage', in *Proceedings of the 5th international conference on Future energy systems*, in e-Energy '14. New York, NY, USA: Association for Computing Machinery, June 2014, pp. 3–13. doi: 10.1145/2602044.2602064.
- [116] G. Limpens and H. Jeanmart, 'Electricity storage needs for the energy transition: An EROI based analysis illustrated by the case of Belgium', *Energy*, vol. 152, pp. 960–973, June 2018, doi: 10.1016/j.energy.2018.03.180.
- [117] G. Palmer, 'A Framework for Incorporating EROI into Electrical Storage', *Biophys Econ Resour Qual*, vol. 2, no. 2, Art. no. 2, Apr. 2017, doi: 10.1007/s41247-017-0022-3.
- [118] J. Dumas *et al.*, 'The Energy Return on Investment of Whole-Energy Systems: Application to Belgium', *Biophys Econ Sust*, vol. 7, no. 4, p. 12, Oct. 2022, doi: 10.1007/s41247-022-00106-0.
- [119] N. Kittner, S. H. Gheewala, and D. M. Kammen, 'Energy return on investment (EROI) of mini-hydro and solar PV systems designed for a mini-grid', *Renewable Energy*, vol. 99, pp. 410–419, Dec. 2016, doi: 10.1016/j.renene.2016.07.023.
- [120] A. Clerjon and F. Perdu, 'Matching intermittency and electricity storage characteristics through time scale analysis: an energy return on investment comparison', *Energy Environ. Sci.*, vol. 12, no. 2, pp. 693–705, Feb. 2019, doi: 10.1039/C8EE01940A.
- [121] Ministerio para la Transición Ecológica, Real Decreto 244/2019, de 5 de abril, por el que se regulan las condiciones administrativas, técnicas y económicas del autoconsumo de energía eléctrica, vol. BOE-A-2019-5089. 2019, pp. 35674–35719. Accessed: Aug. 05, 2025. [Online]. Available: https://www.boe.es/eli/es/rd/2019/04/05/244
- [122] 'Prosumers (Individual Self-Consumption) | Clean energy for EU islands'. Accessed: Aug. 05, 2025. [Online]. Available: https://clean-energy-islands.ec.europa.eu/countries/spain/legal/community-energy-framework/prosumers-individual-self-consumption
- [123] L. Losada-Puente *et al.*, 'Cross-Case Analysis of the Energy Communities in Spain, Italy, and Greece: Progress, Barriers, and the Road Ahead', *Sustainability*, vol. 15, no. 18, Art. no. 18, Jan. 2023, doi: 10.3390/su151814016.
- [124] C. Alaton, J. Contreras-Ocaña, P. de Radiguès, T. Döring, and F. Tounquet, 'Energy Communities: From European Law to Numerical Modeling', Aug. 07, 2020, *arXiv*: arXiv:2008.03044. doi: 10.48550/arXiv.2008.03044.
- [125] Á. Manso-Burgos, D. Ribó-Pérez, M. Alcázar-Ortega, and T. Gómez-Navarro, 'Local Energy Communities in Spain: Economic Implications of the New Tariff and Variable Coefficients', *Sustainability*, vol. 13, no. 19, Art. no. 19, Jan. 2021, doi: 10.3390/su131910555.
- [126] A. J. Gil Mena, V. F. Nasimba Medina, A. Bouakkaz, and S. Haddad, 'Analysis and optimisation of collective self-consumption in residential buildings in Spain', *Energy and Buildings*, vol. 283, p. 112812, Mar. 2023, doi: 10.1016/j.enbuild.2023.112812.
- [127] D. Rebollal, M. Carpintero-Rentería, D. Santos-Martín, and M. Chinchilla, 'Microgrid and Distributed Energy Resources Standards and Guidelines Review: Grid Connection and Operation Technical Requirements', *Energies*, vol. 14, no. 3, Art. no. 3, Jan. 2021, doi: 10.3390/en14030523.
- [128] Spanish National Markets, BOE-A-2020-1066 Circular 3/2020, of January 15, of the National Commission of Markets and Competition, which establishes the methodology

- for calculating electricity transportation and distribution tolls., 2020. doi: https://www.boe.es/eli/es/cir/2020/01/15/3/con.
- [129] A. H. Fathima and K. Palanisamy, 'Optimization in microgrids with hybrid energy systems A review', *Renewable and Sustainable Energy Reviews*, vol. 45, pp. 431–446, May 2015, doi: 10.1016/j.rser.2015.01.059.
- [130] S. Sinha and S. S. Chandel, 'Review of recent trends in optimization techniques for solar photovoltaic–wind based hybrid energy systems', *Renewable and Sustainable Energy Reviews*, vol. 50, pp. 755–769, Oct. 2015, doi: 10.1016/j.rser.2015.05.040.
- [131] L. Herc, A. Pfeifer, N. Duić, and F. Wang, 'Economic viability of flexibility options for smart energy systems with high penetration of renewable energy', *Energy*, vol. 252, p. 123739, Aug. 2022, doi: 10.1016/j.energy.2022.123739.
- [132] M. G. Prina *et al.*, 'Multi-objective optimization algorithm coupled to EnergyPLAN software: The EPLANopt model', *Energy*, vol. 149, pp. 213–221, Apr. 2018, doi: 10.1016/j.energy.2018.02.050.
- [133] F.-A. Fortin, F.-M. D. Rainville, M.-A. Gardner, M. Parizeau, and C. Gagné, 'DEAP: Evolutionary Algorithms Made Easy', *Journal of Machine Learning Research*, vol. 13, no. 70, Art. no. 70, 2012.
- [134] J. A. Duffie, W. A. Beckman, and N. Blair, *Solar Engineering of Thermal Processes, Photovoltaics and Wind.* Newark, UNITED STATES: John Wiley & Sons, Incorporated, 2020. Accessed: May 21, 2025. [Online]. Available: http://ebookcentral.proquest.com/lib/brunelu/detail.action?docID=6123275
- [135] B. Baiyin, K. Tagawa, and J. Gutierrez, 'Techno-Economic Feasibility Analysis of a Stand-Alone Photovoltaic System for Combined Aquaponics on Drylands', Sustainability, vol. 12, no. 22, Art. no. 22, Jan. 2020, doi: 10.3390/su12229556.
- [136] Z. R. Dogaheh and V. Puig, 'Tilt Angle Optimization of Photovoltaic Panels', in 2019 6th International Conference on Control, Decision and Information Technologies (CoDIT), Apr. 2019, pp. 1847–1852. doi: 10.1109/CoDIT.2019.8820549.
- [137] A. S. Al-Ezzi and M. N. M. Ansari, 'Photovoltaic Solar Cells: A Review', *Applied System Innovation*, vol. 5, no. 4, Art. no. 4, Aug. 2022, doi: 10.3390/asi5040067.
- [138] B. R. Paudyal and A. G. Imenes, 'Investigation of temperature coefficients of PV modules through field measured data', *Solar Energy*, vol. 224, pp. 425–439, Aug. 2021, doi: 10.1016/j.solener.2021.06.013.
- [139] X. Zhao, H. Bai, X. Lu, Q. Shi, and J. Han, 'A MILP model concerning the optimisation of penalty factors for the short-term distribution of byproduct gases produced in the iron and steel making process', *Applied Energy*, vol. 148, pp. 142–158, June 2015, doi: 10.1016/j.apenergy.2015.03.046.
- [140] J. Silvente and L. G. Papageorgiou, 'An MILP formulation for the optimal management of microgrids with task interruptions', *Applied Energy*, vol. 206, pp. 1131–1146, Nov. 2017, doi: 10.1016/j.apenergy.2017.08.147.
- [141] DESA, 'Goal 7 | Department of Economic and Social Affairs', Ensure access to affordable, reliable, sustainable and modern energy for all. Accessed: Aug. 21, 2024. [Online]. Available: https://sdgs.un.org/goals/goal7#targets\_and\_indicators
- [142] Directive (EU) 2018/2001, Directive (EU) 2018/2001 of the European Parliament and of the Council of 11 December 2018 on the promotion of the use of energy from renewable sources., vol. 328, no. 2018/2001. 2018, p. 82. Accessed: June 14, 2023. [Online]. Available: http://data.europa.eu/eli/dir/2018/2001/oj/eng
- [143] VPP4ISLANDS, 'VPP4ISLANDS'. Accessed: June 14, 2023. [Online]. Available: https://vpp4islands.eu/
- [144] NASA POWER DAV, 'NASA Prediction of Worldwide Energy Resources (POWER)'. Accessed: Aug. 06, 2024. [Online]. Available: https://power.larc.nasa.gov/data-access-viewer/
- [145] Endesa, 'Electricity access tariffs for businesses', Endesa. Accessed: Aug. 06, 2024.
  [Online]. Available: https://www.endesa.com/en/companies/electricity-access-tariffs-for-businesses

- [146] Eurostat, 'Electricity price statistics'. Accessed: June 15, 2023. [Online]. Available: https://ec.europa.eu/eurostat/statistics-explained/index.php?title=Electricity\_price\_statistics
- [147] Consell de Formentera, 'The installation of solar panels in the facilities of the Formentera Sailing School is finished Press room', Nov. 18, 2023. Accessed: Aug. 20, 2024. [Online]. Available: https://saladepremsa.consellformentera.com/en/2023/11/18/finalitza-la-instal%c2%b7lacio-de-panells-solars-a-les-instal%c2%b7lacions-de-lescola-de-vela-de-formentera/
- [148] Pylontech, 'US5000-Pylon Technologies Co., Ltd.' Accessed: Aug. 20, 2024. [Online]. Available: https://en.pylontech.com.cn/products/c23/134.html
- [149] Intelligent Energy, 'IE-POWER 1T', Intelligent Energy Limited. Accessed: Aug. 20, 2024. [Online]. Available: https://www.intelligent-energy.com/our-products/ie-power-hydrogen-fuel-cell-module/ie-power-1t-and-1u/
- [150] A. Kampker, H. Heimes, M. Kehrer, S. Hagedorn, P. Reims, and O. Kaul, 'Fuel cell system production cost modeling and analysis', *Energy Reports*, vol. 9, pp. 248–255, Mar. 2023, doi: 10.1016/j.egyr.2022.10.364.
- [151] J. Benz, 'POWER Magazine Enapter Makes Headway on AEM Electrolyzer Mass Production', *Enapter*, June 17, 2021. Accessed: Aug. 20, 2024. [Online]. Available: https://www.enapter.com/media-coverages/enapter-makes-headway-on-aem-electrolyzer-mass-production/
- [152] I. Guaita-Pradas and A. Blasco-Ruiz, 'Analyzing Profitability and Discount Rates for Solar PV Plants. A Spanish Case', Sustainability, vol. 12, no. 8, Art. no. 8, Jan. 2020, doi: 10.3390/su12083157.
- [153] Euro indicators, 'Annual inflation up to 2.0% in the euro area'. Accessed: Aug. 10, 2025. [Online]. Available: https://ec.europa.eu/eurostat/web/products-euro-indicators/w/2-17072025-ap
- [154] J. S. R. and S. A. M. and F. Peschiera, *PuLP : PuLP is an LP modeler written in python. PuLP can generate MPS or LP files and call GLPK, COIN CLP/CBC, CPLEX, and GUROBI to solve linear problems.* (2024). Python.
- [155] Gurobi Optimization, LLC, gurobipy: Python interface to Gurobi. (2024).
- [156] R. Roy and J. M. Pearce, 'Is small or big solar better for the environment? Comparative life cycle assessment of solar photovoltaic rooftop vs. ground-mounted systems', *Int J Life Cycle Assess*, vol. 29, no. 3, pp. 516–536, Mar. 2024, doi: 10.1007/s11367-023-02254-x.
- [157] S. Troy *et al.*, 'Life Cycle Assessment and resource analysis of all-solid-state batteries', *Applied Energy*, vol. 169, pp. 757–767, May 2016, doi: 10.1016/j.apenergy.2016.02.064.
- [158] A. Moradzadeh, K. Pourhossein, A. Ghorbanzadeh, M. Nazari-Heris, I. Colak, and S. M. Muyeen, 'Optimal sizing and operation of a hybrid energy systems via response surface methodology (RSM)', Sci Rep, vol. 14, no. 1, p. 20226, Aug. 2024, doi: 10.1038/s41598-024-71035-9.
- [159] L. Yepes-Bellver, A. Brun-Izquierdo, J. Alcalá, and V. Yepes, 'Artificial Neural Network and Kriging Surrogate Model for Embodied Energy Optimization of Prestressed Slab Bridges', *Sustainability*, vol. 16, no. 19, Art. no. 19, Jan. 2024, doi: 10.3390/su16198450.
- [160] L. Hegely, Ö. F. Karaman, M. T. Szucs, and P. Lang, 'Surrogate model-based optimisation of a batch distillation process', *Chemical Engineering Research and Design*, vol. 192, pp. 456–467, Apr. 2023, doi: 10.1016/j.cherd.2023.02.043.
- [161] A. Mukhtar, A. S. H. M. Yasir, and M. F. M. Nasir, 'A machine learning-based comparative analysis of surrogate models for design optimisation in computational fluid dynamics', *Heliyon*, vol. 9, no. 8, p. e18674, July 2023, doi: 10.1016/j.heliyon.2023.e18674.
- [162] A. Mukhtar, K. C. Ng, and M. Z. Yusoff, 'Passive thermal performance prediction and multi-objective optimization of naturally-ventilated underground shelter in Malaysia',

- Renewable Energy, vol. 123, pp. 342–352, Aug. 2018, doi: 10.1016/j.renene.2018.02.022.
- [163] G. James, D. Witten, T. Hastie, and R. Tibshirani, 'Linear Regression', in *An Introduction to Statistical Learning: with Applications in R*, G. James, D. Witten, T. Hastie, and R. Tibshirani, Eds, New York, NY: Springer US, 2021, pp. 59–128. doi: 10.1007/978-1-0716-1418-1 3.
- [164] R. Kohavi, 'A study of cross-validation and bootstrap for accuracy estimation and model selection', in *Proceedings of the 14th international joint conference on Artificial intelligence Volume 2*, in IJCAl'95. San Francisco, CA, USA: Morgan Kaufmann Publishers Inc., Aug. 1995, pp. 1137–1143.
- [165] Y. Guo and Y. Niu, 'The capacity optimization and techno-economic analysis of standalone hybrid renewable energy systems based on a two-stage nested optimization approach', *Journal of Energy Storage*, vol. 85, p. 111143, Apr. 2024, doi: 10.1016/j.est.2024.111143.
- [166] A. I. Atteya and D. Ali, 'Benchmarking a Novel Particle Swarm Optimization Dynamic Model Versus HOMER in Optimally Sizing Grid-Integrated Hybrid PV–Hydrogen Energy Systems', *Eng*, vol. 5, no. 4, Art. no. 4, Dec. 2024, doi: 10.3390/eng5040170.
- [167] F. Fodhil, A. Hamidat, and O. Nadjemi, 'Potential, optimization and sensitivity analysis of photovoltaic-diesel-battery hybrid energy system for rural electrification in Algeria', *Energy*, vol. 169, pp. 613–624, Feb. 2019, doi: 10.1016/j.energy.2018.12.049.
- [168] F. Firdouse and M. Surender Reddy, 'A hybrid energy storage system using GA and PSO for an islanded microgrid applications', *Energy Storage*, vol. 5, no. 7, p. e460, 2023, doi: 10.1002/est2.460.
- [169] N. Niveditha and M. M. Rajan Singaravel, 'Optimal sizing of hybrid PV–Wind–Battery storage system for Net Zero Energy Buildings to reduce grid burden', *Applied Energy*, vol. 324, p. 119713, Oct. 2022, doi: 10.1016/j.apenergy.2022.119713.
- [170] J. Hossain, A. F. A. Kadir, H. Shareef, R. Manojkumar, N. Saeed, and A. N. Hanafi, 'A Grid-Connected Optimal Hybrid PV-BES System Sizing for Malaysian Commercial Buildings', *Sustainability*, vol. 15, no. 13, Art. no. 13, Jan. 2023, doi: 10.3390/su151310564.
- [171] T. Kaewnukultorn, S. B. Sepúlveda-Mora, and S. Hegedus, 'The impacts of DC/AC ratio, battery dispatch, and degradation on financial evaluation of bifacial PV+BESS systems', *Renewable Energy*, vol. 236, p. 121402, Dec. 2024, doi: 10.1016/j.renene.2024.121402.
- [172] D. Meneghel, E. da C. Bortoni, and A. Karimi, 'Boosting DC/AC Ratio of PV Plant for BESS Integration on DC side', in 2018 IEEE Conference on Technologies for Sustainability (SusTech), Nov. 2018, pp. 1–4. doi: 10.1109/SusTech.2018.8671354.
- [173] J. Good and J. X. Johnson, 'Impact of inverter loading ratio on solar photovoltaic system performance', *Applied Energy*, vol. 177, pp. 475–486, Sept. 2016, doi: 10.1016/j.apenergy.2016.05.134.
- [174] E. Mohammadi and G. Moschopoulos, 'Optimization of PV Array-to-Inverter Power Ratio in Grid-Connected Systems to Maximize System Profit', in *2021 IEEE Applied Power Electronics Conference and Exposition (APEC)*, June 2021, pp. 2084–2089. doi: 10.1109/APEC42165.2021.9487276.
- [175] Á. Arcos-Vargas, D. Canca, and F. Núñez, 'Impact of battery technological progress on electricity arbitrage: An application to the Iberian market', *Applied Energy*, vol. 260, p. 114273, Feb. 2020, doi: 10.1016/j.apenergy.2019.114273.
- [176] A. H. Schleifer, C. A. Murphy, W. J. Cole, and P. Denholm, 'Exploring the design space of PV-plus-battery system configurations under evolving grid conditions', *Applied Energy*, vol. 308, p. 118339, Feb. 2022, doi: 10.1016/j.apenergy.2021.118339.
- [177] Andrew. J. Hutchinson and Daniel. T. Gladwin, 'An Analysis of Solar Inverter Ratios, Battery Inverter Ratios, and Their Effects on Capacity Factor and Economics of a DC-Coupled PV/BESS Site', in 2023 IEEE PES Innovative Smart Grid Technologies Latin America (ISGT-LA), Nov. 2023, pp. 270–274. doi: 10.1109/ISGT-LA56058.2023.10328358.

- [178] J. Hurtt and K. Baker, 'Minimum Battery Energy Storage System Sizing Integrated with a Photovoltaic Plant Considering Practical Limitations', in *2021 IEEE Madrid PowerTech*, June 2021, pp. 1–6. doi: 10.1109/PowerTech46648.2021.9494981.
- [179] A. H. Schleifer, C. A. Murphy, W. J. Cole, and P. Denholm, 'Exploring the design space of PV-plus-battery system configurations under evolving grid conditions', *Applied Energy*, vol. 308, p. 118339, Feb. 2022, doi: 10.1016/j.apenergy.2021.118339.
- [180] A. Al-Quraan and B. Al-Mhairat, 'Economic predictive control-based sizing and energy management for grid-connected hybrid renewable energy systems', *Energy*, vol. 302, p. 131795, Sept. 2024, doi: 10.1016/j.energy.2024.131795.
- [181] I. R. Ibrahim, M. N. B. Azman, N. A. Kamarzaman, and R. Darus, 'Maximum Demand Peak Shave Approach Utilising a Hybrid Solar PV and Battery Energy Storage System', in 2023 IEEE 13th International Conference on Control System, Computing and Engineering (ICCSCE), Aug. 2023, pp. 243–248. doi: 10.1109/ICCSCE58721.2023.10237141.
- [182] E. S. Chatzistylianos, G. N. Psarros, and S. A. Papathanassiou, 'Export Constraints Applicable to Renewable Generation to Enhance Grid Hosting Capacity', *Energies*, vol. 17, no. 11, Art. no. 11, Jan. 2024, doi: 10.3390/en17112588.
- [183] M. Castañeda, A. Cano, F. Jurado, H. Sánchez, and L. M. Fernández, 'Sizing optimization, dynamic modeling and energy management strategies of a stand-alone PV/hydrogen/battery-based hybrid system', *International Journal of Hydrogen Energy*, vol. 38, no. 10, pp. 3830–3845, Apr. 2013, doi: 10.1016/j.ijhydene.2013.01.080.
- [184] C. Yang, X. Li, L. Chen, and S. Mei, 'Intra-Day and Seasonal Peak Shaving Oriented Operation Strategies for Electric–Hydrogen Hybrid Energy Storage in Isolated Energy Systems', *Sustainability*, vol. 16, no. 16, Art. no. 16, Jan. 2024, doi: 10.3390/su16167010.
- [185] T. S. Le, T. N. Nguyen, D.-K. Bui, and T. D. Ngo, 'Optimal sizing of renewable energy storage: A techno-economic analysis of hydrogen, battery and hybrid systems considering degradation and seasonal storage', *Applied Energy*, vol. 336, p. 120817, Apr. 2023, doi: 10.1016/j.apenergy.2023.120817.
- [186] C. Blum and A. Roli, 'Metaheuristics in combinatorial optimization: Overview and conceptual comparison', *ACM Comput. Surv.*, vol. 35, no. 3, pp. 268–308, Sept. 2003, doi: 10.1145/937503.937505.
- [187] F.-A. Fortin, F.-M. D. Rainville, M.-A. Gardner, M. Parizeau, and C. Gagné, 'DEAP: Evolutionary Algorithms Made Easy', *Journal of Machine Learning Research*, vol. 13, no. 70, pp. 2171–2175, 2012.
- [188] K. Deb, 'An efficient constraint handling method for genetic algorithms', *Computer Methods in Applied Mechanics and Engineering*, vol. 186, no. 2, pp. 311–338, June 2000, doi: 10.1016/S0045-7825(99)00389-8.